GOX-Ethanol Resonance Ignition System Design

Design and Modeling of the Gas Dynamic Heating in a GOX-Ethanol Resonance Ignition Device

Z. Dickert

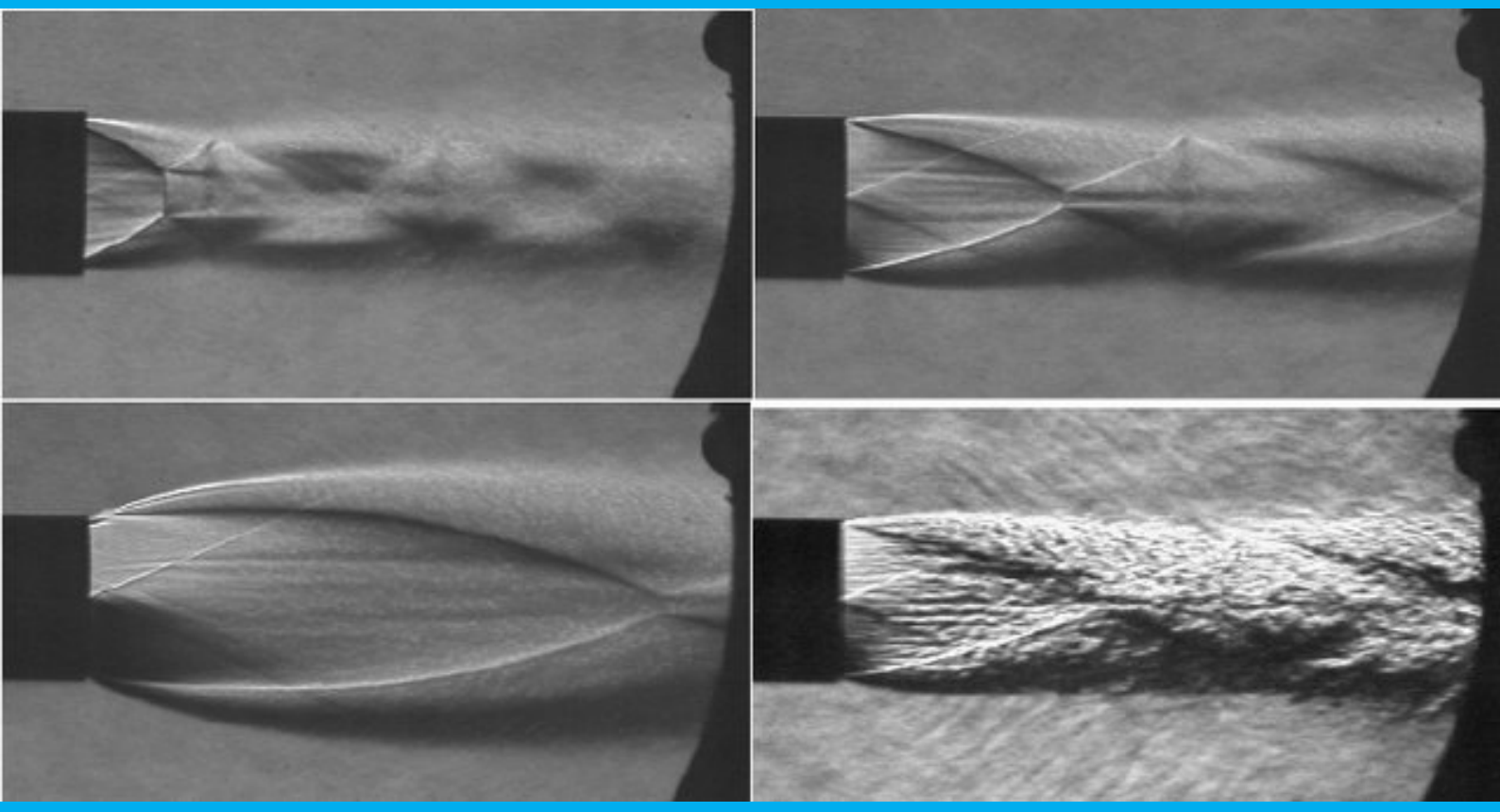

TU Delft

GOX-Ethanol Resonance Ignition System Design

Design and Modeling of the Gas Dynamic Heating in a GOX-Ethanol Resonance Ignition Device

by

Z. Dickert

to obtain the degree of Master of Science
at the Delft University of Technology,
to be defended publicly on Monday October 26, 2020 at 13:00.

Student number:	4701992	
Project duration:	February 14, 2020 – October 26, 2020	
Thesis committee:	Dr. A. Cervone	TU Delft, Chairman
	Ir. B. T. C. Zandbergen	TU Delft, Supervisor
	Dr. ir. AH van Zuijlen	TU Delft

An electronic version of this thesis is available at http://repository.tudelft.nl/.

TU Delft

Glossary

D_n Injection Nozzle Exit Diameter.

L_{conv} Injection Nozzle Convergent Length.

P_c Combustion Chamber Pressure.

P_o Oxidizer Injection Pressure.

d_{in} Injection Nozzle Inlet Diameter.

r_a Injection Nozzle Converging Radius.

r_u Injection Nozzle Radius.

ANSYS ANSYS Fluent CFD software.

CFD Computational Fluid Dynamics.

CRYO DARE Cryogenic Team.

DARE Delft Aerospace Rocket Engineering.

GOX Gaseous Oxygen.

H2 Hydrogen Molecule.

ISP Specific Impulse.

LOX Liquid Oxygen.

LRE Liquid Rocket Engine.

NPR Nozzle Pressure Ratio.

OF Mixture Ratio.

STP Standard Temperature and Pressure.

TRL Technology Readiness Level.

Preface

The purpose of a MSc thesis at Delft University of Technology Aerospace Faculty, is to deliver a body of work that contributes to the chosen field of research. As such, the topic of this thesis was derived as part of an effort to innovate on ignition systems in rocket engines. Aerospace engineering is a very broad field, but my focus has been on propulsion, and for this project, more specifically ignition systems. From my research in the Literature Study I saw that a majority of rocket engines utilize the same 3 types of ignition systems that were developed in the onset of the space program in the 1960s– pyrotechnic, hyperbolic, and spark. I understood a real opportunity to research a more innovative solution, resonance ignition, which I believe will play a major role in future propulsion systems.

After spending a year as the Chief Propulsion Engineer of the Delft Aerospace Rocket Engineering (DARE) Stratos Team, I became very experienced with testing of propulsion systems. Therefore it had initially been the plan to design the resonance ignition system using python and then perform experiments on the manufactured design to test and analyse the design. However, that plan became impossible when in February 2020 Covid-19 spread around the globe leading to the shutdown of many facilities. Therefore in order to complete the testing aspect of this thesis, a pivot was made to using numerical simulation. Numerical simulation tools, such as ANSYS Fluent, are widely used in aerospace engineering to test systems prior to manufacturing and physical testing. The Covid-19 related closure of the manufacturing and testing spaces at TU Delft, dictated that numerical simulations were the most feasible way to test this design.

As a graduate student in the Space Department, I had very little experience with ANSYS prior to this thesis. This meant that there was a significant learning curve before being able to use the software to run the necessary simulations.. I would like to send my deep regards to Weibo Hu, a PhD in the Aerodynamics group and Dr. Ir. A.H. van Zuijlen, an Assistant Professor in the TU Delft Aerospace Engineering Aerodynamics group, for taking the time to review my work in ANSYS Fluent and providing me with an enormous amount of help in understanding how to use the software. Through their guidance I was able to understand how the software worked and how to apply it to my thesis in order to generate results. I would also like to thank my Supervisor, Ir. Barry Zandbergen for providing a great deal of feedback on my work and always asking thoughtful questions.

I will be handing over all of the work to the DARE team, so that new students can use my work to build and test a resonance ignition system in the future. I have learned so much during my time at TU Delft, and am happy to conclude it with this thesis. I am proud of the work presented in this thesis and I believe it contributes to the work on ignition systems in aerospace engineering by exploring an innovative and promising system, resonance ignition.

Z. Dickert
Delft, October 2020

Contents

Summary

Since the 1940s, rocket engines have been ignited by 3 primary methods–hypergolic fuels, spark plugs/torches, and pyrotechnic devices. While much innovation has been made in the design and manufacturing of rockets, the ignition systems are still quite traditional. As the industry looks towards developing vehicle that will take mankind on longer missions to further destinations, it is vital to innovation in our ignition systems. The current systems will face challenges due to long mission duration, limited resources, and the high reusability required for these long missions. As part of this effort to innovate on ignition systems, this thesis explores the promise of resonance ignition. In resonance ignition systems, gas dynamics are used to rapidly heat a propellant gas to above its auto-ignition temperature. This allows the system to achieve combustion of the propellants, without any external energy sources. The goal of this thesis was to develop a design method and testing strategy to generate a detailed design of a resonance ignition system.

The preliminary design of this system was completed using empirical equations in a custom-made python script. Much work went into developing this script, with the intention that the preliminary design generated from this code would be able to heat the gas to the auto-ignition temperature. However, as this script only used empirical equations, which are only estimations and therefore unable to very accurately model this gas dynamic behavior, numerical models were necessary. These numerical models were used to make adjustments to the preliminary design in order to develop a working heating system.

The design was tested using a numerical simulation tool, ANSYS Fluent, in order to model its behavior. Much experimentation took place in order to develop the ANSYS Fluent meshing and solver method, 'Steady-Transient Hybrid Model,' that was capable of accurately simulating the gas dynamic phenomenon, within a reasonable amount of computational time. This method was validated against 2 existing resonance heating numerical studies and a mesh refinement study was conducted. The simulations began with a study on only the injection nozzle, in order to characterize the exhaust flow. These results were used to adjust the preliminary design, that was then used in the cavity simulations.

Three different cavity simulations were conducted, each with one parameter changed in order to find the design that was capable of achieving sufficient heating in the base of the cavity. The results of these simulations is a Detailed Design of a functional resonance heating device. This study found that the resonance cavity design that was capable of achieving the highest heating, at 160K over the ethanol auto-ignition temperature., had a cavity opening diameter twice as large as the nozzle exit diameter, the cavity opening located just before the first shock in the compression zone, and a 3° cavity angle. In order to learn more about the performance of this detailed design, 3 additional cases were run with different inlet pressures to learn how the change in Nozzle-Pressure-Ratio, effected the heating.

This thesis provided the detailed design of a resonance ignition system and validated is functionality through numerical simulation testing. It is recommended that further testing of different parameters be conducted, so that the python code can be modified to produce a more accurate and functional design. It is also recommended that this detailed design be tested in physical experiments to see how well the simulation agrees with the physical behavior. Overall this thesis was successful in designing and testing a resonance heating device, that was capable of heating the injected gaseous oxygen to well above the ethanol auto-ignition temperature.

1

Introduction

In order to initiate combustion in rocket engines, most propellants require a separate ignition system to ignite the main propellants. The purpose of the igniter is to provide the energy required to heat the propellants to the combustion temperature, through a combination of temperature of the ignition gases and time of ignition [66, p.406]. As companies like SpaceX and Blue Origin push the boundaries on what we believe to be possible in the realm of rocketry, a new and innovative ignition system must rise to meet these demands. Designing a reliable and robust igniter that meets the needs of future propulsive systems has proven to be a challenging task. New systems equipped with dozens of rockets and requiring multiple restart in space, will need precise and reliable ignition systems, or else risk mission failure. As such, the aerospace industry is researching future ignition capabilities to meet these demands. One system that has proven to be hardy, reliable, and precise is resonance ignition. This system passively ignites propellants using gas dynamics to put them into a hypergolic-like state. Since the 1970s extensive laboratory testing has demonstrated the potential for resonance ignition to reshape the aerospace industry[56] [60]. The next step will be to show its applicability on vehicles. Resonance ignition presents a safe, reliable, strong, and precise means to meet the ignition needs of the future.

In the 1970s NASA and Rocketdyne performed numerous tests to optimise the design of Hydrogen-Oxygen (H-O) resonance ignition systems [56] [60]. Research in this area subsequently slowed, but has recently re-surged due to the new enthusiasm for space travel. In 2019 the Technical University of Munich, wrote a paper in which they stressed the reliability of resonance ignition systems because they do not require high-powered electronics, long cables or mechanical systems to operate. Additionally they pointed to the safety of these systems over hypergolic or catalytic ignition systems, as resonance igniters do not require any toxic elements [45, p.2]. While this system has proved to be reliable in laboratory settings, there has been little momentum in taking this technology and applying it to flight vehicles. Additionally, little research has been conducted when one of the propellants is in a liquid state. NASA's Technology Readiness Level (TRL) chart indicates the level of development of a system [46]. Based on this chart, resonance ignition has a TRL of 5 (out of 9), meaning a fully functional prototype of this system has been tested in a laboratory environment. The median TRL of this technology will prove to be a challenge. However the simplicity, safety, and low cost of the system, make it ideal for rapid testing and development.

In addition to the far reaching applications of this technology for large scale rocket engines, this system provides an opportunity for innovation at TU Delft. Not only is there the chance to design and analyze such a system, but it also can be tested on a flight vehicle in the future. The Delft Aerospace Rocket Engineering (DARE) society allows students to gain hands-on experience with rocketry in order to bolster their academic experience at TU Delft. The Cryogenics Team (CRYO) is developing Blizzard, a 2.6kN liquid bi-propellant rocket engine[63, p.1] [23]. The ignition system designed in this thesis was made to be tested on the CRYO Blizzard engine. While this system can be used on a wide range of vehicles, collaborating with the student team provides an opportunity for students to gain hands-on experience in manufacturing and testing an ignition system. The goal of this project is to design an innovative ignition system based upon the principles of resonance heating, that will contribute to future ignition technologies for the aerospace industry at large.

1.1. Scope and Context

Ignition systems are an integral part of the development and functionality of all types of engines, from cars to planes to rockets. How they operate and the resources they require have had a large impact on the overall design of these vehicles. Designing a reliable and robust igniter that meets the needs of future propulsive systems has proven to be a challenging task. New systems equipped with dozens of rockets and requiring multiple restart in space, will need precise and reliable ignition systems, or else risk mission failure. As such, the aerospace industry is researching future ignition capabilities to meet these demands.

The DARE society allows students to gain hands-on experience with rocketry in order to bolster their academic experience at TU Delft. The CRYO Team is developing Blizzard, a 2.6kN liquid bi-propellant rocket engine. This thesis will be completed in collaboration with CRYO because DARE provides the resources and experience necessary to develop and test new technologies. Over the past 3 years I have gained great experience as first a member of CRYO, and then the Chief Propulsion Engineer for the DARE Stratos IV Dreamteam. In my role I was responsible for the manufacturing and testing of the DHX-400 Nimbus motor, a 26kN peak thrust hybrid motor. In my role I learned a great deal not only about the technical aspects of rocket engine design, manufacturing and testing, but also about how to be a good leader. As my experience in DARE has helped me grow into an intelligent and capable engineer, I find it important that my thesis project benefit DARE as well as be widely applicable to the aerospace industry at large. To that end, I have chosen to focus my thesis on the development of a Future Ignition System.

The goal of this thesis is to develop an innovative ignition system that is applicable both for CRYO and the wider aerospace industry. A literature study was utilized to gather information on all possible ignition systems, layout the requirements for this system and perform a trade-off to choose one system to develop. From this literature study, it was decided to pursue the study and design of a resonance ignition system [24]. The aim of this thesis is to present a thorough design process for a resonance ignition system using a gaseous oxygen and liquid ethanol propellants. It begins with extensive research into the system, and explanations on the various design parameters. A python script was developed which amalgamates all of these design options and equations in order to design a system. ANSYS simulations were utilized to test the preliminary design and complete the detailed design. Finally recommendation on design improvements and future testing are described, such that this work can be continued on either in DARE or as a subsequent thesis.

The TU Delft faculty of Aerospace Engineering aims to research and develop innovative technologies, so as to make meaningful contributions to the aerospace sector. With the recent rise in launch providers and launch systems, research into methods to improve these systems is more critical than ever. Ignition forms an integral part of rocket engine development and is on a scale of development that is well suited to a university environment. TU Delft is especially well positioned for such a project as it not only has a well equipped research facility in the Aerospace faculty, it also has a motivated and mature student rocket team that can contribute to the faculty's research projects. Therefore it is the goal of this thesis to develop the design of a innovative ignition system that can contribute to both the faculty and student rocket team.

In the final year of the TU Delft MSc Aerospace Engineering thesis, students complete a 12 week literature study, write a paper for the research methodology course, and then complete their 7 month thesis project. This is a technical thesis and requires adequate research, depth and contribution to their academic field.

1.2. History of Resonance Ignition

In the 1970s, NASA conducted a series of experiments to characterize resonance ignition systems and test their capabilities. In 1971, Bert Phillips and Albert Pavli, as part of NASA Lewis Research Center, performed a multitude of tests on a Hydrogen-Oxygen resonance igniter, where they adjusted a range of design parameters in order to characterize the optimal design of the system. Through their research they found an optimal Hydrogen-Oxygen resonance ignition design that proved reliable for propellants at ambient temperature [56, p.1]. In 1973, Leon Stabinsky performed a series of experiments of resonance ignition systems, on behalf of the Rocketdyne Division of Rockwell International. His goal was to perform tests to optimize a resonance ignition system and determine its usability with low temperature propellants [60, p.iii/iv]. At the conclusion of his experiment it was found that once the design of

the ignition system was optimized every test resulted in a successful ignition, furthermore the igniter performed reliably with cryogenic propellants [60, p.2].

Research in this area subsequently slowed, but has re-surged due to a new enthusiasm for space travel. In 2019 the Institute for Turbomachinery and Flight Propulsion, Rocket Propulsion Group at Technical University of Munich, wrote a paper on the *Numerical Investigation of a Resonance Ignition System*, in which they stressed the reliability of resonance ignition systems because they do not require high-powered electronics, long cables or mechanical systems to operate. Additionally they pointed to the safety of these systems over hypergolic or catalytic ignition systems, as resonance igniters do not require any toxic elements [44, p.2]. Additionally in 2007 after extensive experimentation, the Beijing University of Aeronautics and Astronautics concluded that resonance ignition systems were well suited for aerospike nozzles due to their precision timing and high reliability [32, p.1]. This long history of successful experimentation and resurgence of enthusiasm, demonstrates why resonance ignition offers a new and unique solution to the problem of reliable and mass-effective ignition designs. In this thesis, a GOX-Ethanol resonance ignition system is designed, and demonstrates the promise of this new future ignition technology.

1.3. Problem Statement

CRYO has made two unsuccessful attempts to produce a GOX and H2 spark torch ignition system for their LRE Blizzard engine. Forensics of these systems indicate that they likely failed due to pressurization and thermal issues [65]. While this forensic study was not conclusive, these failures are mentioned to highlight the challenges associated with developing an ignition system. Further details on these systems and the forensics of their failures can be found in the literature study [24]. The experiences with both of these designs highlighted the many challenges in designing ignition systems.

Ignition of a rocket engine can be accomplished in numerous ways and the method chosen is dependant on many factors such as the type of engine, propellants used, mass restrictions, etc. In the preceding literature study, a number of ignition system options were analysed and a trade-off was conducted to pick a system that would accomplish the system needs and innovate the field. More information on this trade-off can be found in the accompanying literature study [24]. The result of this trade-off was the decision to design a resonance ignition system using gaseous oxygen and liquid ethanol as propellants. Resonance ignition systems are a promising ignition option and have seem much development in lab environments. This thesis seeks to build on this work by designing a resonance ignition system for a small rocket engine that uses a propellant combination, gaseous Oxygen and liquid Ethanol, which have not yet been used on this ignition system. From this, the central problem statement of the thesis is as follows.

The problem is to design a GOX-Ethanol resonance ignition system that is robust enough to handle the extreme thermal environments in a rocket engine.

1.4. Challenges

During the Literature Study, it was discovered that there exists very little available information on the sizing of ignition systems, specifically when it relates to power and pressure requirements. It was not possible to find clear guidance on how much power an ignition system should provide to achieve a reliable ignition of a rocket engine, depending on the main engine type and power level. Therefore it was decided to make educated, conservative estimates on igniter power requirements, with the understanding that these power requirements could be adjusted based on future engine tests. This was the conclusion reached after discussions with those who are currently working in the field of large LRE testing. To make these estimates, all available information on existing LRE and their igniters was reviewed and trends in power ratio between the main engine and igniter were assessed. A conservative estimate on power was made, and guidance on how to adjust the igniter power output during testing is given. The purpose of this strategy is to allow the tester to decrease the power of the igniter to suit the engine, and prevent the development of an ignition system that is too weak to ignite the engine. Results of testing can be used to improve future estimations on ignition sizing.

Another area of difficulty was on setting the pressure of the igniter propellants and igniter combustion, in relation to the main engine combustion, as well as the timing of ignition. One of laws of fluid dynamics is that gases will always flow from high to low pressure. This is quite useful when needing

to move propellants from high pressure storage tanks to the lower pressure engine for injection and combustion. However if the pressure of the system does not cascade properly and there happens to be a lower pressure area prior to a higher pressure area (ex. a high pressure combustion and a low pressure propellant injection), it can cause the higher pressure gases to 'flow backwards.' This can lead to catastrophic failures in the engine as hot combustion gases can melt ignition or injection systems or even cause detonations in propellant lines. As the ignition system flows into the main engine combustion chamber, it was deemed vital that rules for setting the pressures of the ignition system, relative to the main engine chamber be set. This is especially important in the time after ignition occurs, when the main engine combustion is at a sustained high pressure, and flow of the hot combustion gases into the ignition chamber must be prevented by purging. However very little information on how to set these rules could be found in textbooks, journals or research papers. Therefore advice was sought from an engineer who is one of the top rocket engine testers in the field. A combination of research gathered and guidance given on how to properly set pressures of the systems and ignition timing is described in chapter 4. The pressures and timing of the ignition system set in the thesis are understood to be recommendations, with the necessity to perform testing of the ignition system and main engine combustion chamber to finalize these values. It is recommended to make replaceable ignition system components as it is quite likely melting will occur during testing.

Finally in March 2020, the world was hit with the Covid-19 pandemic. This caused massive closures of facilities, including the TU Delft Aerospace faculty and TU Delft Dreamhall. The original intention of this thesis was to construct a physical ignition system and perform testing, using these facilities. However, as the pandemic has stretched on and the facilities remain either entirely or partially closed, it became infeasible to perform a physical test campaign without great difficulty and months of delay. Therefore in order to complete the thesis in a reasonable amount of time and produce a substantial piece of work, it was decided to pivot the project from a focus on experimentation to a focus on design and development. To this end, a great deal of time was spent on the development of a substantive python code for the design of the system. Then numerical simulation work in ANSYS Fluent was done to test and validate these designs. In their paper, "Numerical investigation on thermo-acoustic effects and flow characteristics in semi-conical Hartmann–Sprenger resonance tube," Afzali and Karimi were able to demonstrate that a numerical simulation of the gas dynamics in a resonance cavity very closely matched the results of experimental testing of that same design [6]. Their work is discussed in more detail in subsequent chapters, but is mentioned here to provide confidence that a numerical simulation done in a similar matter to theirs can be used to demonstrate the validity of a resonance ignition system design. Finally a test campaign was described such that a future researcher can pick up where this thesis ends and perform experimentation. However even without the physical experiment portion, this thesis presents clear, substantive work on the design of an ignition system and provides innovation in the field of ignition.

1.5. Project Planning

The Literature Study for this thesis was conducted from mid-November 2019 to mid-February 2020. After that point the core work on the thesis project began and lasted from mid-February to the end of October 2020. In the original planning for this project, the python code would be written to develop a preliminary design and a set of alternative options for testing. Then a physical test setup was to be manufactured and a series of tests would be run. The first set of test would comprise of only a nozzle and cavity, to test how different parameters effecting the heating of the gas. The second set of tests would be of a prototype ignition system that included the nozzle, cavity and fuel injector, inside of a injector body. However in March 2020, when Covid-19 lead to massive closures of facilities, it was determined to be infeasible to continue with any physical testing. All manufacturing facilities were closed and coordinating and running tests had become impossible to arrange. Therefore, in April, when it appeared that the situation would not improve, it was decided to pivot to a fully numerical approach for testing. This lead to some time delays, as I needed to learn a new software, ANSYS Fluent. In the Aerospace Engineering Master's for Space Flight, we take an introduction to CFD course on ANSYS CFX. While having this background in CFD was helpful, there was still a great deal to learn. First I needed to become familiar with how to use the program, and then I needed to learn how to deal with the very common cases of numerical instabilities. Additionally, the cases in this thesis are complex to set up and run as they require a great deal of time and are prone to numerical instability due to the

presence of shock waves. It took a few months for me to become proficient enough to complete the cases for this thesis and generate accurate and meaningful results. I am grateful to Dr. Ir. A.H. van Zuijlen for his guidance with this software.

In addition, I spent most of August applying for a job at Relativity Space as a Propulsion Test Engineer. This job required an intensive interview process with many rounds of interviews and long technical interviews that required weeks of studying and preparation. I chose to take time during my thesis to apply and interview for this position, as this is when the job opportunity became available, and I thought it responsible to have a job ready after graduation. I was offered and accepted the position as a Propulsion Test Engineer at Relativity Space at the NASA John C. Stennis Space Center in Mississippi. Overall, I was able to overcome these challenges and I believe that I have produced a strong thesis in a timely manner.

2

Research Objectives and Design Methodology

In this chapter the research objectives, questions and design methodology are covered. This is meant to provide information on the goals of the thesis work and the methodology used to accomplish them.

2.1. Research Objectives

The *Main Research Objective* of this thesis states the goal of the project, defining what is hoped to be achieved and the method required to do so. It is as follows.

"The objective of this research project is to design an innovative resonance ignition system that is highly reliable, re-testable, and robust."

2.1.1. Sub-Objectives

In order to achieve this, the established main objective is broken down into a number of *sub-objectives*. These sub-objectives provide a tangible set of tasks that must be completed in this project and provide guidance in the development of the research questions. More in-depth descriptions on how to complete these sub-goals is written in section 2.3.

Sub-Goal 1: Generate the preliminary design requirements of the ignition system. These requirements cover the system performance, reliability, testability and robustness.

Sub-Goal 2: Complete the Preliminary Design Phase. Generate a list of major design parameters and develop a python script to generate the preliminary design of the system.

Sub-Goal 3: Use Ansys Fluent CFD simulations to test the preliminary design and produce the detailed system design.

2.2. Research Questions

From the stated main objective and sub-objectives, a set of research questions is developed. These questions help focus the research of the project and guide the design process. Each question is listed concisely and followed by a further explanation and sub-questions. These questions were developed using the S.M.A.R.T. criteria, which stands for Specific, Measurable, Achievable, Realistic and Time-Based [47].

1. What are the system requirements?
First a set of requirements for the ignition system must be generated. These requirements are based on the needs of the main engine, as well as the specific ignition system needs. These include topics such as determining the minimum ignition energy required to ignite the main propellants and the ignition time required. Additionally, the design of an ignition system must take into account certain operational requirements.

2. Which methodologies and tools will be used to design this system?
A 'road map' of the design of this system must be developed, which lays out the tools used and the steps taken to complete the design process.

3. What are design parameters needed to complete the preliminary design of a resonance ignition system?
Research on the functionality and components of resonance ignition must be performed in order to coalesce a list of design parameters. This set of parameters will form the structure for the design of this system and tools will be used to determine the values for these parameters.

4. What types of CFD simulations are needed to test the preliminary design and generate the detailed system design?
In the case of being unable to perform physical experimentation, it is helpful to perform simulations in order to test the preliminary design. These will also serve to generate the detailed design of the system. What parts of the design are useful to simulate? What tools should be used? How extensive to make these simulations?

2.3. Methodology

The design of the resonance ignition system is accomplished in 2 phases–the preliminary design phase and the detailed design phase. The preliminary design phase utilized python and empirical formulas to develop the initial design of the system. This centered around a custom-built python script, which aggregated all of the performance and geometric equations necessary to design a resonance ignition system. After completing the preliminary design, the next step in the design process is the detailed design phase. Due to the inherent uncertainties of ignition systems, it is important to include testing as part of the detailed design phase. This can be accomplished with physical experimentation or numerical simulation. The choice of whether to perform physical or numerical testing, is dependant on a number of factors, including budget, time, complexity of the test setup and accessibility of testing facilities. Most projects choose to do a combination of physical and numerical testing, the ratio of these dependant on the needs and constraints. Due to the logistical challenges posed by Covid-19, the decision was made to use numerical simulations to complete the testing portion of the design in order to obtain the detailed design. The purpose of the numerical simulations is two-fold, First, to test the preliminary design under the expected operating conditions to see if it performs as expected. Second, it will provide results that contribute towards completing the detailed design of the system. Before discussing the work that went into these design sections, the next chapter will be used to provide the reader with sufficient knowledge on resonance ignition and under-expanded jet flow so that they can follow the work presented.

2.4. Conclusion

The purpose of this chapter was to outline the research objectives and design methodologies for this project. This was accomplished by stating the research main objective and sub-objectives, and providing research questions used to focus and direct the design process. Finally, an overview of the design methodologies was provided to explain the approach taken in the design. More details on the full design methodology is provided in chapter 5.

3

Resonance Ignition

Resonance ignition systems use gas dynamics to rapidly increase the pressure and temperature of a gas. They give the propellants the qualities of hypergolics, without requiring any input energy, catalytic reactions or dangerous fluids [29, p.17]. In this chapter, the basic operations and major components of resonance ignition systems are covered. The purpose of this chapter is to provide context for the chosen design parameters and requirements. This chapter makes reference to a substantial amount of research that is used to support choices made during the design process, and more in depth information can be found in the literature study [24] and references. In this chapter the basic principles of resonance ignition are covered as well as some of the major design parameters. This is followed by an overview of under-expanded jets and gas-dynamics, as they play a central role in the functionality of these systems. The purpose of this chapter is to provide an overview of the information used to generate the system design.

3.1. Basic Principle of Resonance Ignition

Resonance ignition systems utilize the natural phenomenon of gas dynamics to rapidly increase the pressure and temperature of a gas. These devices give the gas the systematic qualities of hypergolic propellants, without requiring any input energy, catalytic reactions or dangerous hypergolic fluids. The central component of these devices is the Hartmann-Sprenger tube comprised of a cavity open at one end and closed at the other, into which a jet of high-speed gas is injected [29, p.17]. Professor Hartmann performed tests with a simple setup consisting of a nozzle, through which a jet of air was directed into a coaxial cylindrical cavity. Gas injected through a nozzle at supersonic speeds forms regions of instability. Hartmann discovered that if the distance between the exit of the injection of the nozzle and the entrance of the cylindrical cavity (gap distance) was adjusted such that the opening of the cavity was within one of the jets regions of instability, the air would oscillate within the cavity at a high frequency. This jet travels down the tube producing a shock wave, is reflected at the end and travels back towards the opening where it meets the incoming jet and pulls the jet into the cavity, thus restarting the cycle [13, p.75]. The oscillations formed by the HS-tube heat a section of the gas due to entropy caused by shock wave irreversibilities and frictional heat losses [50, p.814].

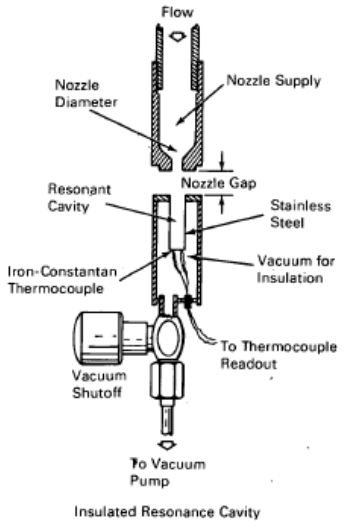

Figure 3.1: Resonance Igniter with insulated resonance cavity and temperature sensors. [20]

By integrating the Hartmann-Sprenger tube into an ignition system, resonance igniters have been developed as a means of reliable and passive ignition [20]. Resonance ignition systems are comprised of 4 main components, the

injection nozzle, the HS tube resonance cavity, the mixing chamber and the exit nozzle, as seen in Figure 3.1 [56, p.3]. The system works by injecting a gaseous propellant into the resonance cavity, using a nozzle. The oscillations formed in the HS tube rapidly increase the temperature of the gas. This rate of heating and maximum temperature reached are dependant on many factors, including the type of gas used and the distance between the injection nozzle and the opening of the resonance cavity. After the oscillating gas passes the ignition threshold temperature, the second propellant is then injected and combustion occurs. The two propellants continue combustion in the mixing chamber, which gives time for the propellants to achieve a more full combustion, before the flame is directed out into the main combustion chamber through the exit nozzle, where it ignites the main propellant flow [60, p.4].

Experiments conducted with Hartmann-Sprenger tubes have been capable of generating extremely high temperatures in a very short period of time making it a good option for ignition systems of rocket engines. Such systems can be customized for specific propellant needs by adjusting certain parameters, including the geometry of the injection nozzle, shape of the resonance cavity, jet pressure and distance between the nozzle exit and cavity inlet, to name a few [50, p.814]. The Hartmann-Sprenger tube can come in the classic right angle cylinder, stepped or tapered shapes. Stepped cavities function similarly to tapered but are easier to machine and therefore well suited for testing. Experimentation has shown that the temperature of the gas can be greatly increased by using a tapered or stepped resonance cavity [50, p.814]. This is well demonstrated by Figure 3.2 which provides the results of a test that demonstrated how a stepped cavity substantially increased the temperature of the gas, when compared to a cylindrical one [13, p.100]. The tapered shape of the cavity generates a higher temperature gas because the converging shape of the tube increases the strength of the shock waves [29, p.21]. From experimentation, it has been found that it requires a few seconds to achieve a steady state high temperature in the resonance tubes, and adding insulation to the tubes can significantly decrease the heat dissipated to the cavity walls [29, p.21].

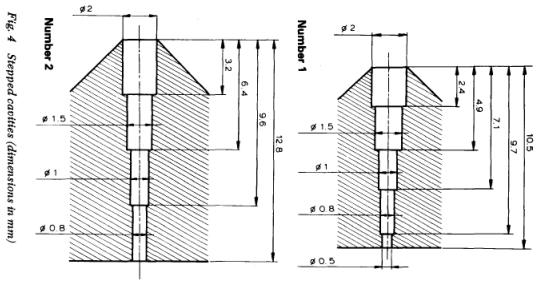

(a) 2 Stepped Cavities [13]

Table 1 Temperature measured after 100 ms

Gas	Cavity temperature (°C)		
	Cylindrical ($L/D = 20$)	Stepped (1)	Stepped (2)
Nitrogen	167	372	218
Argon	290	512	327
Helium	480	928	564

Driving pressure = 7 bar

(b) Cavity Shape Effect on Temperature [13]

Figure 3.2: Brocher Experiments, Effect of Resonance Cavity Shape on Gas Temperature [13]

Since resonance ignition systems use passive means to heat gases above their auto-ignition temperature to achieve ignition, they eliminate the reliance on limited resources or mechanical systems [44, p.1]. Such impressive heating capabilities and limitations on extraneous systems make resonance ignitions an attractive option for rocket engines. While this system has proved to be reliable in laboratory settings, there has been little momentum in taking this technology and applying it to flight vehicles. Additionally, little research has been conducted when one of the propellants is in a liquid state. NASA's Technology Readiness Level (TRL) chart indicates the level of development of a system [46]. Based on this chart, resonance ignition has a TRL of 5 (out of 9), meaning fully functional prototypes of the system have been tested in a laboratory environment. The median TRL of this technology will prove to be a challenge. However the simplicity, safety, and low cost of the system, make it ideal for rapid testing and development. Furthermore, their simplicity, low mass, and reliability make them ideal for rocket engines that require multiple ignition sites [29, p.17].

3.2. Propellants

In order to design a resonance igniter that is able to achieve the required temperature and be robust enough to survive multiple ignitions, a number of components need to optimized. These include the propellants used, resonance cavity geometry and material, geometry of the injection nozzle, distance between the nozzle and opening of the cavity, and the layout of components. The type of gas used

has a great impact on the maximum possible temperature achieved by the device. While it is possible to use any gas, theory establishes that monatomic gases should be capable of achieving much higher temperatures then diatomic gases because they have greater shock wave irreversibilities [13, p.100]. This theory has been

substantiated by multiple experiments, where lower molecular gases, such as Helium and Hydrogen heated much more rapidly than heavier gases [29, p.17]. A sample of the results of such experiments is shown in Figure 3.3a. While these tests used different set-ups and parameters, they show an overall trend in monatomic gases achieving higher temperatures, in a shorter amount of time, when compared to diatomic gases and molecules. In experiments conducted by Brocher, a HS-tube was capable of heating Helium in a 10mm tube at a rate of over $10^6\ K/s$ [13, p.75].

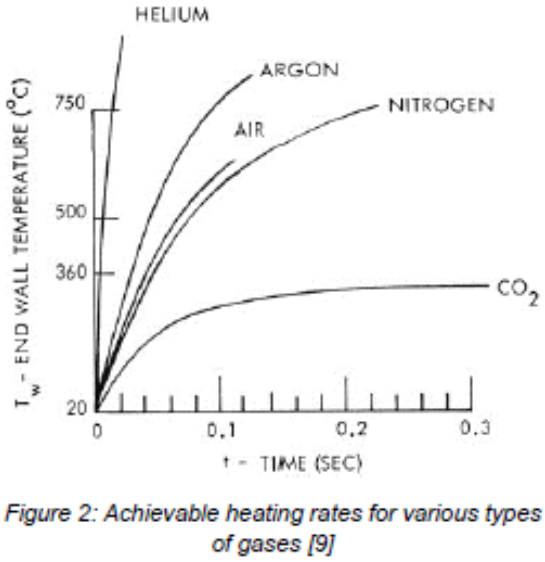

(a) Helium, Argon, Air, Nitrogen, and Carbon Dioxide [45]

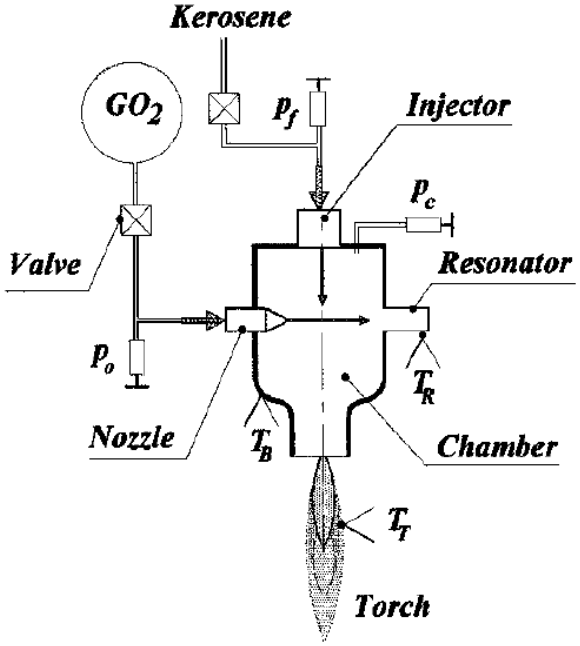

(b) Gaseous Oxygen and Liquid Kerosene Resonance Igniter Schematic, Source: [54, p.996]

Figure 3.3: Propellant heating and a Kerosene Resonance Ignition System

In order to reduce the system mass and complexity the igniter will use the main engine propellants, LOX and Ethanol(l). As the system requires at least one gaseous propellant, one of these must be vaporized. Oxygen is only liquid at cryogenic temperatures and boils at $-183°C$ [4]. Ethanol is a liquid at STP and boils at approximately $78°C$ [25]. This means that by simply flowing LOX through ambient piping it will change phase to a gas. Additionally, the maximum temperature achieved by the resonant gas is dependant on the size of the molecule. From theory and experimentation, lighter gases are capable of achieving higher temperatures because they have greater shock wave irreversibilities [13, p.100] [29, p.17]. Oxygen and Ethanol, have molecular weights of 31.999 and 46.07, respectively [4] [25]. Therefore Oxygen will be the resonant gas.

In 2001, researchers in Brazil successfully tested a GOX-Kerosene resonance ignition system, shown in Figure 3.3b. It proved that one could use the GOX as the resonant gas and achieve ignition by injecting a few drops Kerosene [54]. In this project a similar design will be used where GOX will be the resonant gas and Ethanol(l) will be injected. Some challenges foreseen are the corrosive nature of Oxygen and the lower temperature Oxygen can achieve, compared to the smaller Hydrogen atom. Therefore research will be done to choose materials that are robust enough to handle such an environment. If the corrosive nature of the Oxygen proves to be too detrimental or if the temperature reached is not sufficient, then a H-O version of the resonance igniter will be developed. This has already proven to be very reliable, but comes with added system mass. Recent academic research on resonance ignition has been very successful and provides an excellent basis for the development of a design and testing for a system at TU Delft [26] [45].

Introducing a liquid propellant, alters the configuration and procedures of the igniter, as it is vital to avoid the situation where the liquid fills up the resonance cavity, disrupting the ignition [54, p.995]. This also eliminates the practice of using a premixed stoichiometric mixture, as has been done in some Hydrogen Oxygen resonance igniters. Resonance ignition with a liquid fuel and gaseous oxidizer is accomplished by using the gaseous oxygen as the resonance gas and injecting it into the resonance cavity. Once the oxygen is heated above the auto-ignition temperature of the fuel, with margin, a small amount of the liquid fuel is injected into the hot oxygen to achieve combustion. This liquid fuel injection has the advantage that it can assist in cooling the walls of the ignition device. The setup of such an igniter is depicted in Figure 3.3b, which includes pressure and temperature sensors that can be included in a test bench version. Experimentation, designs and results from this paper will be vital in the thesis work, as this type of igniter most closely resembles the imagined product of this thesis. However it must be noted that the auto-ignition temperature of Kerosene is lower than ethanol, they are approximately $210°C$ and $400°C$, respectively [22] [25]. This means that the design produced for the thesis will need to achieve a higher temperature than that achieved in this paper.

3.3. Under-expanded Jets and Gas Dynamics

The simplified working principle of resonance cavity heating devices is that when an under-expanded jet of gas is injected into a closed-end cavity, the compression of the shock waves causes a rapid increase in the pressure and temperature of the gas in the cavity. This physical phenomenon is dependant on a number of parameters, most vitally being the geometries of the gas injection nozzle and the resonance cavity. In his paper, *Small Scale Supersonic Combustion Chamber with a Gas Dynamic Ignition System*, Marchan was able to develop a working resonance ignition system and characterize the most important design parameters. His work found that the ”operating mode of an HSG depends primarily on the geometric parameters of the supersonic jet (shock wave structure), the size of the resonance tube, the form of the resonance cavity, and the position of entry edges of the resonance tube relative to the shock waves in a free supersonic jet. under-expanded jets are most often used in HSGs” [48, p.1242]. This conclusion highlights the importance of the geometry of the under-expanded jet, as well as the igniter components. Therefore a short review on the structure of under-expanded jets and how they effect the gas dynamics of a resonance ignition system is provided.

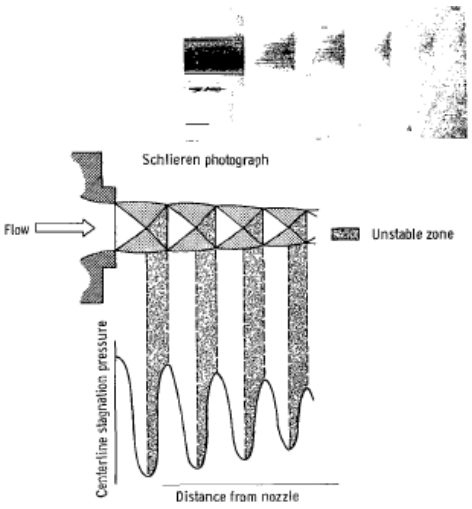

Figure 3. - Typical variation of stagnation pressure in an underexpanded choked jet.

Figure 3.4: Stable and unstable zones in the flow of an under-expanded choked jet, Source: [56]

In a perfectly expanded system, the exit pressure of a nozzle or orifice matches the ambient pressure of the region it flows into. If the gas exits the device at a lower pressure than the ambient region, it is said to be over-expanded. If the gas exits at a higher pressure than the ambient region it forms an under-expanded jet. The gas in this under-expanded jet will undergo an isentropic expansion after the exit until it eventually reaches equilibrium pressure with the surrounding ambient gas. The exact shape and characteristics of the under-expanded jet are defined by the pressure ratio between the gas at the exit of the nozzle and the ambient gas. However all under-expanded jets consist of a core region and a mixing region. The core region is dominated by compressible effects and is composed of isentropic expansion and compression regions and shock cells, with regions of supersonic and subsonic mach flow. This is surrounded by the mixing region where the flow is subsonic and mixes with the outer fluid region. These regions are separated by a sonic boundary, as depicted in Figure 3.5 [28, p.11]. In the core region of expansion and contraction exist the zones of stability and instability, as depicted in Figure 3.4. The exact location of these zones is very important to the functionality of the resonance ignition system. The gas dynamics that drive the process of resonance heating and the subsequent ignition and combustion, are rather complex. For

a full explanation one should review the Literature Study that accompanies this thesis and *Advanced Ignition Systems* [24]. A concise explanation of the steps in the gas dynamic process are described below and illustrated by Figure 3.6 [29, p.19]. ’

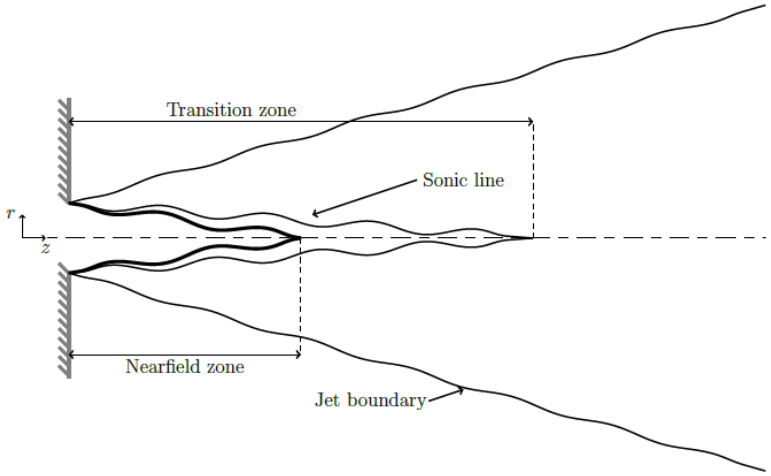

Figure 3.5: under-expanded Jet Main Parameters [28, p.11]

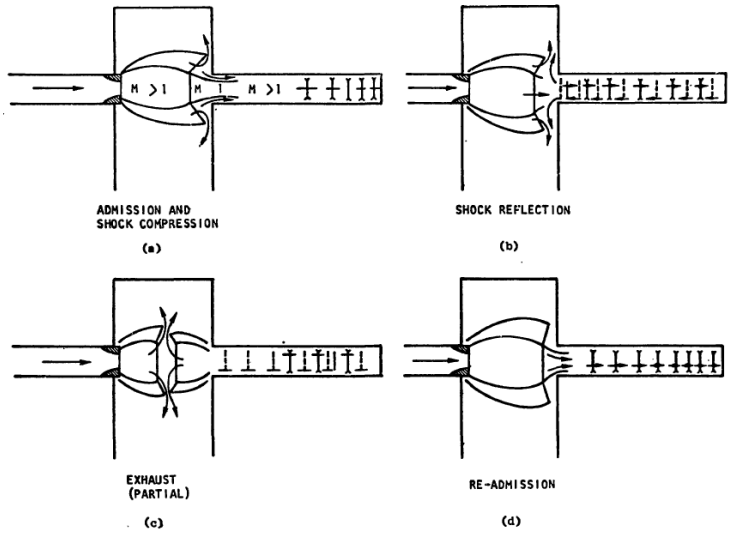

Figure 12. Resonance Heating Phenomenon

Figure 3.6: Resonance Heating Diagram [29, p.20]

Steps in Gas Dynamics of Resonance Tube Heating

1. **Admission and Shock Compression**: The injection nozzle shoots a jet of high pressure under-expanded gas into the resonance cavity. This creates a series of shocks in the tube which ”irreversibly compress a fraction of the gas volume [29, p.19].”
2. **Shock Reflection:** The shock waves reflect on the closed end of the cavity and the shock waves exit the tube towards the incoming jet.
3. **Exhaust (Partial)**: The incoming jet and the reflected shock impinge on each other in the region formed between the nozzle and cavity opening where the shock disks are present.
4. **Re-Admission**: As there is only a fixed amount of gas in the tube, as it empties out the pressure in the closed end of the tube drops. This allows the nozzle gas to be readmitted into the tube, thus repeating the process.

The shock wave irreversibilities in the resonance cavity and frictional losses cause the increase in pressure and temperature of the gases. Once this gas reaches the required temperature, which is above the auto-ignition temperature of the 2nd propellant, that 2nd propellant is injected, and combustion begins in the resonance cavity. A mixing cavity exists to provide the additional space required to achieve a more complete combustion of the propellants [29, p.22]. In order to create the environment in which the gas dynamics can occur to heat the injected gases, the geometry and location of the resonance cavity must be compatible with the NPR (Nozzle Pressure Ratio) of the injection nozzle. As stated, the exact shape of the under-expanded jet is dependent on the injection nozzle NPR. In addition in order for the resonance cavity to achieve heating of the injected gases, the opening of the cavity must be large enough to intake the core of the exhaust jet.

In Figure 3.7a-Figure 3.8 the structure of a moderately (1.1≤ η_e ≥2, 2≤ η_o ≥4), highly (2≤ η_e ≥4, 4-5≤ η_o ≥7) and very highly under-expanded (η_e ≥3-4, η_o ≥7) jet are shown, as well as the approximate location of these stability zones, relative to the exhaust jet structure [28, p.14]. NPR is a ratio of the nozzle injection pressure and ambient pressure at the exit. These figures show that as the NPR increases and the jet becomes more under-expanded, the shape and location of these shock cells change. For lower NPR the shock cells create a pattern of diamond machs with a narrow core diameter that is close to the device exit diameter. As the NPR increases, the diameter of the jet increases and the shock cell develops a rounder, more barrel like shape and ends with a more vertical normal shock called a mach disk. The length between the beginning of the exhaust and the mach disk increases as well. For the very highly under-expanded jet, these changes are even more pronounced with a longer mach disk length and a more defined vertical mach at the end of the first shock cell. Therefore when designing the resonance ignition system, it is important to consider the shape of the under-expanded jet as it relates to the chosen NPR. This is important in the design of the shape and location of the resonance cavity.

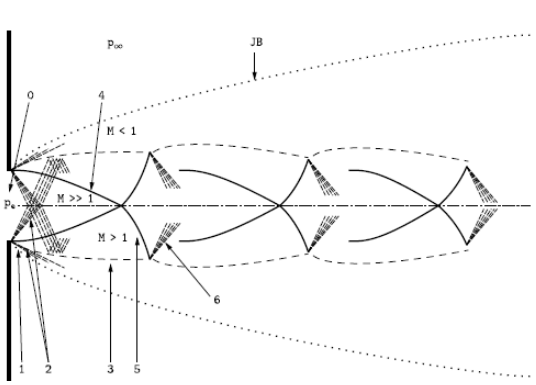

(a) Structure of a Moderately Under-expanded Jet (1.1≤ η_e ≥2, 2≤ η_o ≥4

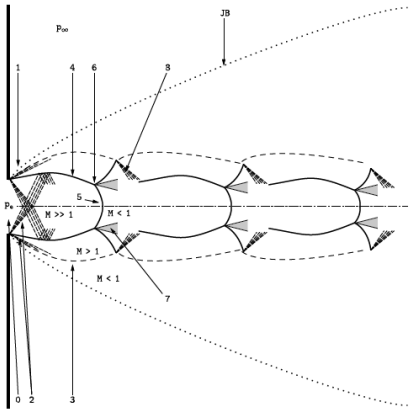

(b) Structure of a Highly Under-expanded Jet (2≤ η_e ≥4, 4-5≤ η_o ≥7)

Figure 3.7: Structure of Moderately and Highly Under-Expanded Jets

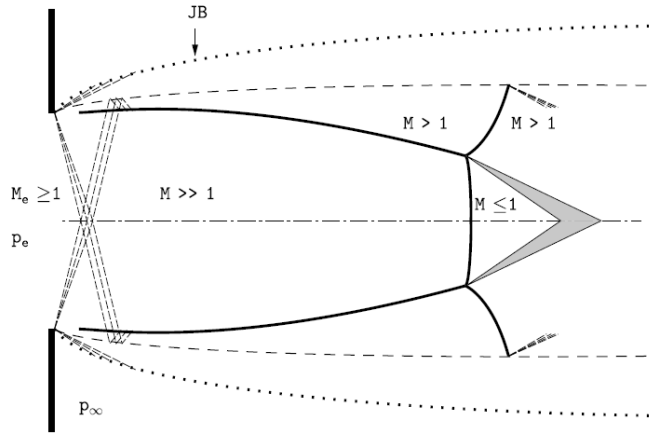

Figure 3.8: Structure of a Very Highly Under-expanded Jet (η_e ≥ 3-4, η_o ≥ 7) [28, p.44]

3.4. Conclusion

Resonance ignition is promising because of its high reliability, precision, reusability, simplicity and safety. This chapter presents the research gathered on state-of-the-art resonance ignition systems in order to provide an overview of the major system parameters. The purpose of this section is to organize those sources and present them in a clear and logical manner. This chapter has been kept concise for the thesis, but more information on resonance systems can be read in the accompanying literature study [24]. Using this information and sources cited, a list of the major design parameters can be generated and the design requirements and design process developed. These design parameters, requirements and process are covered in the subsequent chapters.

4

Preliminary Design Requirements

In this chapter a set of requirements are defined in order to complete the preliminary design of the resonance ignition system. This is being designed for operation on the DARE Blizzard Engine, which drives some of these requirements. Detailed information and discussion on the requirements of this engine can be found in the literature study and engine documentation. An excerpt of important information is contained in Appendix A. When developing the preliminary design requirements, it is important to utilize system engineering tools to guide the process. The lecture slides from the TU Delft Systems Engineering course [30] and the corresponding reading materials, such as the *International Council on Systems Engineering Handbook* [3] were used to create a systems engineering architecture for this project. In the beginning of a project it is important to define a preliminary set of requirements because if this is done too late it can become very difficult or even impossible to make the changes required to meet these requirements. Developing a requirements list is an iterative process that involves many factors, including evaluating constraints, defining performance parameters, and performing trade-offs, to name a few [3, p.130]. The *Systems Engineering Fundamentals* handbook by the US Department of Defense, states that for a requirement to be good it must have the qualities of being *Achievable, Verifiable, Clear, Complete, and Consistent* [55, p.36]. The INCOSE handbook was also consulted to help generate a clear list of requirements. These include functional, performance and design requirements. Functional, or operation, requirements define the tasks that the system must complete. Performance requirements set the performance parameters that the system must meet, and design requirements set rules on how to design and manufacture the system, to ensure it meets its capabilities. In order to properly define the design requirements, the major system parameters must be defined. Therefore in this chapter these system parameters and operational requirements are explained and result in a set of preliminary design requirements.

4.1. Major Design Parameters

After completing the baseline research on resonance ignition systems for the Literature Study, a more thorough and structured approach was taken for the thesis. This began with compiling a list of the major design parameters of these systems and determining how to set each parameter in the most accurate way. This list of parameters was compiled from resources on general ignition and resonance ignition. The general ignition resources were used in the calculation of the ignition power requirements, propellant mass flow rates, orifice sizing, and nozzle geometry and were derived from works by Sutton [61], Huzel and Huang [39], Zandbergen [66], Akkermans [9], Repas [58], Lawver [43], and Coronado.

Parameters that focused on the gas dynamics, geometric calculations and procedures relating to resonance ignition were derived mainly from works by Bauer [10] [11], Brocher [16] [17] [13] [15][14], Guozhou [32], Chang [18], Hamed [34], Lungu [44] [45], Marchan [48], Marchese [49], Phillips [56] [57], Hartmann [35], Stabinsky [60], among others. Upon reviewing all of these works, a table of the most important and reoccurring parameters was established and are listed in Table 4.1. This should not be taken to be an exhaustive list of parameters, but rather a concise list that provides a path towards a focused design process.

The following tables list the many design parameters that factor into the design of a resonance

ignition system. The parameters are listed in the following table and then explained further on. The corresponding python code is referenced when used. This is meant to provide a clear guide of the design process and decisions. While this thesis does not include calculations of the ignition timing, the related parameters are included in the table as they are important and need to be investigated in future work.

Table 4.1: Resonance Ignition Device Propellant and Combustion Design Parameters

Parameter	Unit	Description
R. Gas		Resonance Gas
Fuel		
P_{ign}	kW	Minimum Required Ignition Power
$\dot{m}_o$	kg/s	Oxidizer Mass Flow Rate
$\dot{m}_f$	kg/s	Fuel Mass Flow Rate
ϵ		Combustion Equivalence Ratio
T_c	K	Combustion Temperature
P_c	Bar	Combustion Chamber Pressure
P_o	Bar	Oxidizer Injection Pressure
P_f	Bar	Fuel Injection Pressure
NPR		P_o/P_{atm} Nozzle Pressure Ratio
δt_{res}	s	Resonance Gas injection time
δt_{burn}	s	Time from fuel injection to end of burn
T_{res}	K	Temperature at Base of Resonance Tube

Table 4.2: Resonance Ignition Device Geometric Design Parameters

Parameter	Unit	Description
D_n	mm	Gas Injection Nozzle Exit diameter
D_{res}	mm	Resonance Tube Inlet diameter
d_e	mm	Resonance Tube end diameter
β	Degree	Injection Nozzle Convergent Angle
D_{res}/D_n		Ratio Res. Tube inlet D/Nozzle Outlet D
Δ S	mm	Gap Distance
L_{res}	mm	Resonance Tube Length
t_w	mm	Resonance Tube wall thickness
Shape		Resonance Tube Shape
Material		Resonance Tube Material

4.2. Operational Requirements

Before proceeding with the preliminary design process of the igniter, it is important to take into consideration igniter operations that will have a direct effect on the design decisions. In this section, a few key aspects of igniter operations are explained relating to pressure settings and purging. These guidelines in ignition operation are important to ensure proper functioning of the system and to avoid failures. The resulting preliminary design requirements from this section are included in Table 4.3. This thesis does not include physical testing of the system, in which these operational requirements would be necessary. However, as this thesis will be handed to members of the DARE team, it is important that they be made aware of these vital operational requirements. Therefore it was chosen to include this information in the thesis, to support future testing. These requirements were derived from researching ignition experiments as well as from my personal experience in propulsion testing at SpaceX, and consultation

with an industry professional.

4.2.1. Positive DP

Boyle's Law states that for a given mass of gas at a constant temperature, the multiplication of the pressure and volume of the gas are constant, $PV = c$ [12]. In practical terms, this explains why when two regions of different pressure are connected, gases will naturally move from regions of high pressure to regions of lower pressure: to equalize the pressure between the regions. This can be seen in weather patterns where warm, high pressure air rises to colder, lower pressure regions. This phenomenon is used broadly in aerospace applications to direct the movements of propellant gases in feedsystems. A good example is the propellant blow-down systems, which accomplishes moving propellants from the storage tanks to the combustion chamber with no pumps. It achieves this by storing the gases at high pressures, connecting the tanks to the lower pressure combustion chamber and allowing the gas to freely move from the high pressure tanks to the low pressure combustion chamber, as the gases work to achieve pressure equilibrium between the regions. When designing gaseous systems, it is necessary to consider the movement of gases due to pressure differentials. Gas will always flow from regions of higher to lower pressure. Thus in order to design for predictable gas movement, it is necessary to maintain a positive difference in pressure across regions, or positive differential pressure (DP). In rocket engines, the pressures of the systems must cascade down the feedsystem, from high to low pressure, to ensure that the gases flow in the proper direction. If the feedsystem does not maintain this positive DP in the correct direction, the gases will flow backwards in the system, or "back-flow." LREs must always maintain a positive DP between the propellant injectors and the combustion chamber, and between the ignition system and the combustion chamber. If the nearly 3000K combustion chamber gases were to back-flow from the combustion chamber into either of these areas, the components would melt and/or massive explosions of the propellant in these systems could occur. These failure modes would cripple the engine and potentially lead to a loss of vehicle. Therefore it is vital that this positive DP relationship is maintained.

4.2.2. Purging

Once the igniter achieves complete and self-sustaining combustion of the main engine propellants, it is no longer needed. At this point, the igniter must deploy methods to prevent back-flow and protect its components from the high temperature, 3000K, combustion chamber gases. If gas from the combustion chamber were to flow back into the igniter, it can cause the components to melt or even cause explosions in the propellant feed lines. As discussed in the previous section, in order to prevent back-flow in systems, a positive DP must be maintained for the duration of operation. There are various strategies that are used to achieve this and protect ignition systems. These include continuing to operate the igniter for the full duration of the main engine burn, purging through the igniter chamber with high pressure fluids, or using check valves in hypergolic ignition systems.

In systems that choose to continue to operate the igniter for the duration of the main engine burn, the pressure of the ignition combustion must be greater than the pressure of the main engine combustion, else the main engine combustion gases would flow from the high pressure main engine combustion chamber back into the lower pressure ignition combustion chamber. This is possible in engines that have relatively low main engine combustion pressure. However the drawbacks to this option are that while it is efficient to burn a portion of the propellants in the igniter during the main burn, the higher pressure and increased time of combustion in the igniter would require much more robust components. This can lead to much heavier parts and decreases the lifetime and reliability of the igniter parts. Due to these reasons, this is not the solution chosen for this case.

The other option to protect the igniter during the main engine burn is to purge the ignition system with a high pressure fluid for the duration of the main engine combustion. In this case the pressure of that purge fluid is kept higher than the main engine combustion pressure, in order to prevent back-flow. NASA's spark-torch igniter, designed by George Repas, utilizes this method of operation. The igniter chamber pressure is set to 135 psig during its igniter combustion. The main engines that use this igniter have combustion chamber pressures that far exceed the igniter chamber pressure, such as the Rs25 which has a chamber pressure of 2994 psig. Therefore, once ignition is detected in the main engine combustion chamber, the spark-torch igniter ceases combustion and switches to purging with an inert gas (HE or N2) that is set to 60 psig above the combustion chamber pressure of the main engine. This purge continues for the entire main engine burn and prevents the back flow of the hot combustion

chamber gases into the ignition system [58]. This option of purging with a high pressure fluid through the ignition system for the duration of the main engine burn will be used in this design.

The choice of purging fluid is dependant on the size and needs of the system. Ignition systems can either use their fuel supply or a separate supply of an inert gas, such as Helium or Nitrogen, to purge the system. In systems where the mass flow rate of the ignition fluids is minor compared to the main engine propellants, using inert gases is a reasonable option, as their inerting affects will be negligible. This is why the Repas spark-torch igniter can use inert gases for purging, as they are used on such massive engines. However in our case the mass flow rate of our ignition system is relatively high compared to the main engine, and expelling inert gases for the duration of the main engine burn can have significant inerting affects on the main engine combustion. The other option is to set the igniter propellants to a higher pressure than the main engine combustion pressure and use one of the propellants to purge the ignition system during the main engine burn. The industry standard is to use the fuel for purging, as opposed to the oxidizer, as oxidizers are must more reactive and corrosive than fuels, and can cause damage in the system. The highly reactive nature of oxidizers means that if it is used to purge the system, there is a risk of the oxidizer igniting and causing an explosion that travels along the oxidizer feedsystem to the propellant tank, leading to a massive explosion. There is also the danger of the oxidizer igniting inside of the ignition system and melting the components. In addition to being safer and less corrosive than oxidizers, fuel is preferred due to its cooling capabilities, which extends the lifetime of system components. This is why most combustion reactions, including our igniter combustion, run fuel rich in order to achieve a cooler combustion.

As a positive DP is required, the pressure of the purge fuel must be set to higher than the main engine combustion pressure, taking into account any pressure losses across the fuel injector and ignition system orifice, to prevent back-flow. It is recommended that the pressure difference between the purge gases and the main engine chamber pressure be kept at about 60 psig (4 bar), as seen in the Repas Spark-torch ignition system [58]. As the Blizzard engine does not include any propellant pumps, a solution to maintain this pressure difference is to supply the igniter fuel line directly from the main engine fuel tank. This will ensure that the fuel supply pressure is sufficiently higher than the main engine combustion pressure. The Blizzard engine uses a blow-down pressurization system, thus the pressure will trend down, but if both the main engine and igniter fuel are supplied by the same source, the positive DP during the main engine burn can be maintained. It is recommended to install pressure sensors across the system during testing to ensure that these positive DPs are maintained during operation.

Finally, this ignition system is relatively large compared to the main engine and fuel will be injected for the duration of the main engine burn. Therefore it is necessary to take into account the mass flow rate of the injected igniter fuel into the total main engine mixture ratio. The main engine fuel injector holes must be sized, taking into account the injector fuel supply, such that the designed main engine mixture ratio is achieved.

4.3. Preliminary Design Requirements

Based upon these operational requirements and major design parameters, and after consultation with the system engineering documents, a list of requirements was developed [47]. These requirements are not meant to be quantitative at this stage. Their purpose is to provide guidance for the calculations performed in the preliminary design. During the preliminary design the values for all of the parameters given in Table 4.1 and Table 4.2 are calculated based upon the requirements described in Table 4.3. Information on the Blizzard Main Engine can be found in Appendix A. It is recommended that the reader review this appendix to see how the main engine affects a selection on the requirements. Table 4.3 lists the preliminary design requirements of the ignition system.

4.4. Conclusion

In this chapter, the main design parameters of resonance ignition systems and operational requirements were discussed, in order to generate the preliminary design requirements. This set of requirements is used in the development of the preliminary design python script and guides the entire design process. In the next chapter an explanation of the design process used in the preliminary and detailed design is presented.

Table 4.3: Preliminary Design Requirements

ID	Category	Requirement
1	Power (P_{ign})	The power requirement of the ignition system will be set based upon the amount of power required to vaporize and achieve stable ignition of the main engine propellants. A percentage of the main engine propellant flow necessary to ignite will be set, as well as a safety factor. The minimum ignition system power requirement will then be set.
2	Mass Flow ($\dot{m}$), Mixture ratio (O/F) & Combustion Temperature (T_c)	Based upon the P_{ign}, the ignition system propellant mass flow rates, and combustion temperature must be set. These 3 values are all dependant on one another. Once T_c is set, O/F can be determined based on the propellants.
3	Temperature (T_{res})	The temperature achieved at the base of the resonance cavity must be sufficient to vaporize the liquid ethanol and heat it to above the auto-ignition temperature, 700K.
4	Geometry	The geometry of the nozzle, cavity and gap distance must be set to allow for the gas dynamic heating phenomenon to occur.
5	Pressure (NPR)	The NPR of the gas injection nozzle must be high enough to produce an under-expanded jet.
6	Pressure (P_c, P_f, P_o)	The pressure of the ignition propellants and the ignition combustion pressure must be set to prevent back-flow. A positive DP must exist between the ignition system and the main engine combustion chamber during the entire engine operation.
7	Purging	The ignition system must purge with fuel during the duration of the main engine combustion. A positive DP must be maintained for the duration of the purging and the main engine mixture ratio must take this fuel mass flow into account.
8	Reusability	The ignition system must be able to be fired a specified number of times, consecutively, before need to approach the system. Must be able to be used for multiple test campaigns.
9	Robustness	The ignition system must be robust enough to survive the combustion gases. Materials chosen must be able to survive T_c as well as the corrosive nature of these propellants.
10	Reliability	High reliability in igniting engine and a system to shut off engine in case ignition is not achieved. This is given as a recommendation but not implemented.
11	Safety	Ignition system must meet the safety regulations dictated by Dutch law and within the allowable limits of the student team, DARE. This includes toxicity levels, classifications of propellants and explosives used, and PPE required.

5

Design Methodologies

The following chapters provide a guided explanation of the design of the resonance ignition system. The design of this system was divided into two sections, the preliminary design phase, and the testing and detailed design phase. In this chapter, the design methodologies utilized in each of the design phases is explained. These methodologies include the resources consulted, design procedures followed, and tools utilized.

5.1. Preliminary Design

The preliminary design phase began with reviewing the requirements and reading through many research papers on design of resonance ignition systems, in order to generate a list of major design parameters. This list of parameters was used to guide the preliminary design process. Through various scientific articles, papers and textbooks on related topics–including ignition, resonance ignition, Hartmann-Sprenger tubes and under-expanded compressible flow–a set of empirical equations and design rules were compiled to calculate these design parameters. Using the list of parameters and review of designs of similar ignition systems, an outline of the design plan was created. This design plan detailed the equations used for calculations, resources used to support the calculations performed and the order of the calculations. The design plan was then overlaid with a python script that performed the set of calculations required for each section. Below I briefly describe each section of the preliminary design process, explaining the calculations performed and the corresponding set of code. The next few chapters of this paper then provide detailed information on the design assumptions and theory behind all of the calculations performed and choices made as a part of the preliminary design process.

The preliminary design begins with calculating the igniter power requirements. This is the minimum amount of power the igniter must supply in order to ignite a specified percentage of the main engine propellants and is engine specific. As stated earlier, this system is being designed for use on the DARE CRYO Blizzard engine, and therefore this engine will set the ignition power requirements. Once the power requirement is calculated, the igniter propellant combustion temperature and mixture ratio are calculated based on propellant flammability limit. Then the material choices for the igniter injection nozzle, resonance cavity and combustion chamber are chosen based on the combustion temperature and material properties. After this the operating pressures, mass flow rates and geometries of the exhaust, injection nozzle and resonance cavity can be calculated. Next, the total exhaust parameters are calculated. The total mass flow rate of the igniter exhaust is calculated using the relationship between power, enthalpy and mass flow rate. Then the oxidizer and fuel mass flow rates are determined based on this total mass flow rate and the predetermined mixture ratio. Then the geometry of the exhaust orifice as a function of the combustion pressure is calculated and tabulated. After that, the geometric and pressure parameters of the GOX injection nozzle and resonance cavity are calculated. These calculations rely on equations of compressible, under-expanded flow from converging nozzles. These equations provide a relationship between the gaseous oxygen injection pressure, temperature, mass flow rate and nozzle exit area. The pressures in the system–injection, combustion, and purging pressure–are set based on maintaining choked flow in the GOX injection nozzle, and a positive glsDP across the system for the duration of operation. Then an iterative process is used to choose a combination of the injection

pressure and exit diameters of the injection nozzle and igniter exhaust, such that the system operates at a manageable pressure and mass flow rate, and has exit geometries that can fit in the current main engine manifold and are easy to manufacture. Estimations of the gap distance and opening diameter of the resonance tube are made based on empirical calculations of the exhaust jet of the injection nozzle and a review of similar systems. Finally, the geometry of the fuel injector is calculated based on the calculated mass flow rate and pressure requirements. The resulting system is then summarized in the preliminary design results.

Python Code Sections

This code is comprised of a *Main.py* file and a number of supporting custom functions. In Figure 5.1, a flow chart is displayed which details which python functions are used in each section of the main code. This is followed by a short summary of each section of the code, with the subject of each part in bold, and the name of the corresponding python script(s) in italics. The complete python script and output file can be read in Appendix B. In the appendix, the functions listed below are included in order with the name of each function written on the top of the first page of that function.

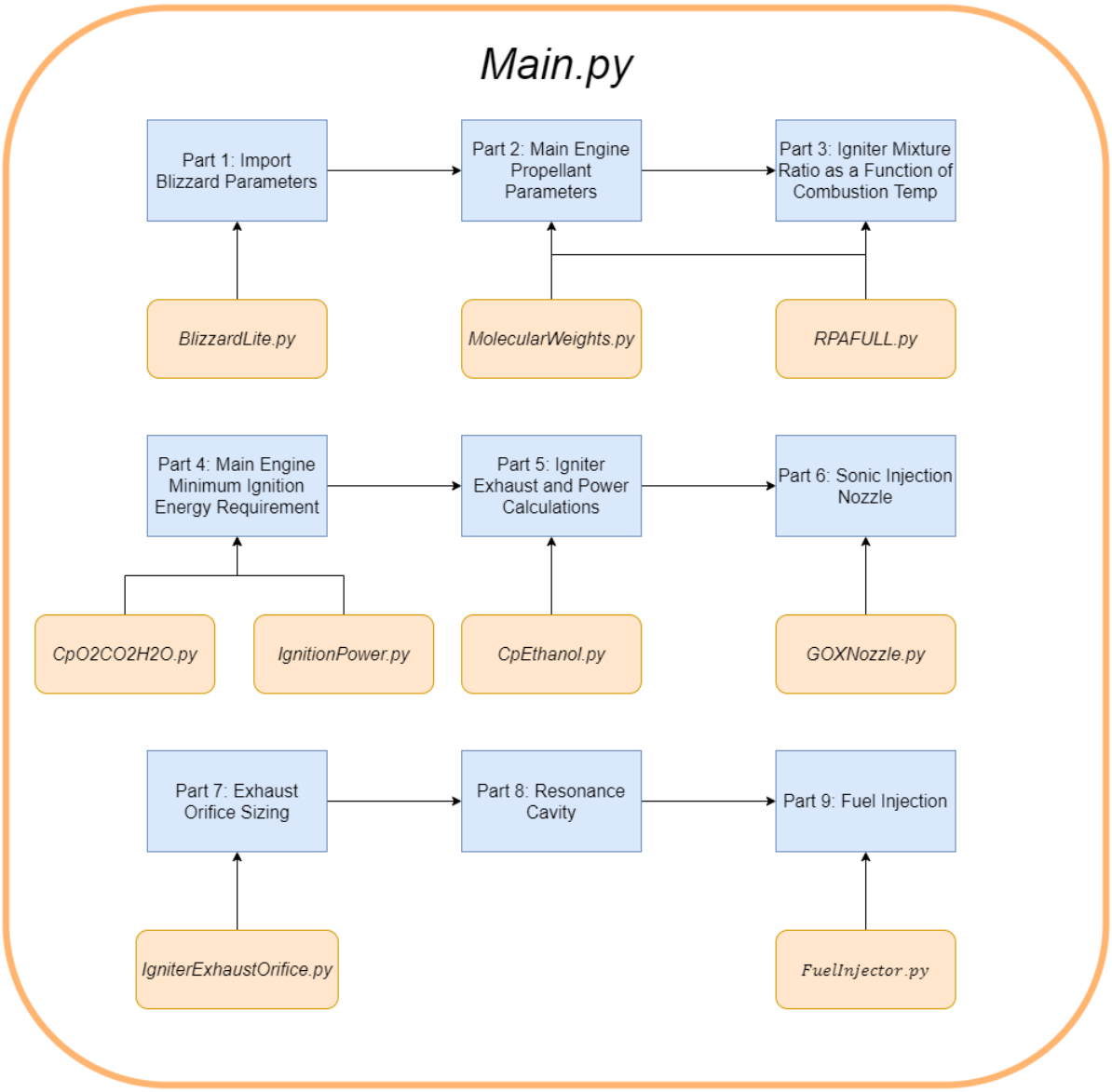

Figure 5.1: Flow Chart of Python Code

Main Python File: $Main.py$

Part 1: Import Blizzard Parameters $BlizzardLite.py$
Imports main engine parameters.

Part 2: Main Engine Propellant Parameters $MolecularWeights.py$
Calculate the stoichiometric Mixture Ratio for the main engine propellants, weighted molar mass and density of the fuel (as it is a mixture 85% Ethanol 15% Water), and equivalence ratio of the main engine propellants.

Part 3: Igniter Mixture Ratio as a Function of Combustion Temp. $RPAFULL.py$, $MolecularWeights.py$
Create a plot of the combustion temperature as a function of the propellant mixture ratio for the igniter combustion, using glsRPA. Choose a mixture ratio and corresponding combustion temperature, based on research. Create a chemical balance equation for the chosen propellant mixture ratio of the igniter.

Part 4: Main Engine Minimum Ignition Energy Requirement $CpO2CO2H2O$, $IgnitionPower.py$
Calculate the total power required to raise a chosen percentage of the main engine propellants to the ignition temp. To do so, calculate how much power is required to raise the propellants from their injection temp to the auto-ignition temp of ethanol as well as the amount of power required to change the phase of the propellants from liquid to vapor. Must calculate the specific heat at constant pressure values over the temperature range, as they are a function of temperature, and use the results to calculate the change in enthalpy of the propellants. Choose a percentage of the main engine propellant flow to ignite and calculate the power required.

Part 5: Igniter Exhaust and Power Calculations $CpEthanol.py$
Using a simple orifice for the igniter exhaust, calculate the total change in enthalpy achieved by the given Tc (which is a function of the selected OF). Use this to calculate the total mass flow rate of the igniter exhaust, given the required power and the change in enthalpy. Additionally calculate the weighted mass, specific heat ratio of the exhaust products.

Part 6: Sonic Injection Nozzle $GOXNozzle.py$
Calculate the pressures and geometries required to achieve choked flow in the GOX sonic injection nozzle during the igniter heating and combustion phases of operation. The GOX sonic nozzle must maintain choked flow during this time, to prevent back-flow of hot ignition combustion gases up the GOX line, which could cause an explosion. A range of GOX nozzle areas was chosen based on comparable systems.

Part 7: Exhaust Orifice Sizing $IgniterExhaustOrifice.py$ Calculate the size of the exhaust orifice, based on the allowable pressure drop across it.

Part 8: Resonance Cavity $Main.py$
Geometric parameters of the resonance cavity, including the opening diameter size, cavity shape, length, and angle.

Part 9: Fuel Injection $FuelInjector.py$
Calculations on the sizing of the fuel injection holes needed to achieve the required fuel mass flow rate and necessary atomization of a liquid fuel.

The preliminary design of the system using empirical calculations in the python script, result in a preliminary design of the injection nozzle and resonance cavity. This output file can be viewed in APPENDIX PYTHON.

5.2. Testing and Detailed Design: ANSYS Fluent Simulations

After completing the preliminary design, the next step in the design process is the detailed design phase. Due to the inherent uncertainties of ignition systems, it is important to include testing as part of the detailed design phase. This can be accomplished with physical experimentation or numerical simulation. The choice of whether to perform physical or numerical testing, is dependant on a number of factors, including budget, time, complexity of the test setup and accessibility of testing facilities. Most

projects choose to do a combination of physical and numerical testing, the ratio of these dependant on the needs and constraints. Due the logistical challenges poised by Covid-19, the decision was made to use numerical simulations to complete the testing portion of the design in order to obtain the detailed design. The purpose of the numerical simulations is two-fold, First, to test the preliminary design under the expected operating conditions to see if it performs as expected. Second, to provide results that contribute towards completing the detailed design of the system. This will be accomplished by performing numerical simulations of an under-expanded jet from a converging nozzle and of an under-expanded jet of a converging nozzle directed into a resonance cavity.

This preliminary design is tested using glsANSYS Fluent and the results of the simulation are used to create the detailed design. In lieu of performing physical calculations, ANSYS Fluent is used to test the design with a numerical simulation. ANSYS Fluent simulates the gas dynamics of the sonic injection nozzle and the resonance cavity. A steady state model was used to determine the geometries of under-expanded jet flow from a nozzle, as this is difficult to calculate empirically. This serves to test the preliminary geometric design of the system, with regards to the gap distance and resonance cavity opening diameter. Then both steady and transient solutions are used to model the resonance heating effect in the cavity. These resonance cavity numerical simulations were designed based on the works of Murugappan [50], Afzali and Karimi [6], and Khoshkbijari and Karimi [42] who first performed such simulations and then physically tested these systems. Their experiment with both their simulations and physical testing demonstrated provided quite the accuracy of these types of simulations, thereby, making them a valuable resource. These simulations serve to test the preliminary design and are used to generate the detailed design of the system.

5.3. Conclusion

As the preliminary design of the ignition system is extensive, it has been divided into three chapters for clarity. In the subsequent 3 chapters the theory and equations used to develop the custom-made Python script are detailed. chapter 6 covers the power, sizing, material choices, and mass flow rate calculations for the ignition system. chapter 7 explains the calculations of the injection nozzle geometry and pressures. Finally, chapter 8 details the design of the resonance cavity, exhaust orifice and fuel injector elements.

In chapter 6 the main engine is set, so the calculation of these parameters is straight forward and does not require trade-offs. However the calculations performed in chapter 7 and chapter 8, require an iterative process, with trade-offs throughout. These geometric and pressure parameters not only take into account performance requirements, but must consider design limitations on space and manufacturing capabilities. Every section explains the theory and equations used to calculated each parameters and ends with a table summarizing the results. The preliminary design ends with a trade-off to choose a final preliminary design to use in the numerical simulations.

6

Preliminary Design: Power, Sizing and Mass Flow Rates

In this chapter the preliminary design of the power, sizing and mass flow rates of the ignition system are calculated. The theory behind the equations used is provided and the calculations can be viewed in the python code in Appendix B. In this chapter, the percentage of the main engine propellant that must be ignited to achieve full combustion is determined, followed by the amount of power that the igniter must generate to achieve this. Information on the process of ignition and the ignition systems of other engines is provided. Once the power is determined, the allowable igniter combustion temperature and propellant mixture ratio can be set based on material thermal limits and propellant flammability limits. The placement of this system on the engine manifold must be considered, as space limitations can effect the sizing of the injection holes. Finally the mass flow rates of the propellants can be calculated be evaluating all of this information.

6.1. Ignition Power

The preliminary design begins with the calculation of the power requirements of the ignition system, which is a function of the main engine propellant properties and mass flow rates. Once the power requirement is established the ignition propellant mixture ratio can be determined, based upon the propellant flammability limits and the thermal limits of the system materials. This ignition system is designed for use on the Dare Cryo Blizzard Lite Engine [63] [23]. The ignition system is required to provide enough power to achieve a stable and self-sustaining combustion of the main engine propellants. Based on extensive research, there are no set rules on how to establish the power requirements of an ignition device. Rather, most system designers seem to make an educated estimation of the power requirements and then use testing to refine the power output of the ignition system, based on its performance.

Therefore the strategy for setting the power requirement of the ignition system is accomplished by making an educated, conservative guess based upon comparison with existing sets of LREs and their ignition systems. This is similar to the method described in another TU Delft thesis *Ignition modeling in methane-oxygen rocket engines* by C. Akkermans [9, p.18]. In Westbrook's paper on the chemistry of Ignition, he establishes that in chemical reactions there are four main types–initiation, propagation, branching and termination. In initiation, stable species react to form radicals, the amount of which are kept constant by chain-propagation reactions. Chain-branching reactions result in an increased number of radicals and are the key to ignition and creation of stable combustion. Chain termination is the opposite of branching, for it reduces the number of radicals as they recombine to reform stable species [62, p.1564]. For aerospace engine ignition, the most important chain-branching reaction is when one Hydrogen atom reacts with an Oxygen molecule O_2, creating 2 radicals, $H + O_2 \rightarrow O + OH$. These Hydrogen atoms come from the fuel source and these reactions require a high activation energy to take place [62, p.1564]. In Paul Ronney's paper, "Laser versus conventional ignition of flames," he gives a detailed explanation of the two types of ignition: deflagration and detonation. These two types of ignition are differentiated based on the type of flame propagation. In deflagration, the flame moves

at a subsonic rate and therefore the energy spreads through they system by means of conduction where the pressure stays relatively constant. In detonations, the flame spreads at a supersonic rate with massive pressure increases caused by shock waves. In this case a deflagration style ignition will be utilized.

In deflagration, energy is added to a system of combustible material until a kernel forms. If the energy added is below E_f, then the energy will dissipate into the surrounding material until the kernel is extinguished and the ignition will be unsuccessful. If the energy added is above E_f, then the heat created inside the kernel is larger than the amount that is lost as the energy dissipates into the surrounding material. The kernel survives and begins to consume the combustion material around it, thus creating a self-sustaining flame. Flame propagation distance as a function of temperature provides a quantifiable value of the success of an ignition, as depicted in Figure 6.1. In order to characterize the ignition requirements for deflagrations, a minimum total energy or a minimum flame kernel radius must be identified [59, p.2]. The main takeaway from these works, is that it is not necessary for an igniter to provide power to ignite 100% of the propellant flow. Rather, if the igniter provides enough power to ignite a specified minimum threshold percentage of the main propellant flow, it will provide the power that will in-turn ignite another percentage of the propellant flow, and so on and so forth, until eventually the combustion propagates into the full propellant flow, through the process of deflagration. If the igniter provides too little power and ignites too small a percentage of the propellant flow, the combustion will not have the energy needed to propagate the combustion through the entire propellant flow, and instead the initial ignited propellant flow will die out and be 'drowned' by the rest of the propellant flow.

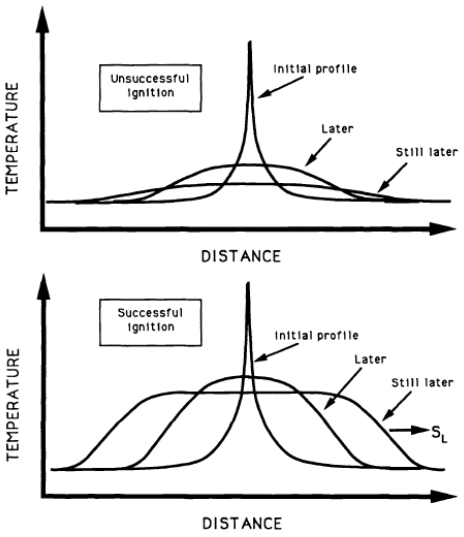

Fig. 2 Schematic diagrams of unsuccessful and successful ignition.

Figure 6.1: Successful and Unsuccessful Ignition, Source: [59]

An ignition's success is dependant upon if the amount of energy added to the system is above this *minimum ignition energy*, E_f. The minimum ignition energy of the system is product of the power and the ignition time. Ignition systems generally operate in the range of 1-2 seconds, with the exact timing determined through experimentation[61]. At this point it will be assumed that the ignition system operates for approximately that length of time, and this section will focus on calculating the minimum power requirement of the ignition system. There does not exist a simple equation that can be used to set this ignition power. Therefore, information on a selection of LREs and their companion ignition systems was reviewed, in order to establish a pattern for ignition power as a function of main engine power. This information is detailed in Figure 6.2, the table was compiled by Akkerman in his thesis work [9].

Engine			Igniter			Fraction	
Name	Propellants	Power [kW]	Type	Propellants	Power [kW]		
HYPROB			Spark-torch		64		[8]
Vinci	LOX/LCH4	35927	Catalytic	H2O2	440	0.0122	[21] [23]
Vinci	LOX/LCH4	35927	Spark-torch		440	0.0122	[10] [23]
LE-7	LOX/LH2	542584	Spark-torch	GOX/GH2	22971	0.00512	[51]
LE-7 Preburner	LOX/LH2	377158	Spark-torch	GOX/GH2	38000	0.101	[51]
LE-5	LOX/LH2	63516	Spark-torch	GOX/GH2	1320	0.0208	[51]
LE-5 Preburner	LOX/LH2		Spark-torch	GOX/GH2	120		[51]
SSME RS-25	LOX/LH2	1048191	Spark-torch	GOX/GH2	51529	0.0492	[51]

Table 3.3: Overview of reviewed rocket engines, their igniters, igniter output power, power required to heat the main combustion chamber propellant stream to autoignition temperature and the fraction of this power delivered by the igniter.

Figure 6.2: LRE engine and igniter powers from Akkermans Thesis [9, p.19]. Here 'Fraction' is analogous to mixture ratio.

It is important here to stress that there exists very little clear guidance on the proper power sizing of an ignition system. The overall consensus seems to be that it is highly variable and requires testing to confirm. However when creating a design it is necessary to establish a starting point. Therefore it is decided to review existing ignition systems and base the ignition power requirements on their systems. A conservative estimate will be used and it is advised that the team developing the engine perform testing on the igniter's capability to ignite the main engine over a range of igniter propellant mixture ratios and pressures. From Figure 6.2, the ratio of igniter power and main engine power is calculated, called the propellant fraction. The propellant fraction can be used to solve for the percentage of the main engine propellant flow that must be ignited by the igniter[61]. As all of these engines are proven, they provides a good estimate on how much power the igniter must provide, relative to the main engine, in order to ensure combustion. On average, these ignition systems provided 5% of the power of the main engine. A highly conservative safety factor of 2 is chosen, in order to take into account estimation errors, design assumptions, and manufacturing errors [9, p.19]. It is decided to set the power design requirement as such. Energy is power times time. The takeaway here is that the power requirement has been modified, stating that the ignition system must provide enough power to ignite 10% of the main engine propellant flow. This includes a safety factor of 2.

6.1.1. Calculating Ignition Power

In order to determine the power requirement of the igniter, it is necessary to examine the main engine propellants and calculate the amount of power required to ignite a specified percentage of the main propellant flow. The main design parameters of relevance of the Blizzard main engine are in Table A.1. More information on the Blizzard engine can be found in Appendix A. From Table A.1, it can be observed that the main engine oxidizer is 100% Liquid Oxygen and the fuel is Ethanol 85% + Water 15%. Ignition systems achieve combustion by raising a portion of the main propellant flow to its auto-ignition temperature, which is the temperature at which a substance will self-ignite. The power calculation begins by solving for the total amount of power required to raise 10% of the total flow of the main engine propellants from their injection temperature to the auto-ignition temperature of the fuel. This includes the amount of power required to change the phase of the propellants from liquid to vapor.

Table 6.1: Most Important Design Parameters of Blizzard V1 [23]

Parameter	Value	Unit
Fuel	Ethanol 85% + Water 15%	
Oxidizer	100% Liquid Oxygen	
Thrust (Nozzle)	2.6	kN
Chamber Pressure, Pc	20	bar
Combustion Temperature, Tc	3167	K
Engine Exit Velocity	2400.38	m/s
ISP	230.54	s
O/F	1.489	
Total Mass Flow	1.1	kg/s
Oxidizer Mass Flow	0.666	kg/s
Fuel Mass Flow	0.477	kg/s
Vandenkerchove Function	0.633	

In Table 6.3, the injection temperature of the main engine propellants in listed, the fuel is stored at 298K, however as the injector manifold will be cooled from the preflow of the liquid oxygen, for the power determination, to create a safety margin, the injection temperature of the fuel will be set to 200K. This table also lists the mass flow rates of 10% of the main engine propellants. An important factor to highlight is that the fuel in this engine is not pure Ethanol, but contains 15% water by mass. Therefore when calculating the power it is vital to remember to include the power required to vaporize and heat the water to the ethanol auto-ignition temperature. The water in the fuel does not contribute to the combustion, but requires a significant amount of power to heat. Therefore Table 6.3 divides the fuel mass flow rate into its components. The auto-ignition temperature and boiling temperature of the

ethanol, and the boiling temperature of liquid oxygen are also listed. These boiling temperatures are below the auto-ignition temperature, which necessitates their vaporization.

To calculate the mass flow rates of the ethanol and water components of the fuel, it is necessary to determine the chemical balance equation for the combustion. It is not so simple as splitting the fuel mass flow rate into 85% for ethanol and 15% for water, because they both have different molecular weights. Therefore in order to calculate the chemical balance equation, the percentage of ethanol and water in the fuel as well as weighted molecular masses are used in order to determine the proper coefficients for each of the molecules. The molecular weights of all of the elements in the chemical balance equation are listed in Table 6.2. The chemical balance equation for CRYO Blizzard engine with 85% Ethanol(l) 15% Water(l) as fuel, and 100% Liquid Oxygen oxidizer is detailed in Equation 6.1. The components on the left side of the arrow are referred to as the reactants and those on the right side of the arrow are the products. More detail on this can be found in the function *MolecularWeights.py*. The calculated mass flow rates of the fuel components are listed in Table 6.3.

$$1.0 * C_2H_5OH(l) + 0.4513 * H_2O(l) + 3.0 * O_2(l) \longrightarrow 2.0 * CO_2(g) + 3.4513 * H_2O(l) \tag{6.1}$$

Table 6.2: Molecular Weights, from Periodic Table

Element	Abbr.	Value	Unit
Carbon	C	12.011	g/mol
Hydrogen	H	1.008	g/mol
Oxygen	O	15.999	g/mol

Table 6.3: Main Engine Propellant Injection Temperature and Mass Flow Rate

Propellant	Parameter	Value	Unit
Fuel	Injection Temperature [23]	298 (200)	K
Fuel	Phase at Injection [23]	Liquid	
Oxidizer	Injection Temperature [23]	90	K
Oxidizer	Phase at Injection [23]	Liquid	
Ethanol	Auto-ignition Temperature [25]	763	K
Ethanol	Boiling Temperature	351.6	K
Liquid Oxygen	Boiling Temperature [4]	90.19	K
Oxidizer	10% of total mass flow rate [23]		kg/s
Fuel	10% of total fuel mass flow rate [23]		kg/s
Ethanol	Mass flow rate of ethanol in 10% of total fuel flow [23]		kg/s
Water	Mass flow rate of water in 10% of total fuel flow [23]		kg/s

The following equations used in the power calculations are listed and described below. The full calculations are contained in the python script, which can be viewed in Appendix B. The power requirement for phase change and change of temperature are calculated using Equation 6.2 and Equation 6.3. These contain two important values: **L, Latent Heat of Vaporization**, which is the amount of heat that must be added to change the phase of the element, and c_p**, Specific Heat at constant pressure**, which is the amount of heat that must be added to change the temperature of the element by $1°C$. The Latent Heat of Vaporization Values are listed in Table 6.4.

Equation for Raising the Temperature

$$Q = \dot{m} * c_p * \Delta T \tag{6.2}$$

Equation for Changing the Phase

$$Q = \dot{m} * L \tag{6.3}$$

where Q: power $[W]$, $\dot{m}$: mass flow rate $[kg/s]$, c_p: specific heat, at constant pressure, T: change of temperature $[K]$, L: latent heat of vaporization $[J/kg]$

Table 6.4: Latent Heat of Vaporization

Propellant	Value	Unit
Ethanol	854000	J/kg
Water	2256000	J/kg
Oxygen	214000	J/kg

The c_p, Specific Heat at constant pressure, values for ethanol, water, and liquid oxygen are temperature dependant. Therefore for each propellant, the value of the specific heat at each temperature from the injection temperature of the propellant to the ethanol auto-ignition temperature must be calculated. The summation of these c_p values known as the change in enthalpy, d_h, and the change in enthalpy is defined in Equation 6.4.

$$c_{=p} * \Delta T = \Delta H \tag{6.4}$$

The mathematical equation for calculating c_p as well as the relevant values for each propellant are taken from NIST, and the process can be reviewed fully in the code, see function *CpO2CO2H2O.py* [19]. The total power required to vaporize each propellant and raise it to the ignition temperature is described in Equation 6.5. The total power required is a sum of the mass flow multiplied by the sum of the enthalpy change and latent heat of vaporization, for each propellant. The ethanol fuel is separated into the water and ethanol in this equation.

$$\begin{aligned} Q = (\dot{m}_{eth} \cdot (\Delta H_{eth,sum} + L_{vap,eth})) + (\dot{m}_{water} \cdot (\Delta H_{water,sum} + L_{vap,water})) + \\ (\dot{m}_{ox} \cdot (\Delta H_{ox,sum} + L_{vap,ox})) \end{aligned} \tag{6.5}$$

Amount of power the igniter must provide in order to achieve ignition of 10% of the main engine prop flow is $Q = 152.1kW$

6.2. Igniter Combustion Temperature

The power of the igniter is a function of the total propellant mass flow rates and the enthalpy difference between the enthalpy at the combustion temperature, H_{ign} and the enthalpy at the autoignition temperature, H_{ref} [66, p.417]. Equation 6.6 states that for a constant power, there is an inverse relationship between the mass flow and enthalpy difference. This means that for a constant power, as the combustion temperature increases, the $Hign$ increases, causing the enthalpy change $H_{ign} - H_{ref}$ to increase, and the mass flow rate, $mign$ to decrease, and vice versa.

$$P_{ign} = m_{ign} * (H_{ign} - H_{ref}) \tag{6.6}$$

Equation 6.6 provides the means to calculate the total igniter mass flow rate for a given power and a chosen combustion temperature. In order to select the combustion temperature, a number of variables must be considered, including combustion flammability limits, material thermal compatibility, and igniter size.

6.2.1. GOX/Ethanol Flammability Limits

The first factor to consider is the flammability limits of the propellants. For every propellant combination there is a range of mixture ratios above and below which ignition will not occur, under a set of specific conditions. The exact range of ignitable glsmixture ratios, O/F, is dependant on numerous factors, most notably being the propellant injection pressures, propellant temperatures, and combustion chamber size. The mixture ratio is a fraction of the mass flow rate of the oxidizer propellant and the fuel propellant, $O/F = m_o/m_f$. For every propellant combination there exists a stoichiometric mixture ratio, where all of the reactants (propellants) are consumed and converted into the products (exhaust

gases)[61, p.163]. At this ratio there are no unburnt reactants (propellants) in the exhaust flow. The glsstoichiometric mixture ratio is the most mass efficient mixture ratio and results in the maximum combustion temperature for these propellants. However, most propulsion systems do not burn at the glsstoichiometric mixture ratio and instead a majority choose to burn fuel-rich. At a fuel-rich ratio, there is unburnt fuel molecules in the exhaust products and this is advantageous for numerous reasons. First, it results in a cooler combustion, which is necessary because most materials would not survive sustained exposure to the high stoichiometric combustion temperatures. Additionally, for certain fuels–such as Hydrogen which is extremely lightweight–having unburnt fuel molecules in the exhaust lowers the molecular mass of the exhaust products and leads to a higher specific impulse [61, p.163]. The other option to obtain a lower temperature combustion is to operate fuel-lean, in which there are unburn oxidizer molecules in the exhaust. This has been used in some applications, however because of the highly corrosive and reactive nature of oxidizers these systems often require a lot of maintenance and are careful handling. For this application, the specific impulse is not relevant but the combustion temperature is extremely important. If this combustion temperature is too high for the given materials, then the system will require active cooling capabilities, which greatly increases the system complexity. Therefore it is decided to operate this ignition system at a glsfuel-rich mixture ratio. In order to choose the mixture ratio, the flammability limits of the propellants must be determined. Then an analysis of material options for the system components will be conducted and a mixture ratio will be chosen that falls within the flammability limits and burns at an allowable combustion temperature. The following assumptions will be made when selecting the mixture ratio.

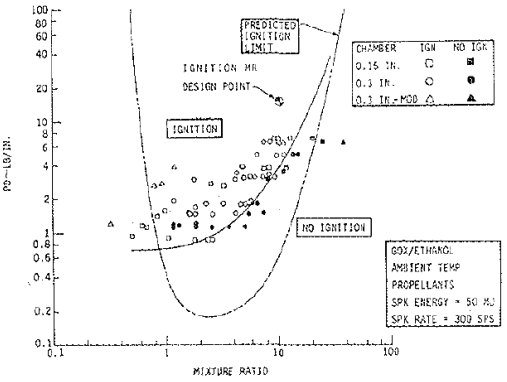

Figure 9. Effect of Cold Flow Pressure and Chamber Diameter on Ignition

Figure 6.3: GOX/Ethanol Flammability limits Mixture Ratio vs Cold Flow Pressure [43]

Assumptions:

- The mixture ratio will be fuel-rich.
- The Ethanol and GOX propellants are assumed to be at ambient temperature when injected.
- The combustion pressure, P_c will be less than 40 bar, in order to keep the required pressure in the oxygen, nitrogen and ethanol supply tanks at a safe and workable pressure.
- The fuel used in the igniter is 85% Ethanol and 15% Water, this will likely narrow the ignition flammability limits, as the water will absorb a portion of the energy required for ignition.

To establish a set of flammability limits, the research paper *Ignition Characterization of the GOX/Ethanol Propellant Combination* by Lawver from NASA Johnson Space Flight Center, and *Flammability limits: A review with emphasis on ethanol for aeronautical applications and description of the experimental procedure* by Coronado from the National Space Research Institut in Brazil were consulted [43]. In the glsNASA paper, an experimental study was conducted that defined the ignition characteristics of GOX/Ethanol propellant combinations in order to define ignition limits for the propellants as a function of mixture ratio, cold flow pressure, combustion chamber diameter and propellant temperatures [43]. After reviewing the results in this paper and using the assumptions stated above, an education choice on the acceptable range of mixture ratios for the GOX/Ethanol propellants was made, so as to have reasonable certainty that an ignition event would occur. The goal of this exercise was not to find the precise range of flammability, as that would be prohibitively difficult to do, but more-so to provide an educated guess of where one can be fairly confident that an ignition event will occur. The paper conducted two major sets of relevant experiments, which are surmised below.

Experiment Set 1: Pulse Mode Tests A spark torch GOX/Ethanol igniter was used to conduct 52 pulse mode tests with the following conditions.

- $O/F = 0.78$ to 3.29
- $P_o = 5.1$ to 13.58 bar

Table 5
Flammability limits in air and in oxygen [1,32].

Fuel	LFL (%)		UFL (%)	
	Air	O_2	Air	O_2
Hydrogen	4	4	74	94
Carbon monoxide	12	16	74	94
Ammonia	15	15	28	79
Methane	5	5	15	61
Propane	2	2	10	55
Ethane	3	3	12.5	66
Isobutene	1.8	1.8	8.4	48
Ethylene	2.7	2.9	36	80
Propylene	2	2	11	53
Coal gas	5.3	5.3	32	70

Figure 6.4: Flammability in air and oxygen of gases [21]

- Propellant temperatures $= -104^{\circ}C$ to ambient.

Experiment Set 2: Large O/F Range Tests A spark torch GOX/Ethanol igniter was used to conduct 205 hot fire tests with the following conditions.

- $O/F = 0.4$ to 40
- $P_o = 0.23$ to 3.4 bar
- Chamber diameter $=$ 3.8mm, 5mm, and 7.6mm.

The results of the experiments demonstrate that the igniter achieved ignition achieved and maintained a smooth and stable combustion over the entire range of conditions [43]. Figure 6.3 illustrates the predicted flame quench limits and plots the resulting flame limits from the experiments. From this figure it can be seen that ignition was only achieved between $O/F = 0.4$ to 20, and as the mixture ratio increased the minimum cold flow pressure required to achieve ignition increased. Based on these tests and considering the given assumptions, a range of acceptable mixture ratios is $O/F = 0.4$ to 3.3. To reaffirm this choice, the work of Coronado was also consulted, in which different gases were tested for flammability limits with air and oxygen. The results of these tests are in Figure 6.4. This research did not conduct testing of ethanol flammability in pure oxygen, but the gases used are similar to ethanol and provide a good approximation of the flammability limits of ethanol. Here we see that the flammability limits of Ethane are 3.3% to 66% by volume. This satisfies the chosen range of $O/F = 0.4$ to 3.3.

6.2.2. Mixture Ratios and Combustion Temperature

Now that a range of mixture ratios has been chosen that falls within the flammability limits, RPA and the custom python code (*RPAFUll.py*) are used to generate plots of the combustion temperature, T_c as a function of mixture ratio, O/F. The chosen combustion pressure, P_c, effects the combustion temperature and therefore a set of pressures, $P_c = 5$, 11, 20, 35 bar, were plotted to observe the relationship between combustion pressure and temperature. As RPA does not include the Ethanol85 fuel, a fuel file was created, the details of which are included in Appendix C. The code also calculates the stoichiometric chemical balance equation and the stoichiometric mixture ratio. This value is displayed on Figure 6.5 as a vertical grey line. The stoichiometric mixture ratio for GOX/Ethanol is, $O/F_s = 1.77$

As it has already been assumed that the combustion will be fuel-rich, one should focus on the values to the left of the grey, vertical stoichiometric line. Notably, in the range of mixture ratios from approximately $O/F = 0.6$ to 1.3 the combustion pressure has a negligible effect on the combustion temperature. This is ideal from a design standpoint, because it eliminates a pressure dependence for the combustion temperature which simplifies the design. From this, the potential mixture ratio can be narrowed to a value between $O/F = 0.6$ to 1.3. As can be seen from Figure 6.5, this range of mixture ratios result in a combustion temperature between approximately 1400-2800K. In order to choose an exact mixture ratio, it is necessary to review the properties of a selection of material for the system, and choose a mixture ratio that is thermal compatible with the chosen material.

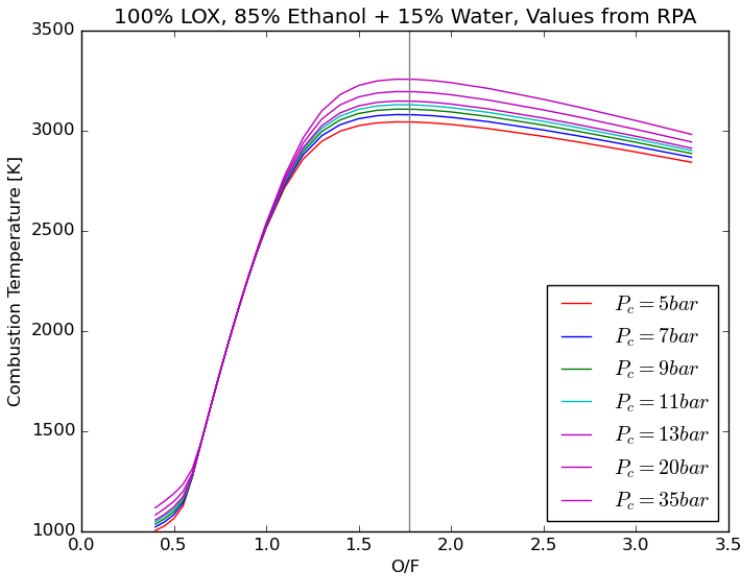

Figure 6.5: GOX/Ethanol85 O/F vs T_c over a range of P_c

6.2.3. Material Selection

There are three main components of the resonance igniter, whose operating conditions must be evaluated when choosing materials for manufacturing–gas injection nozzle, igniter body, and resonance cavity. While all three components have to deal with thermal loads, the resonance cavity has very specific needs and therefore will be reviewed first.

The role of the resonance tube is to provide a cavity which captures the compression of shock waves of the incoming sonic jet, so as to raise the pressure and temperature of the gas in the base of the cavity. Once this gas reaches the auto-ignition temperature of the fuel, the fuel is injected into the igniter chamber, mixes with the hot gases in the resonance cavity and ignites. There are many design factors that contribute to the success of a resonance tube, the material choice being a main factor. Based on evaluation of a selection of laboratory Hartmann-Sprenger tubes and resonance devices, 3 properties have been identified as crucial to the proper functioning of the cavity: low thermal conductivity, high structural strength and impermeability [56].

Low Thermal Conductivity: The material must have low thermal conductivity because the resonance gas needs to reach an extremely high temperature in a short period of time. If the thermal conductivity of the material is too high, then much of the heat generated by the gas dynamics will transfer from the gas into the walls of the cavity. If this occurs, the gas will be unable to reach the auto-ignition temperature. Therefore the ideal cavity material must have a low thermal conductivity, such that the majority of the heat generated by the gas dynamics remains in the gas.

High Structural Strength: The gas dynamics that occur inside of a resonance cavity cause rapid temperature and pressure increases, leading to thermal shocks, as well as high vibrations. This means that the resonance cavity material must have high structural strength so that it can survive this extreme environment. Materials like ceramics and asbestos, which are good insulators, would not be suitable for this cavity because they have low structural strength and would crack and crumble when exposed to these conditions [56].

Impermeability: For a resonance cavity to produce high temperature gases, the sonic jet must be able to form compression waves in the cavity. However, if the resonance cavity is made out of a porous material, it will absorb the compression waves and the gas dynamic phenomenon that causes resonance tube heating will be unable to occur. This is why a material like foamed zirconia, which has high strength and low thermal conductivity, but high porosity is unsuitable for this application [56].

Table 6.5 contains a set of possible materials, their thermal conductivity κ (assume at ambient temperature, unless otherwise stated) and their melting temperatures, T_m. This was compiled based upon a review of resonance cavity heating experiments as well as other types comparable of ignition systems. An important consideration is the length of time these materials will be exposed to the high temperature gases. Based on the review of a few different resonance ignition experiments, one can expect the gaseous oxidizer jet injection into the resonance cavity and the time it takes to heat up to the ethanol auto-ignition temperature (800K) to last a few seconds. Then the actual ignition time–from when the fuel is injected to when the fuel valve is closed and ignition stops–will be less than 2 seconds.

Table 6.5: Materials TC Values from [5].

Material	**Thermal Conductivity (W/mK)**	**Melting Temp (K)**
Titanium	17	1941
Nickels (600s)	14.9	1627-1686
Haynes 188 Alloy	19.3 at $777K$	1588-1683
SS 304	21.4 at $773K$	1627-1728
Alu 2024	205	775-911
Copper	385	1358
Glass	0.8	1673-1873
Fiberglass	0.04	1400
Asbestos	0.08	1144
Asbestos Composite Martine 65	0.245	
Acrylic	0.2	433
PTFE	0.25	600.15

Therefore the resonance cavity material must be able to survive up to about 5 seconds at around 1000K, and then less than 2 seconds at the combustion temperature. This is an extremely short period of time from a thermal perspective, meaning that while the stated melting temperature of a material may be below the combustion temperature chosen, if that combustion lasts less than 2 seconds, the material will in all likely-hood be able to survive the ignition in a reasonable condition. A good example of this is the NASA GOX/H2 spark torch igniter, which has a combustion temperature of 2050K. Even though this temperature is above the stated melting temperature of the material, the author states that because it has a ”low temperature and short operating time (0.75sec ignition), it eliminates the need to cool the chamber” [58]. This igniter uses the Haynes 188 alloys, which is a cobalt-nickel-chromium-tungsten alloy that has ”excellent high temperature strength and good resistance to oxidizing environment up to 1095C for prolonged exposures.” It is made of 22% chromium which protects it from oxidizer damage and corrosion[1]. In the NASA igniter, the combustion has a temperature of 2050K for 0.75 seconds, uncooled. The stated melting temperature of the Haynes 188 alloy is between 1588-1683K. This means that the combustion temperature in the igniter is between 367K and 462K hotter than the melting temperature of the material. This is an ignition system that is widely used by NASA, has a very long lifetime, high reusability, and has a great history of success. It proves that even if the combustion temperature is higher than the melting temperature of the material, as long as the ignition is quick, the material will survive[58]. This probably has to do with the low thermal conductivity of the material, since the ignition is so rapid and the thermal conductivity so low, there is not enough time for the heat of the combustion to penetrate into the material and cause damage.

Based on Table 6.5, the most promising materials from a thermal perspective are Titanium, Nickel (600), Haynes 188 Alloy, SS304, Glass, Fiberglass, glsPTFE and Asbestos. All have lower thermal conductivity values and high melting temperatures. Some other things that should be considered when choosing a material for the resonance cavity are hardness, machinability, cost, melting temperature, and oxidation and corrosion resistance. This device must be able to operate multiple times in a high temperature, oxygenated environment and it must be feasible to manufacture. These additional parameters remove a few options. Titanium is very expensive, hard and difficult to machine, therefore it is eliminated. Nickel (600) and Haynes 188 Alloy are expensive and difficult to source so they are eliminated. Asbestos is hazardous and is eliminated. Glass is too brittle and is removed. That leaves

SS304, PTFE and Fiberglass. Fiberglass is too porous to be used for the resonance cavity, but perhaps it could be used to insulate around the cavity.

The best options are SS304 and PTFE. The testing of this system, begins with heating tests of the resonance cavity, in which a sonic nozzle will inject an under-expanded jet of gaseous oxygen into resonance cavity test articles. The purpose of this phase of testing is to refine the geometry and placement of the cavity. This will likely require a half dozen cavity test pieces that vary in geometry, opening diameter, length, and shape. Once a geometry is found that allows for sufficient heating, that will be chosen as the final cavity geometry. Then ignition testing can occur, in which the resonance gas is heated and the fuel is injected to test for ignition. More information on the testing can be found in the Literature Study [24]. While one could make all of these test articles out of one material, it is more time and cost effective to choose a cheap and easy to manufacture material for the heating tests, in order to allow for rapid testing of a wide range of options and quickly refine the geometric parameters. Then the final material choice, which is best suited to the operating conditions can be manufactured for the ignition tests.

PTFE is a great choice for the initial heating tests because it is easy to machine, cost-effective, and has proven to be a great option in experiments done by Khoshkibijari and Karimi [42]. While PTFE does have a relatively low melting temperature of $600K$, these initial tests are just meant to demonstrate if the cavity can achieve heating. Once this has been proven successfully, then the testing can switch to a more thermally compatible material. PTFE is simple to manufacture because it is quite soft, and one can easily machine very small diameters, down to 1mm, as well as complex shapes, such as cones and tapers, which will be required in this application. This makes PTFE an ideal option for being able to manufacture and test many different geometries for the resonance tubes. The price, manufacturing ease, low thermal conductivity, and relatively high melting temperature make PTFE the best choice for initial resonance cavity heating tests.

SS304 has 18% chromium composition, which makes it highly corrosion and oxidation resistant. It has excellent toughness, is easy to manufacture, and is affordable since it is widely used. The high chromium content of SS304 enhances its ability to withstand high temperature and oxygen-rich environments. However, long term, repeated exposure to high oxygen environments will lead to oxidation and corrosion of the system. Therefore for the durability and longevity of this ignition system, a fuel-rich mixture ratio will be used, as previously stated. As the geometry of the injection nozzle will likely remain unchanged, it is recommended to manufacture the injection nozzle out of SS304 because it is tough and it will not wear down much during testing which will make for reliable results. Regarding the resonance cavity, it is recommended to make the initial heating test pieces from PTFE and once the geometry is validated, the test articles can be manufactured from SS304 for the hot fire testing. PTFE is cheaper than SS304 and is easier to manufacture, which is necessary in the resonance cavity heating tests. However for the test bench and flight models it is recommended to manufacture the injection nozzle, resonance cavity and combustion chamber from SS304.

Since SS304 will be used as the material in the final system, it will be used to set the maximum allowable temperature boundaries. The melting temperature of SS304 is 1627-1728K and based on guidance from the NASA Spark Torch Ignition System, the max combustion temperature can be set at 367-467K above this. Therefore the chosen maximum ignition temperature is $T_{c,max} = 2000K$. For most LRE hydrocarbons, the combustion efficiency is quite high, near 98%. Since there is already a large safety factor on the power calculations, there will be no safety factor applied on the combustion efficiency. Applying this $T_{c,max}$ to the O/F vs T_c plot in Figure 6.5, results in a maximum allowable O/F of 0.8. At $O/F = 0.8$, $T_c = 1960$. The effect of combustion chamber pressure is negligible at this mixture ratio.

6.3. Size Considerations

As shown in Equation 6.6, the ignition power is a function of the propellant mass flow rate and enthalpy difference. The larger the enthalpy difference (ie the higher the combustion temperature), the lower the mass flow must be to achieve the same amount of power, and vice versa. The larger the cross-sectional area of the injector nozzle and the exhaust orifice, the higher the mass flow rates through them. The size of these exit orifices affects the overall size of the ignition system. Therefore it is necessary to examine the engine manifold, where the ignition system will be mounted, to set boundaries on the physical size of the system. If the igniter is too large it may not fit on the manifold and conversely if it

is too small, then it will be difficult to manufacture.

The technical drawings of the Blizzard Lite test bench engine contained in the Appendix A, provide information on the sizing of the engine. The main geometries to consider are the inner diameter of the combustion chamber, the injector plate internal diameter, and the inlet and outlet diameters of the injector, which are listed in Table 6.6. The engine uses a pintle tipped injector placed in the center of the engine manifold. The igniter must be mounted close enough to the injector to be able to shoot a flame into the injector flow. As the combustion chamber walls are quite thin, the engine manifold provides the most feasible mounting location for the igniter, as it provides enough material to secure the igniter in place and it is located close to the injector spray Appendix A. The technical drawing of the Blizzard Injector, Figure A.7 shows the injector plate which is mounted below the manifold and illustrates how much space is left on either side of the injector place the igniter outlet. The igniter will be threaded into the manifold above this plate, but its outlet must be able to fit in the space between the outer diameter of the injector flow inlet and the inner diameter of the injector place internal diameter. Additionally, the internal diameter of the combustion chamber is even smaller than the injector plate internal diameter, so in face the outer diameter limit is 90mm. This leaves 17mm on each side. The final design of the manifold can be adjusted to ensure there is enough material to properly thread and secure the igniter in place, but the drawings provide guidance on what a reasonable size is.

Table 6.6: Blizzard Lite Geometries [23]

Parameter	**Value**	**Unit**
Inner Diameter Combustion Chamber	90	mm
Injector Plate Internal Diameter	110	mm
Injector Inlet Diameter	56	mm
Injector Outlet Diameter	25.32	mm

Another consequence of the physical size of the igniter is heat transfer to the igniter material. With resonance ignition, it is better to have a smaller surface area inside of the resonance tube–which is dependant on the diameter of the inlet–because the larger the inner surface area of the resonance tube, the more heat is transferred to the walls of the resonance tube and lowering the maximum achievable temperature of the resonance gases. Therefore it is optimal to have a smaller resonance tube surface area, which requires a smaller resonance tube inlet diameter, resulting in a smaller injection nozzle diameter. Based on the relationship between cross-sectional area and mass flow rate, this translates to a lower oxidizer mass flow rate and a lower total mass flow rate. In order to achieve the required power level at a lower mass flow rate, Equation 6.5 dictates that a higher temperature combustion is required. Therefore it is optimal to design for a system with a small geometry that operates at the highest possible combustion temperature that the chosen materials can safely withstand.

In the power equation Equation 6.6, the total change in enthalpy multiplied by the total propellant mass flow rate, results in the ignition power. As the power requirement has been set, the next section will explain how to solve for the total change in enthalpy for the given propellants at the chosen combustion temperature. Then the mass flow rate of the exhaust gases can be calculated, as well as its corresponding orifice diameter. Using this information and the chosen mixture ratio, the mass flow rates of the injected propellants and the associated geometries of their injectors can be solved. Once all of the equations are set up, an iterative process is used where the chosen mixture ratio and combustion temperature, $O/F = 0.8\ T_c = 1960K$ are input into the python script to see how they affected the dimensions of the oxidizer injector nozzle and exhaust orifice. After reviewing the results and the discussed size considerations, the geometry of the ignition system is chosen. First all of the calculations used in the process will be explained and then the results of this iterative process will be discussed.

6.4. Total Enthalpy Change

The total enthalpy change, also known as the 'heating value' $H_{ign} - H_{ref}$ of the igniter exhaust products, describes the change in enthalpy of the propellants as they are raised from a reference temperature–in

this case the auto-ignition temperature of ethanol–to the combustion temperature, T_c. Calculating the total change in enthalpy requires solving for the heating value of each exhaust product and summing them. This begins with identifying the combustion reactants and products, which is accomplished by calculating the chemical balance equation for the combustion reaction with the chosen mixture ratio. The chemical balance equation was previously calculated for the main engine propellant combination of Oxidizer: 100% LOX + and Fuel: 85% Ethanol + 15% Water. The ignition system uses the same propellants, apart from the oxidizer being in the gaseous form. Therefore a similar method for solving the chemical balance equation will be utilized, with the ignition system mixture ratio. As stated previously, the chosen mixture ratio of $O/F = 0.8$ makes this combustion fuel rich, meaning there will be excess fuel left over in the products. While this lowers the efficiency of the reaction, it is the necessary as it lowers combustion temperature to a more feasible $1960K$, as opposed to the $3200K$ combustion temperature at the stoichiometric ratio, as seen in Figure 6.5. Choosing a lower temperature eliminates the need for a cooling system and choosing a fuel-rich ratio is less damaging then a fuel-lean ratio because oxidizers are extremely corrosive. Below the chemical balance equations for the stoichiometric mixture ratio and the chosen mixture ratio are given, details of these calculations are in Appendix B. The stoichiometric chemical equation for the propellants, where the reactants are on the left-hand side and the products are on the right hand side is:

$$(1.0 * C_2H_5OH(l) + 0.4513 * H_2O(l)) + 3.0 * O_2(l) \longrightarrow 2.0 * CO_2(g) + 3.4513 * H_2O(g) \tag{6.7}$$

The chemical equation for the reaction, with $O/F = 0.8$ is:

$$\begin{aligned} 3.2 * (1.0 * C_2H_5OH(l) + 0.4513 * H_2O(l)) + 3.0 * O_2(l) \longrightarrow \\ 2.0 * CO_2(g) + 3.4513 * H_2O(g) + 2.2 * (1.0 * C_2H_5OH(l) + 0.4513 * H_2O(l)) \end{aligned} \tag{6.8}$$

In the fuel-rich reaction, Equation 6.8, there is excess of fuel on the product side of the equation. Therefore when calculating the heating value of the exhaust products, this unburnt fuel must be included in the exhaust products. A weighted sum of all of the exhaust products, $CO_2(g)$, H_2O,and C_2H_5OH, must be calculated based on the chemical balance equation. The heating value is the summation of the specific heat values at each temperature from the auto-ignition temperature to the combustion temperature. Since the specific heating value, cp is temperature dependant, for each product it is calculated at every temperature from the auto-ignition to combustion temperature, then divided by the product's molecular weight and summed. See *cpO2CO2H2O.py* and *CpEthanol.py* for the detailed calculations. This is repeated for each of the exhaust products, and then the weighted mass of the dH for the exhaust products is calculated with the following equation. The coefficients are taken from Equation 6.8.

$$\begin{aligned} A * (C2H5OH(l) + 0.45127 * H2O(l)) + B * O2(l) - > \\ C * CO2(g) + D * H2O(g) + E * O2(g) + F * (C2H5OH(l) + 0.45127 * H2O(l)) \end{aligned} \tag{6.9}$$

The calculated heating value, dH Exhaust: $2079469\ J/kg$

6.5. Igniter Mass Flow Rates

With the igniter power requirement and the total change in enthalpy calculated, the igniter propellant mass flow rates can be determined. This begins by solving for the total exhaust gas mass flow rate using the equation, Equation 6.5. Equation 6.10 rewrites this power equation to solve for the mass flow rate. As mass is conserved, the mass flow rate of these exhaust gases is the sum of the oxidizer and fuel mass flow rates, defined in Equation 6.11. There is also a relationship between the fuel and oxidizer mass flow rates and the mixture ratio, defined by Equation 6.12.

$$m_t = \frac{P}{H_{ign} - H_{ref}} \tag{6.10}$$

$$m_t = m_o + m_f \tag{6.11}$$

$$\frac{O}{F} = \frac{m_o}{m_f} \tag{6.12}$$

6.6. Conclusion

In this chapter, the calculations for all of these parameters were conducted, as well as explanations of all of the relationships between the variables. Understanding these relationships is important in the event that one wishes to make changes to the design. The power equation, Equation 6.5, states that the combustion temperature and propellant mass flow rate are inversely proportional, so that in order to maintain a set power requirement, these both must be adjusted proportionally. In order to increase the power output, either the combustion temperature or mass flow rate must be increased, and vice-versa. From the RPA outputs for the given propellant combination, the relationship between mixture ratio and combustion temperature was provided. It showed that the closer the mixture ratio was to the stoichiometric ratio, the higher the combustion temperature, and the further away the mixture ratio was from the stoichiometric ratio, in either the fuel-rich or fuel-lean, direction, the lower the combustion temperature. In Table 6.7 the final values for the power, material and mass flow rate parameters for the preliminary design are provided. This igniter is being designed to test on the Blizzard engine, therefore the power parameters given in Table 6.7 are set to achieve ignition in the Blizzard Engine. Using the equations in section 6.5 and the mixture ratio, $O/F = 0.8$ the total, fuel and oxidizer mass flow rates or the Blizzard engine are calculated and the results are listed in Table 6.7. More details on these calculations can be viewed in *IgniterExhaust.py* in Appendix B.

Table 6.7: Resonance Ignition Device Preliminary Design Parameters: Power, Materials, and Mass Flow Rates. (subscript 0 indicates total conditions)

Parameter	Symbol	Value	Unit
Power			
Resonance Gas		Oxygen	
Fuel		Ethanol85	
Oxidizer Injection Temperature	$T_{0,ox}$	288.15	K
Fuel Injection Temperature	$T_{0,f}$	288.15	K
Minimum Required Ignition Power	P_{ign}	152.1	kW
Combustion Temperature	T_c	1960	K
Mixture Ratio	O/F	0.8	
Heating Value Exhaust	dH	2079469	J/kg
Materials			
Injection Nozzle Material	Material	SS304	
Resonance Tube Material	Material	PTFE/SS304	
Igniter Chamber Material	Material	SS304	
Mass Flow Rates			
Total Propellant Mass Flow Rate	m_o	70.12	g/s
Oxidizer Mass Flow Rate	m_o	31.165	g/s
Fuel Mass Flow Rate	m_f	38.956	g/s

7

Preliminary Design: Injection Nozzle Geometry and Pressures

In this chapter the preliminary design of the gaseous oxygen injection nozzle will be covered. Using the propellant mass flow rates calculated in the previous chapter, the geometry of the nozzle can be calculated using isentropic equations for choked flow converging nozzles. The geometry of the nozzle is dependant on the nozzle pressure ratio (NPR), which itself has a large effect on the design and performance of the resonance heating phenomenon. Therefore a large portion of this chapter is dedicated to understanding the relationships between gas mass flow rate, gas temperature, gas pressure and exit area of the nozzle. In addition, the choice of supply pressure is dependant on the desired combustion pressure and exhaust pressure of the ignition system, as pressure losses and risks of back-flow must be considered. Therefore in this chapter an integrated approach is used to design an injection nozzle and resonance cavity that are able to achieve sufficient heating for a chosen NPR, combustion pressure and ignition system exhaust pressure.

7.1. Igniter Geometric Relationships

Given the igniter power (P), combustion temperature (T_c) and mass flow rates, the injection nozzle parameters can be calculated, all of which are listed below. As a converging nozzle will be used the geometric parameters of this type of nozzle must be calculated [66].

Injection Nozzle Parameters to Calculate:

- D_n: Injection Nozzle Exit Diameter
- d_{in}: Injection Nozzle Inlet Diameter
- β: Injection Nozzle Convergent Angle
- ϵ: Injection Nozzle Area Ratio
- L_{conv}: Injection Nozzle Convergent Length
- r_u: Injection Nozzle radius
- r_a: Injection Nozzle Converging Radius
- NPR: NPR, Nozzle Pressure Ratio
- P_o: Oxidizer Injection Pressure
- P_c: Combustion Chamber Pressure

Before beginning the calculations, it is important to establish the relationship between the gaseous oxygen mass flow rate, temperature, pressure and area, such that informed decisions can be made. This relationship is described in Equation 7.1, which states that at any point in the flow of these combustion gases, the ratio of the mass flow rate (m) times the square root of the total temperature (T_t) divided by the cross-sectional area (A) times the total pressure (P_t), equals a constant [31]. This defines the relationship between all of these parameters and helps in making design decisions.

$$\frac{m * sqrt(T_t)}{A * P_t} = C \tag{7.1}$$

This means that for a chosen combustion temperature, which here is equivalent to the total temperature $T_c = T_t$, and a mass flow rate calculated from Equation 6.5, Equation 7.1 can be used to determine the best area and pressure combination. As discussed, the diameters of the igniter exhaust nozzle must be small enough to fit on the manifold, and the diameters of the GOX injection nozzle and ethanol injection holes must be large enough to easily manufacture, but on the small size to prevent too much heat loss in the resonance tube (whose size is directly related to the size of the GOX injection nozzle.) From Equation 7.1, it can be seen that for a chosen mass flow rate and total temperature at any point in the flow, as the cross sectional area increases, the total pressure decreases and vice versa. Therefore if one is trying to decrease the diameter of the exit of the exhaust nozzle, they should increase the total pressure at that point, which means that they need to increase the combustion pressure. This is a cascading design, meaning that the design choices in the injection nozzle will affect the design choices for the combustion pressures, resonance cavity and exhaust orifice. The most important relationship is that between the geometries of the components and the pressures. As explained in the Requirements chapter, in order to function, the ignition system must maintain a positive DP in the flow direction. However there are limitations in available space and supply pressures. Therefore in this chapter an iterative process will be used for the design of the main components. The equations and theory will be explained, then the python code is used to calculate the resulting parameters for a set of options, and finally a trade-off is conducted and a set of parameters is chosen.

7.2. Example Systems and Design Constraints

In the next sections we will solve for the geometries of the injection nozzle and resonance tube. Their geometries are extremely dependant on one another. Before solving for the geometries of the injection nozzle and resonance tube it is useful to gather values from similar experiments, which will help set some boundaries on parameters, and provide confidence in design choices. To provide guidance on sizing, two tables. Table 7.1 lists the geometries of a selection of working Hartman-Sprenger Generator (HSG) heating and sound devices, that use $O2$, $N2$, and air as resonance gases. Table 7.2 lists major design parameters of complete resonance ignition systems. While all 3 experiments listed in the table use air instead of gaseous oxygen, they have very similar specific heat ratios and act similarly enough to provide guidance. The experiments do not list the complete set of parameters and only those values given are included in the table. These values provide a good starting point on sizing of the injection nozzle exit and resonance tube inlet, and will be consulted throughout the design.

Table 7.1: Hartmann Sprenger Devices Geometries, all dimensions are in mm

Device Type	D_n	D_{res}	**Optimal** D_{res}/D_n	**Paper**
HSG Heating	5	6.3	1.26	Karimi/Khosh. [42]
Res. Igniter	4	2		Niwa [54, p.996]
HSG Heating	2	2	1.0	Broucher [13]
HSG Heating		3	1.0	Narayanan [52]
HSG Sound		1.3-2.0		Brun/Boucher [48]
HSG Sound			1.6	Borisov [48]
HSG Heating	508	635	1.25	Phillips/Pavli [56]
HSG Heating			1.3	Stabinsky [48]
HSG Heating			1.33	Marchese [48]
HSG Heating			1.3-2.5	Boutorin [48]
HSG Heating			1.1-1.6	Kessaev [48]
HSG Heating			1.6	Marchan [48]

Apart from Phillips and Pavli, who made a very large device, a majority of the HS heating and resonance ignition devices are rather small, with injection nozzle exit diameters 5mm or less and resonance rube inlet diameters 6.3mm or less. As these geometries have been proven to work and are in the scale of the engine, these will provide the approximate maximum boundaries for our design. There are also some design constraints to consider, which are as follows.

Design Constraints:

- The combustion pressure, P_c will be less than 40 bar, in order to keep the required pressure in the oxygen, nitrogen and ethanol supply tanks at a safe and workable pressure.
- The igniter exhaust orifice outlet must be able to fit in the space on the manifold, which is 17mm.
- Manufacturing: The smallest step size in drills in 0.1mm. however the most common drills are 0.0 and 0.5mm sizes. therefore choose a GOX injector nozzle outlet and/or resonance tube size of 0.0 or 0.5mm if possible to make manufacturing easier.
- To minimize heat losses to the walls of the resonance tube, maximum resonance tube inlet diameter is 7 mm and maximum injection nozzle exit diameter 6mm.
- Resonance cavity opening must be located within the compression zone of the first shock cell of the under-expanded jet [48, p.1242].
- The combustion chamber is assumed to be a cylinder shape.

Table 7.2: HS Heating Experiments, Maximum Temperature Geometries

Paper	Narayanan [52]	Karimi [42]	Marchan [48]
Gas	air	air	air
NPR (P_o/P_a)	5	11	5.5-7.5 (P_e/P_a)
D_n (mm)	3	5	3.8
D_{res} (mm)	3	6.3	6 (D_{cyl} : 2.5)
d_e (mm)	1.4		
L (mm)	39	48	L_{cyl} : 15
ΔS (mm)	9.9	13.5	7
Shape	Conical	Conical	Conical-Cylin. hybrid
Res Material		PTFE	
β (deg)			20

7.3. GOX Sonic Nozzle

When designing a converging, sonic nozzle for a compressible substance (gaseous oxygen), it is vital to understand how the different parameters affect the design. Table 7.3 defines all of the variables used in the next section.

Table 7.3: Variable Definition

Symbol	Definition	Symbol	Definition (Unit)
$\dot{m}$	Mass Flow Rate (kg/s)	R	Specific Gas Constant ($J/mol*K$)
T_t	Total (or Stagnation) Temperature (K)	P_t	Total (or Stagnation) Pressure (Pa)
T	Static Temperature (K)	P	Static Pressure (Pa)
ρ	density (kg/m^3)	u	Velocity (m/s)
A	Area (m^2)	γ	Specific Heat Ratio
M	Mach Number	$*$	Sonic Condition ($M = 1$)
A_e	Exit Area (m^s)	P_B	Back Pressure (Pa)
D(M)	Corrected Mass Flow per Unit Area	P^*/P_t	Critical Pressure Ratio
$P_{ign,cc}$	Igniter Combustion Pressure (Pa)	$P_{me,cc}$	Main Engine Combustion Pressure (Pa)

7.3.1. GOX Nozzle: System Pressures

There are 3 phases of igniter operation:

Phase 1: GOX injection and heating

Phase 2: Ethanol injection and combustion
Phase 3: Ethanol purging

The GOX nozzle needs to maintain choked flow for the duration of phases 1 and 2. In phase 1, the choked flow is necessary to create the under-expanded jet of oxygen necessary for the gas dynamics phenomenon. In phase 2, the choked flow will allow the GOX to continue to flow into the igniter during the combustion, while preventing backflow of these hot igniter combustion gases into the GOX supply line (which could cause an explosion.) In phase 3, the GOX supply will stop and the high pressure ethanol will continue to flow into the igniter to clear out any remaining GOX and maintain a positive differential pressure (DP) between the igniter combustion chamber and the main engine combustion chamber. This positive DP will prevent the backflow of hot main engine combustion gases into the igniter chamber. A check valve will be placed just before the GOX nozzle to prevent fuel from flowing up that line.

At this point it is important to explain what positive differential pressure (DP) means and why it is vital to consider in the design. Gas flows from high to low pressure. Therefore to ensure that the injected gaseous oxygen, the igniter combustion gases and the main engine combustion gases flow in the proper directions, the system must maintain a positive DP in the correct directions at all times. In Appendix H a plot is provided that illustrates of all of the steps in this ignition process, and shows the relative pressures in the igniter and main engine combustion chambers as a function of time. This plot is provided to show that in a working system there is always a positive DP maintained between the igniter combustion chamber and the main engine combustion chamber. This DP is necessary to prevent back-flow because if this positive DP is not maintained, and the pressure of the hot combustion gases in the main engine combustion chamber become higher than the gases in the igniter combustion chamber, then these hot main engine combustion gases will ”back flow” into the igniter and cause thermal damage to the igniter. This could melt the igniter and lead to explosions in the propellant lines.

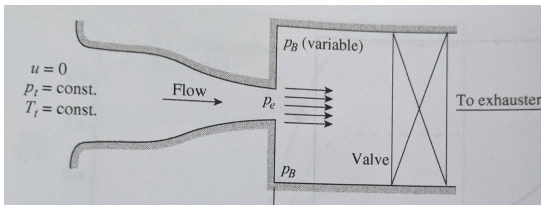

(a)

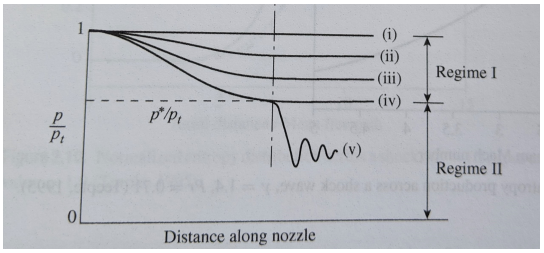

(b)

Figure 7.1: Operation of a converging nozzle at different back pressures. [31, p.72]

Therefore when designing the sonic nozzle for the GOX injection, the designer must choose a P_t that maintains choked flow in the GOX injection nozzle for the duration of the igniter operation, until ethanol purging begins. An important consideration now is how to take into account the Back Pressure, P_B of this system. Figure 7.1 illustrates a converging nozzle that directs gas from a large reservoir into a chamber. The supply gas is at a constant total pressure and temperature, P_t and T_t. The pressure at the exit pane of the nozzle is P_e and the pressure in the chamber downstream of the nozzle is the back pressure, P_B [31, p.72]. This gas is assumed to be isentropic. The plot on the lower half of the figure shows how the ratio of the back pressure to the total (stagnation) pressure, P_B/P_t varies along the length of the nozzle.

Line (i) shows that if $P_B = P_t$, there will be no flow through the nozzle. Lines (ii) and (iii) show that if P_B is a bit less than P_t, then there will be subsonic flow ($M < 1$) in the nozzle. Line (iv) shows what happens when $P_B = P^*$. the critical pressure, and the flow is sonic at the exit, so $M = 1$. ”Further reduction of the back pressure cannot increase the corrected flow and thus cannot alter any of the flow quantities upstream of the exit” [31, p.73]. In other words, the flow is choked and no matter how much lower the P_B is made, it will not have any effect on the flow in the nozzle or upstream. With this in mind, one can now observe how the corrected mass flow per unit area and P_e/P_t are related. Figure 7.2 shows that in Regime I, where $P_B/P_t > P^*/P_t$, the corrected flow per unit area increases while the back pressure decreases. In Regime II once $P_B/P_t = P^*/P_t$, at the critical conditions, no matter how much lower the back pressure is made, the corrected mass flow per unit area and the mach number at the exit are unaffected.

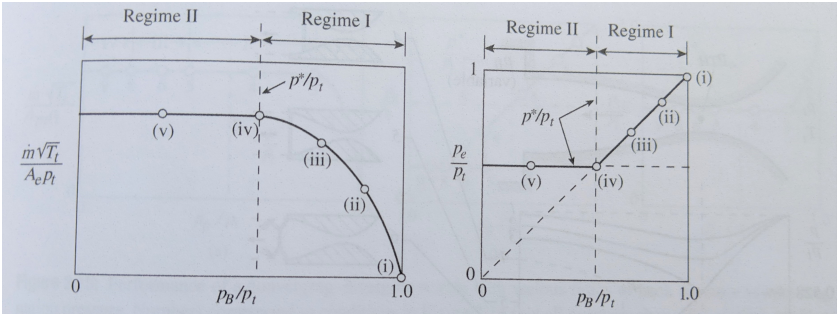

Figure 7.2: Corrected flow per unit area and nozzle exit pressure as a function of the back pressure ratio for a converging nozzle. [31, p.73]

This is very important in this project's case because when the ignition occurs in the igniter combustion chamber, one must ensure that the flow through the nozzle remains choked, to prevent the combustion gases from having any effect in or upstream of the GOX nozzle. This means that one must ensure that the critical pressure ratio, $P_B/P_t = P^*/P_t$ is maintained during the igniter combustion. In this case the back pressure equals the igniter combustion pressure ($P_B = P_{ign,cc}$). However during the GOX heating, the gaseous oxygen will be injected into the igniter chamber which is at ambient pressure, so P_B will be lower than $P_{ign,cc}$ during the resonance heating time. In Figure 7.1, line (v) shows us that if P_B/P_t is lower than critical, "the pressure distribution within the channel, the value of P_e/P_t, and the flow rate are all identical with the corresponding quantities for condition (iv)" [31, p.73]. Therefore it is okay to have a lower P_B/P_t during the resonance heating phase, when only the oxygen is being injected. What is vital in the design is to ensure that when the combustion occurs in the igniter:

$$\frac{P_B}{P_t} <= \frac{P^*}{P_t} \tag{7.2}$$

Applying all of this to the design, one must first calculate the critical pressure ratio P^*/P_t, which is done by solving Equation 7.11 when $M = 1$. For gaseous oxygen, the critical pressure ratio is, P^*/P_t = 0.56. Then using Equation 7.2, one can solve for the minimum supply pressure, P_t as a function of the back pressure, P_B, that guarantees choked flow in the nozzle for the duration of operation from igniter startup to the start of the fuel purge. The design requirement for the gaseous oxygen is written in Equation 7.14.

An important aspect to discuss is the isentropic and incompressible flow assumptions that will be used in the calculations of the sonic injection nozzle. The resonance gas starts from a relatively static position in the storage tank and, when directed through the sonic nozzle, this gas is increased to sonic speed where the Mach number equals 1. At this point the gases have static and dynamic values of temperature and pressure. Liquids are assumed to be incompressible, meaning their density is constant regardless of the speed at which they travel. Gases on the other hand are compressible fluids, meaning that their density will change depending on their flow speed. This change in density has important effects on how the gas functions are different speeds. However, at low speeds, like below $M = 0.3$, it is reasonable to assume that gases are incompressible [31]. Including compressibility effects for flow above $M = 0.3$ are important, but add a great deal of complexity to the calculations. Therefore in these initial empirical calculations, the gas will be treated as an ideal gas and incompressible flow equations will be used. Corrections for compressbility effects will be made using the results of the ANSYS Fluent simulations, which do include the compressibility effects. For now, to make the math easier and get good approximations, the flow will be assumed to be incompressible and thus use isentropic relations and laws. These isentropic equations are approximations and do not account for losses in feedsystem, however as they physical size of the system is small and the volume of gas used is small, it will be assumed that the losses in the system are also small. One very important law of in-compressible flow is: Total Pressure and temperature is conserved, Total = static + dynamic. Therefore when the gas is not moving $v = 0$, (like in the supply tanks and combustion chamber) the dynamic P and T are 0, and the total = static. Once the gas moves the static values decrease as the dynamic values increase, keeping the total value the same, due to the conservation law.

For the GOX injection nozzle, the following set of isentropic equations will be used to approximate

the temperature, pressure, and velocity values of the flow. As this is a sonic nozzle there are the critical ratios for temperate and pressure, CTR and CPR. Both of these critical equations are derived from isentropic relations, in which the Mach number at the sonic throat is set to one, $M = 1$. In all 4 of the isentropic equations below in the left hand side fraction, the upper number is the static value at a chosen point in the flow, and the bottom value (x_t) indicates the total value where velocity is 0, $v = 0$. In the critical equations, the $*$ notation indicates the static value at the sonic point (ie the throat/exit) where $M = 1$. The specific heat ratio here, γ, is the weighted specific heat ratio for all of the exhaust products at the given mixture ratio. The equations used to calculate these values and the results are as such.

Isentropic Equations:

$$\left(\frac{P}{P_t}\right) = \left(\frac{\rho}{\rho_t}\right)^{\gamma} = \left(\frac{T}{T_t}\right)^{\frac{\gamma}{\gamma-1}} \tag{7.3}$$

$$\left(\frac{P}{P_t}\right) = \left(1 + \frac{\gamma-1}{2}M^2\right)^{\frac{-\gamma}{\gamma-1}} \tag{7.4}$$

$$\left(\frac{T}{T_t}\right) = \left(1 + \frac{\gamma-1}{2}M^2\right)^{-1} \tag{7.5}$$

Critical Isentropic Equations

$$\left(\frac{P^*}{P_o}\right)_{CR} = \left(\frac{2}{\gamma+1}\right)^{\frac{\gamma}{\gamma-1}} \tag{7.6}$$

$$\left(\frac{T^*}{T_t}\right)_{CR} = \left(\frac{2}{\gamma+1}\right) \tag{7.7}$$

Next a central non-dimensional variable called the corrected flow per unit area should be defined. It describes the mass flow through a cross-sectional area, for a given gas, as a function of the Mach number only [31, p.60]. To derive this equation, begin with the simple equation for one-dimensional flow of a gas per unit area, Equation 7.8.

$$\dot{m} = \rho u A \tag{7.8}$$

Now incorporating the stagnation quantities the total pressure and temperature values and using the ideal gas law, gives, Equation 7.9.

$$\dot{m} = \frac{p}{p_t}\frac{T_t}{T}\frac{p_t}{RT_t} \tag{7.9}$$

Then use the relations of the stagnation and static values, the velocity in terms of Mach number, and the speed of sound using Equation 7.10 and Equation 7.11 to solve for the corrected flow per unit area equation.

$$\frac{T_t}{T} = 1 + \frac{(\gamma-1)M^2}{2} \tag{7.10}$$

$$\frac{p_t}{p} = \left(1 + \frac{(\gamma-1)M^2}{2}\right)^{\gamma/\gamma-1} \tag{7.11}$$

Corrected Mass Flow per unit Area, $D(M)$:

$$\frac{m\sqrt{RT_t}}{Ap_t\sqrt{\gamma}} = \frac{M}{\left(1 + \frac{\gamma-1}{2}M^2\right)^{\frac{1}{2}\left(\frac{\gamma+1}{\gamma-1}\right)}} = D(M) \tag{7.12}$$

This equation can be used to calculate the corrected flow per unit area for a specified gas. In order to better understand what this equation is describing, a plot of corrected mass flow per unit area, $D(M)$

versus Mach Number (M) is shown in Figure 7.3, for a gas with a specific heat ratio, $\gamma = 1.4$. This is well suited for this situation, as gaseous oxygen has a specific heat ratio, $\gamma = 1.4$ [31].

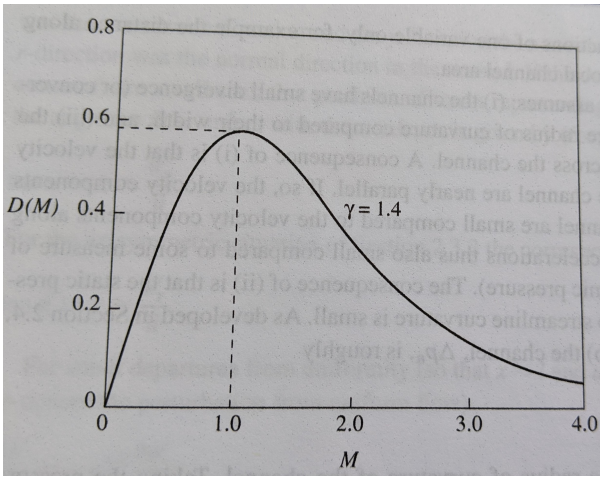

Figure 7.3: Corrected flow function, D(M) versus Mach number for $\gamma = 1.4$. [31, p.62]

From this figure and equation, one can learn the following.

> "For a given Mach number, the physical mass flow per unit area ($\dot{m}/A$, in $kg/(sm^2)$) is proportional to the stagnation pressure and temperature interpreted as local values...corrected flow per unit area rises as the Mach number increases for $M < 1$, falls as the Mach number increases for $M > 1$, and has a maximum at $M = 1$. The value of the maximum depends on γ and is 0.579 for $\gamma = 1.4$....The use of corrected flow allows direct interpretation of the effects of friction and heat transfer....processes which either increase the stagnation temperature of a steady flow (for example, heat addition) or decrease the stagnation pressure (friction) increase D...processes which increase the stagnation temperature or decrease the stagnation pressure increase the area needed to pass a given physical mass flow" [31, p.62,63].

The simplified corrected mass flow equation for a sonic, converging nozzle is as follows.

$$\frac{\dot{m}\sqrt{T_t}}{Ap_t} = \sqrt{\frac{\gamma}{R}}\left(\frac{\gamma+1}{2}\right)^{\frac{-1}{2}\left(\frac{\gamma+1}{\gamma-1}\right)} = D(M)^* \tag{7.13}$$

Equation 7.13 says that for sonic conditions, $\frac{\dot{m}\sqrt{T_t}}{Ap_t}$ equals a constant. Meaning that if one of the variables on the left-hand-side (LHS) of the equation changes, it will have an effect on at least one other variable on the LHS, in order to maintain constant. In order to apply this to the current design, it is helpful to illustrate 2 examples.

Example 1:
Build a sonic, converging nozzle with a fixed exit area (A_e), and keep the supply gas at a constant temperature (T_t). If one were to increase the supply pressure (P_t), then the mass flow rate would also increase, proportionately.

Example 2:
An engineer is designing a sonic, converging nozzle in python and trying to calculate the exit area (A_e). They keep the supply gas at a constant temperature (T_t). From the power requirements, one can calculated a minimum mass flow rate ($\dot{m}$). If supply pressure (P_t) increases, the exit area (A_e) will decrease proportionately, and vice versa.

Example 2 is a perfect summary of this project's situation. This project aims to design a sonic nozzle to create an under-expanded jet of gaseous oxygen, which will be directed into a resonance cavity. This report has already used the power requirements to calculate the gaseous oxygen mass flow rate required and the total temperature of the propellant. Therefore, given that $\dot{m}$ and T_t are fixed, one can

use Equation 7.13 to determine which values of P_t and A_e to use for the nozzle. To do so one must consider their relationship from Equation 7.13, the requirements of the resonant gas phenomenon and the main engine parameters. From the prior sections, guidelines have been established on the sizing of these nozzle-cavity pairs, in order to achieve the resonant gas dynamic phenomenon. Additionally, the relationship between geometric size, supply pressure and power output of the igniter have been described. The goal in the design is to create a sonic nozzle that will be able to maintain an underexpanded flow of gaseous oxygen for the duration of the igniter operation, and maintain a constant mass flow rate to ensure that the mixture ratio of the combustion is stable and accurate.

7.3.2. GOX Nozzle: Shape

In order to build a functioning resonance tube, a jet of underexpanded gas needs to be directed into a cavity. First the shape of the injection nozzle must be chosen, converging or converging-diverging. Phillips and Pavli tested using a converging nozzle, as well as a few different types of converging-diverging nozzles, with varying expansions ratios. They found that the ”maximum pressure wave amplitude at the base of the resonance cavity was found for a simple sonic nozzle, with an area of unity.” [56] In conclusion, a simple converging nozzle provides the maximum pressure and temperature at the base of the resonance nozzle. Therefore a converging, sonic injection nozzle that produces an underexpanded jet of gaseous oxygen will be used.

7.3.3. GOX Nozzle: Pressure and Area Calculations

The GOX nozzle will be a converging, sonic nozzle and the relationship between the nozzle mass flow rate, inlet gas pressure, inlet gas temperature and exit area, has been established. For a sonic converging nozzle with isentropic flow, there is an equation that describes the relationship between $\dot{m}$, T_t, P_t, and A_e, Equation 7.13. Based on the set power requirements of the igniter, a constant valve for $\dot{m}$ has been calculated, and there is a given supply of gaseous oxygen with a constant T_t. For the 2 remaining variables, P_t and A_e, a set of requirements have been developed that provide a range of values to test. For the area, the range of injection nozzle exit diameters has been established based on prior experiments. A range of 1.5 to 6mm nozzle exit diameters will be input into the solver. For the pressure, the range of possible inlet pressures is based on the need for a sonic, underexpanded jet, as stipulated by the resonant gas phenomenon, and is limited by the back pressure in the igniter chamber during operation. By combining Equation 7.13, and the requirements for these two parameters, one can perform a set of iterative calculations for different ranges of A_e and P_t, in order to find the most optimal combination for our design. The required oxidizer mass flow rate of $\dot{m}_o = 31.16$ g/ has already been calculated and it is assumed that the injection gas is gaseous Oxygen with $R = 259.8 J/mol * K$ and $\gamma = 1.4$, and a temperature of $T_t = 300$ K. Therefore in order to achieve the desired mass flow rate the nozzle exit area and gas inlet pressures must be calculated as a pair.

In order to maintain positive DP in the system, the resulting combustion pressure from a chosen GOX inlet pressure and nozzle exit diameter must be greater than the ambient pressure. This combustion pressure should be a few bar above the ambient pressure, to account for some pressure loses across the exhaust orifice. Therefore in order to choose a range of possible nozzle pressure and diameter combination, the resulting combustion pressures for these options is calculated and displayed in Figure 7.4, with a selection of the variables listed in Table 7.4. This table displays the minimum total supply pressure P_t required to maintain choked flow in the oxygen injection nozzle during the igniter combustion, when the back pressure is equal to the combustion pressure. The combustion pressures listed $P_{ign,cc}$ are the maximum allowable combustion pressures for the given supply pressures P_t necessary to maintain choked flow. Therefore when choosing the supply pressure and combustion pressure for a given nozzle exit diameter, the supply pressure must be greater than or equal to the value given in Table 7.4. Then the combustion pressure that corresponds to the chosen supply pressure can be calculated. This iteration is completed in a python script. Note that the igniter combustion pressure $P_{ign,cc}$ was varied over a range, and the minimum P_t based on the given requirement is listed in the table, because $P_{ign,cc}$ drives the value of P_t, as explained by Equation 7.2. In Table 7.4, the 0.0 and 0.5mm diameters are selected from the results and listed with the corresponding total supply and combustion pressures. As these are the easiest to manufacture sizes, they will be focused on.

Requirement: GOX Supply Pressure P_t

$$P_t >= \frac{P_B}{(P^*/P_t)} \tag{7.14}$$

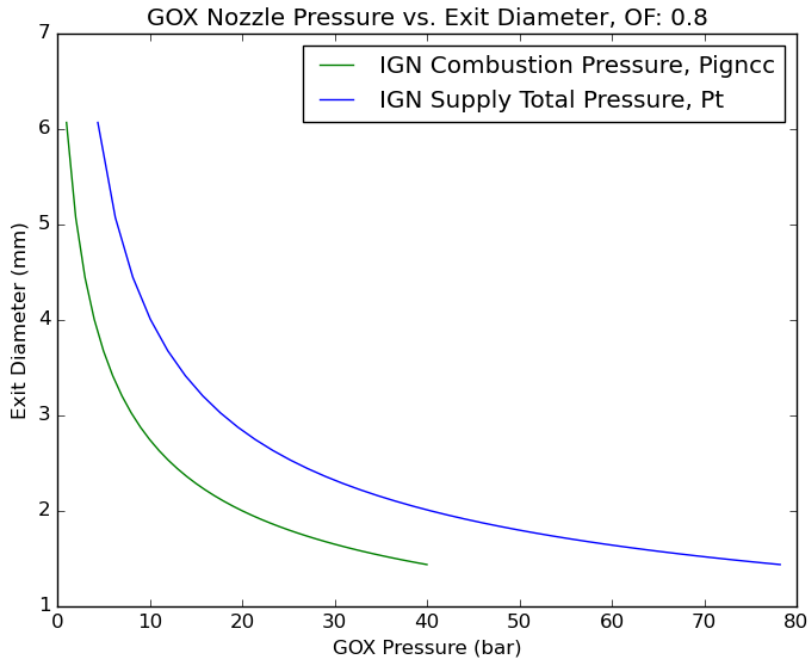

Figure 7.4: GOX Sonic and Converging Nozzle. Plot of combustion and total GOX supply pressure vs. nozzle exit diameter, for a fixed mass flow rate and supply temperature, keeping choked conditions. OF: 0.8

To calculate the P_t (P_o) values for each nozzle exit diameter listed in Table 7.4 the following assumptions and equations were used. It was assumed that the converging nozzle was sonic and choked, with a mass flow rate was of $31.165 g/s$. The gas was assumed to be isentropic, which allowed the following isentropic equations to be used. These isentropic equations were simplified for sonic conditions where $M = 1$, resulting in the following equations for mass flow rate, and area, where A^* is the area of the sonic throat. These equations were combined with the mass flow rate and exit area values as the inputs, and the total pressure as the output. Table 7.4 lists the results of these calculations.

$$m = \frac{A^* P_t}{\sqrt{T_t}} * \sqrt{\frac{\gamma}{R}} * \left(\frac{\gamma+1}{2}\right)^{-\left(\frac{(\gamma+1)}{2(\gamma-1)}\right)} \tag{7.15}$$

$$A = \pi \frac{d}{4} \tag{7.16}$$

where m : mass flow rate , A^* : Sonic throat Area, P_t : Total pressure, T_t : Total temperature, γ : specific heat of gas, R : specific gas constant

The relationship between the gas injection pressure and combustion pressure can be seen in this figure and table. They illustrate how the igniter combustion pressures $P_{ign,cc}$ varies for a given gaseous oxygen supply pressures P_t and nozzle exit areas A_e. Equation 7.14 was used to solve for the P_t values and then Equation 7.13 was used to solve for area. A wide range of combustion pressures, from 1-40 bar was used. In order to keep choked conditions during entire operation, $P_B/P_t <= P^*/P_t$, where $CPR = P^*/P_t$. Therefore $P_t >= P_B/CPR$, where P_B is the igniter combustion chamber pressure. From this one can see that the supply pressure must be greater than or equal to the back pressure divided by the CPR. Therefore as long as the supply pressure is greater than P_B/CPR, choked conditions will be met. As established, for a set P_B, once choked conditions are met, one can increase P_t and still maintain choked flow. Therefore, to ensure that choked conditions take place, a 1 bar margin will be

Table 7.4: GOX Nozzle Parameters: Inlet pressure, combustion pressure and Exit Diameter Relationship

d_e **(mm)**	$P_{ign,cc}$ **(bar)**	P_t **(bar)**
1.5	38.0	72.0
2	21.4	40.4
2.5	13.7	25.9
3	9.5	18.0
3.5	7.0	13.2
4	5.3	10.1
4.5	4.2	8.0
5	3.4	6.5
5.5	2.8	5.3
6	2.4	4.5
6.5	2.0	3.8

added to the calculated minimum P_t, to ensure that the CPR and choked flow are maintained during igniter combustion.

In order to choose which injection nozzle exit diameter and injection pressure combination to use in this design, it is necessary to consider expected pressure losses in the system. When the igniter combustion gases are directed into the main engine combustion chamber through the igniter exhaust orifice, these gases will experience a pressure loss. The size of this pressure loss is dependant on numerous factors, including the diameter of the exhaust orifice, as well as surface roughness across the orifice and manufacturing errors. As stated in the Operational Requirements, the system must be designed to prevent any back-flow. In this case, the exhaust flow is being injected into the main engine combustion chamber at startup, when the exit pressure is at ambient. The ignition system must maintain a positive DP between the igniter and main engine combustion chamber during the entire operation, which is why the ignition system will be purged with high pressure fuel during the main engine burn. The operation time of the igniter must be tested to ensure ignition of the main engine propellants, and then start of purging, before the pressure in the main combustion chamber rises above the exit pressure of the igniter gases. To provide some margin on this, it is best to choose a conservative injection pressure value. Before making a choice, an estimation on expected pressure losses across the exhaust orifice was made, which is described in detail in section 8.2.

After testing different values of exhaust gas pressure at each of the nozzle exit diameter options, taking into consideration the limited space for the exhaust orifice on the injector manifold, and considering the need for a large margin, it was decided to choose a 3mm nozzle exit diameter with a 19.0 bar injection pressure. This geometry was selected because it is an easy machine diameter (for smaller drill sizes it is best to use 0.0 or 0.5mm diameter drills as they are most common), with a reasonable oxygen supply pressure, and combustion pressure that leaves margin for pressure losses across the exhaust orifice. This geometry will be used in the ANSYS Fluent simulations and refinement to the choice will be made as part of the Detailed Design phase. This option is reasonable as the values are close to those of the working resonance test systems developed by Narayanan, Marchan, and Karimi [52] [48] [42]. The supply pressure of 19 bar is chosen because it is greater than the minimum pressure value of 18 bar necessary to maintain choked flow. This 1 bar increase provides some margin to account for friction losses in the nozzle and feedsystem. During experiments these input pressure values and therefore NPR may be adjusted to find the optimum. However these values provide a reasonable geometry to start designing and for simulations. All of the corresponding geometric and pressure values for this option are listed in Table 7.5. With the main parameters of the nozzle set, the other geometric values can be calculated. When designing converging nozzles, there are some general guidelines. To limit pressure losses, it is recommended to use rounded and smooth converging section in order to keep the flow attached. In addition, the shorter the convergent length the higher the pressure losses in the nozzle.

Figure 7.5 shows the main geometric parameters of a convergent nozzle. The typical NASA recommended values for these parameters are [66], $\frac{r_u}{R_t}$ = 0.5-1.5, $\frac{r_a}{D_c} > 0.5$, and B = 30-60 degrees. The

NPR and exit diameter were held constant and the contraction angle B and the inlet diameter, D_{inlet} were varied between $20 - 40$ degrees, and 8-10mm, respectively, to see how it affected the geometry of the nozzle. The inlet diameters are standard values taken from standard fitting sizes available from Goodridge. From a machining perspective, it is more difficult to machine accurately at very small geometries, which should be kept in mind when making the design choice [2]. After reviewing the resulting nozzle geometries, it was decided to choose B: 20 degrees and d_{in}: 10 mm. These values make for a longer convergent length with a shallow angle to prevent flow detachment, as well as provide a bit larger values to make machining more feasible. The complete list of design parameters calculated in this chapter are listed in Table 7.5.

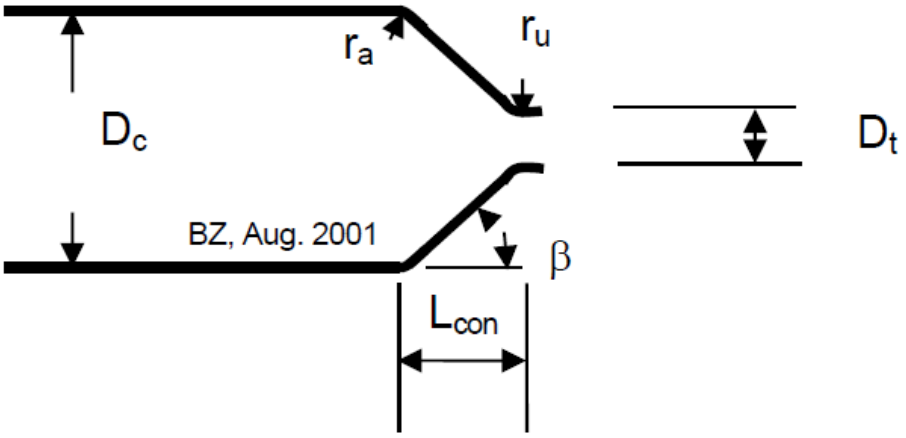

Figure 4: Schematic of chamber convergent

Figure 7.5: Convergent Nozzle Geometric Parameters

7.4. Conclusion

In this chapter the geometry of the gaseous oxygen injection nozzle was calculated, as well as the oxygen supply pressure, NPR, and igniter combustion pressure. The relationships between the gas pressure, temperature, mass flow rate and exit area for a converging, choked, isentropic nozzle were explained in detail. From Equation 7.1, one learned that for a set nozzle geometry and gas temperature, if the supply pressure is decreased, such that the nozzle pressure ratio drops below the critical pressure ratio, the mass flow rate will decrease. However, if the supply pressure is increased but the nozzle pressure ratio remains at or above the critical pressure ratio, the mass flow rate not change, because the nozzle is choked. If the nozzle supply pressure remains and gas temperature remain fixed, then if the nozzle exit area increases the mass flow rate will decrease and vice versa. If any changes are made to the design, these relationships must be considered in order to achieve a system that functions as expected. In addition, an explanation on back-flow and how to avoid it from the igniter combustion chamber into the injection nozzle was covered, in order to set an appropriate igniter combustion pressure. In Table 7.5, the GOX nozzle geometry and system pressures calculated in this chapter are listed.

Table 7.5: GOX Nozzle Preliminary Design Parameters, subscript 0 indicates total conditions

Parameter	**Symbol**	**Value**	**Unit**
Injection Nozzle Exit Diameter	D_n	3	mm
Injection Nozzle Inlet Diameter	d_{in}	10	mm
Injection Nozzle Convergent Angle	β	20	Degree
NPR, Nozzle Pressure Ratio	P_o/P_{atm}	19	
Oxidizer Injection Pressure	P_o	19.0	Bar
Combustion Chamber Pressure	P_c	8.72	Bar
Area Ratio	ϵ	11.11	
Convergent Length	L_{conv}	9.616	mm
Nozzle radius	r_u	2.25	mm
Converging Radius	r_a	1.2	mm

8

Preliminary Design: Resonance Cavity, Exhaust Orifice and Fuel Injector

In this chapter the geometry of the resonance cavity is calculated based upon the inputs of the propellant mass flow rates and GOX injection nozzle sizing from the previous chapters. The available design options and parameters are explained and then calculations performed. After the cavity is designed, the exhaust orifice is sized based upon the allowable pressure drop from the igniter combustion chamber to the main engine combustion chamber. Then a short section on the estimated sizing of the fuel injector is provided. While this tests conducted for this thesis focus on the heating of the gaseous oxygen in the resonance cavity, this section on sizing the fuel injector is included to ensure that fuel injector orifices are able to fit in the engine manifold. That said, the main focus of this chapter will be on the sizing of the resonance cavity and exhaust orifice.

8.1. Resonance Cavity

In designing the resonance cavity there are several main geometric parameters–shape, gap distance (Δ s), inlet diameter (D_{res}), end diameter (d_{end}), angle (α), and length (L)– and the calculations and choices made for all of these geometries are as follows. The resulting geometric parameters are contained in Table 8.1.

8.1.1. Resonance Cavity Shape and Geometry

There is not a clear empirical method that can be utilized in order to calculate a cavity shape, angle and length. However through much experimentation, researchers have determined which geometries are most likely to produce the highest gas dynamic heating effect. The Hartmann-Sprenger cavity can come in the classic right angle cylinder, stepped or conical shapes. Stepped cavities function similarly to conical but are easier to machine and therefore well suited for testing. Experimentation has shown that the temperature of the gas can be greatly increased by using a conical or stepped resonance cavity [50, p.814]. This is well demonstrated by Figure 3.2 which provides the results of a test that demonstrated how a stepped cavity substantially increased the temperature of the gas, when compared to a cylindrical one [13, p.100]. The conical shape of the cavity generates a higher temperature gas because the converging shape of the cavity increases the strength of the shock waves [29, p.21]. In ”Small-Scale Supersonic Combustion Chamber with a Gas-Dynamic Ignition System,” Marchan coalesces the results of a great deal of research on cavity shape, into a set of guidelines. This research also found that the conical cavity produced the highest temperature at the base of the cavity, as compared to a cylindrical shape [48, p.1244]. The tapered cavity also produced a higher temperature than the cylindrical, but lower than the conical. As the conical cavity is difficult to produce, especially at such small sizes, Marchan recommends using a truncated cone, with a very small base diameter. Based on data, it is decided to use a truncated conical resonance cavity.

The resonance cavity opening diameter should be large enough to catch the core of the under-expanded exhaust jet and located within the compression zone of the first shock cell. From experimentation, it was discovered that that the opening diameter of the resonance cavity should be equal to the

jet diameter, such that the entire under-expanded jet flows into the resonance cavity and maximizes heating. As shown in Figure 8.1, there is expansion of the flow as it exits the nozzle, resulting in a jet diameter that is larger than that of the nozzle exit. The exact relationship between the nozzle exit diameter and the jet diameter is hard to calculate because there are many factors that affect it. While there are empirical formulas that attempt to estimate the jet diameter, they are often incorrect. Therefore it is a better strategy to analyse experimental data from other HSG and resonance cavity experiments. The optimal D/d found in these experiments will provide guidance on an educated estimation of the resonance cavity diameter, D_{res} that should be used in this design. These experiments use a combination of Schieleren Imaging to define the jet diameter and full nozzle and cavity combination to detect heating for different resonance cavity diameters [48, p.1243].

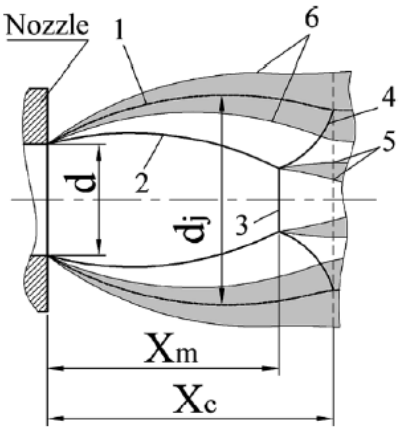

Figure 8 Structure of the first cell of an underexpanded jet. 1, Conventional (shadow) boundary of the jet; 2, oblique shock; 3, Mach disk; 4, reflected shock; 5, boundaries of the internal mixing layer; 6, boundaries of the external mixing layer.

Figure 8.1: First Cell Under-expanded Jet [48, p.1242]

The fact that this nozzle creates an under-expanded jet, means that the diameter of the resonance cavity needs to be larger than that of the exit of the under-expanded nozzle because the jet diameter is larger than the nozzle exit diameter. The resonance cavity needs to be able to capture the full jet flow. The exact relationship between the nozzle exit diameter and the jet diameter is difficult to precisely quantify, even with the empirical equations given. However from the example systems in Table 7.1, the experimental optimal D/d is between 1.2 and 1.6, where D: resonance cavity inlet diameter and d: nozzle exit diameter [48]. To save time at this point, the preliminary design will choose a value in this range that results in a machinable size. In the detailed design, ANSYS Fluent will be used to refine this value. Therefore for the preliminary design a ratio of $D/d = 1.4$ will be used. Using $D_{res}/D_n = 1.4$, for a 3mm nozzle exit results in a $D_{res} = 4.2$ mm.

Given the resonance cavity inlet diameter, the corresponding end-wall diameter can be calculated. In their experiment, Khoshkbijari and Karimi used a conical resonance cavity with an inlet diameter of 6.3mm and a cavity end wall diameter of 1.4mm [42]. This ratio of $D_{res}/d_{res} = 4.5$ is a reasonable estimation. Using this ratio, the diameter of the resonance cavity end-wall should be 0.933 mm, rounding up to the next available drill size, the cavity end-wall diameter will be set to 1 mm.

Marchan states that a number of studies found a 3 °half-cone angle to optimize the heating of the resonance cavities [48, p.1244]. This is supported by the Afzali experiment, where the cavity had a 3 °truncated half-cone angle and was able to produce sufficient heating for ignition. Regarding length, these experiments found that the gas-dynamic heating effect only became apparent when the resonance cavity length (L) to opening diameter ratio (D) of the cavity was greater than 4, L/D 4. Taking all of this into consideration, it is decided to use a truncated conical cone with a 1mm diameter base and a 3 °half-cone angle. With a 3 °half-cone angle, an opening diameter of 4.2mm, and a base diameter of 1mm, the L/D is 7.27, which is sufficient.

8.1.2. Gap Distance

The preliminary design of the resonance system has a nozzle with $\eta_o = 19$, therefore it is expected for the under-expanded jet to have the shape of the very highly under-expanded jet, in Figure 8.2. This first shock cell region, where $M \geq\geq 1$, the gas experiences an expansion, followed by a compression and then a shock. Figure 3.4 depicts these stability zones and shows that the compression zone is located just before the shock. As stated, in order to achieve heating, the opening of the resonance cavity must be contained within this unstable zone (compression region.) This distance between the nozzle exit and the resonance cavity entrance is the Gap Distance, Δ S. From Figure 8.2, one can identify the 2 main geometric parameters of the under-expanded jet, the jet diameter and the length of the first mach disk.

The gap distance, or the distance between the nozzle exit and the opening to the resonance cavity, should be chosen such that the resonance cavity opening sits within the compression region of the first shock cell. From the *Review on the Under-expanded Jet*, the chosen NPR of 19, means that this nozzle is expected to produce a Highly Under-expanded Jet [28, p.44]. This type of jet will have the features shown in Figure 8.2. In this image, it can be seen that there exists a region after that nozzle exit that ends with a vertical shock, which is also called the Mach Disk. This region, called the first shock cell comprises the region between the nozzle exit and the Mach Disk, and contains the first expansion and compression zones. The gas first expands just after the nozzle exits and then compresses until it reaches the Mach Disk, as seen in Figure 3.4.

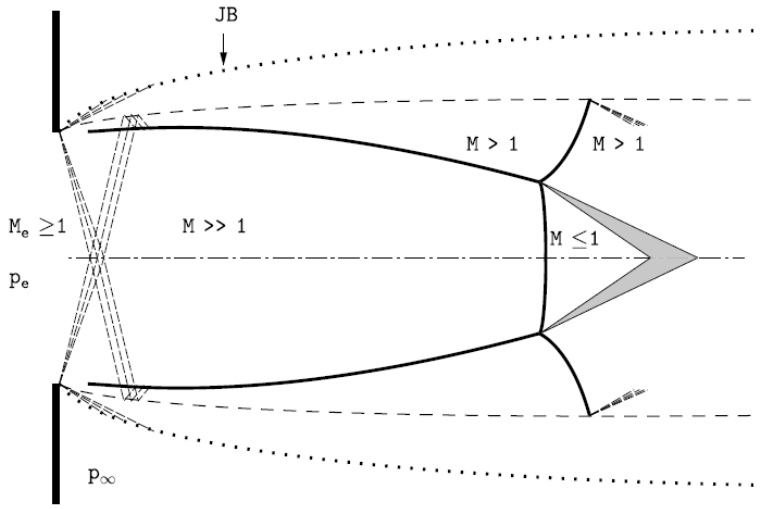

Figure 8.2: Structure of a Very Highly Under-expanded Jet (η_e ≥ 3-4, η_o ≥ 7) [28, p.44]

The location of this first Mach disk is fluid independent and mainly governed by the nozzle pressure ratio. Franquet describes a variety of empirical formulas that can be used to estimate the location of this mach disc, with the most accurate being Equation 8.1 [28, p.44]. The paper concludes that this equation is reasonably accurate and will be used to predict the initial gap distance.

$$\frac{L_{MD}}{D_e} = 0.645497\sqrt{\eta} \tag{8.1}$$

For a GOX Injection Nozzle with an exit diameter of 3 mm and a NPR,η_o: 19, Equation 8.1 predicts that the Mach Disk will be located 8.441 mm from the nozzle exit. In order to set the resonance cavity opening within the compression zone, a gap distance of 8mm will be chosen.

8.2. Exhaust Orifice Diameter

As the igniter exhaust will be ejecting gases into the extreme environment of the main combustion chamber, it runs the risk of melting in these extreme conditions. Therefore for ease of use and testing, it is decided to use a simple orifice for the igniter exhaust, as opposed to a more complex nozzle

design. This will make it easy and fast to replace the exhaust orifice if it melts during the ignition testing. The diameter of the exhaust orifice is sized to allow the necessary mass flow rate, calculated in the power section, with an acceptable pressure drop. As explained previously, it is vital to keep a positive pressure gradient in the system to avoid the backflow of hot combustion chamber gases. The pressure drop across the exhaust orifice can be calculated using Equation 8.2. For an injection nozzle with an exit diameter of 3 mm, the pressure drop for a range of orifice diameters was calculated and plotted in Figure 8.3. From the stated design constraints, due to space limitations, the maximum exhaust orifice diameter is 17mm. From Figure 8.3, it can be seen that the larger the orifice diameter, the lower the pressure drop across the orifice and the lower the velocity of the exhaust flow. Therefore from the perspective of pressure losses, it is advantageous to choose the largest possible orifice, but this comes at the cost of a low velocity flow. Therefore an exhaust orifice diameter of 12 mm was chosen, because it results in an approximately 1.74 bar pressure drop and maintains a flow velocity of 456 m/s.

$$\delta P = m_{tot}^2/(C_d^2 * A^2 * 2 * \rho) \tag{8.2}$$

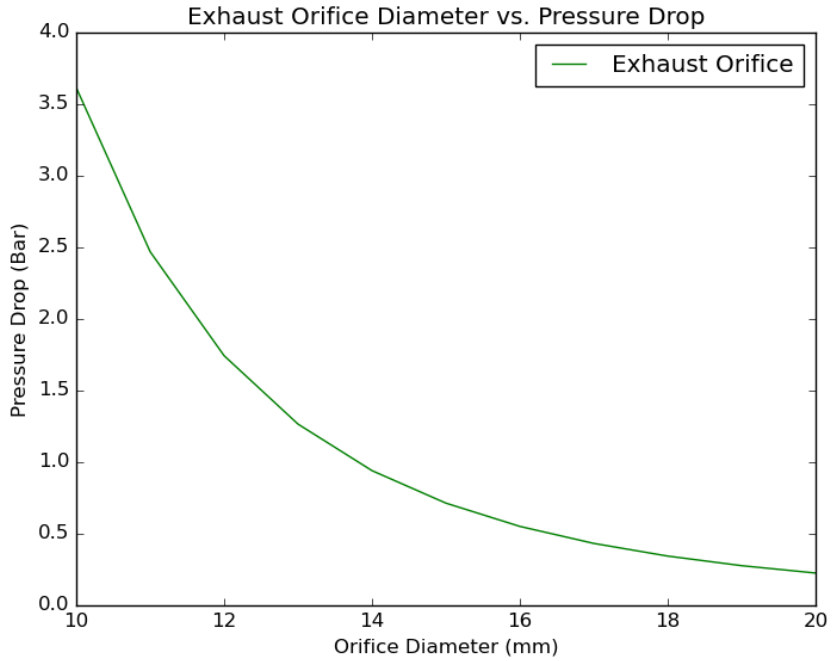

Figure 8.3: Orifice Exhaust Diameter versus Pressure Drop for 3 mm GOX Nozzle Exit Diameter

8.3. Fuel Injection

The liquid ethanol fuel will be injected into the gaseous oxygen stream through a set of small orifices. This will cause the fuel to experience a pressure drop across the injector. In order to better illustrate the relative locations of the GOX injection nozzle, resonance cavity, fuel injection holes and exhaust orifice, a schematic drawing of the igniter has been provided in the conclusion of this chapter. As stated in the requirements section, the fuel will be used to purge the system during the main engine burn, and must travel through the fuel injector and the igniter exhaust orifice. The pressure of the fuel exiting the igniter exhaust orifice must be greater than the main engine combustion pressure, to prevent backflow and protect the ignition system. In order to include some safety margin to account for losses due to manufacturing errors and such, a minimum 4 bar pressure difference between the fuel exiting the igniter and the main engine combustion pressure will be used. The main engine uses a blow down system so the combustion pressure will drop over time, but to size the fuel injector the maximum combustion pressure value will be used, see plot in Appendix H. The main engine combustion pressure is 20 bar,

which results in a minimum fuel exit pressure of 24 bar. In order to set the supply pressure of the fuel so as to achieve the stated minimum exit pressure, the pressure losses across the fuel injector and exhaust orifice must be calculated. In the python code the following equations are used to calculate the pressure drop across the injector and exhaust orifices, as well as the velocity of the fluid. These equations are taken from [66].

$$A = num * \pi * \frac{r^2}{2} \tag{8.3}$$

$$DP = \dot{m}^2/(C_d^2 * A^2 * 2 * \rho) \tag{8.4}$$

$$v = Cd * \sqrt{(2 * DP)/\rho} \tag{8.5}$$

where A: area of the injector hole, num: number of holes, r: hole radius, DP: pressure drop, $\dot{m}$: mass flow rate, Cd: discharge coefficient (0.88 for holes less than 1.5mm diameter and 0.9 for holes greater than 1.5mm diameter.), v: velocity

The size of these holes was kept small to improve the atomization of the fuel, and the exhaust size and number of holes was varied in order to achieve a low pressure drop. A selection of 3 injection holes of 1mm diameter each, resulted in a pressure drop of 2.23 bar, which is relatively low and deemed acceptable. The exhaust orifice is very large, and therefore there is a negligible pressure drop across this orifice for the fuel. Taking into account the pressure losses across the injectors and in order to ensure a positive Dp in the system during the main engine burn, and including the 4 bar margin, the Minimum Fuel Injection Pressure is 26.3 bar. The velocity of the fuel across the fuel injector holes is 21 m/s, and the velocity of the fuel across the exhaust orifice is 0.32 m/s.

8.4. Conclusion

In this chapter the design of the resonance cavity, exhaust orifice and fuel injectors was covered, as well as the consequences of changing these geometries. The different cavity shape options were covered, with the consensus from much experimentation being that the a a conical cavity with a 3 °cone-half angle was optimum. This chapter also explained how moving the location of the opening of the cavity would effect the resonance cavities heating capabilities depending on whether the opening was located in an expansion or compression zone. Then estimation on the sizing of the exhaust orifice was computed based on the allowable pressure drop between the ignition system and main engine combustion chamber. Finally a calculation of the size of the fuel injection holes was performed. The complete python script used in the full preliminary design calculations can be viewed in Appendix B and a flow chart of the code is available in Figure 5.1. The complete list of the preliminary design parameters is contained in Table 8.1 and a schematic of the location of all of the components in this system is provided at the end of this chapter. This is not to scale, and is meant to provide the reader with a sense of the relative location of all of the components. The values in Table 8.1 will be used as the inputs for the Detailed Design in the Simulation Section of this report.

Table 8.1: Resonance Ignition Device Preliminary Design Parameters, subscript 0 indicates total conditions

Parameter	Symbol	Value	Unit
Resonance Gas		Oxygen	
Fuel		Ethanol85	
Oxidizer Injection Temperature	$T_{0,ox}$	288.15	K
Fuel Injection Temperature	$T_{0,f}$	288.15	K
Minimum Required Ignition Power	P_{ign}	152.1	kW
Combustion Temperature	T_c	1960	K
Mixture Ratio	O/F	0.8	
Heating Value Exhaust	dH	2079469	J/kg
Materials			
Injection Nozzle Material	Material	SS304	
Resonance cavity Material	Material	PTFE/SS304	
Igniter Chamber Material	Material	SS304	
Mass Flow Rates			
Total Propellant Mass Flow Rate	m_o	70.12	g/s
Oxidizer Mass Flow Rate	m_o	31.165	g/s
Fuel Mass Flow Rate	m_f	38.956	g/s
GOX Sonic Injection Nozzle			
Injection Nozzle Exit Diameter	D_n	3	mm
Injection Nozzle Inlet Diameter	d_{in}	10	mm
Injection Nozzle Convergent Angle	β	20	Degree
NPR, Nozzle Pressure Ratio	P_o/P_{atm}	19	
Oxidizer Injection Pressure	P_o	19.0	Bar
Combustion Chamber Pressure	P_c	8.72	Bar
Area Ratio	ϵ	11.11	
Convergent Length	L_{conv}	9.616	mm
Nozzle radius	r_u	2.25	mm
Converging Radius	r_a	1.2	mm
Resonance Cavity			
Resonance Cavity Shape	Shape	Conical-Truncated	
Resonance Cavity Inlet diameter	d	4.2	mm
Resonance Cavity end diameter	d_e	1.0	mm
Resonance Cavity Angle	α	3	degrees
Resonance Cavity Length	L_{res}	30.53	mm
Resonance cavity wall thickness	t_w	1.0	mm
Gap Distance	ΔS	8	mm
Exhaust Orifice			
Exhaust Orifice Diameter	d_{exh}	12.0	mm
Exhaust Pressure Drop	ΔP_{exh}	1.74	Bar
Exhaust Velocity	v_{exh}	456	m/s
Fuel Injector			
Fuel Injection No. Holes		3	
Fuel Injection Hole Diameter	1.0	mm	
Fuel Injection Pressure Drop	ΔP_f	2.23	Bar
Fuel Injection Velocity	V_f	21	m/s
Fuel Exhaust Pressure Drop	ΔP_f	0.0009	Bar
Fuel Exhaust Velocity	V_f	0.32	m/s
Minimum Fuel Supply Pressure	$P_{f,min}$	26.3	Bar

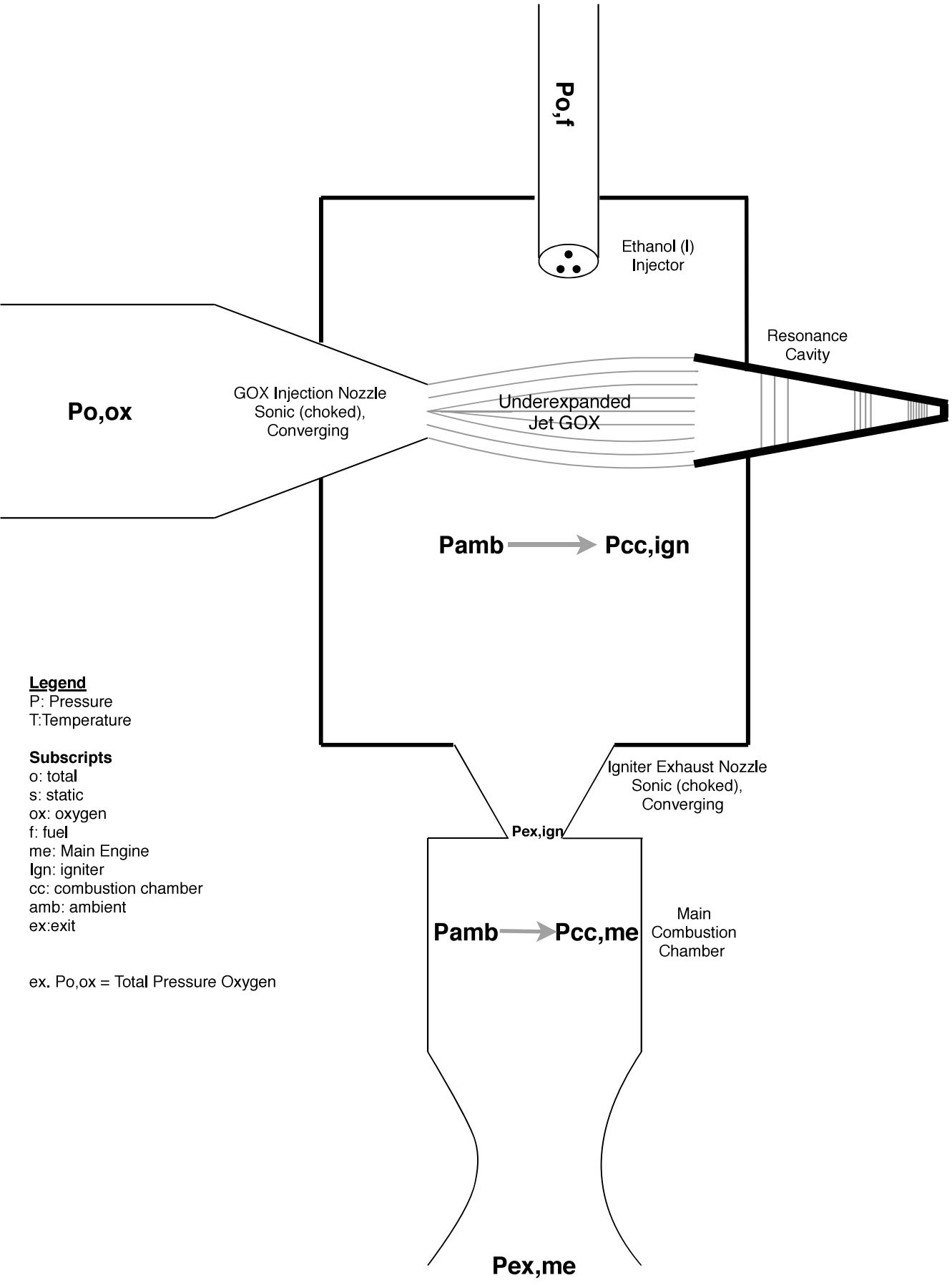
Po,f
Ethanol (l)
Injector
Resonance
Cavity
Po,ox
GOX Injection Nozzle
Sonic (choked),
Converging
Underexpanded
Jet GOX
Pamb
Pcc,ign
Legend
P: Pressure
T:Temperature
Subscripts
o: total
s: static
ox: oxygen
f: fuel
me: Main Engine
Ign: igniter
cc: combustion chamber
amb: ambient
ex:exit
ex. Po,ox = Total Pressure Oxygen
Igniter Exhaust Nozzle
Sonic (choked),
Converging
Pex,ign
Pamb
Pcc,me
Main
Combustion
Chamber
Pex,me
Pamb
Pamb

9

Simulation: Setup and Strategy

In order to characterize the physical behavior of this system, 2 types of numerical analyses were conducted. The first, labeled 'Nozzle-Steady,' is a steady simulation of the under-expanded jet outflow of a converging nozzle. This case serves to characterize the shape of the shock cell formed at the exit of the nozzle, in order to provide information regarding the placement and sizing of the cavity. The results of the 'Nozzle-Steady' simulation are used to make adjustments to the preliminary design before it is input into the following simulation. The second set of cases, labeled 'Cavity,' model the flow of the under-expanded jet from the nozzle into the resonance cavity. In this chapter the introduction to all of the simulation cases is given, covering the simulation strategy, background on setting up the geometry and mesh, the governing equations and turbulence models used and additional flow solver information.

9.1. Goals and Strategy

The goal of the 'Cavity' simulations are to demonstrate if the temperature of the gas at the base of the resonance cavity rises above the auto-ignition temperature of the fuel, when the system has reached a steady state. The idea being that in a physical system the GOX would be directed into the cavity for a few seconds in order to allow the gas in the base of the cavity time to heat up. This means that it is not necessary to simulate the detailed periodic flow of the gas in the cavity, but only to model the change in temperature at the base. The assumption is made that if significant heating occurs at the base of the cavity, then the gas dynamic heating effect of the resonance cavity has occurred. To model the transient oscillations of the gas in the cavity would require a very large amount of computational power and time, which is beyond the scope of this thesis. Therefore, after much experimentation and numerous meetings with Dr. Ir. A.H. van Zuijlen, it was decided to use the following approach which provides all the necessary data in a manageable amount of computational time. For these cases a coarse mesh was used, which has the disadvantage of loss of accuracy, but the advantage of a much faster is computational time. The coarseness of the mesh was adjusted many times in order to find a balance of these factors and choose a mesh that provided a reasonable amount of accuracy and computational time. As the heating of the gas is caused by periodic oscillations of the gas in the cavity, it is not possible to find an accurate steady solution for this case, and therefore a transient solver is required. However in order to save time, a strategy of beginning with a steady solver and then ending with a transient solver was used. The steady solver is able to very quickly solve the full domain and find a result that is somewhat near the actual solution, which is then used as the initialization for the transient solver, which can then solve for an accurate solution. The full strategy on the meshing and solver are described further in subsection 9.6.2 . The 'adjusted preliminary design' is the first case run in this section. After reviewing the results, a set of cases were derived in which different parameters were adjusted to see how they effected the heating. Finally, after analysing all of the results, the Detailed Design is presented and recommendations are given.

For these cases, 2 geometries were generated. The first geometry contained a nozzle and fluid domain, and was used for the 'Nozzle-Steady' case. The second geometry contained a nozzle, cavity and fluid domain, and was used for the 'Cavity' cases. Information on the setup of the geometries and meshes is contained in chapter 11. All of the cases used the same solver setup, apart from the

time component, which varied based on whether the case was steady or transient. Therefore the information described in this chapter applies to all of the fluent simulations conducted. These numerical simulations were conducted using ANSYS Fluent, which is a tool that performs a numerical simulation using the finite volume method. In order to perform a numerical simulation, a geometry with a mesh input is required. This mesh must be constructed in such a way that optimizes the simulation, improves convergence, and prevents numerical errors that can lead to solver divergence. In order to provide guidance on the creation of these simulations and to provide cases with which to use as verification of the results in this paper, a set of research papers that feature numerical simulations and, in some cases, experimental results of resonance cavities were consulted. References are made to these papers throughout the simulation chapters and more information on these cases can be found in the full papers [51] [52] [53] [7] [6] [11] [10] [50]. In this chapter the major aspects of setting up a mesh and numerical simulation are detailed. In ANSYS Fluent, the user must first define a geometry, then apply a suitable mesh, and finally set up the solver with the given models, boundary conditions, and initial conditions, among other parameters. There are many options in all of these sections, dependant upon the flow conditions, and in this chapter a brief overview of the main Fluent parameters is provided. This covers the many optional choices the user has in setting up a mesh and solver, but focuses on those choices that are most applicable to the simulations conducted in this thesis. It also provides explanations into why certain choices were made in setting up the case. The following chapters then detail the specific setup and results of the cases conducted for this thesis.

9.2. Geometry Definition and Mesh Generation

First the user must define the geometry. All cases considered in this study are 2D-axisymmetric, with the x-axis as the axis of rotation, as necessitated by the ANSYS Fluent User's Guide [8, p.128]. While in reality there will be some 3D effects due to turbulence in the flow, a 2D axisymmetric case provides a reasonable estimate of the flow characteristics at a much lower computational cost, as stated by numerous other researchers who have performed similar types of simulations [42] [6] [50] [10]. Fluent utilizes a finite volume method, which means that the computational domain is divided into finite volumes. The solver than applies the conservation laws and solves for the flux balance at each finite volume and the final solution is comprised of the averages of these finite volumes [36]. In order to define these finite volumes, the geometry must be divided into a grid or mesh. When choosing how to build the mesh, the user must consider the complexity of the geometry and have some understanding of the expected flow pattern and flow direction. Fluent allows for two types of meshing—structured and unstructured–which are shown in Figure 9.1.

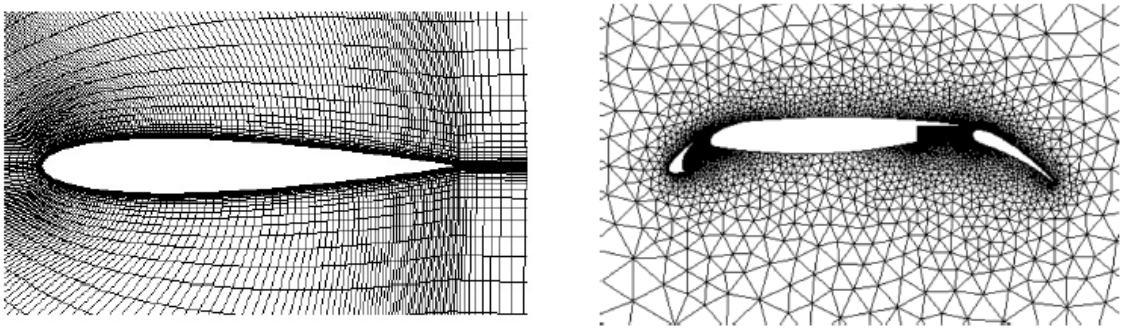

(a) Structured Mesh [36]

(b) Unstructured Mesh [36]

Figure 9.1: Structured and Unstructured Meshes [36]

In a structured mesh all of the cells are similar in topology and are connected in the same manner. Structured meshes are majority rectangles for 2D and hexahedrons for 3D, and can be projected onto a Cartesian domain. Unstructured meshes can have any type of topology which can be very different from other cells in the grid, and there are no rules for how these cells are to be connected. Their shape is mostly triangles for 2D and tetrahedrons for 3D, and their domain can usually not be projected onto Cartesian domains. Meshes can be either structured, unstructured or have a combination of both. Structured meshes are simple, have high quality control and are useful for simple geometries with

flow in a known direction. Unstructured meshes are more complicated and computationally intensive, but are useful for a complex geometry and/or flow pattern because they are very flexible. Structured meshes offer the advantage of reducing the effect of numerical diffusion because their cells can align with the flow direction and produce very accurate results along boundary layers [36]. For the cases in this thesis, the geometry is simple which makes it easy to generate a high quality structured mesh. However the flow pattern is expected to be very turbulent and nonuniform, In the 'Cavity' cases, the flow will form shocks in the exhaust, and is expected to move in the x-direction from the inlet into the cavity, oscillate along the x-axis within the cavity, and then exit the cavity and move in the y-direction towards the outlet/farfield boundaries. For cases when the flow direction is uniform and predictable along boundary layers, it is necessary to include a bias in the mesh along the walls, with a $y+$ value near 1. However in cases where the flow pattern is very turbulent and nonuniform, a very refined mesh in the wall regions can cause divergence in the solver, and therefore it is recommended to use a uniform structured grid for these types of flows. That being said, the nozzle exit and nozzle-cavity region of the domain is the region of interest with a complex flow patterns and shock waves, which require a refined mesh. Whereas the region in the farfield domain away from the cavity does not experience much complex flow and can utilize a coarser mesh. Therefore a structured mesh with a more refinement in the nozzle-cavity region, that then smoothly transitions to a coarser mesh in the farfield domain is used. This type of meshing was used in similar studies by Murugappan and Narayanan, and can be seen in Figure 9.2. In addition this meshing strategy was discussed and validated with Dr. Ir. A.H. van Zuijlen, an Assistant Professor in the TU Delft Aerospace Engineering Aerodynamics group.

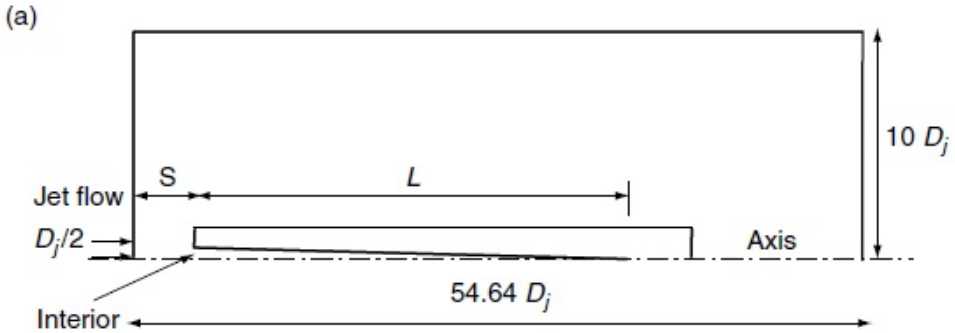

(a) Computational domain and boundary conditions, (b) Computational grid adopted for the current simulation.

Figure 9.2: Narayanan Grid

9.3. Mesh Quality

In order to guarantee that a numerical computation will be accurate and stable, it is necessary to maintain a certain level of quality of the mesh. When building a structured mesh, there are 4 quality factors that can be assessed to judge the quality of the mesh. These factors are Element Quality, Aspect Ratio, Skewness, and Orthogonal Quality. In order to be able to state with confidence that the results of the simulation are accurate, the mesh quality factors should be within the ranges described.

9.3.1. Element Quality

A structured mesh has the highest Element Quality when all of its cells are orthogonal and square. The orthogonal quality, skewness and aspect ratio factors describe each of these, while the Element Quality aggregates all of the quality factors into a single value. For a structured mesh, the closer the Element Quality is to 1, the better. However due some areas having higher refinement and unorthogonal geometric shapes, it is not possible to achieve an Element Quality of 1. Therefore after a discussion with Weibo Hu, a TU Delft PhD student in the Aerodynamics group, a minimum Element Quality of 0.75 was set.

9.3.2. Aspect Ratio

Aspect Ratio is used to describe how stretched a cell is[8, p.130] . In the case of a 2D mesh, an Aspect Ratio of 1:1 means that the width and height of the cell are equal, and it is a square. As the cell becomes lengthened into a rectangular shape, the ratio between the width and height of the cell increases, increasing the Aspect Ratio. Figure 9.3a visualises how the Aspect Ratio is calculated. It is important to note that the Aspect Ratio is always above 1, which is achieved by placing the larger value on the top of the fraction. This way the Aspect Ratio describes how far away from square the shape of the cell is, regardless of whether the width or height has been increased. When the Aspect Ratio of a cell becomes very large, it can cause numerical errors and instabilities. Therefore the official ANSYS Fluent guide states that, in general, it is recommended to maintain an Aspect Ratio of maximum 5:1 for the bulk fluid regions, and 10:1 for the wall, boundary layer regions [40]

9.3.3. Skewness

For a tetrahedral mesh, skewness is used to describe the difference between a theoretical perfectly square cell, whose vertex angles are all $90°$, and the actual cells which may be rectangular with vertex angles greater or less than $90°$ [8, p.132]. In a 3D mesh the skewness describes a difference in volume, and in a 2D mesh it describes a difference in cell area. Figure 9.3b shows the difference between a perfect cell and a highly skewed cell, and describes the equation to calculate skewness. The larger the value the more skewed the cell is, and therefore it is desirable to have a very low skewness. A high skewness can make it difficult or impossible for the solver to converge. The official ANSYS Fluent guide recommends that the maximum skewness be below 0.95 and the the average be below 0.33 [40].

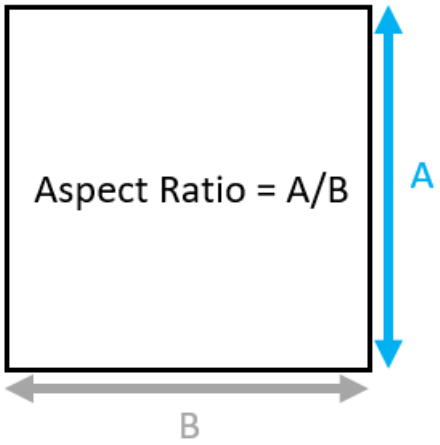

(a) Aspect Ratio 2D Cell

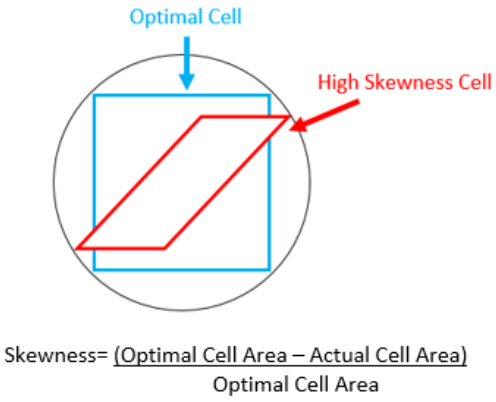

(b) Skewness 2D Cell

Figure 9.3: Aspect Ration and Skewness

9.3.4. Orthogonal Quality

The orthogonal quality of a mesh describes how near the angle between the adjacent cells are to $90°$. An orthogonal quality near 1 indicates high orthogonality, and a value near 0 indicates poor orthogonality. It is desirable to have an orthogonal quality close to 1. Orthogonal quality is calculated using

the equations and vectors shown in Figure 9.4. The first equation is the normalized dot product of the area vector ($\vec{A_i}$) and the vector from the cell center to the center of the face ($\vec{f_i}$). The second equation calculates the dot product of the area vector and a vector from the center of the cell to the center of an adjacent cell ($\vec{c_i}$) [8, p.130].

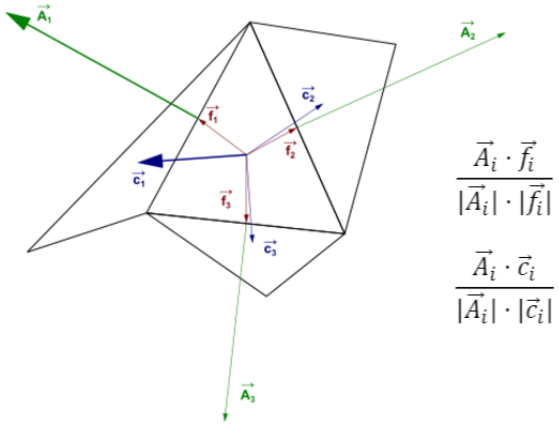

Figure 9.4: Orthogonality, vectors used to compute the orthogonal quality and equations [8, p.130]

9.4. Governing Equations

These cases feature compressible, turbulent flow, which means that the flow contains fluctuating quantities including velocity fields, energy, and momentum. It is impractical to attempt to directly calculate these fluctuations as they can be very small and occur at a high frequency. Therefore ANSYS Fluent uses governing equations which drastically decrease the computational load of these calculations, by using different methods to eliminate the very small scale fluctuations that are expensive to calculate [37]. ANSYS Fluent has many different turbulence model options, which have different strengths and weakness. This means that one must consider many factors in choosing which turbulence model is best suited to the specific application. The main tradeoff is between resolution of the model and computational expense [27]. While there is no way to say for certain which model will work best in advance, there are strategies that can be used to narrow down the choice of models to those that perform well under the conditions of the case.

The Fluent governing equations belong to two major categories–Reynolds-Averaged Navier Stokes (RANS) and Large Eddy Simulations (LES). The RANS equations utilize the full range of turbulence scales to generate average flow quantities. The use of averaged quantities greatly simplifies the solver and lessens the computational expense. RANS models are typically 2D, coarser than LES models, and are often used for steady cases or transient cases with a low number of time-steps [37]. The LES model computes large eddies using a time-dependent simulation and filtered Navier-Stokes equations. This makes for a more accurate solution, but has a much greater computational cost, as opposed to the RANS models. The LES model is used for 3D geometries, with a higher level of refinement and many more timesteps than RANS models [37]. As the cases in this thesis are 2D and the focus is more on the changes in temperature and pressure, as opposed to generating a very detailed model the flow pattern, the RANS models are sufficient. Therefore in order to save time and computational energy, a RANS turbulence model will be chosen for all the simulations in this thesis [40, section 4.2.1]. As stated, in the RANS model, the Navier Stokes equations are computed using the averaged values for each of the fluctuating quantities, including velocity, pressure, and energy. Equation 9.1 shows the equations used to calculate the mean values foe each of these quantities, where $\overline{u}_i$: mean component, u_i': fluctuating components ($i = 1, 2, 3$). The equations were found in the "Reynolds-Averaged Navier-Stokes: RANS" lecture slides from the TU Delft *CFD for Aerospace Engineers* course, which can be viewed if a a further explanation of these equations is required [38].

$$u_i = \overline{u}_i + u_i' \tag{9.1}$$

In the RANS model it is assumed that momentum, mass and energy are conserved, which is a valid assumption for both incompressible and compressible flows. The general equations for the conservation of mass is written in Equation 9.2, and the equation for conservation of momentum in an inertial reference frame is in Equation 9.3 [40, section 1.2].

$$\frac{\delta\rho}{\delta t} + \nabla \cdot (\rho\vec{v}) = S_m \tag{9.2}$$

$$\frac{\delta}{\delta t}(\rho\vec{v}) + \nabla \cdot (\rho\vec{v}\vec{v}) = -\nabla p + \nabla \cdot (\bar{\bar{\tau}}) + \rho\vec{g} + \vec{F} \tag{9.3}$$

where p: static pressure, $\bar{\bar{\tau}}$: stress tensor, $\rho\vec{g}$: gravitational body force, $\vec{F}$: external forces.

Using these equation of continuity, but replacing the instantaneous quantities with the mean values calculated with Equation 9.1 and assuming a 2D, axisymmetric geometry, results in the following 2 RANS equations, written in their Cartesian form [40, section 4.2.2].

$$\frac{\delta\rho}{\delta t} + \frac{\delta}{\delta x_i}(\rho u_i) = 0 \tag{9.4}$$

$$\frac{\delta}{\delta t}(\rho u_i) + \frac{\delta}{\delta x_j}(\rho u_i u_j) = -\frac{\delta p}{\delta x_i} + \frac{\delta}{\delta x_j}\left[\mu\left(\frac{u_i}{x_j} + \frac{u_j}{x_i} - \frac{2}{3}\delta_{ij}\frac{u_l}{x_l}\right)\right] + \frac{\delta}{\delta x_j}(-\rho\overline{u_i' u_j'}) \tag{9.5}$$

9.5. Turbulence Models

The RANS governing equations have around a dozen different turbulence models, which are split into Eddy Viscocity Models (EVM) and Reynolds Stress Models (RSM) [38]. The EVMs are based on 0-equation algebric or one or more transport equations, and the RSMs are based on nonlinear EVMs or full RST with additional transport equations. EVMs are simpler than RSMs, which means that they are less accurate but much quicker to solve. This thesis work does not require the detailed results provided by RSMs, and therefore they will not be discussed. The algebraic EVMs are not suitable for internal flows with boundary layers, whereas the transport equations were designed to handle these types of flows. As the cases in this thesis are internal flows with boundary layers, the EVMs with transport equations will be used. A quick explanation of each type and a recommendation on which model is model is most suitable is given below [38].

9.5.1. k-epsilon model

The $k-\epsilon$ model is a 2-equation RANS model, and is widely used in industry. It is computationally efficient because it only uses 2 transport equations and performs well for external flows. The TU Delft CFD course does not recommend using this model for large pressure gradients or flow separation [38]. That being said, the vast majority of numerical simulations of resonance cavities reviewed for this thesis utilized the $k-\epsilon$ model.

9.5.2. k-omega model

The $k-\omega$ model is also a 2-equation RANS model that is widely used in industry. It is computationally efficient because it only uses 2 transport equations and it is provides good results for flows with pressure gradients, separation and along boundary layers. It it highly sensitive to the boundary conditions set at the inflow and freestream, which is why the $k-\epsilon$ model is preferred for external flows. [38].

9.5.3. Spalart-Allmaras model

The Spalart-Allmaras 1-equation model is a very robust model that was designed for aerospace applications and performs well in cases that contain wall-bounded flows and/or large pressure gradients [40, section 4.3.1] [52, p.569]. It was designed to combine the best features of the $k-\epsilon$ and $k-\omega$ models. In addition it is a a simple model with only one-equation which makes it computationally efficient [38]. This model is less sensitive to numerical errors as compared to the k-ϵ and k-ω models.

9.5.4. Turbulence Model Choice

As stated, it is impossible to be certain which turbulence model will perform most accurately for the given case. However a turbulence model was chosen after evaluating the performance characteristics of the given models, as well as reviewing which models were used by all of the numerical simulation of resonance cavities reviewed for this thesis. All of the other works used either the $k-\epsilon$ or Spalart-Allmaras model, with the vast majority using the $k-\epsilon$ model. The most robust way to choose a model would be to run cases with all options and compare accuracy, which can be done for a future paper that continues this work. However due to time constraints it was decide to use the $k-\epsilon$ model, as it was the most used model for resonance cavity numerical analyses and it has proven to be a very accurate model for this type of case.

9.6. Flow Solver

9.6.1. Pressure and Density Based

There are two numerical methods available in Fluent, pressure-based and density-based. The pressure-based solver was originally designed for use on low-speed incompressible flows and the density-based solver was designed for high-speed compressible flows. However, since their created these solvers have both been greatly adjusted to allow for more widespread use. This means that the pressure-based solver can be used for high-speed compressible flows in the ANSYS Fluent 18.0 version [40]. Both methods use the momentum equations to generate the velocity fields. The difference between the solvers is that the pressure-based solver creates the pressure field by solving a pressure equation derived from the equations of continuity and momentum, whereas the density-based solver calculates the pressure field using the equation of state and calculates a density field using the continuity equation. More information on the specifics of each solver can be found in the ANSYS Fluent Theory Guide 12.0, section 18.1 Overview of Flow Solvers [40, section 18.1]. The ANSYS Fluent theory guide recommends using a density-based solver for compressible flows, and all of the papers on numerical simulations of resonance cavities reviewed for this thesis used a density-based solver. As such, a density-based solver will be used for these cases. In additional the energy equation must be turned on, and the working fluid, gaseous oxygen, should be set to an ideal gas.

9.6.2. 'Cavity' Cases: Steady-Transient Hybrid Model

Numerical simulations can be solved as either steady or transient problems. Steady cases only discretize spatial values and work to generate a solution at equilibrium. They are much less computationally intensive, as compared to transient cases. Transient problems add a 4th dimension, time, to the simulation and are parabolic. This means that they are useful in demonstrating flows that are naturally parabolic in nature. The case resets to the initial values at the beginning of each time step while inputting information from the previous time step to help the solver move towards a parabolic convergence, which means that the values oscillate around an average value. The gas dynamics of a resonance cavity exhibit parabolic behavior, since the gas oscillates in the cavity. As such, the majority of the papers on the numerical simulation of resonance cavities use a transient model to simulate the oscillating flow in the cavity. The transient model is useful if the researcher wants a detailed model of the movement of the gas in the cavity, however it comes at a very high computational cost. These transient cases often require very small time-steps and take a large number of iterations just to converged to a steady periodic state. For example in the paper, "Numerical investigation on thermo-acoustic effects and flow characteristics in semi-conical Hartmann–Sprenger resonance tube" by Afzali, for their transient model a time step of $2e-08$s was used, which required 1,000,000 time steps to model 0.018 seconds of flow[6]. The first 0.004 seconds of this run, which required 200,000 time steps, was spent on converging to the periodic flow. An attempt was made to run a model like this on an HP z-book with 4 parallel processors, to estimated how long such a case would take to run. With a very refined mesh, it was able to solve 2 iterations per minute, meaning that it would take around 500,000 minutes or 8,333 hours. This is an infeasible amount of time and out of the scope of this project.

The ANSYS theory guide details examples of transient cases, in which a steady case is run first in order to help the solver converge [41]. This allows the solver to skip over a large part of the initialization time that would be required if it was run purely transient and is a strategy to save computational time. As stated, the function of the 'Cavity' simulations are to demonstrate if the temperature of the gas at the base of the resonance cavity rises above the auto-ignition temperature of the fuel, when

the system has reached a steady state. However it is not accurate to attempt to model the temperature at the base using *only* the steady solver. This is because of the nature of this case and the method that the steady solver uses in an attempt to reach convergence. This case features periodic flow of gas in the cavity, meaning there will never be a constant (steady) solution. The pressure, temperature and velocity of the gas will vary due to these oscillations. Therefore the steady solver will never be able to reach a convergence. In its attempt to find a solution, the steady solver makes a series of guesses on the values of the pressure/temperature/velocity/etc. at every cell in the domain. That is why the plots of pressure, temperature and velocity at different points in the flow vary widely in the early iterations of the flow, but as the solver gets closer to the actual value, the amplitude of these oscillations decreases. However, as stated the steady solver will never be able to fully converge and therefore the final value it finds will be near the actual solution, but cannot be trusted to be accurate. This is why a transient solver must also be used. It is true that a transient solver could be used for the entire simulation, but his would add a extremely long computational time for initialization. In Figure 9.5 the plot of pressure and temperature versus time at a point in the cavity are shown from a transient simulation of a similarly sized nozzle-cavity system by Afzali [6]. In this plot the values are chaotic for the first 0.003s, and then the oscillate around a mean value for the rest of the time. This chaotic 0.003s is the initialization of the solver. The nice periodic section after that is where the solver has converged and the actual pressure and temperature values at this point are the average value of these oscillations. Based on the oscillation frequency, it can be seen that one full cycle of the gas in the cavity takes approximately 0.0004s for a 48mm long cavity. This means that the time for initialization is an order of magnitude longer than the actual cycle time. Solving this initialization time in the transient solution would take an excessive amount of time. Using a steady solution as the initialization for a transient case is common practice and saves a great deal of computational time. Therefore the 'Cavity' cases will first be run steady, until all of the values are relatively static. Then these steady results will be used to initialize a transient solver which will be run for approximately 2 cycles of the gas in the cavity. As the mesh used in this thesis is much coarser and with larger time-steps that that used by Afzali, it is unable to model the full transient behavior of the domain parameters (pressure, temperature, velocity, etc.) However it is able to calculate the average values, which is sufficient to determine if the temperature at the cavity base meets requirements. Therefore we should expect that in the transient portion of the solution, the values will vary, but with a much smaller amplitude, as compared to Afzali. In order to keep the workload manageable, it was decided to use this strategy of running the simulation as a steady case first to speed up the initialization, and then run the transient case [41]. This strategy will be referred to as the 'steady-transient hybrid model.'

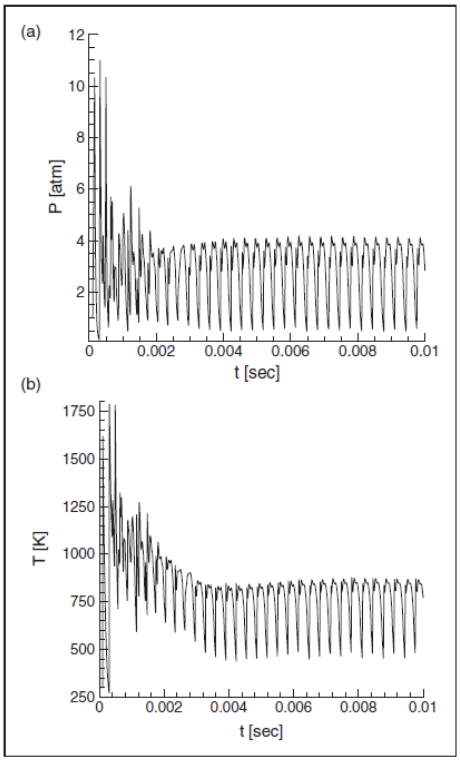

Figure 5. Simulation results for flow properties vs time at point P_4: (a) pressure, (b) temperature.

Figure 9.5: Pressure and Temperature versus time at P2 in Afzali cavity, transient case [6]

9.7. Solution Methods and Controls

For the Solution Methods, an implicit time marching method with a Roe-FDS flux type was used. For the Spatial Discretization factors, the Least Squares Cell Based Gradient and Second Order Upwind is used for the flow, turbulent kinetic energy, and turbulent dissipation rate. A Second Order Implicit transient formulation is used. These are all set to 2nd order because it will better resolve the shock

regions, as compared to the first order method.

In the Solution Controls a Flow Courant Number of 0.9 is used. The size of Courant number is directly proportional to the solver time-step. This low Courant number was chosen to improve stability of the solver and prevent divergence. Due to the adverse pressure gradients formed by the shocks in these cases, very small time-steps are required to properly resolve these regions and prevent divergence, which is why a very small Courant number is used. In addition, to mitigate instabilities caused by the presence of large pressure gradients in the shock region, Gradient Adaption is used, in which cells are refined and coarsened around large pressure gradients dynamically during the calculation. In this case the cells are adapted every 10 intervals using the Gradient Method and Scale Normalization, with a maximum of 60,000 cells. The solver requires initialization and the setup of boundary conditions for the full domain. Details on these, as well as the data gathered for each of the cases are covered in the next chapter.

9.8. Conclusion

This chapter served to outline the set of the numerical simulations conducted in this thesis, present the goals of each of these cases, and explain the strategy used to define this set of simulations. It then provided an overview of the most important aspects of setting up these simulations–geometric definition, mesh generation, and solver inputs. These sections described the many option available and explained why certain options were selected for this specific study. Finally is provided some detailed information on the meshing and solver setup, that is applicable to all numerical simulations performed in this thesis. In the next 3 chapters, the geometry, meshing, and solver setup for all of the numerical simulation cases are described, followed by a description of the cases run and ending with a presentation and analysis of the results. First the 'Nozzle-Steady' case was run to characterize the geometry of the under-expanded jet. The results from this were used to make adjustments to the preliminary design, regarding the location and geometry of the resonance cavity. The parameters of this 'adjusted preliminary design' are listed in Table 10.4, and these are the inputs used in the initial 'Cavity' simulations. After performing a mesh refinement study and validation of the 'Cavity' mesh and solver, a set of alternative designs are tested. These are used to test whether changing certain parameters effects the gas-dynamic heating process. Upon reviewing the results of all of the 'Cavity' tests, a Detailed Design is presented which is the design that achieves the highest gas dynamic heating. As the setup of the 'Cavity' cases require the results of the 'Nozzle-Steady' case, the next 3 chapters will be presented in the following manner for clarity. First the setup and results of the 'Nozzle-Steady' case will be presented. This chapter will conclude with a table of the 'adjusted preliminary design' parameters, Table 10.4. Then in chapter 11, the setup of the 'Cavity' cases will be presented. An analysis of these results will be discussed in detail in chapter 12.

10

Nozzle-Steady Simulation: Setup and Results

In this chapter the setup and results of the 'Nozzle-Steady' Simulations is covered. This includes the geometry definition, meshing strategy and solver setup. The results of this case are then presented and analyzed with the goal of better understanding the shape of the nozzle jet flow. With this additional information on the geometry of the nozzle jet flow, adjustments can be made to the preliminary design in order to improve its performance.

10.1. Geometry

All cases in the simulations were 2D and axisymmetric. Figure 10.1 displays the geometry of the 'Nozzle-Steady' case with the dimensions and boundaries labeled. Table 10.1 details the value of the dimensions in this geometry. The shape of the 'Nozzle-Steady' case was kept simple with only a converging nozzle and a large fluid domain for the exhaust. The width and height of the outlet region were made large to prevent the outlet from effecting the the nozzle exhaust flow [50] [52] [6].

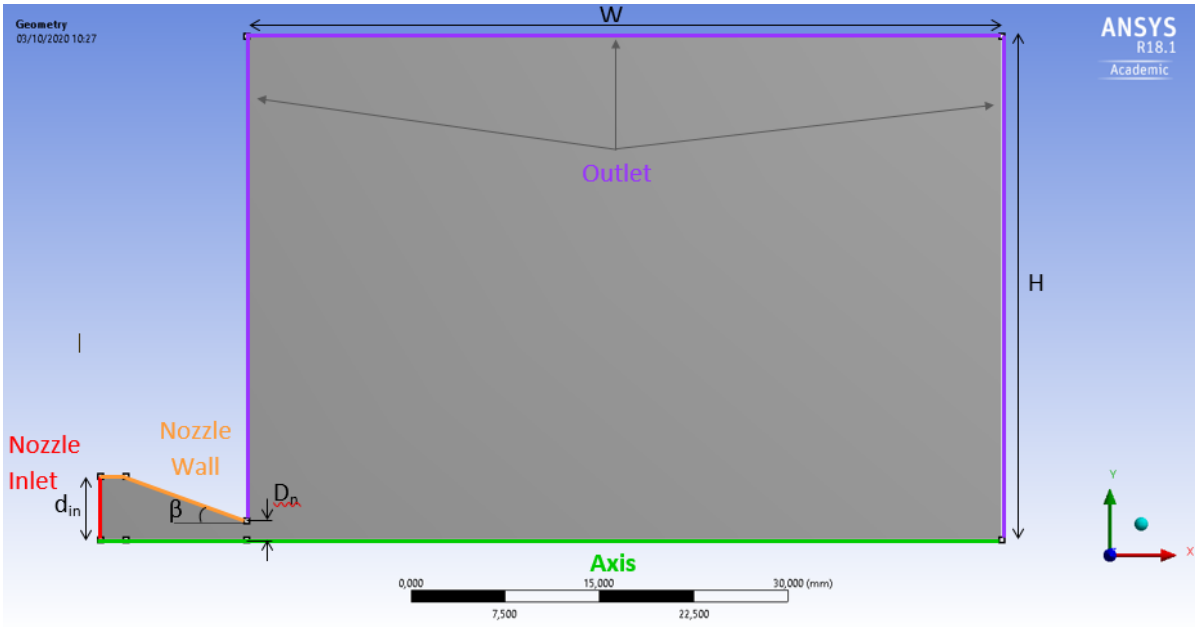

Figure 10.1: 'Nozzle-Steady' Geometry Labeled, 2D axisymmetric

Table 10.1: 'Nozzle-Steady' Geometry Dimensions

Dimension	Symbol	Value	Unit
Injection Nozzle Inlet Diameter	d_{in}	10	mm
Injection Nozzle Exit Diameter	D_n	3	mm
Injection Nozzle Convergent Angle	β	20	Degree
Fluid domain Height from x-axis	H	40	mm
Fluid domain Width from y-axis	W	60	mm

10.2. Mesh

The major decisions that are made when generating a mesh are the type of mesh, sizing, quality and level of refinement. As explained in section 9.2, all cases in this thesis were meshed using a structured, rectangular mesh. The mesh was more refined in the nozzle exit region and coarser in the far away fluid domain. The cells in the fine and coarse regions were relatively uniform in size, with a smooth transition between the fine and coarse regions. When deciding how to setup make the mesh, the works of Murugappan, Narayanan and Afzali, which have similarly sized and shaped computational domains, were examined to provide guidance [50] [52] [6]. Images of the full mesh and a closer view of the refined region are given in Figure 10.2 and Figure F.1. The mesh details are included in Appendix F.

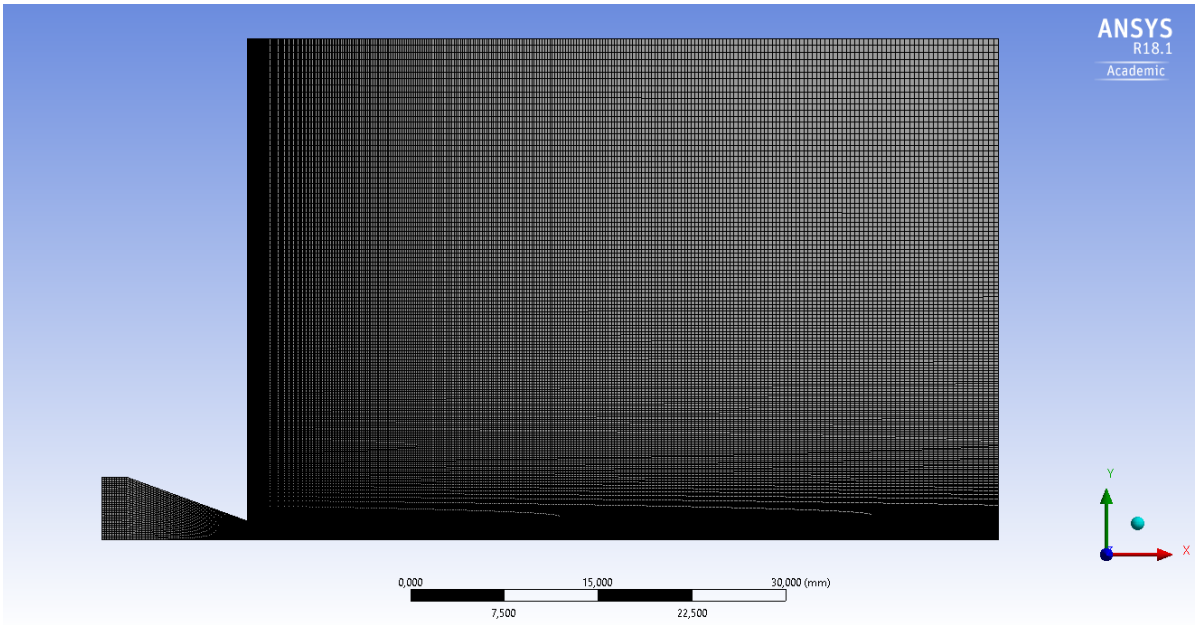

Figure 10.2: 'Nozzle-Steady' Full Mesh

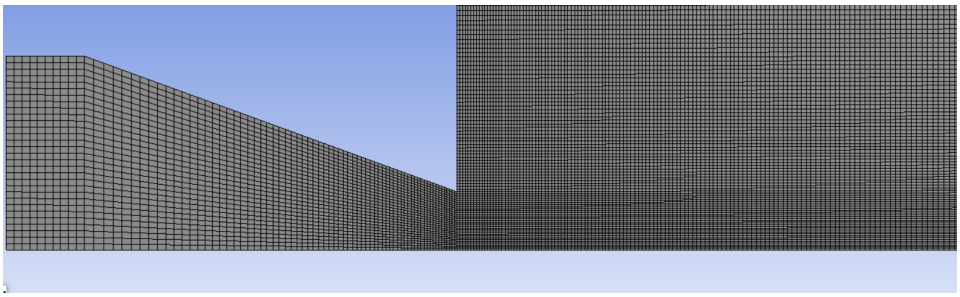

Figure 10.3: 'Nozzle-Steady' Mesh, zoom in nozzle-gap-cavity region

Table 10.2: 'Nozzle-Steady' Mesh Quality Factors

Quality Factor	Value
Element Quality	
Average	0.7617
Stnd. Deviation	0.21
Aspect Ratio	
Max	8.9957
Average	2.3778
Stnd. Deviation	1.3807
Orthogonal Quality	
Average	0.99928
Stnd. Deviation	5.126e-03
Skewness	
Max	0.22222
Average	4.6625e-03
Stnd. Deviation	2.4177e-002

10.3. Solver Setup

The main parameters of the solver setup are the same for the 'Nozzle-Steady' and 'Cavity' cases, apart from the transient component of the 'Cavity' simulations. Therefore the information provided here can also be applied to the 'Cavity' simulations, with the transient inputs and any other differences described in chapter 11. The final setup of the solver was derived after reviewing other resonance cavity numerical simulations, running many tests with different options and finding that the setup presented here was able to run smoothly without diverging, and provided results that matched predictions. A density-based, axisymmetric, steady case was set up with the energy equation turned on. The k-epsilon, realizable turbulence model with enhanced wall treatment was used. As this is compressible flow the working fluid, gaseous oxygen, was set to an ideal gas. An implicit, Roe-FDS time method was used with 2nd order upwind for flow, turbulent kinetic energy and turbulent dissipation rates. In order to prevent divergence, a low Courant number of 0.9 was used. The entire domain was initialized with the assumption of being static at atmospheric conditions. This means that the pressure was set to 1 atm, the temperature to 300 K and the velocity to 300 K. The operating condition was set to 0 atm. As shocks develop in this domain, which cause large pressure gradients, the dynamic mesh refinement tool was used with gradient and scale settings. This tool automatically adds refinement every 10 iterations to the regions that exhibit these large pressure gradients, and was set to apply to a maximum of 60,000 cells. This was used after reviewing an example in the ANSYS Theory Guide that used a similar strategy to deal with adverse pressure gradients in shocks in a supersonic nozzle [40].

10.3.1. Boundary Conditions

Table 10.3 lists the boundary conditions for the 'Nozzle-Steady' case, which correspond to the labeled boundaries of the geometry in Figure 10.1. The choice of boundary layers was made after reviewing the example cases and consultation with Weibo Hu, a PhD student in the Aerospace Aerodynamics Faculty and Tu Delft, who is very experienced with Fluent. A description of each of the boundary conditions is provided below.

Inlet: Pressure Inlet

The inlet is a pressure constant inlet. As this nozzle is designed to be choked, setting a constant pressure inlet with the 3mm exit diameter should result in the choked mass flow rate calculated in the preliminary design. This type of inlet is most representative of the experimental conditions, as in that case a bottle of oxygen will be set to a constant pressure and supplied to the nozzle. The pressure inlet is set to 18.7385 atm gauge total pressure, which is equivalent to 19 bar. The supersonic/initial gauge pressure is set to 1 atm, as the fluid domain is meant to be static, empty and at standard atmospheric

Table 10.3: Boundary Conditions: 'Nozzle-Steady'

Boundary	Type
Inlet	Pressure Inlet
Outlet	Pressure-Farfield
Axis	Axis
Nozzle Wall	Wall, stationary, no slip, adiabatic

conditions. The turbulent viscosity percentage and ratio are left at the given values of 5% and 10.

Outlet: Pressure-Farfield
All the outlet boundaries function as the outlet of the fluid domain and are set to pressure-farfields with Mach $= 0.1$, 1 atm pressure and 300 K temperature. A pressure-farfield is most applicable here because it allows the solver to decide if fluid should flow in or out of the boundary, which prevents errors when reversible flow occurs, which is very likely with turbulent flow. The turbulent viscosity percentage and ratio are left at the given values of 5% and 10. The outlet pressure is set to 1 bar because the igniter is only expected to operate for a few seconds during startup when the pressure in the igniter combustion chamber will be at ambient. Once the ignition occurs in the igniter combustion chamber, the gas dynamic phenomenon will no longer occur and will not be required as the propellants injected will be able to maintain the combustion.

Axis: Axis
As this is an axisymmetic geometry, the axis is set to an axis.

Nozzle Walls: Wall
The nozzle walls are set to stationary, no-slip, and adiabatic walls.

10.3.2. Calculation Activities

The contour plots of the mach number, temperature and pressure were calculated every 100 iterations to observe how the solution developed. In CFD post, plots of the pressure, temperature and mach number along the axis as well as at different points in the exhaust were calculated. In addition, contour plots of the solution were generated. All of this was exported and plots of the data were generated using Microsoft Excel.

10.4. Results

The following figures and plots illustrate the result of the simulations of the 'Nozzle-Steady' case. A selection of these results, which are most relevant to the analysis are presented in this chapter, with the complete set included in Appendix F. As this flow includes shocks, the solver is unable to converge down to residuals of 1e-05. After discussions with Dr. Ir. A.H. van Zuijlen on the best methods to validation of convergence for a flow with shocks, it was decided to observe both the residuals and mass flow rates. All of these figures are contained in Appendix F. The residuals, shown in Figure F.2 do steadily drop towards convergence, with the k and epsilon residuals converging. The other residuals drop to between 1e-02 and 1e-04, but never really decrease further because of the instabilities in the shock regions. However these residuals do level out in the last 3,000 iterations, indicating a level of convergence. As a second means of convergence the mass flow rates of the inlet and outlet are compared. Figure F.3 plots the mass flow rate per iteration of the inlet and outlet over the entire simulation. A positive value indicates mass moving into the domain, and a negative value indicates mass moving out of the domain. This is why when the simulation converges, past 20,000 iterations, the inlet mass flow rate is positive and the outlet mass flow rate is negative. In the first 4,000 iterations, the mass flow rates are very chaotic. This is because the solver cannot solve all of the cells at once, but is beginning at the inlet boundary and moving towards the outlet, as the iterations progress. This is why the outlet mass flow rate takes longer to converge, as compared to the inlet. Therefore in these initial iterations the solver is just making wild guesses, until those regions are reached. In order for the simulation to

be deemed converged, the percent difference between the absolute value of the mass flow rates at the inlet and outlet, also called 'flux' should be close to 1%. The flux for the entire simulation is displayed in Figure F.4, and the flux of the final few iterations is shown in Figure F.5. They show that by the end of the simulation the flux is around 4.75%. While this is higher than the desired 1%, this was the lowest flux achieved after many days of attempts. As these results are meant to serve as more of an estimation of the exhaust jet shape and in the interest of time, it was decided to accept this offset.

The pressure, temperature, velocity and mach contours of the 'Nozzle-Steady' case are provided in Figure 10.4-Figure 10.7. Figure 10.7 illustrates the mach contour of the exhaust jet. For validation, this should be compared to the schematic of the highly under-expanded jet, seen in Figure 8.2. While the end of the cell is more tapered in the Fluent contour than in the schematic, the overall shape of the shock cell and the mach number distribution match the schematic well. As stated, for optimal performance, the resonance cavity opening should be located within the compression zone of the shock cell and the opening diameter of the resonance cavity should be wide enough to capture the core of the jet flow. In Figure 10.8, the mach number along the axis boundary is plotted. Here (0,0) is the location of the nozzle exit on the axis. From this figure, it can be seen that the nozzle is sonic because the mach number at the throat ($x = 0$) is equal to 1. Around $x = 11.5$mm, there is a steep drop in the mach number, indicating the presence of a normal shock. Plots of the temperature, pressure and velocity along the x-axis are contained in Appendix F, and all show the same pattern as the mach plot. Therefore the location of the normal shock is around 11.5mm. This is further than the value calculated using Equation 8.1, meaning that the gap distance in the preliminary design must be adjusted. In order to determine what gap distance to use, the figure of the velocity vectors in this shock cell must be observed.

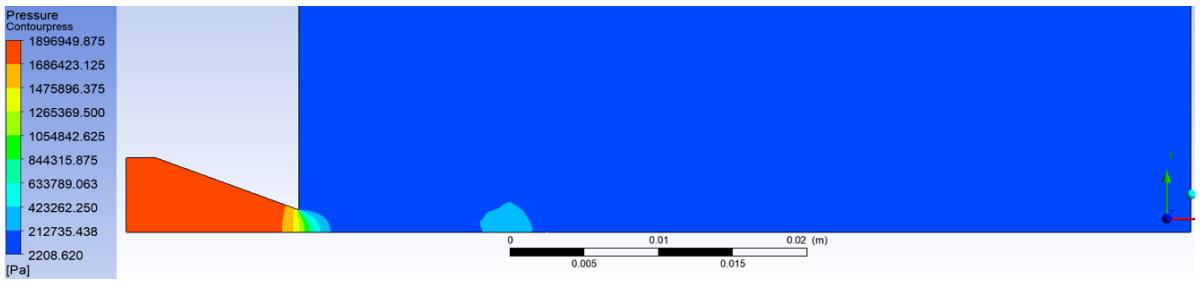

Figure 10.4: Nozzle-Steady, Pressure Contour

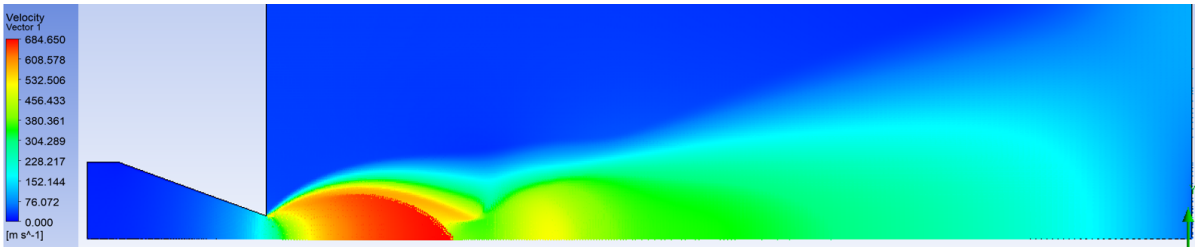

Figure 10.5: Nozzle-Steady, Velocity Contour

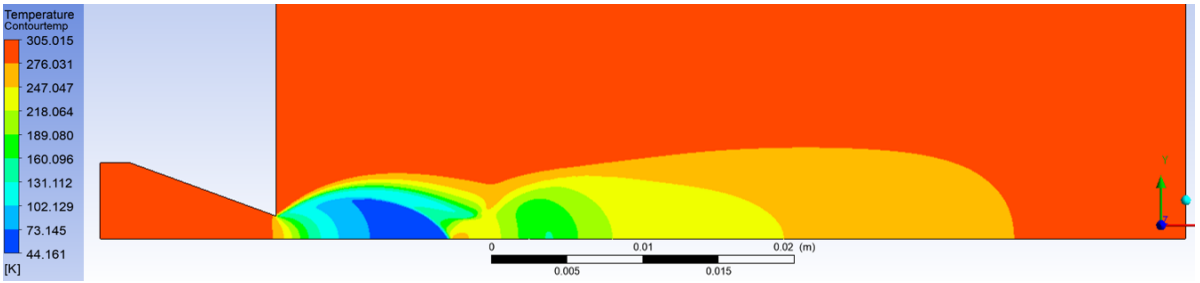

Figure 10.6: Nozzle-Steady, Temperature Contour

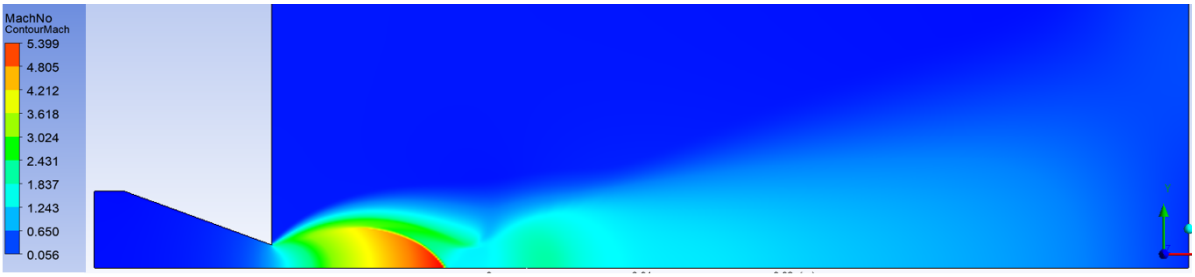

Figure 10.7: Nozzle-Steady, Mach Contour

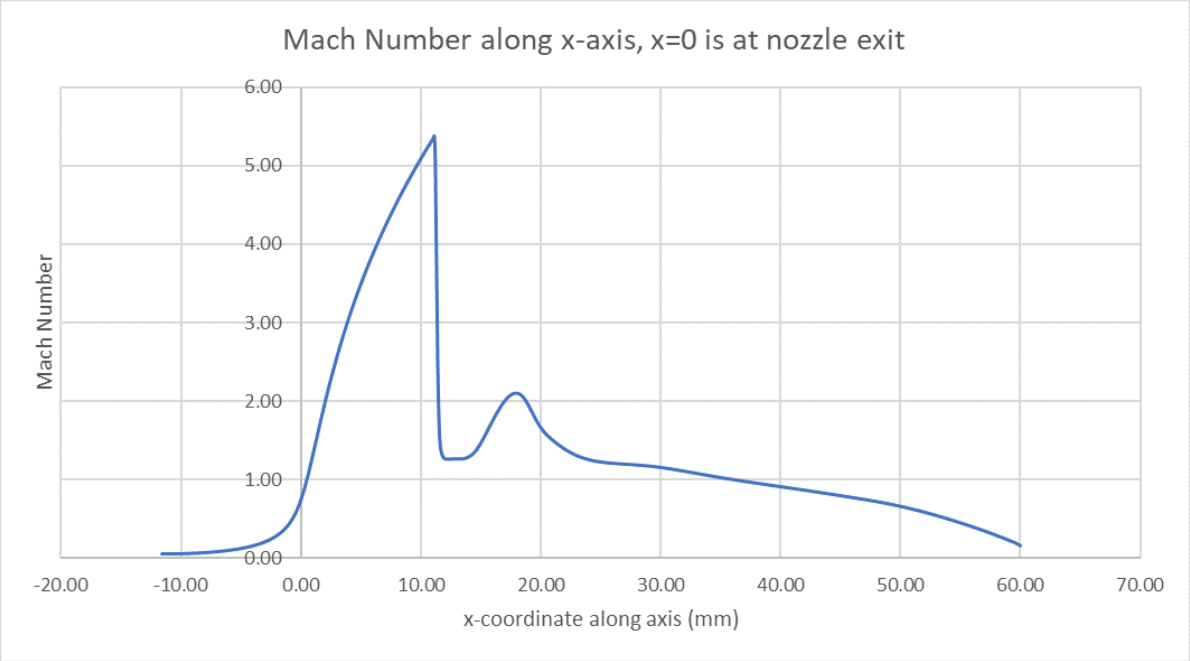

Figure 10.8: Nozzle-Steady, Mach Number along x-axis, x=0 is at nozzle exit

In Appendix F, the velocity vectors of the entire first shock cell are displayed. Figure 3.4 illustrates that the gas first expands, with velocity vectors point up and out, and then compresses, with the vectors pointing down and in towards the axis. A closer image of the velocity vectors in the compression zone are displayed in Figure 10.9. This vector contour plot from ANSYS CFD-Post has been edited by adding black arrows on top of the vectors in order to improve the visibility of the arrows. In addition the x-axis distances from the exit of the nozzle have been added such that the location of the transition between the expansion and compression zones can be determined. As stated, in this velocity vector plot, the expansion zone can be identified as the region just after the nozzle exit, where the velocity vectors are pointed up and away from the axis. At around 6mm from the nozzle exit, the velocity vectors are parallel to the axis and then begin to point downwards as the compression zone begins. Black squares and labels have been added to designate the expansion and compression zones. For this study the cavity entrance must be placed within the compression zone, which can be seen in Figure 10.9 as 6-11.5mm from the exit of the nozzle. In order to ensure that the opening of the resonance cavity is locate with the compression zone of the exhaust, it was decided to move the Gap Distance to just before the normal shock, at 11mm from the nozzle exit. The adjusted preliminary design parameter is listed in Table 10.4.

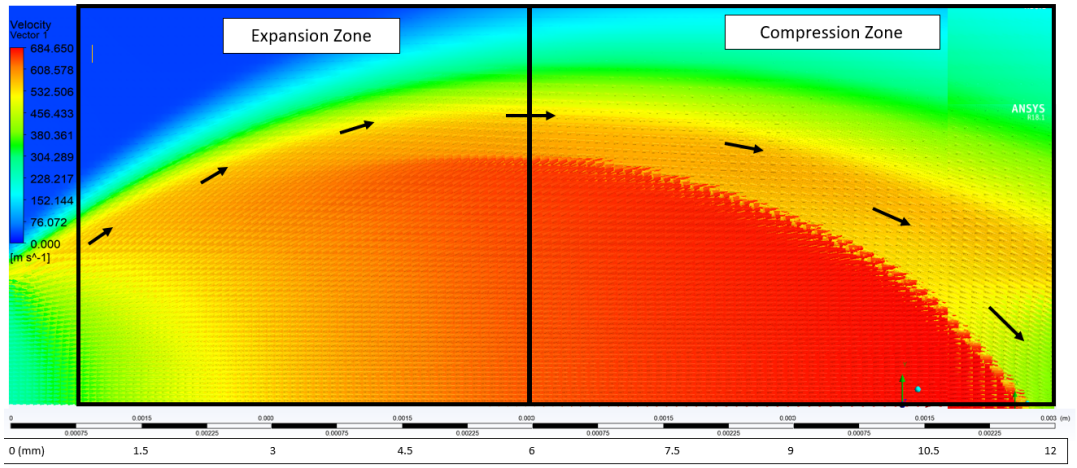

Figure 10.9: Nozzle-Steady, Velocity Vectors in exhaust, zoomed in on the 1st shock cell

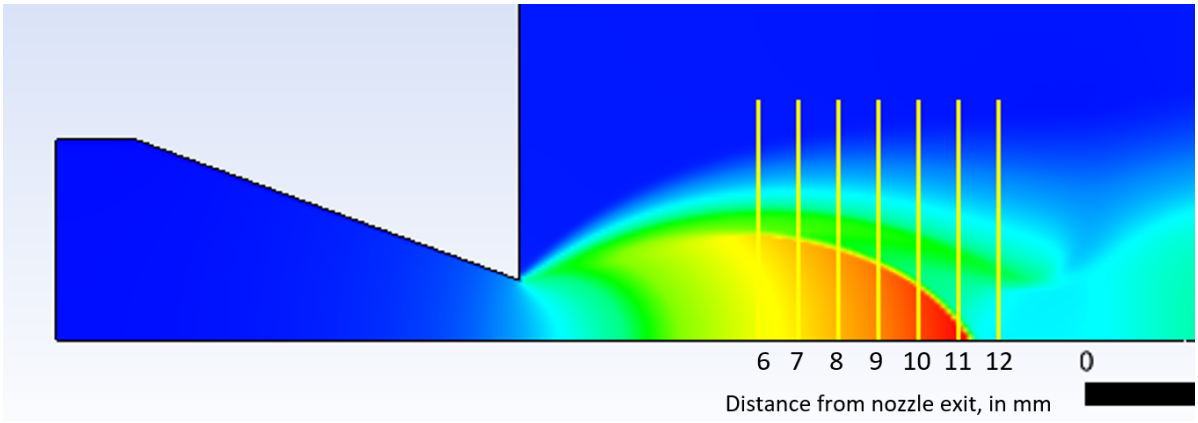

Figure 10.10: Nozzle-Steady, Distance Markers at various distances away from the nozzle exit.

As the gap distance has changed, the opening diameter of the resonance cavity may need to be adjusted. To aid this decision, a plot of the mach number in the y-direction at a set of points in the exhaust are plotted in Figure 10.11. These points are located 7-12mm from the nozzle exit, and correspond to the lines in Figure 10.10. This plots details the mach number in the y-direction at each of these points to illustrate how the diameter of the exhaust jet decreases in the 2nd half of the first shock cell, which is illustrated by the decreasing mach number of the flow in the y-direction. At 11mm distance from the nozzle exit, the mach number starts at over 5, then drops to 2 at 1mm height, then rises back to 2.5 at 2mm height, and then decreases to 0. This means that the majority of the core of this exhaust flow is located between the axis and 2mm height at the distance of 11mm from the nozzle exit. In order to only include the high speed flow in the cavity, the opening diameter of the nozzle in the preliminary design is changed to 4mm. As the cavity angle is kept at $3°$, and the base diameter is also kept at 1mm, this results in a change in cavity length. In Table 10.4, the adjusted parameters for the preliminary design are listed. These will be used as the inputs in the 'Cavity' simulations.

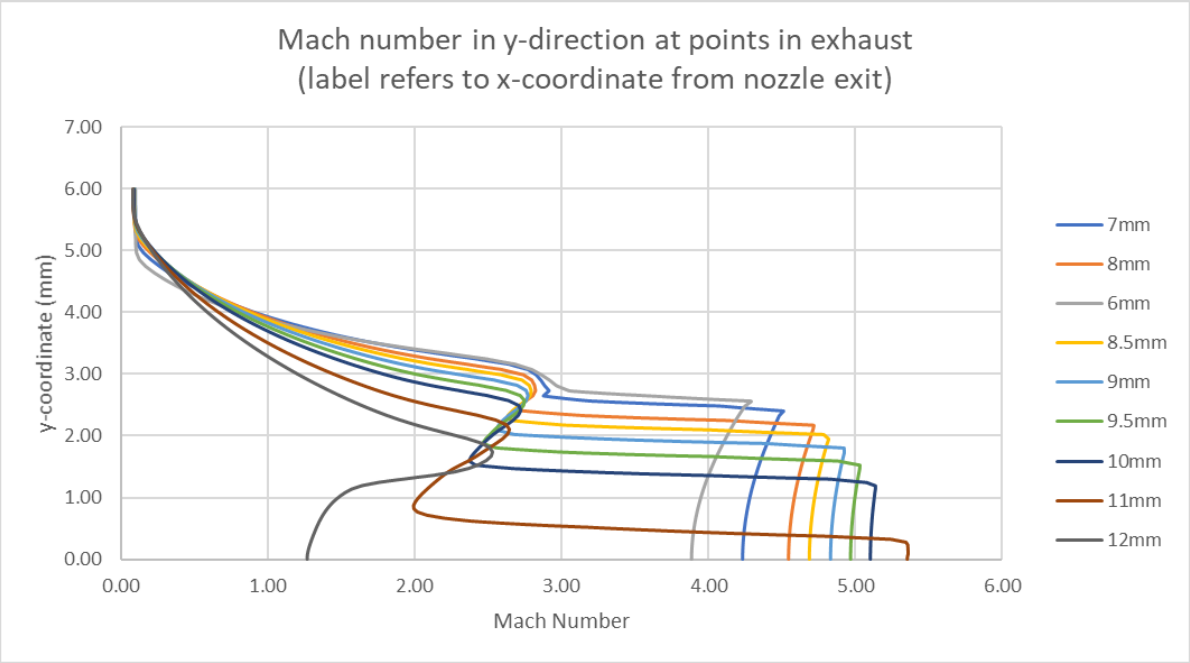

Figure 10.11: Nozzle-Steady, Jet Diameter at various distances away from the nozzle exit.

10.5. Conclusion

In this chapter an introduction and explanation of the setup of the 'Nozzle-Steady' numerical simulation was given. The geometry, meshing and solver setup strategy were described. Finally the results of the simulation were presented and analyzed, resulting in a new 'adjusted preliminary design' to be used in the 'Cavity' simulations. The results of the 'Nozzle-Steady' simulation showed that the length of the first shock region of the nozzle exhaust jet is longer than that predicted by the empirical results. Due to this new information, the gap distance between the nozzle exit and cavity inlet was increased based on the simulation results. Since the gap distance was increased, the opening diameter of the preliminary design had to be adjusted as well in order to better match the jet diameter at that location. These new 'adjusted preliminary design' parameters, listed in Table 10.4, are used as the inputs to the next set of simulations.

Table 10.4: Resonance Ignition Device *Adjusted* Preliminary Design Parameters

Parameter	**Symbol**	**Value**	**Unit**
Resonance Cavity			
Resonance Cavity Shape	Shape	Conical-Truncated	
Resonance Cavity Inlet diameter	d	4.0	mm
Resonance Cavity end diameter	d_e	1.0	mm
Resonance Cavity Angle	α	3	degrees
Resonance Cavity Length	L_{res}	28.622	mm
Resonance Tube wall thickness	t_w	1.0	mm
Gap Distance	ΔS	11	mm

11

’Cavity’ Simulations Setup

In this chapter, all of the numerical simulation preparation work is outlined for the ’Cavity’ cases. This begins with an explanation of the geometry and meshing strategy. As there is a transient component to this simulation, an explanation of the grid sizing, as it relates to time, is covered. In order to qualify the accuracy of the mesh, a mesh refinement was conducted and the results are analyzed. Then, additional solver input information and geometric boundary conditions are provided. The chapter concludes with a mesh and solver validation study, that seeks to determine the accuracy of this setup by using it to solver a known case and comparing the results.

11.1. Geometry

Figure 11.3 displays the 2D, axisymmetric geometry for the ’Cavity’ simulations with the dimensions and boundaries labeled. All cases in the ’Cavity’ simulations used a nearly identical geometry, apart from the parameters that were adjusted for specific cases. Table 11.1 provides the values associated with these dimensions. These values given as constants remained unchanged throughout all the cases, whereas those described as ’variable’ were adjusted based on the conditions of each case. The only exception is that the width of the fluid domain had to be elongated for the longest cavity length, but this does not effect the results of the simulations.

This geometry was styled after the works of Murugappan, Narayanan and Afzali, which can be seen in Figure 11.1, Figure 11.2, and Figure 11.3 [50] [52] [6]. All these designs used a 2D, axisymmetric geometry, contained a cavity, either included the nozzle or set the inlet as the nozzle exit, and set the fluid domain boundaries far from the nozzle-cavity region to prevent the outflow from effecting the gas dynamic phenomenon. In these geometries the height of the fluid domain is between 7.5 to 10 times the diameter of the nozzle exit. In this thesis, the height of the fluid domain is set to 15 times the nozzle exit. In the Murugappan case, the width of the fluid domain is only equal to the gap distance, but this is acceptable because the sides of the environment are set as walls and as such there is no flow across these boundaries. However in this thesis, it was decided to use the boundary conditions set by Narayanan and Afzali, in which all the environmental boundary were set to pressure-farfields, which allow flow in and out. Further explanations of boundary conditions is given in subsection 11.3.1. Therefore the width of this fluid domain must be set far from the cavity entrance to prevent flow disturbances. In the two example cases the width of the fluid domain was set to 4.5 times the gap distance for Afzali and 54.64 times the nozzle exit diameter for Narayanan. Therefore in this thesis, the width of the fluid domain is set to approximately 4.5 times the preliminary design gap distance [50] [52] [6].

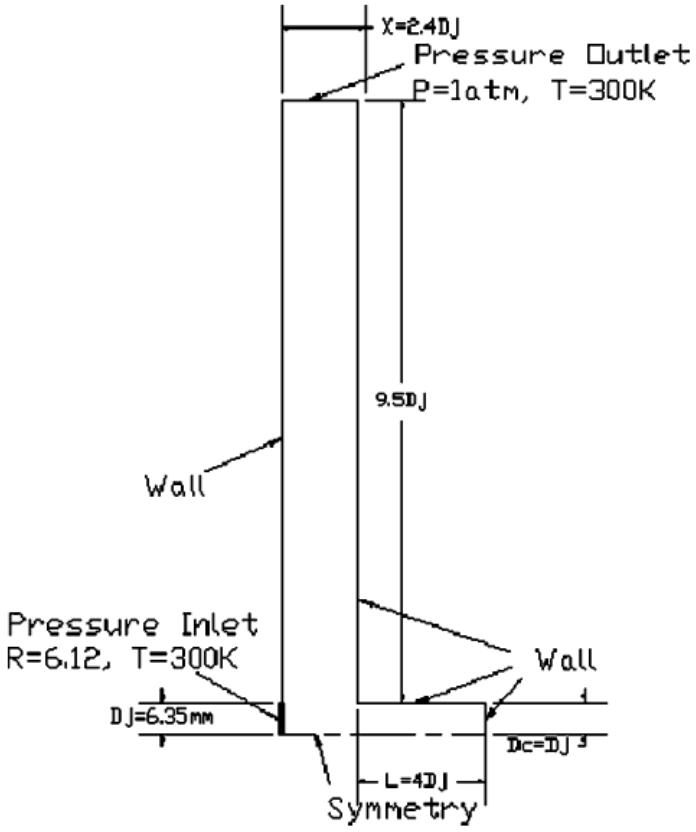

Figure 11.1: Murugappan Geometry [50]

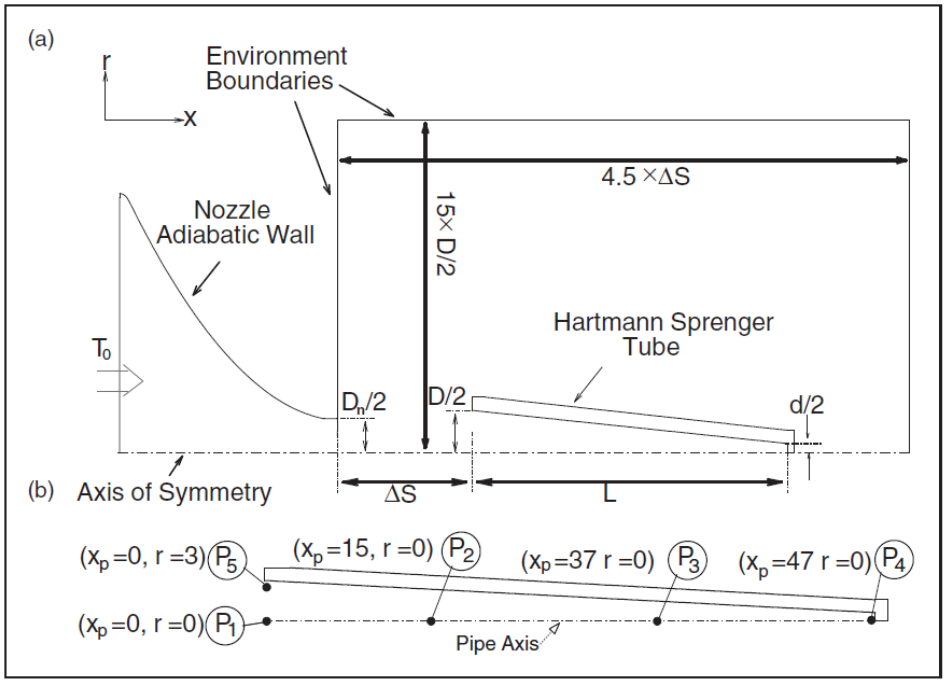

Figure 11.2: Afzali Geometry [6]

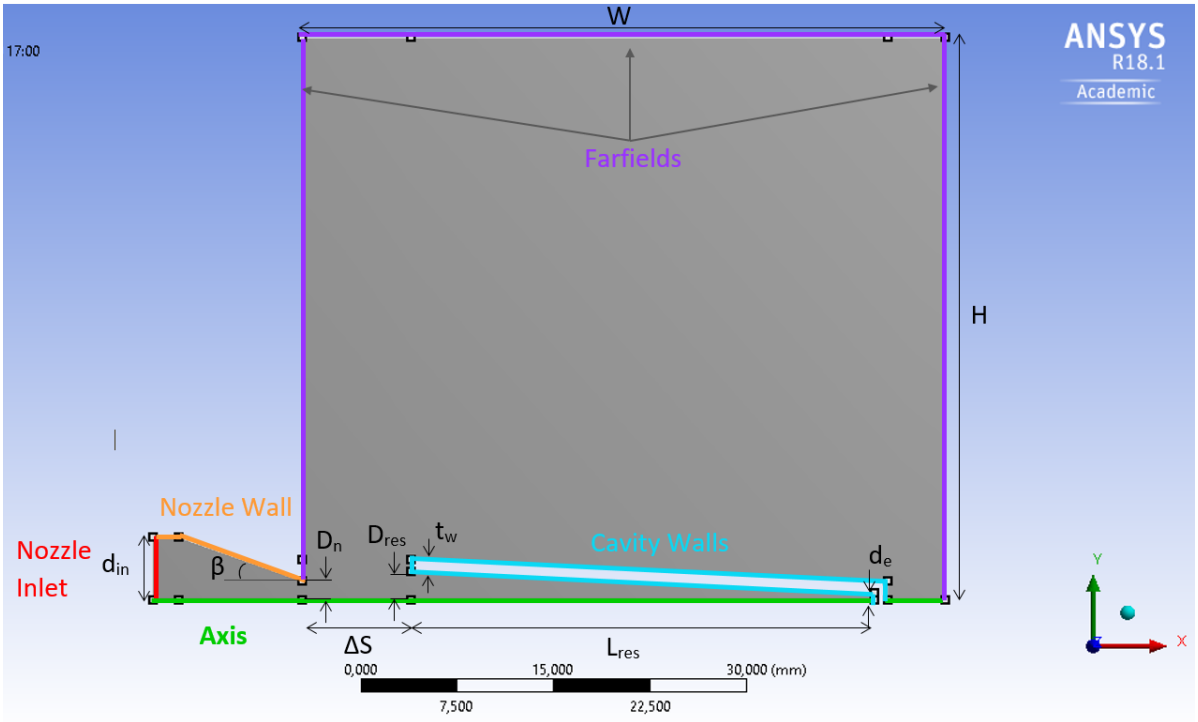

Figure 11.3: 'Nozzle-Cavity-Steady'/'Nozzle-Cavity-Transient' Geometry Labeled, 2D axisymmetric

Table 11.1: 'Nozzle-Cavity-Steady'/'Nozzle-Cavity-Transient' Geometry Dimensions

Dimension	Symbol	Value	Unit
Injection Nozzle Inlet Diameter	d_{in}	10	mm
Injection Nozzle Exit Diameter	D_n	3	mm
Injection Nozzle Convergent Angle	β	20	Degree
Gap Distance	ΔS	variable	mm
Resonance Cavity Inlet diameter	D_{res}	variable	mm
Resonance Cavity end diameter	d_e	1.0	mm
Resonance Cavity Length	L_{res}	variable	mm
Resonance Tube wall thickness	t_w	1.0	mm
Fluid domain Height from x-axis	H	45	mm
Fluid domain Width from y-axis	W	50	mm

11.2. Mesh

11.2.1. Grid Sizing

As these simulations use both a steady and transient solver, a complex and detailed approach and to be taken when generating the mesh. This is due to the relationship between cell width, time-step size and computational time. The more refined the mesh the smaller the size of the cell width and time-step, resulting in a longer computational time. In order to balance accuracy with computational time, calculations on cell sizing and time-step had to be conducted and a selection of different levels of mesh refinement were tested and analysed. This geometry uses a structured, rectangular mesh, with a uniform grid that is more refined in the nozzle-gap-cavity section, and coarser in the faraway fluid domain. As explained in, section 9.2,the cells in the fine and coarse regions were relatively uniform in size, with a smooth transition between the fine and coarse regions. Murugappan, Narayanan and Afzali all ran numerical simulations of similarly sized resonance cavities, and their meshing strategies

were examined to provide guidance [50] [52] [6]. The sizing and total number of nodes for each of these cases are as such. Murugugappan used a total of 34,237 nodes with a uniform grid size over the entire domain [50, p.815]. In the steady case run by Narayanan, shown in Figure 9.2, between 100,000 and 164,000 nodes were used with a finer grid in the nozzle, gap and cavity region and a coarse grid in the further away fluid domain. Afzali used approximately 127,000 nodes with more refinement in the nozzle, gap and cavity region [6, p.2709]. However it should be noted that these works ran fully transient, as their aim was to characterize the periodic motion of the flow. As this occurs extremely quickly, it requires a very fine mesh and extremely small time-steps to capture, on the order of 2e-08s [6]. For this study, a partially transient case is solved in order to find the average temperature a the base of the cavity. This means a much lower level of refinement is necessary, as the movement of the flow will not be simulated. The reason for this is that to simulate such a fully transient solution would take over 8,000 hours of computational time, which is infeasible for this thesis. This strategy of beginning with a steady solver and ending with a transient one is described in full in subsection 9.6.2. Therefore for this set of simulations a coarse mesh was used, that balanced accuracy with computational time.

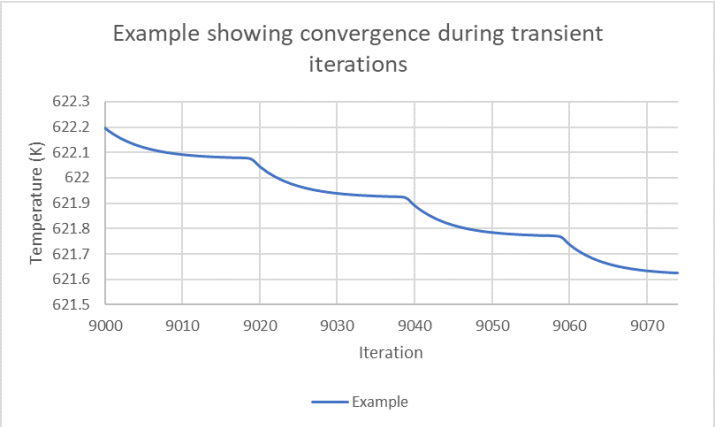

Figure 11.4: Example of Convergence in each Time-Step in a Transient Solution

When determining the refinement of the 'Cavity' cases, calculations of the required time-step size were conducted. In transient cases the user must input the 'time-step size (s)', 'number of time steps,' and 'iterations per time-step.' The time-step is dependant on the average cell size, which is the distance from one side of the cell to the other, and the maximum speed at which information propagates through the domain, which is the sum of the speed of sound and the maximum flow velocity. If the time-step is too large, the solver will not be able to converge during each time-step, resulting in an inaccurate solution. If the chosen time-step is too small the solver will be able to converge during each time-step, meaning it will be accurate, but it will take a very long time. Therefore it is necessary to use Equation 11.1 to calculate the required time-step. Each time-step performs a number of iterations, in this case the given value of 20 iterations per time-step will be used. If the solution succeeds in converging during each time-step, then in the plots of the temperature, pressure, and velocity values versus iteration, the lines are expected to have a 'staircase-like' appearance. In that at the beginning of the time-step the solver make a guess, then as the iterations progress the line begins to curve (up or down) and if it reaches convergence, the final 5-10 iterations are static and form a flat line in the plot. This characteristic of the final plots will be checked for validation purposes. An example of a converged transient temperature plot is shown in Figure 11.4.

The time-step size is directly dependant on the grid size, the smaller the grid size the smaller the time-step. The number of time-steps required is related to the total simulation time and time step size, shown in Equation 11.2. From this, it can be seen that the smaller the time-step size, the larger the number of time-steps required to simulate the stated total physical time. The more iterations required, the longer the computational time of the simulation. Before calculating the time-step size, one should first calculate the total time required for the simulation. Then an iterative approach can be taken to choose the grid size. This entails choosing different grid sizes, computing the required time-step size for that grid size and the number of iterations required to perform the total simulation time. Short simulations (100 iterations) can be run using these grid-size/time-step size options to determine how

much time the computer takes to complete each iteration. From there an estimation of total computation time for each grid size option can be calculated and a decision made on how much time can reasonable be spent computing. First, an explanation on how to calculate the total iteration time is given below. Then a table of the grid size options, with the corresponding time-step size and number of iterations is given, followed by a choice of grid-size.

$$\text{Time step size (s)} = \frac{\text{Avg. Cell size (m)}}{\text{Speed of sound (m/s)} + \text{ Maximum Flow Velocity (m/s)}} \tag{11.1}$$

$$\text{Total Physical Time (s)} = \text{Time step size (s)} \cdot \text{\# Time-Steps} \tag{11.2}$$

In the study by Afzali, for a similarly sized resonance cavity, plots of the pressure, temperature and velocity at different points in the cavity are displayed in Figure 11.5. Here point 1 is at the inlet of the cavity, point 4 at the base and points 2 and 3 in between. In transient cases, there is a region of initialization where the solver is trying to converge. Every iteration it gathers information which it uses as an input to the following iteration, eventually converging and oscillating periodically around the converged solution. This initialization time can be observed in the first 0.004 seconds of Figure 11.5a. At 0.004s, the solver has reached a convergence, which is observable based on how for the remaining time, the solution oscillates around an average value. This average value is the calculated pressure and temperature at that point. This is a very large amount of time, for example if a time-step of 1e-07s was used, it would take 40,000 time-steps, with 20 iterations each, resulting in 800,000 iterations required just for the initialization. This would take thousands of hours of computational time, which is why the steady solver is used first to eliminate this long initialization time. Once the steady portion of the solver is complete, the transient solution will begin at a value near to the solution. Therefore in the transient solver, it is only necessary to compute a few cycles of the flow oscillations, in order to determine the average value.

The time required for the gas to complete one oscillation in the cavity is equal to twice the cavity length, divided by the average velocity of the flow in the cavity, see Equation 11.3. This requires an estimation of the speed of the flow in the cavity. From the preliminary design, the expected speed of the flow at the nozzle exit is 301.563 m/s, and from the data collected of the velocities measured at 4 points along the cavity in the adjusted preliminary design 'Nozzle-Steady' case an average velocity of 320 m/s was calculated. As noted, the velocity values in this steady case may not be extremely accurate, but they are just used as an estimated of flow speed. A flow speed of 300 m/s will be used in the calculation and the speed of sound in oxygen is 326 m/s [67]. This results in total speed of information in the cells of 646m/s, to be used in Equation 11.1.

The length of the cavity in the preliminary design is 28.622 mm. The amount of time required for the fluid to travel twice the length of the cavity, to complete one oscillation at 320m/s, is 0.0001788 seconds. From the Afzali study, it was found that once cycle for the 48mm long cavity took approximately 0.0004 seconds, as illustrated in Figure 11.5b [6]. Using Equation 11.3, one full oscillation of the Afzali cavity should take 0.0003s. This is close to the simulated value and gives support to using Equation 11.3 to predict the cycle time. Therefore the estimated total time required for the simulation to complete one cycle is 0.00018s.

$$\text{Time Per 1 Cycle (s)} = \frac{2 * \text{Cavity Length (m)}}{\text{Avg Flow Velocity (m/s)}} \tag{11.3}$$

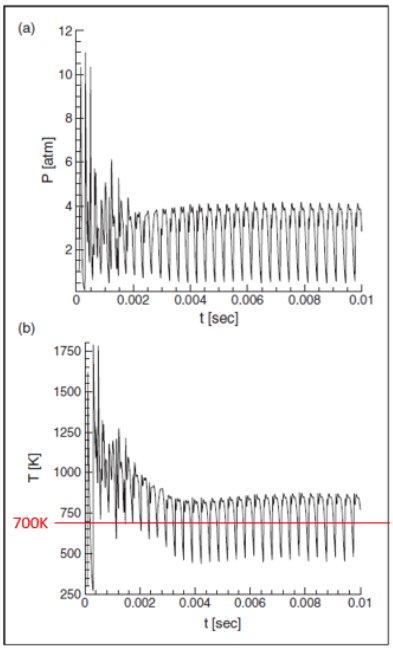

Figure 5. Simulation results for flow properties vs time at point P_4: (a) pressure, (b) temperature.

(a) Pressure and Temperature versus time at P2 in cavity, transient case. Average Temp 700K.

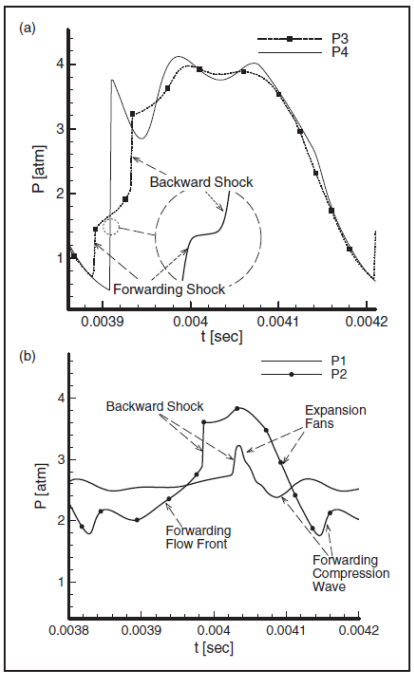

Figure 8. Incident shock, reflected shock, expansion fans, and forwarding flow front within diagrams of pressure fluctuations at (a) points P_3 and P_4 and (b) points P_1 and P_2.

(b) Pressure vs. Time at 4 points in cavity, illustrating the the movement of forward and backwards shock [6]

Figure 11.5: Afzali Resonance Cavity Transient Simulation Results [6]

In order to keep the computational time reasonable, it was decided that the minimum allowable time-step size was 1e-07s. From experimentation, it was found that when the time-step is lower than this the value, the simulation takes 10s of thousands of iterations and 10s of hours of computational time to converge. The range of time-steps presented in Table 11.2 took between 5,000-20,000 iterations to converge and the simulations were completed in 3-8 hours. In Table 11.2, 3 options of grid-refinement are given with their corresponding time-step size and number of iterations for 1 cycle. As the refined region consists of the nozzle, gap and cavity, the cavity is used here to calculate the cell width. The same cell width is to be used in the nozzle and gap regions, with a larger cell width used in the coarse faraway regions. In Table 11.2, the cell width was calculated by dividing the cavity length by the number of divisions. The time-step size was then calculated using Equation 11.1 with a total information speed of 646m/s. Then Equation 11.2 was used to calculated the # of time-steps required to complete 1 cycle. Additionally, after running some test simulations, it was found that the time-steps sized calculated using Equation 11.1 were too large and convergence was not occurring during each time-step. This is not a surprise as this equation was only an estimation of the time-steps. After testing it was found that if the time-step sized was lowered a bit the solutions converged. These lowered time-step values used in the solver are listed as 'TS size, Fluent' in Table 11.2 and the number of iterations required is calculated using this value.

11.2.2. Mesh Refinement Study

In order to choose which mesh to use for these simulations, a mesh refinement study was conducted, in which the 3 options in Table 11.2 were computed. The average values during the transient phase of the pressure and temperature at the base of the cavity, P4 were compared. If only a small difference was found between 2 of the meshes, then it proved that the refinement was not affecting the simulation result. Plots of the pressure and temperature at P4 for 10,000 iterations for the LOW, MEDIUM and HIGH refined mesh are displayed in Figure 11.6 and Figure 11.7. In Table 11.3 the average values of the pressure and temperature at P4, during the transient period are compared for each mesh refinement option. In addition, in Figure 11.8-Figure 11.13, the contour plots of the pressure and temperature for each option are displayed. Note that the pressure and temperature values in these contour plots

Table 11.2: Estimation of time-step size and number of time-steps for different levels of grid refinement. Assume 1-Cycle-Time: 0.00018s. TS: Time-Steps

Option	Region, Length (m)	# Divisions	Cell Width (m)	TS Size, Calc (s)	TS Size, Fluent (s)	# TS 1-Cycle
1: HIGH	Cavity, 0.028622	60	0.000477	7.38e-07	4e-07	450
2: MED.	Cavity, 0.028622	40	0.0007155	1.1e-06	6e-07	300
3: LOW	Cavity, 0.028622	29	0.000986	1.53e-06	8e-07	225

are at the final iteration and therefore are not representative of the average value. These contour plots are included to show how developed the result is and to see if the size of the temperature and pressure regions are similar. All refinement mesh information and the other parameter contour plots are in Appendix D for the 3 options.

In order to decide which mesh refinement is sufficient, the average values in Table 11.3 are compared. If only a small difference exists between a mesh and the next more refined option, than that lower refined mesh is sufficient. Other levels of refinement were also computed in the study, but for brevity only 3 options are analysed here. First, the pressure and temperature contour plots were reviewed to see if they were fully developed. The contour plots of the MEDIUM and HIGH mesh are both fully formed and their high temperature regions cover approximately the same area, whereas the LOW contour plots looks to be underdeveloped. Now reviewing the values in Table 11.3, when the LOW and MEDIUM mesh were compared, a 11,313 Pascal pressure difference and 35 K temperature difference were found. This pressure difference is not very large, only 0.1 Bar, but 35 K in temperature difference is enough to require further refinement. When the MEDIUM and HIGH mesh were compared a 5,869 Pascal pressure difference and 0 K temperature difference were found. This is a negligible difference and proves that the MEDIUM mesh is sufficiently refined to produce an acceptable simulation result, that is unaffected by the level of mesh refinement. With these results, the MEDIUM level of refinement is chosen as the level of refinement for the remainder of this study.

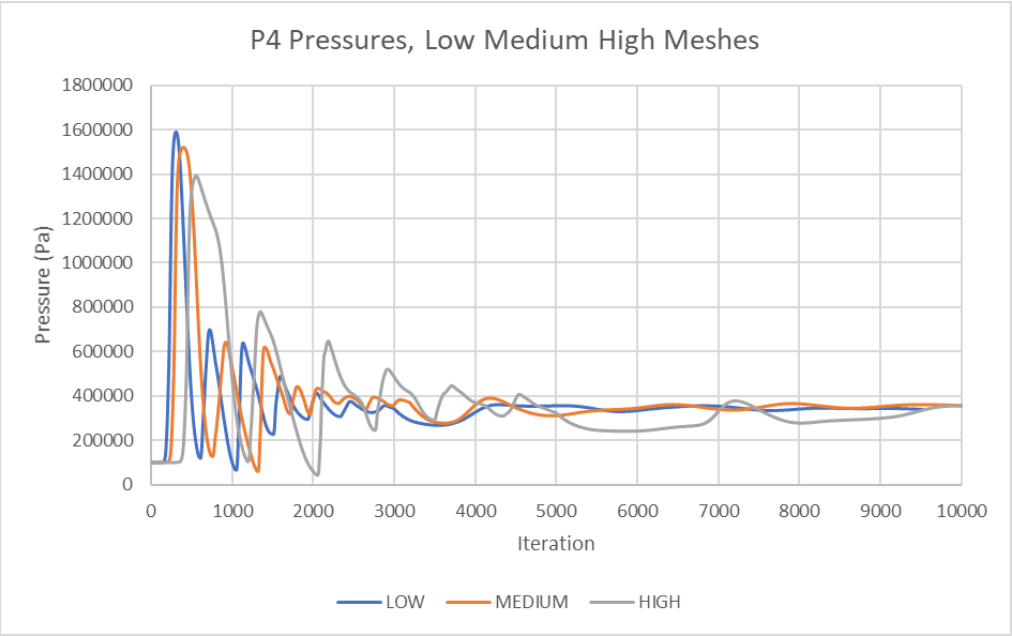

Figure 11.6: Mesh Refinement Pressure for 10,000 iterations

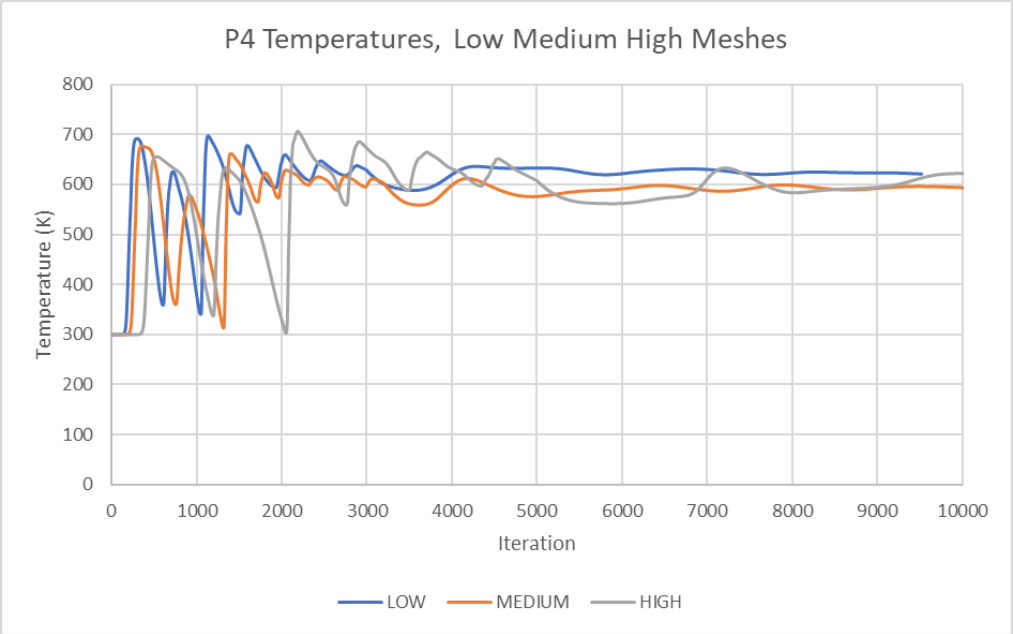

Figure 11.7: Mesh Refinement Temperature for 10,000 iterations

Table 11.3: Mesh Refinemnet, comparison of Pressure and Temperature at P4, all values are average in transient

Parameter	LOW	MEDIUM	HIGH
P4 Pressure (Pa)	344368	355681	361550
P4 Temp (K)	625	591	591

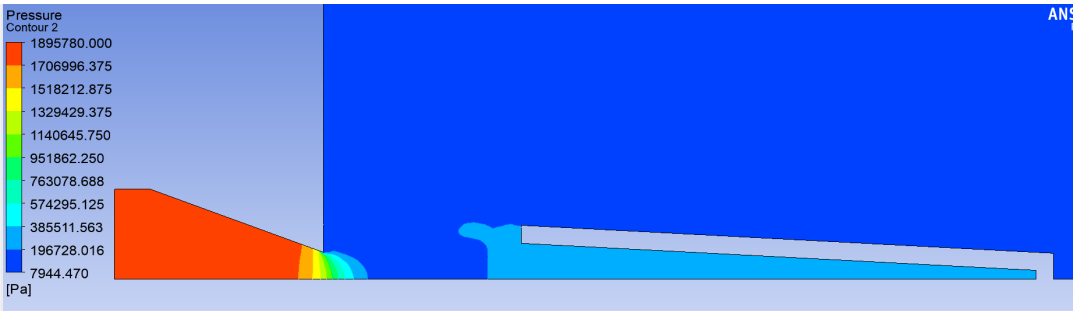

Figure 11.8: 1: HIGH Mesh Pressure Contour

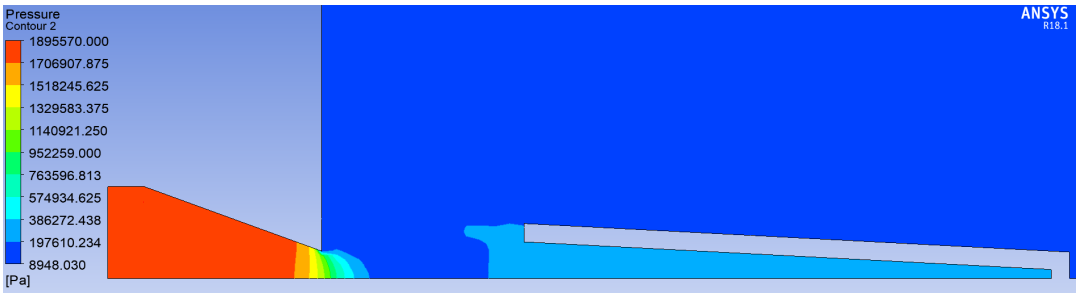

Figure 11.9: 2: MEDIUM Mesh Pressure Contour

Figure 11.10: 3: LOW Mesh Pressure Contour

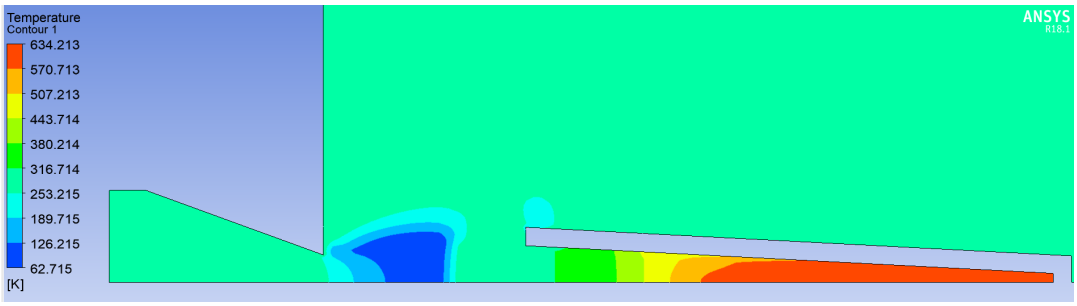

Figure 11.11: 1: HIGH Mesh Temperature Contour

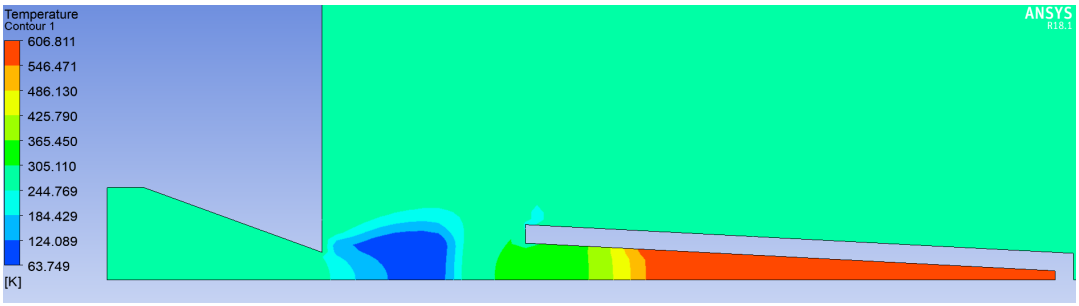

Figure 11.12: 2: MEDIUM Mesh Temperature Contour

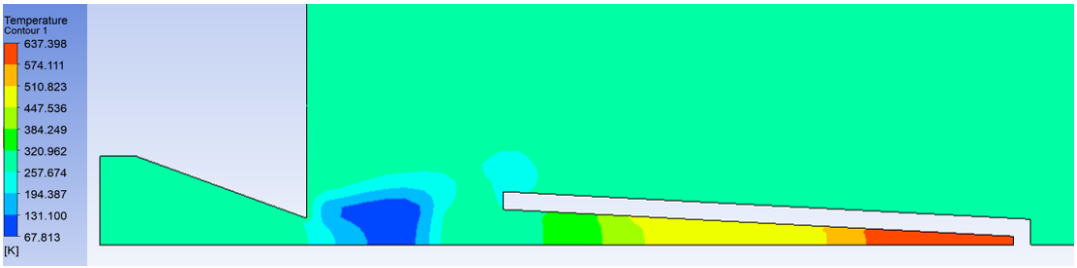

Figure 11.13: 3: LOW Mesh Temperature Contour

11.2.3. Final Mesh Chosen

After completing the mesh refinement study, the final mesh chosen to use in all of the 'Cavity' is presented below. The mesh of the full domain and a closer view of the more refined nozzle-gap-cavity region are displayed in Figure 11.14 and Figure 11.15. The mesh details are displayed in Figure 11.16 and the quality factors for this mesh are listed in Table 11.4. As discussed in chapter 9, there is expected to be complex flow in the nozzle-cavity region, thus requiring a uniform structured mesh with a finer mesh in the nozzle-cavity region and a coarser mesh in the far away fluid domain. A bias is used in x-direction of the farfield domain to generate a smooth transition between the fine and coarse grid

regions. Figure 11.15 zooms into the refined nozzle-cavity region to show the level of refinement and the smooth transitions between regions. The mesh contained approximately 64,000 nodes, and the details of the mesh are displayed in Appendix G. Table 11.4 lists the mesh quality parameters for the preliminary design mesh. The geometry is adjusted a bit for the sets of cases, but the quality values do not fluctuate very much and therefore only the preliminary design values are provided.

Table 11.4: 'Cavity' Mesh Quality Factors

Quality Factor	Value
Element Quality	
Average	0.77
Stnd. Deviation	0.19
Aspect Ratio	
Max	8.9957
Average	2.3778
Stnd. Deviation	1.3807
Orthogonal Quality	
Average	0.9988
Stnd. Deviation	4.2e-03
Skewness	
Max	0.22222
Average	1.84e-02
Stnd. Deviation	2.45e-002

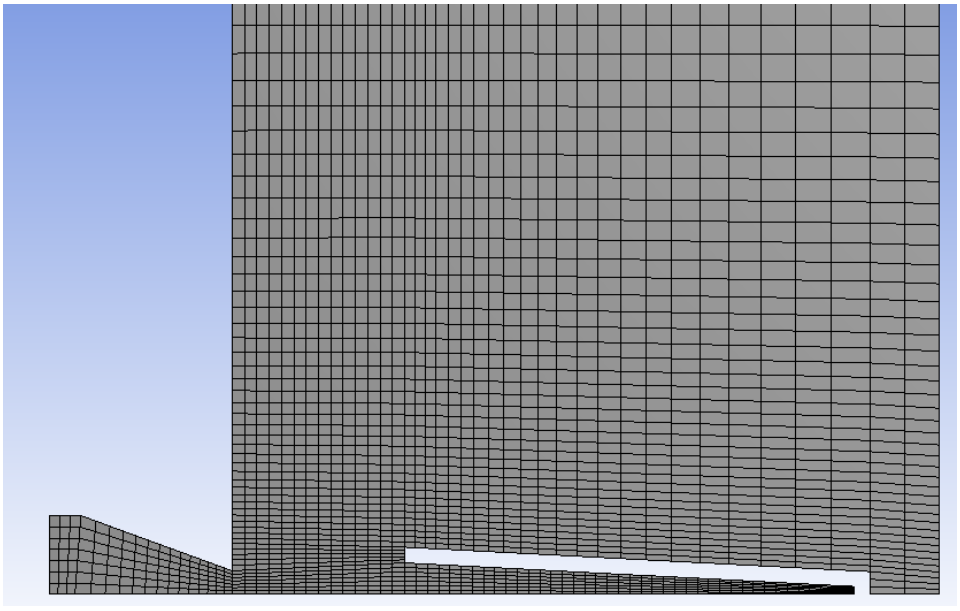

Figure 11.14: 'Cavity' Full Mesh

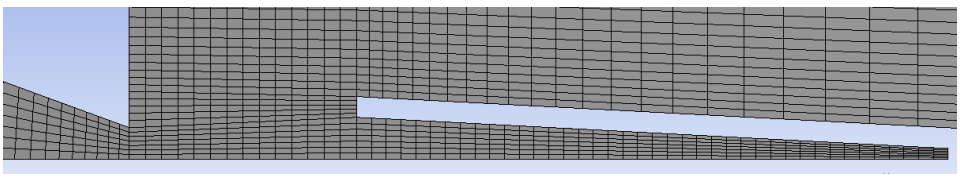

Figure 11.15: 'Cavity' Mesh, zoom in nozzle-gap-cavity region

Details of "Mesh"	
Display	
Display Style	Body Color
Defaults	
Physics Preference	CFD
Solver Preference	Fluent
Relevance	0
Export Format	Standard
Element Order	Linear
Sizing	
Size Function	Proximity and Curvature
Relevance Center	Coarse
Span Angle Center	Fine
Curvature Nor...	Default (18,0 °)
Num Cells Acr...	Default (3)
Proximity Size Fu...	Faces and Edges
Min Size	Default (3,4552e-002 mm)
Proximity Min ...	Default (3,4552e-002 mm)
Max Face Size	Default (3,45520 mm)
Growth Rate	Default (1,20)
Automatic Mesh ...	On
Defeature Size	Default (1,7276e-002 mm)
Minimum Edge L...	0,50 mm
Quality	
Inflation	
Assembly Meshing	
Advanced	
Statistics	
Nodes	2172
Elements	2022

Figure 11.16: 'Cavity' Mesh details

11.3. Solver Setup

All of the cases use the same solver setup, with the only exception being the difference in inlet pressure required for the pressure cases. The final setup of the solver was derived after reviewing the other resonance cavity numerical simulations, running many tests with different options and finding that the setup presented here was able to run smoothly without diverging, and provided results that matched predictions. A density-based, axisymmetric, steady case was set up with the energy equation turned on. The k-epsilon, realizable turbulence model with enhanced wall treatment was used. As this is compressible flow the working fluid, gaseous oxygen, was set to an ideal gas. An implicit, Roe-FDS time method was used.

In order to improve numerical stability in solver, experimentation was done using 1st and 2nd order equations for the flow, turbulent kinetic energy and turbulent dissipation rates. 1st order equations are more robust than 2nd order and therefore are more stable. However they are not as accurate, which is why a common strategy to keep stability is to begin with 1st order equations and then switch to 2nd order [40]. After much testing a strategy was developed to maintain stability during the case. It is expected that when the solver begins the parameters (P,T,V) will vary greatly with large amplitudes as the solver makes its initial guesses. As the iterations progress this amplitude will decrease until it stabilizes around a small amplitude. At this point the case is stable enough to serve as the initialization for the transient case. However if the steady solver begins with 2nd order equations, the solution diverges and fails. In order to maintain stability, approximately 1000 iterations are run as 1st order steady, then around 1,000 iterations are run as 2nd order steady, and if at this point the plots look stable, the transient case begins. The exact number of 1st an 2nd order iterations varied a bit for each case and they are listed in Table 12.4.

In order to prevent divergence, a low Courant number of 0.9 was used. The entire domain was initialized with the assumption of being static at atmospheric conditions. This means that the pressure was set to 1 atm, the temperature to 300 K and the velocity to 300 K. The operating condition was set

to 0 atm. As shocks develop in this domain, which cause large pressure gradients, the dynamic mesh refinement tool was used with gradient and scale settings. This tool automatically adds refinement every 10 iterations to the regions that exhibit these large pressure gradients. This was used after reviewing an example in the ANSYS Theory Guide that used a similar strategy to deal with adverse pressure gradients in shocks in a supersonic nozzle [40].

11.3.1. Boundary Conditions

Table 11.5 lists the boundary conditions, which correspond to the labeled boundaries of the geometry in Figure 11.3. The boundaries are the same as the 'Nozzle-Steady' case apart from the added Cavity wall, which is explained. All of the other boundary conditions are described in subsection 11.3.1.

Table 11.5: Boundary Conditions: Nozzle-Cavity

Boundary	Type
Inlet	Pressure Inlet
Farfield (outlet)	Pressure-Farfield
Axis	Axis
Nozzle Wall	Wall, stationary, no slip, adiabatic
Cavity Wall	Wall, stationary, no slip, heat-transfer

Cavity Walls: Wall The cavity walls are set to stationary, no-slip walls with heat transfer. The material choice from the preliminary design is SS304, therefore the cavity wall is set to have the SS304 heat transfer coefficient of $16W/mK$, with a free stream temperature of 300K, and a wall thickness of 1mm.

11.3.2. Calculation Activities

For each case, 4 points (P1, P2, P3, P4) were set along the x-axis in the resonance cavity, with P1 located at the opening of the cavity, P4 at the base of the cavity and P2 and P3 spaced in between. The exact coordinate location of these points varied per case and are listed in Table 12.3. The solver recorded the pressure, temperature and velocity at each of these points, as well as the mass flow rate at the inlet and outlet boundaries. The contour plots of the mach number, temperature and pressure were calculated every 100 iterations to observe how the solution developed. All of this was exported and plots of the data were generated using Microsoft Excel.

11.3.3. Mesh and Solver Validation Study

In order to verify if this strategy can predict the average value of the periodic temperature at the base of the cavity, the Medium Mesh and solver setup used in this thesis was tested on the design in the Afzali paper [6]. The geometry and inputs were adjusted to match the Alfazi case, whose geometries are shown in Figure 11.2. As these figures contain variables, the values used for these geometric variables are listed in Figure 11.17 [6].

Table 1. Physical specification of numerical and experimental case.

Variable	Value	Variable	Value	Variable	Value
D_n	5	A_{0n}/A_n	7.5	P_a	1
D	6.3	L	48	T_a	300
d	1.4	NPR	11	k	0.25
ΔS	13	T_0	300	t_{pipe}	1

Figure 11.17: Afzali Validation Case Inputs [6]

The parameters at 4 points in the cavity were measured. The coordinate location of each of these points, labelled P1, P2, P3, P4, are given, in mm, in Table 11.6. In order to keep the solution stable,

the Steady-Transient Hybrid Model was used. The solver inputs required for this stabilization and the total calculation time is given in Table 11.7. The case was run until it stabilized and the average value of each parameter did not vary greatly. Information on the mesh details, quality factors, and images of this mesh are contained in Appendix E.

Table 11.6: Alfazi Validation Simulation Case Points 1-4 x-coordinate locations in mm ($x = 0$ at nozzle exit)

Case	P1	P2	P3	P4
Afzali Validation	13	29	45	60.75

Table 11.7: Alfazi Validation Case: Solver Info

Case	Afzali Validation
# **Iterations: Steady 1st Order**	1400
# **Iterations: Steady 2nd Order**	1200
Time-Step Size (s)	6e-07
# **Iterations: Transient 2nd Order**	5300
Transient Flow Time (s)	1.55502e-4

The results of the pressure at the base of the cavity (P4) in the Afzali study, seen in Figure 11.5a, show the fully transient solution. Here after 0.003s the solution has converged and the temperature at P4 oscillates around an average value 700K. The aim of the steady-transient hybrid approach used in this thesis is to calculate the average value of this very refined transient solution, in a much more time effective way. Therefore the Afzali case is prepared using the same mesh sizing as in this thesis and run using the same solver approach. If the result predicted at P4 using the mesh from this thesis results in a value of temperature near to the average of the periodic values in the transient solution, then it validates this meshing and solver strategy. An image of the mesh, table of the mesh quality factors and all of the resulting plots and figures are in Appendix E.

Figure 11.18 shows the resulting contour plot of the temperature at P4 using the Medium Mesh with the steady-transient hybrid solver after 7550 iterations, or 0.0001464s in total flow time. A graph of the temperature versus time at all the points is shown in Figure 11.19. The solution was quite stable at this point and therefore it was ended. 1400 iterations were run steady with 1st order discretization equations, then 1200 iterations were run steady with 2nd order equations, which is listed in Table 12.4. The use of 1st and 2nd order discretization equations are explained in section 11.3. After this point, the transient case was run with a time-step of 6e-07s. In these results, the last 1,500 iterations is equal to approximately 1 flow cycle. The average values of Pressure, Temperature and Velocity at Points 1-4 for these last 1,500 iterations are listed in Table 11.8.

Taking the average temperature of this final cycle results in a temperature of 705K. This extremely close to the average value calculated in the complete transient case run by Afzali and required much less computational time. This steady-transient hybrid case this took approximately 6 computational hours to run, as compared to the 9,000 hours required to run the fully transient case. Therefore the final values in the steady-transient hybrid model is validated to use, and the resulting values are to be taken as the average values of a fully transient model. A more extensive set of results for the validation can be viewed in Appendix G.

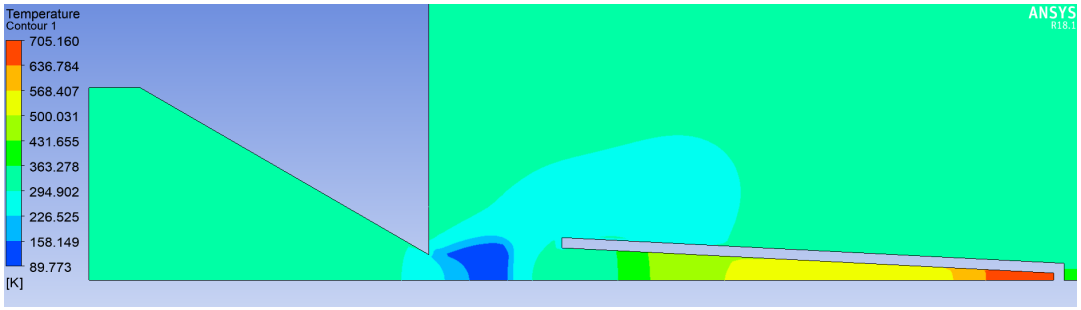

Figure 11.18: Afzali Verification Temperature Contour

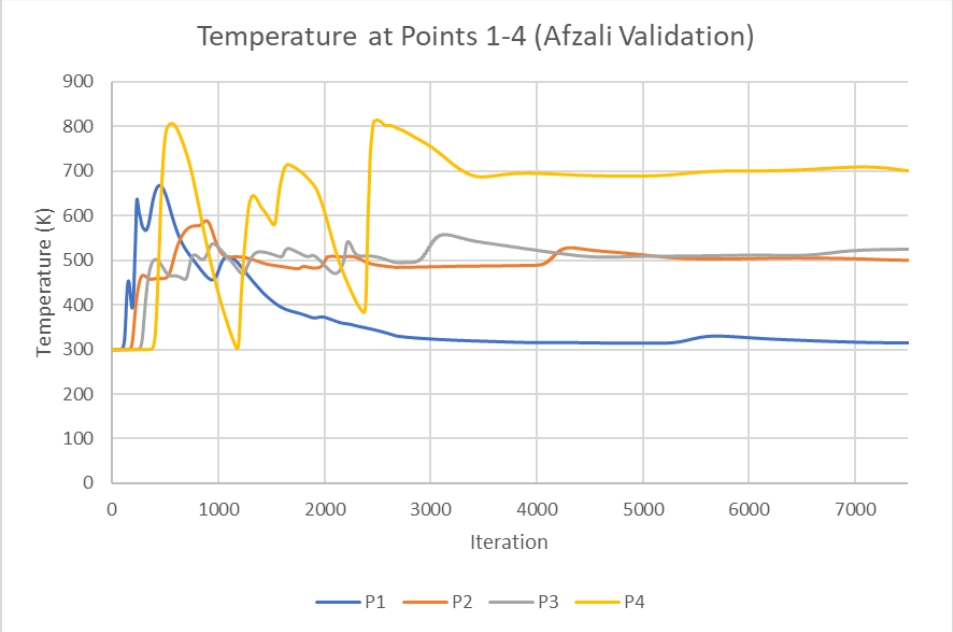

Figure 11.19: Afzali Verification Temperature vs. Iteration plot

Table 11.8: Results Afzali Validation, average values at P 1-4 in transient

Parameter	P1	P2	P3	P4
Pressure (Pa)	322066	352688	377003	358202
Temp (K)	315	501	524	705
Velocity (m/s)	12.56	15.6	20	0.5

11.4. Conclusion

In this chapter, an introduction and explanation of the setup of the 'Cavity' numerical simulation was given. Here, the background behind the mesh grid sizing, and refinement and validation studies were given. The mesh refinement study was successful in determining which level of refinement was sufficient to generate a solution, without the grid sizing affecting the accuracy of the results. Then the setup of the solver is provided, including the boundary conditions used. Finally, the chapter presented a mesh and solver validation study, which demonstrated that the mesh and solver setup were accurate in their results, by testing them on 2 documented cases and finding agreeable results.

12

Results and Discussion

In this chapter, a description of all of the cases run as part of the 'Cavity' cases are given. As part of this description, the geometric parameters, solver inputs, and the strategy behind the choices for each case are presented. An explanation of the convergence and solver validation strategy is provided. Finally the resulting data is provided and analysed in order to choose the Detailed Design.

12.1. Description of Cases

The purposes of these 'Cavity' cases is to test whether the resonance heating effect occurs for the preliminary design, and to run other options in order to generate the 'Detailed Design.' First *Case 1: Preliminary design*, was tested to see if the preliminary design calculated using the python code and nozzle simulation results was able to heat the gas to the required temperature. When Case 1 resulted in a base temperature lower than the required ethanol auto-ignition temperature of 640K, 2 more options were tested. In *Case 2: Large* α, the resonance cavity half angle was increased from 3 to 6 °to see how the cavity angle effected the heating and if the 3 °half-cone angle is optimum, as stated by other researchers. When this also proved to be incapable of heating the gas sufficiently, *Case 3: Large* D_{res} was run, in which the opening diameter of the resonance cavity was increased. A description of each of these cases is listed in Table 12.2. Case 3: Large D_{res} was successfully able to heat the gas at the base of the cavity above the auto-ignition temperature and was chosen for the system 'Detailed Design.' In order to gather more information on how the resonance gas input pressure affects performance, 3 additional cases were run with Case 3 using different input pressures. In this section an overview of each case is given. For each of these cases, it should be assumed that all parameters, other than what is described in Table 12.2 are those from the preliminary design. For clarity, a table of the adjusted preliminary design values is provided, see Table 12.1, whose dimensions correspond to those labeled in Figure 11.3.

Table 12.1: Resonance Ignition Device *Adjusted* Preliminary Design Main Parameters

Parameter	Symbol	Value	Unit
Injection Nozzle Exit Diameter	D_n	3	mm
NPR, Nozzle Pressure Ratio	P_o/P_{atm}	19	
Resonance Cavity Shape	Shape	Conical-Truncated	
Resonance Cavity Inlet diameter	d	4.0	mm
Resonance Cavity end diameter	d_e	1.0	mm
Resonance Cavity Angle	α	3	degrees
Resonance Cavity Length	L_{res}	28.622	mm
Resonance Tube wall thickness	t_w	1.0	mm
Gap Distance	ΔS	11	mm

The coordinate locations of P1, P2, P3, P4 are given, in mm, in Table 12.3, as they vary for each case. Table 12.4 provides the solver stabilization information and total calculation time for each case. All of the Case 3 studies use that same point coordinates and solver stabilization information. The cases were run for differing lengths of transient iterations because after approximately 4,000 transient iterations, the average value of each parameter does not vary greatly. Continuing to run beyond this many iterations serves to provide increased accuracy to the solution. As it took approximately 5 hours of run time to compute 6,000 transient iterations, once it was seen that the average values for Cases 1 and 2 were not sufficient, they were ended. Case 3 was run for 43,000 transient iterations because it was successful in heating the gas at the cavity base to above the auto-ignition temperature. This long run-time was completed to increase the accuracy of the data for this case, as it would be chosen for the system Detailed Design. After this point, it was decided to investigate the effect that changes to the resonance gas input pressure would have on the dynamic heating of the gas. Cases 3.1-3.3 were conducted, in which the input pressure was set to 10.25, 15 and 25 bar. The resulting mass flow rate, and temperature and pressure in the cavity for these difference input pressures were compared. Before presenting and analysing the results, an explanation of the solver convergence and validation is provided.

Table 12.2: Cavity Simulation Case Descriptions

Case	**Cavity Half-Cone Angle, α**	D_{res}	**Gap Distance, ΔS**	**Cavity Length, L_{res}**
Case 1: Preliminary Design	$3°$	4mm	11mm	28.622mm
Case 2: Large Angle	$6°$	4mm	11mm	14.272
Case 3: Large D_{res}	$3°$	6mm	11mm	47.7mm

Table 12.3: Cavity Simulation Cases Points 1-4 x-coordinate locations in mm ($x = 0$ at nozzle exit)

Case	**P1**	**P2**	**P3**	**P4**
Case 1: Preliminary Design	11	20.5	30	39.5
Case 2: Large Angle	11	16	21	25
Case 3: Large D_{res}	11	27	43	58.5

Table 12.4: Cavity Cases: Solver Info

Case	**1: Preliminary**	**2: Large α**	**3: Large D_{res}**
# **Iterations: Steady 1st Order**	1200	1000	1200
# **Iterations: Steady 2nd Order**	2000	1000	1000
Time-Step Size (s)	6e-07	6e-07	6e-07
# **Iterations: Transient 2nd Order**	10000	4500	43000
Transient Flow Time (s)	2.934e-4	1.3203e-4	1.2906e-3

12.2. Convergence and Solver Validation Check

In order to prove that the solver has converged, the plot of the residuals and the convergence plots of one of the parameters is included for each case. As this flow is periodic in nature, its residuals will not resolve to an extremely low value, like 1e-6 as is seen in static flows. However in the residual plot for Case 3, Figure 12.1 which was run the longest of all the cases, to 45,000 iterations, the average value

of each of the residuals was between 1e-04 and 1e-06. The residuals for Cases 1 and 2,Figure G.1 and Figure G.6, are a bit higher, but this is due to the fact that these cases were not run as long, and it is predicted that if they were run for 45,000 iterations, their residuals would match the range shown in Case 3. In order to verify if the transient portion has converged, plots of a small section of the temperature versus iteration were produced. As previously stated, in the transient portion each time-step performs 20 iterations, and if the time-steps is correctly sized, then the solver should converge by the end of each time-step. This convergence can be observed by a 'staircase-like' plot. The convergence plot for Case 3 is displayed in Figure 12.2, and its stair-case shape demonstrates that this solution has converged at each time-step. Similar plots for Cases 1 and 2 are in Appendix G.

Another method to verify convergence is to measure the mass flow rates of the inlet and outlet, and check the flux value. The flux is a measure of the difference in these values. As this is a closed system, it is expected that the mass flow rate at the inlet and outlet will be equal. In Figure 12.3, Figure 12.4 and Figure 12.5, the mass flow rates and flux for Case 3 are shown. As explained in chapter 10, the mass flow rates are chaotic at the beginning when the solver is making wild, initial guesses. As the solution progresses, the absolute values of the mass flow rates get closer. The mass flow rate of the choked injection nozzle was calculated to be 31.165g/s in the preliminary design python script. The results of the simulated inlet mass flow rates cases are extremely close to this value, between 31-32g/s. Therefore it can be said that the numerical solution is accurately modeling the inlet mass flow rate. To state with 100% certainty that convergence has been reached, the mass flow flux should be less than 1%. However in all of the cases presented, this flux varies between 2-8%. In Case 3, which ran the longest, the solution was able to converge to a flux of 2-4%. This flux greater that 1% is likely due to the fact that the in this model, the outlet is set to a pressure-farfield, which allows flow in and out. This means that there may be some gas flowing back into the model at the outlet boundaries, which is preventing it from reaching a 1% flux. In turbulent flows, it is common to experience what the solver calls 'reversed flow' at the outlet. As the flux continued to drop the longer the solution was iterated, it is expected that this flux would approach 1% after a very long time. For reference, the 45,000 iterations in Case 3 took over 15 hours to compute. Therefore in the spirit of using time efficiently, it was decided to accept these flux values.

Finally, it is important to compare these results to other similar studies, to see if the values are within the expected range. In the Afzali resonance paper, with an NPR of 11, the cavity base temperature and pressure were approximately 700K and 2.5atm, respectively[7] . In the Narayanan resonance device, with an NPR of 5, the cavity base temperature and pressure were approximately 980K and 3 bar. Comparing these to the results of Case 3, where $NPR = 19$, the average cavity base temperature and pressure were 800K and 3 bar. We do not expect the results this simulation to be identical to these examples, as many factors effect the final pressure and temperatures, such as geometry and NPR. However, the results found in all 3 cases are similar in scale to the example cases, which lend support to the results of this simulation. The residuals, mass flow rate, flux and convergence plot for all of the cavity cases are included in Appendix G.

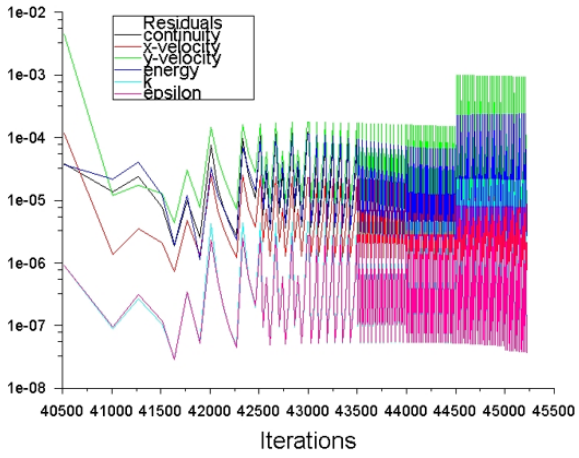

Figure 12.1: Case 3: Large D_{res} , Residuals

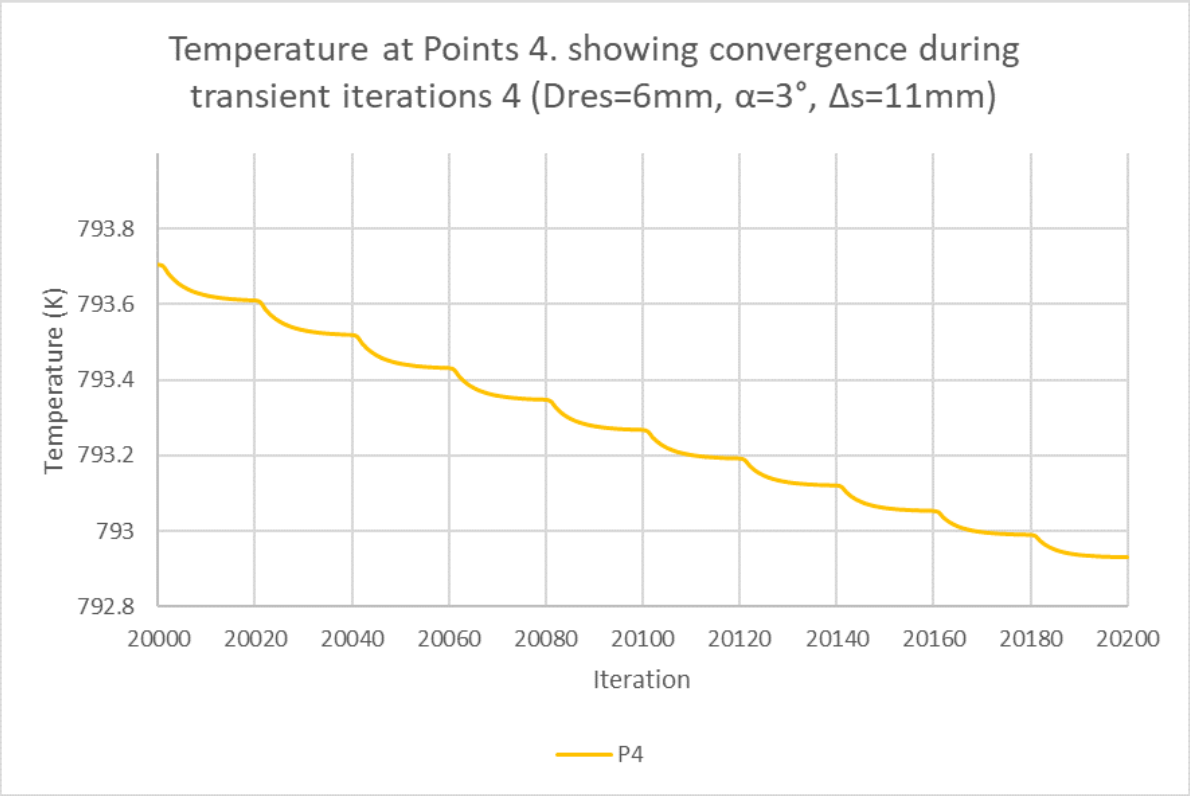

Figure 12.2: Case 3: Large D_{res}, Transient Convergence

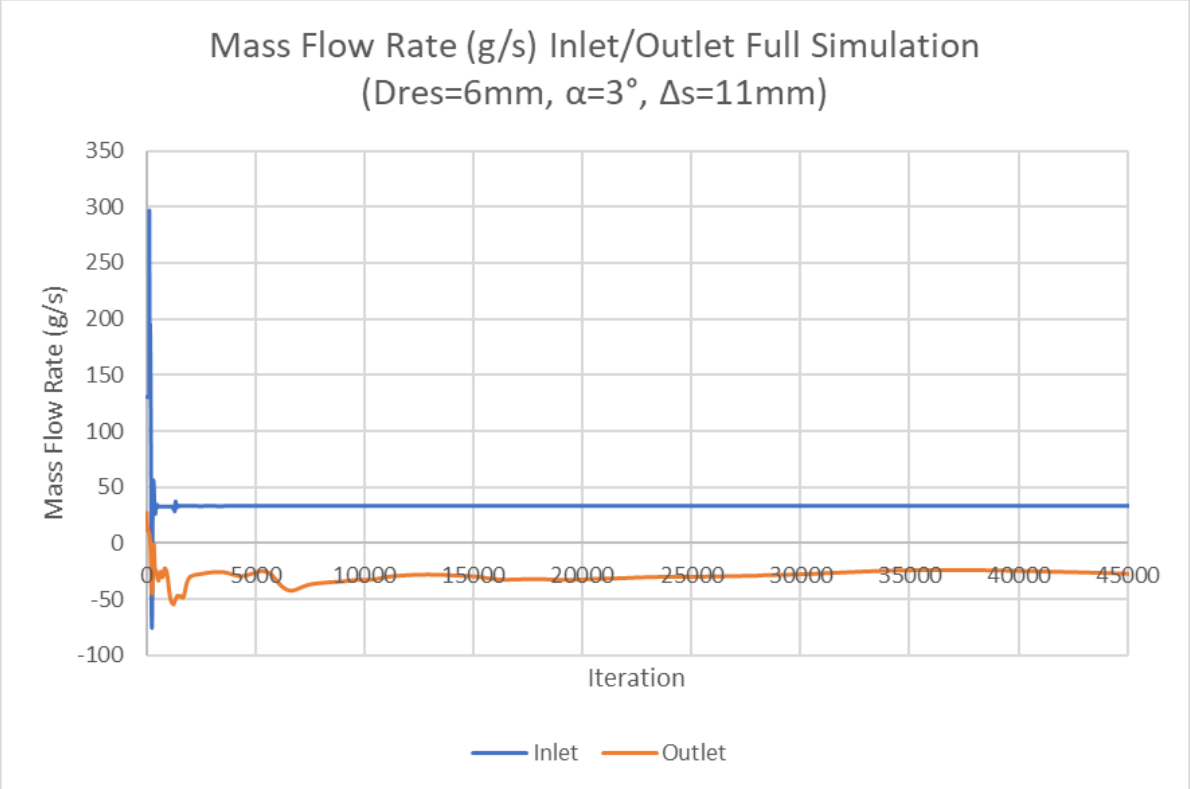

Figure 12.3: Case 3: Large D_{res}, Mass Flow Rate Inlet/Outlet Full Simulation

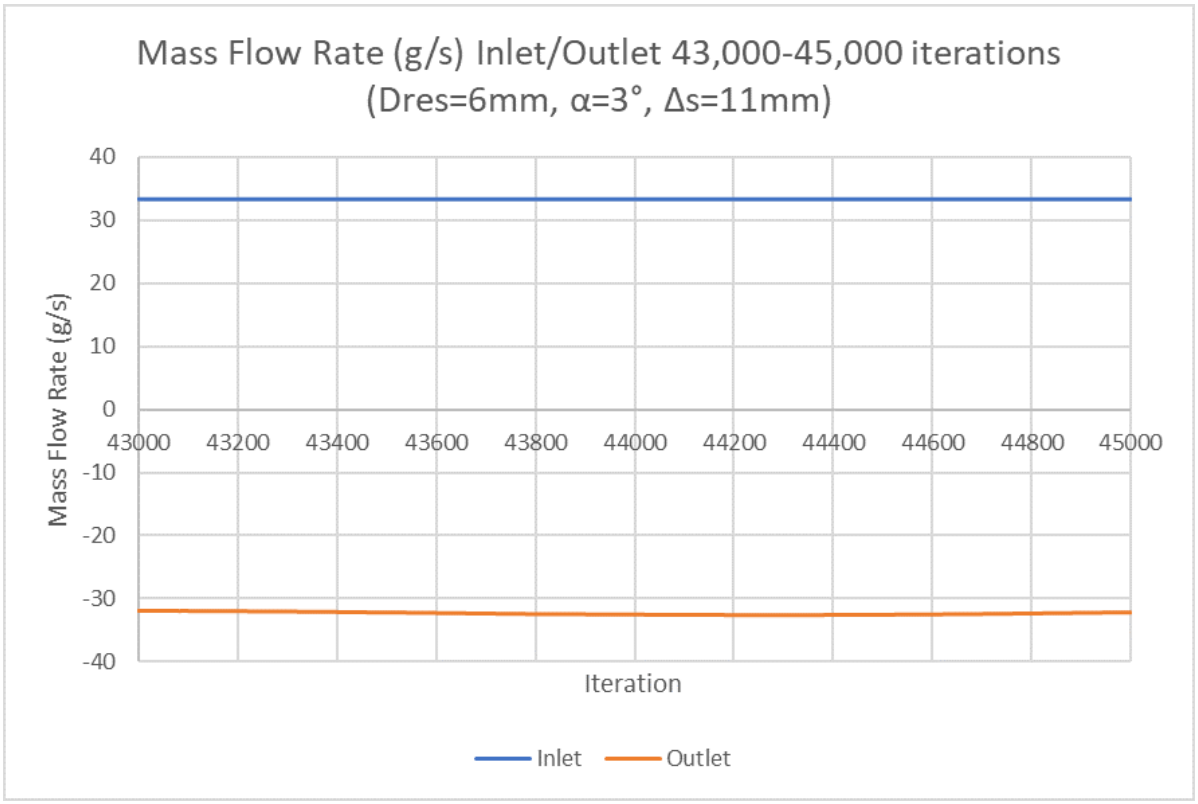

Figure 12.4: Case 3: Large D_{res}, Mass Flow Rate Inlet/Outlet End of Simulation

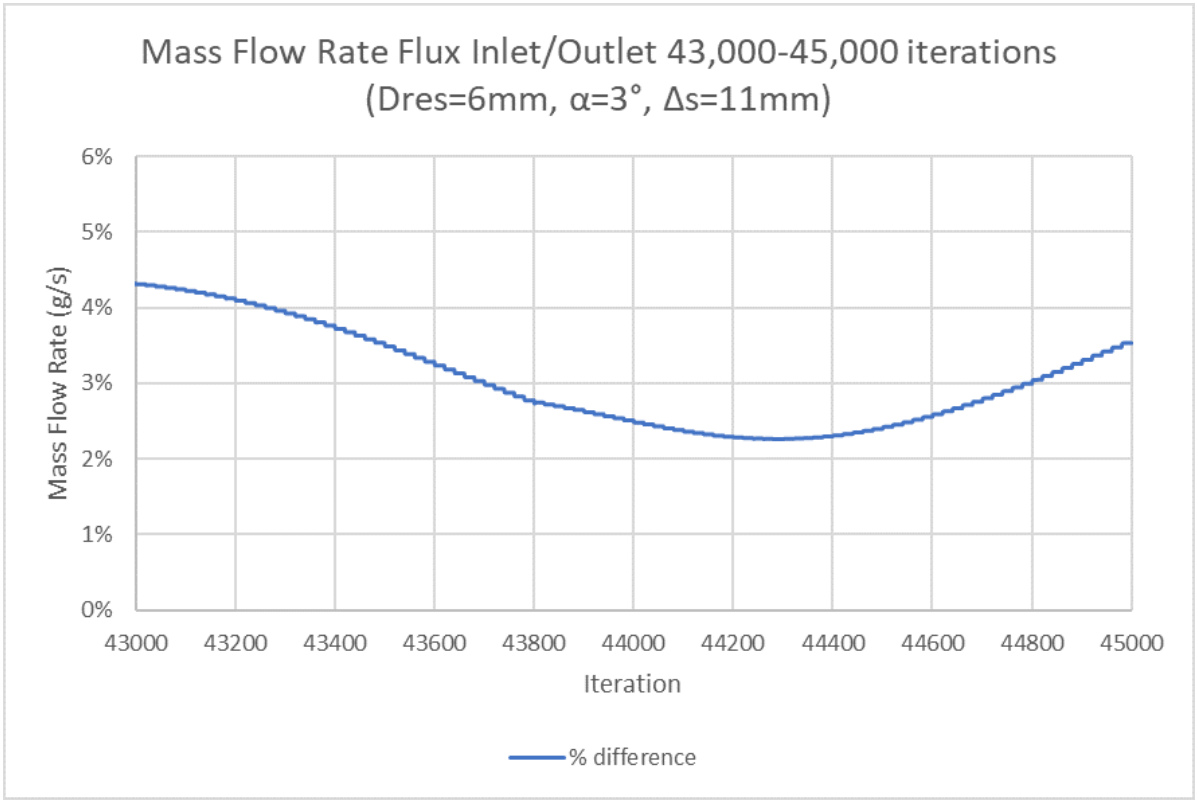

Figure 12.5: Case 3: Large D_{res}, Mass Flow Rate Inlet/Outlet Flux, End of Simulation

12.3. Cases 1-3 Results

Now that the setup and description of all of the 'Cavity' cases have been presented, the results of these numerical simulations are analyzed and the Detailed Design is presented. Table 12.5-Table 12.7 list the average pressure, temperature and velocity values at points 1-4 during the transient phase for each of the cases. The average value was taken because the parameters oscillate with a very small amplitude during the transient phase, due to the periodic nature of the flow. As stated, in order for the resonance ignition system to achieve combustion of ethanol, the temperature of the gas at the base of the cavity must be greater than the ethanol auto-ignition temperature of 642k. As the numerical simulation does not take into account friction losses that will occur in the physical system, it will likely calculate a temperature slightly higher than the physical value. Afkali and Narayanan estimated this difference to be around 25K [7] [51]. Therefore a conservative minimum temperature requirement of 680K for the base of the cavity is set. Cases 1-3 were conducted in numerical order, with the results of the prior case providing input to the changes made between cases. The tables of the average values at each of the 4 points and the contour plots of are presented below for Cases 1-3. As a note, these contour plots are taken from the last iteration in the transient case, and therefore the values given are instantaneous and do not correspond to the average values. However they are shown to provide insight onto the shape of the different contour plots. The values given in Table 12.5-Table 12.7 are the average values at each of the points in the transient phase, and are the values that will be compared for each case. First the most important results of Cases 1-3 are presented and then the analysis of these results is given. An explanation of the convergence and validation of these cases is provided later on in section 12.2, and additional figure are given in Appendix G. Afterwards, the setup of cases 3.1-3.3 are given and their tables and contour plots are presented and analyzed.

12.3.1. Results Case 1: Preliminary Design

Table 12.5: Results Case 1: Preliminary Design, average values at P 1-4 in transient

Parameter	P1	P2	P3	P4
Pressure (Pa)	330953	353165	353909	354548
Temp (K)	320	598	599	593
Velocity (m/s)	11.9	2.1	1.55	0.17

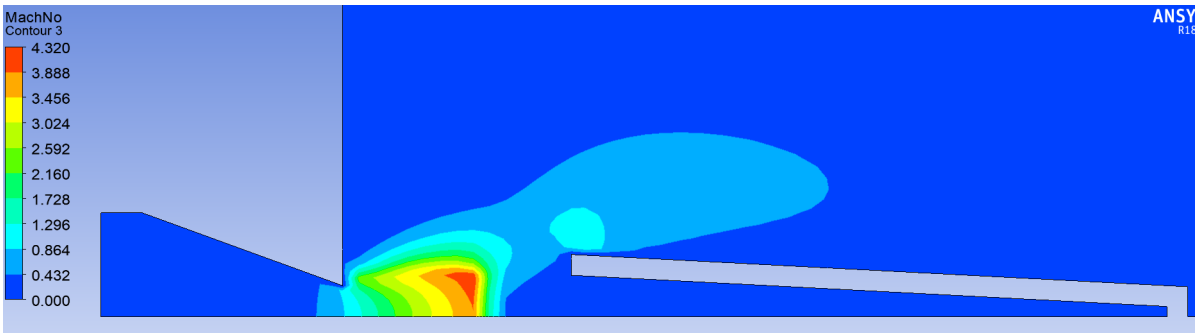

Figure 12.6: Case 1: Preliminary Design, Mach Contour at End of Simulation

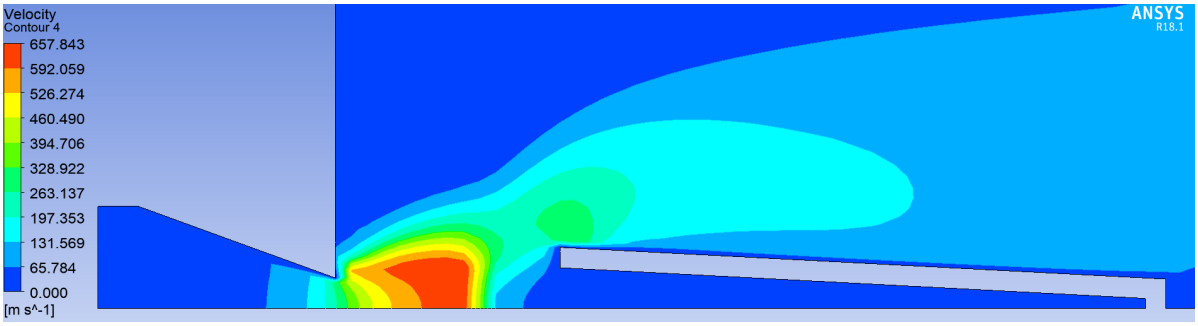

Figure 12.7: Case 1: Preliminary Design, Velocity Contour at End of Simulation

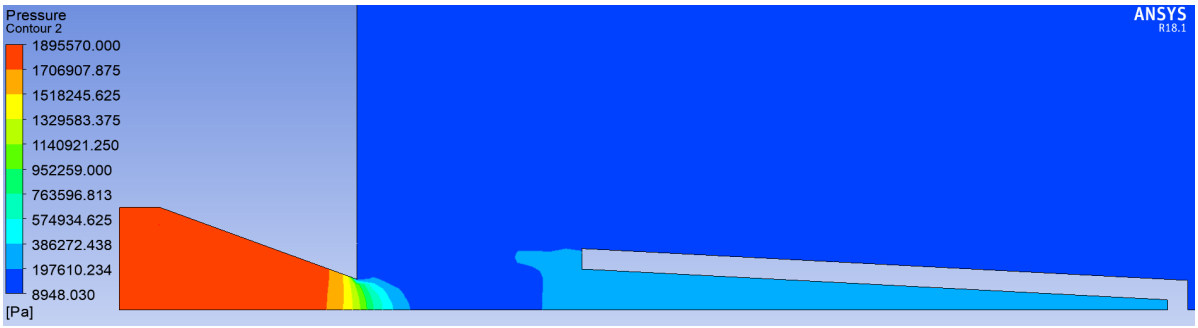

Figure 12.8: Case 1: Preliminary Design, Pressure Contour at End of Simulation

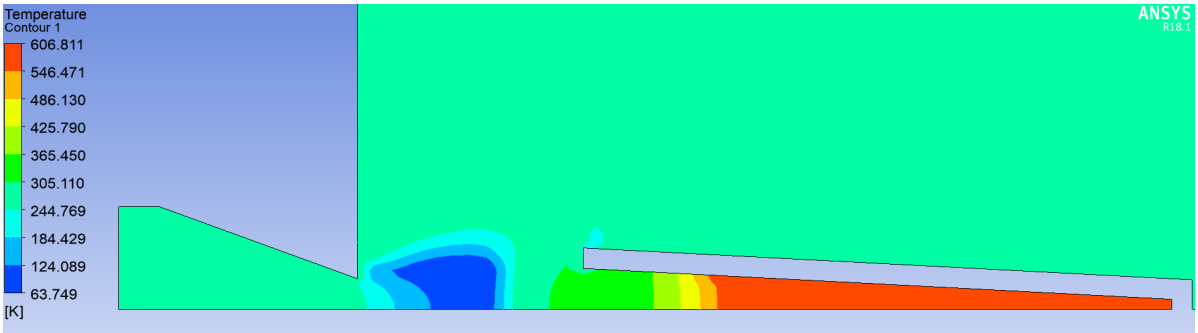

Figure 12.9: Case 1: Preliminary Design, Temperature Contour at End of Simulation

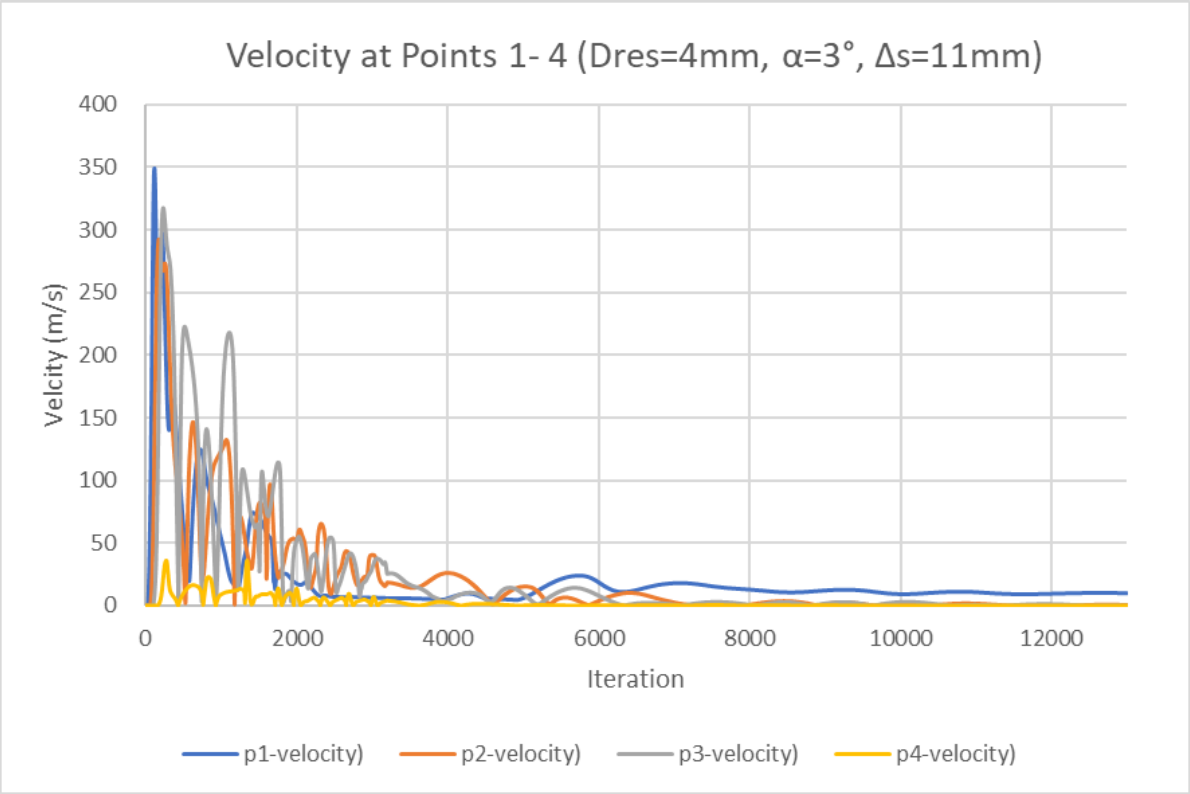

Figure 12.10: Case 1: Preliminary Design, Velocity Plot

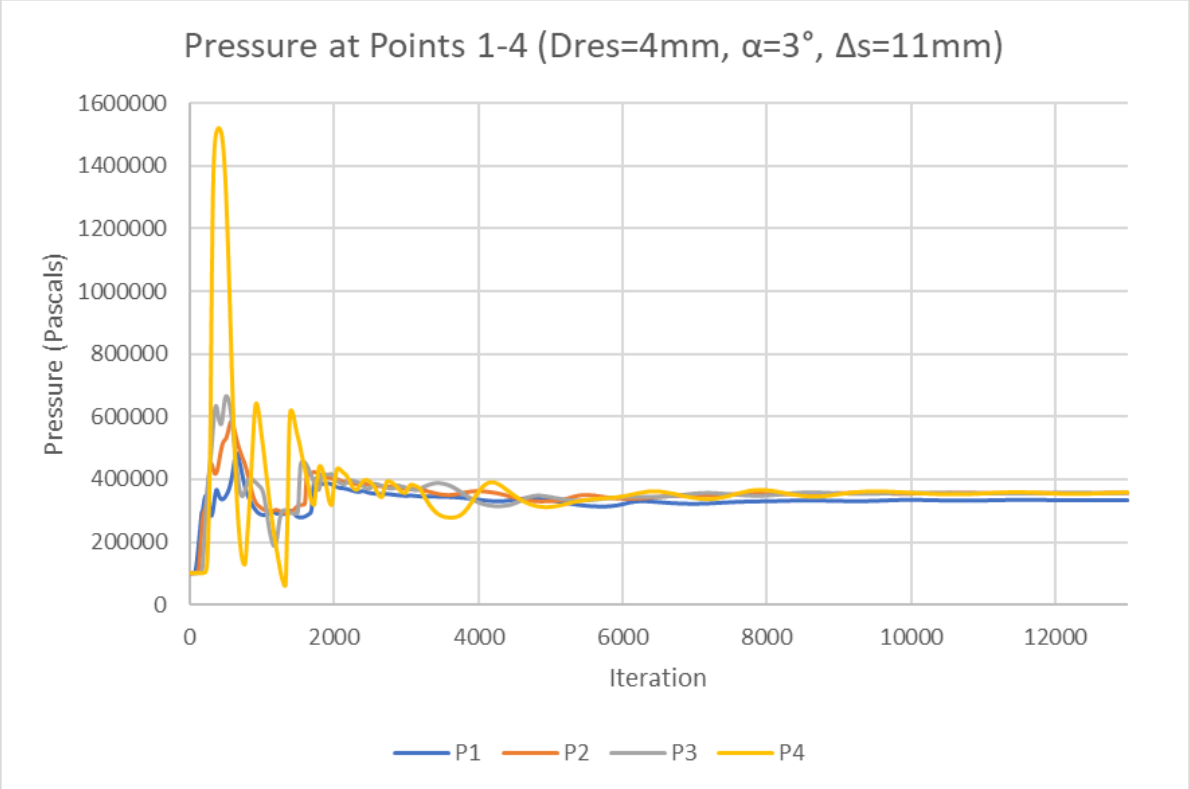

Figure 12.11: Case 1: Preliminary Design, Pressure Plot

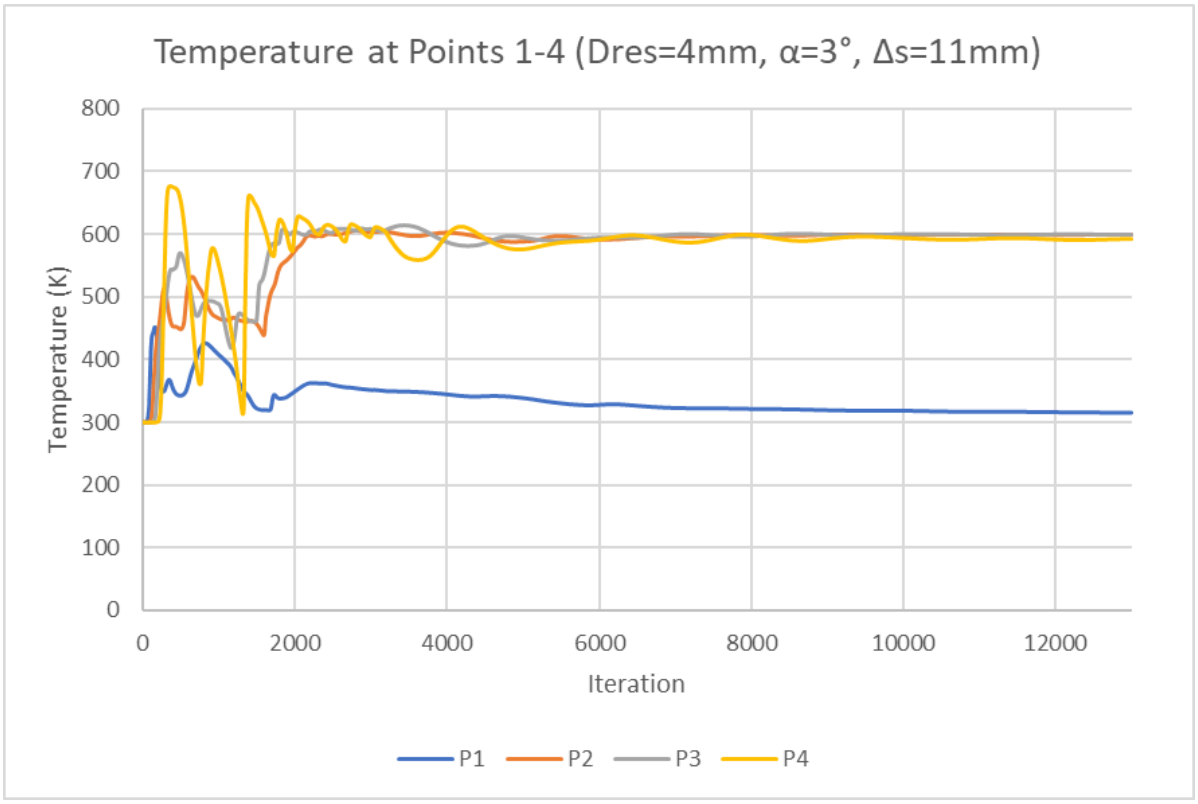

Figure 12.12: Case 1: Preliminary Design, Temperature Plot

12.3.2. Results Case 2: Large Alpha

Table 12.6: Results Case 2: Large α, average values at P 1-4 in transient

Parameter	P1	P2	P3	P4
Pressure (Pa)	361223	386604	385800	385464
Temp (K)	311	361	446	468
Velocity (m/s)	8.15	2.04	1.5	0.14

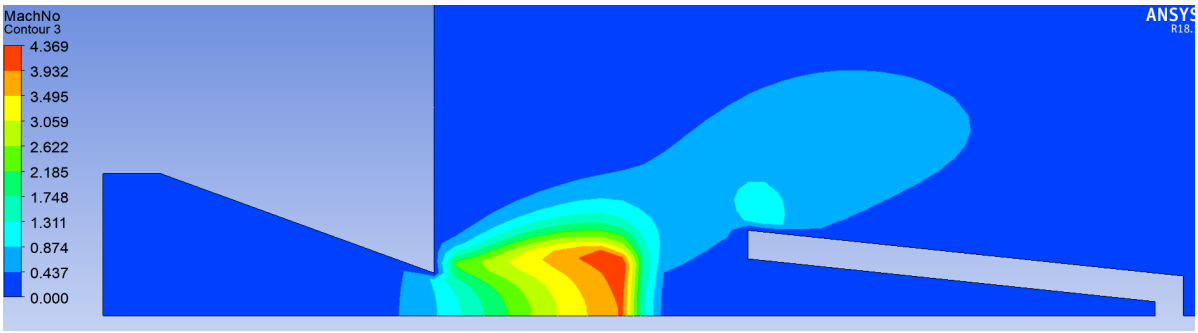

Figure 12.13: Case 2: Large α, Mach Contour at End of Simulation

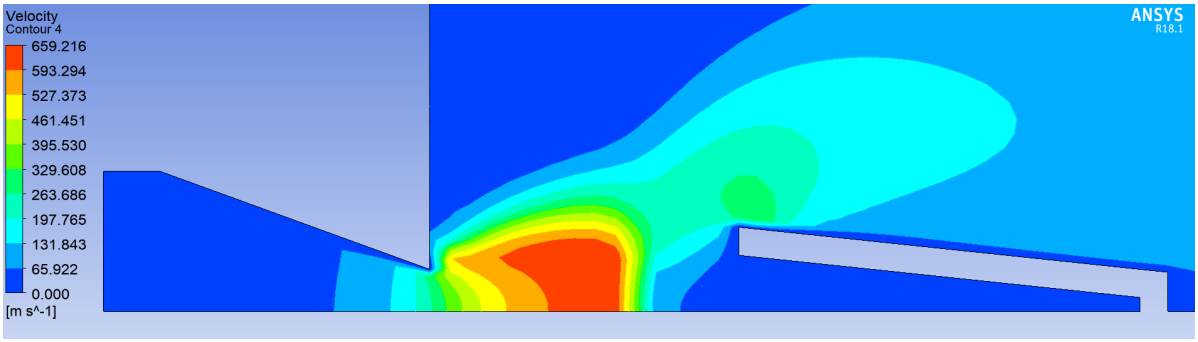

Figure 12.14: Case 2: Large α, Velocity Contour at End of Simulation

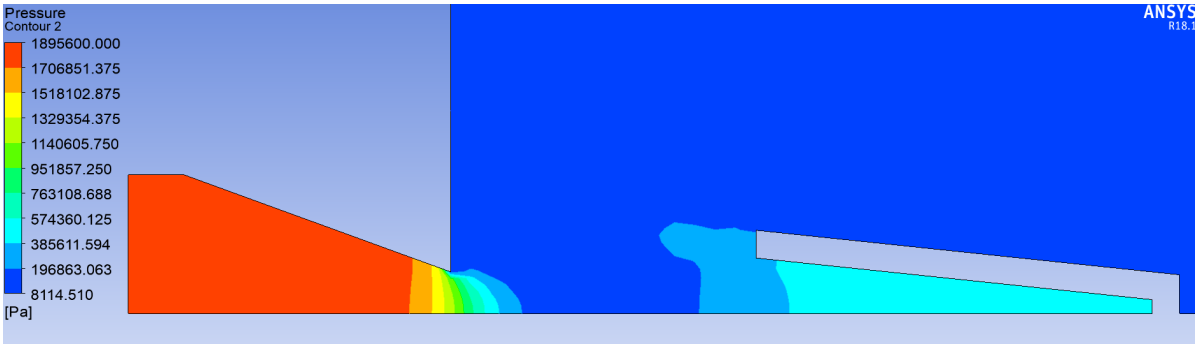

Figure 12.15: Case 2: Large α, Pressure Contour at End of Simulation

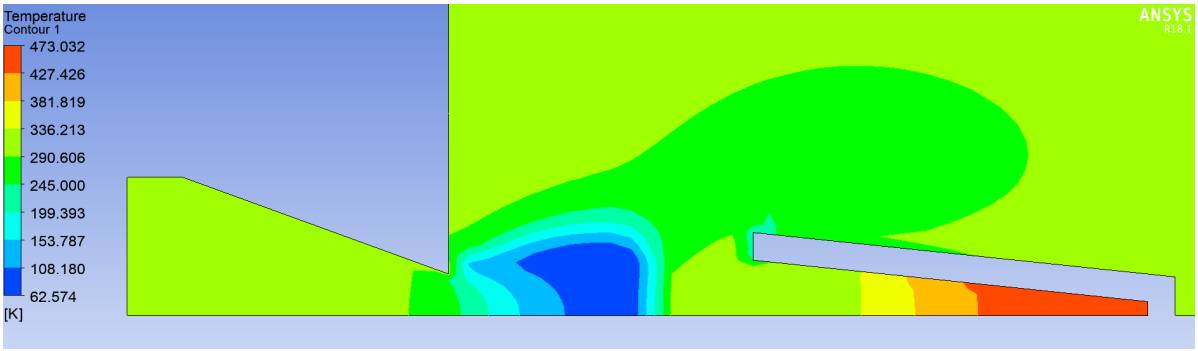

Figure 12.16: Case 2: Large α, Temperature Contour at End of Simulation

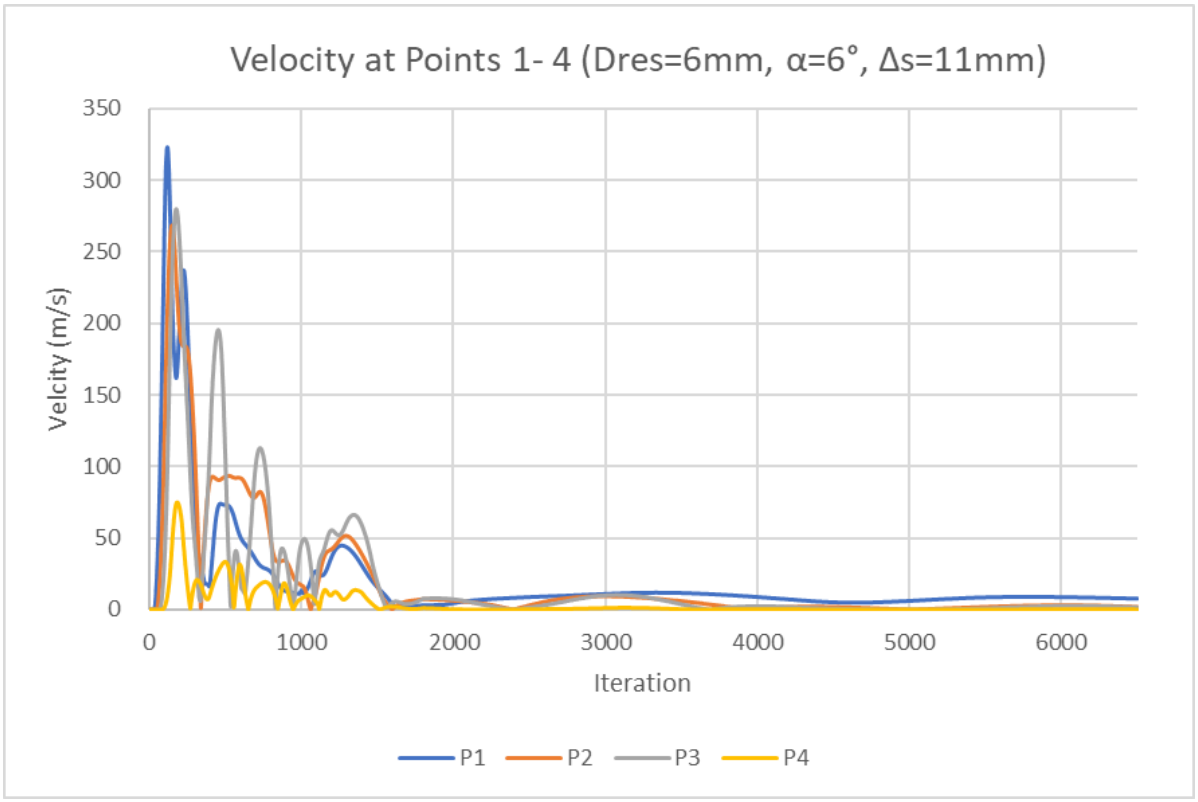

Figure 12.17: Case 2: Large α, Velocity Plot

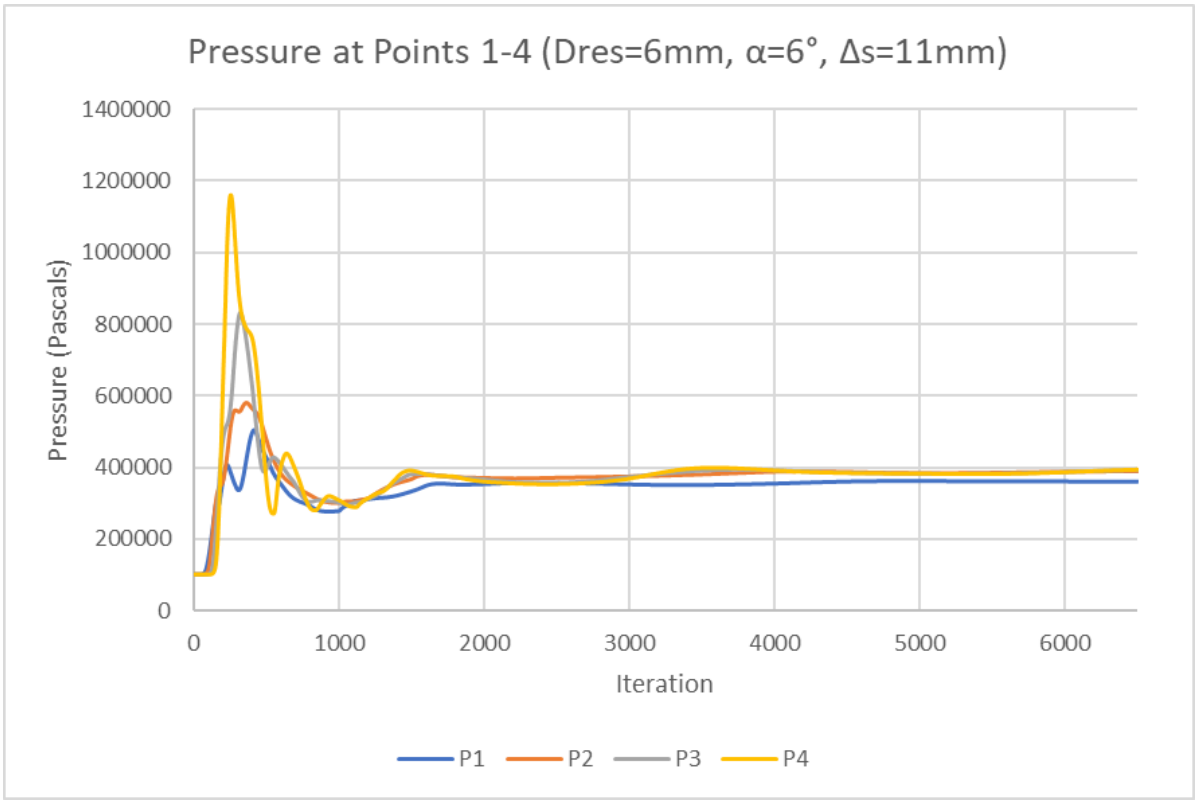

Figure 12.18: Case 2: Large α, Pressure Plot

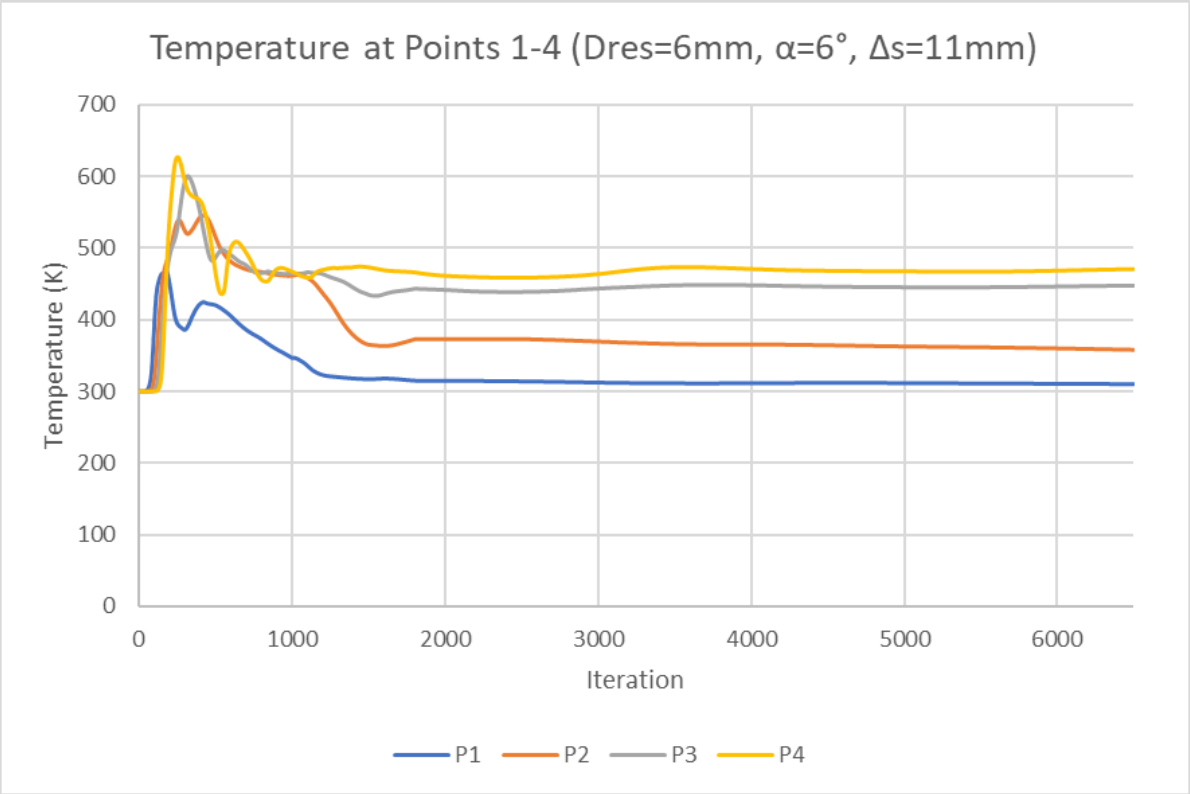

Figure 12.19: Case 2: Large α, Temperature Plot

12.3.3. Results Case 3: Large Dres, Po= 19 bar

Table 12.7: Results Case 3: Large D_{res}, $P_o = 19$ bar average values at P 1-4 in transient

Parameter	P1	P2	P3	P4
Pressure (Pa)	276160	306524	306437	306381
Temp (K)	315	446	670	800
Velocity (m/s)	24	1.03	1.02	0.03

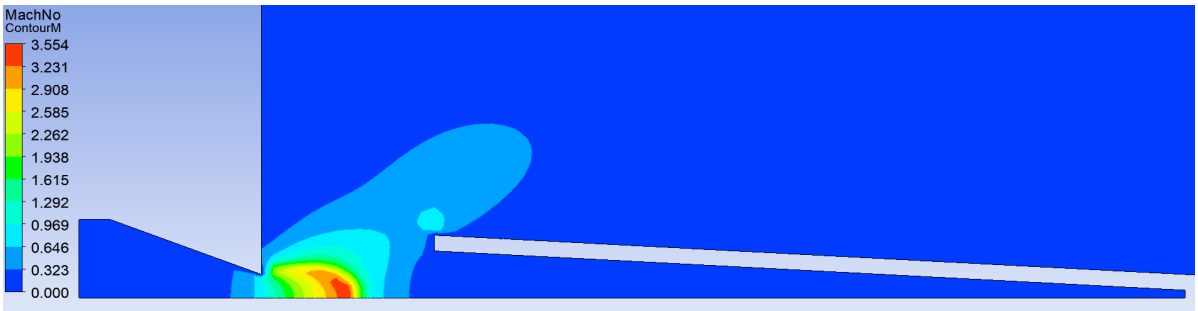

Figure 12.20: Case 3: Large D_{res}, Mach Contour at End of Simulation

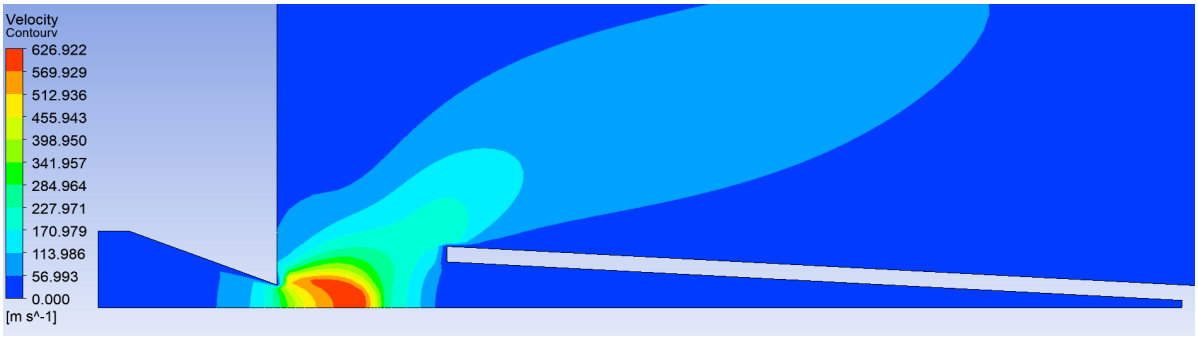

Figure 12.21: Case 3: Large D_{res}, Velocity Contour at End of Simulation

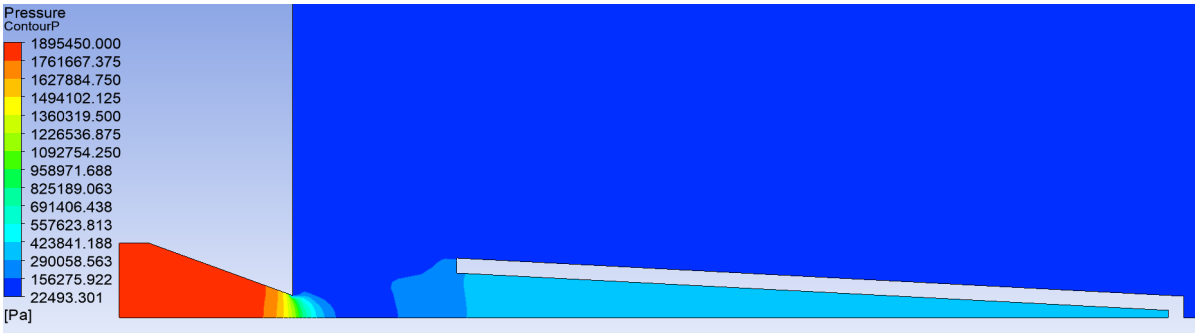

Figure 12.22: Case 3: Large D_{res}, Pressure Contour at End of Simulation

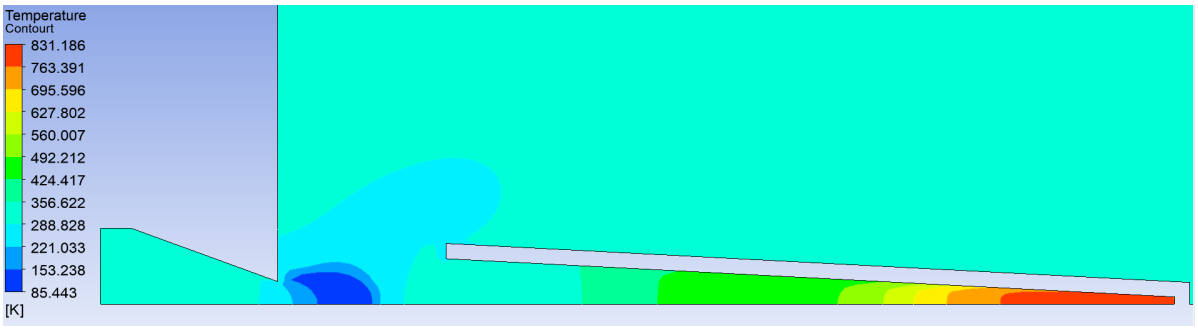

Figure 12.23: Case 3: Large D_{res}, Temperature Contour at End of Simulation

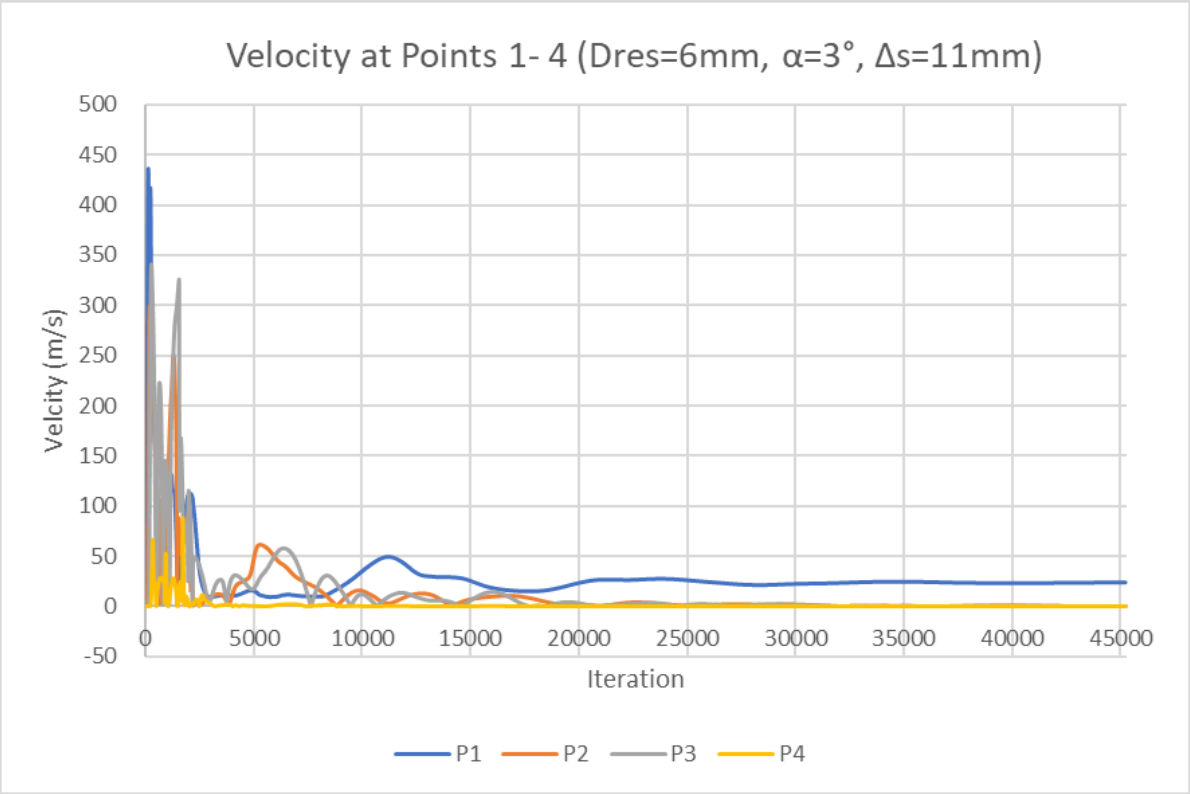

Figure 12.24: Case 3: Large D_{res}, Velocity Plot

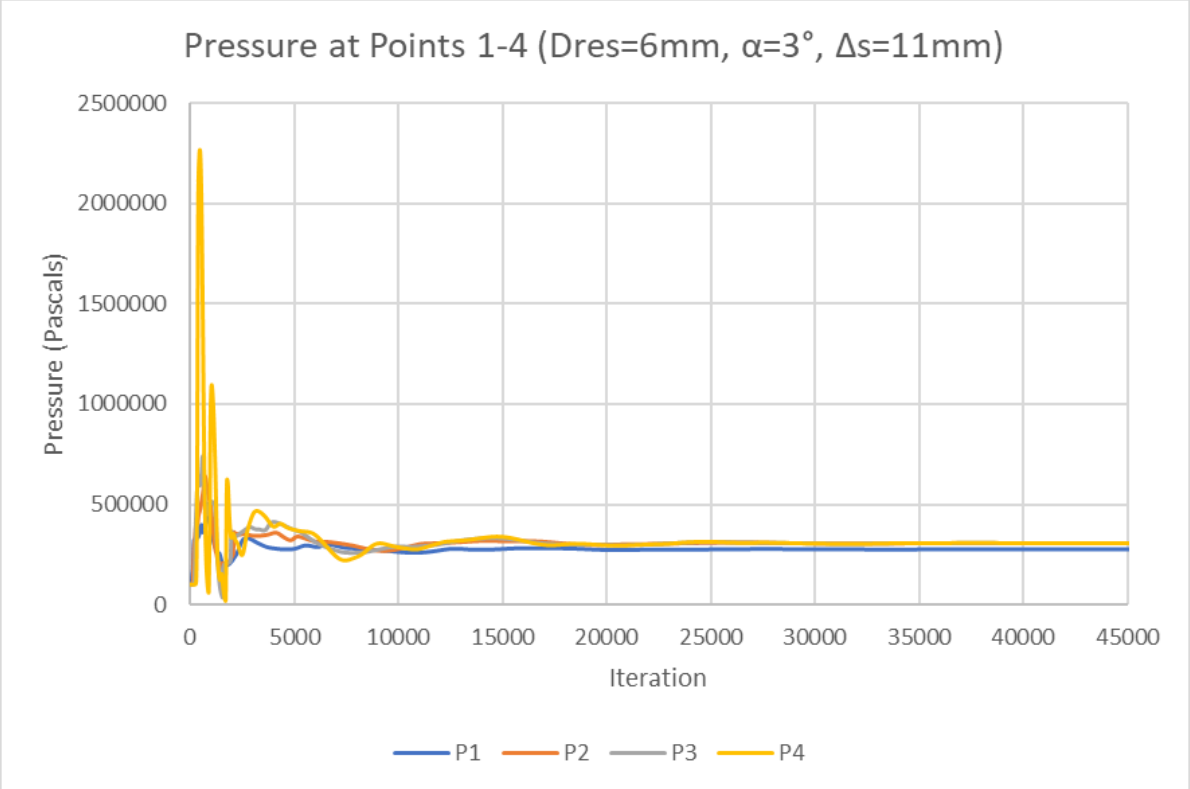

Figure 12.25: Case 3: Large D_{res}, Pressure Plot

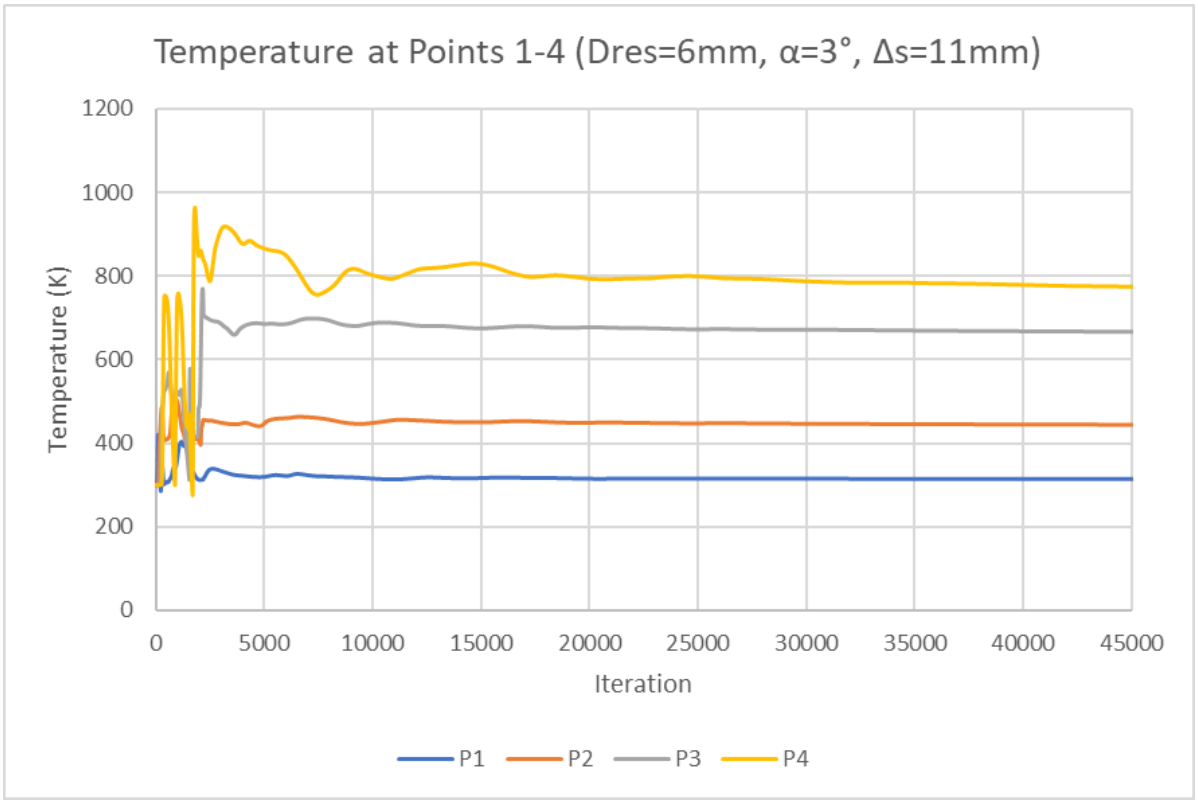

Figure 12.26: Case 3: Large D_{res}, Temperature Plot

12.3.4. Cases 1-3 Analysis

First, the resulting plots and values will be analysed to see if they correspond to the expected behavior of the resonance heating cavity. Then the results for Cases 1-3 will be compared to see which was able to meet the ignition temperature requirements. The plots of the pressure, temperature and velocity at each iteration for Cases 1-3 all follow the same pattern of very chaotic values during the initialization phase in the first 2 thousand iterations. As listed in Table 12.4, the 1st order equations are used at the start for around 1000 iterations to help with stability, followed by approximately 1000 iterations of the 2nd order equations. Once the amplitude of the parameters decreased substantially and the plots stabilized, the transient case was started using these steady results as inputs. All the parameters became very static after around 10,000 iterations, with a very small change in value during each flow cycle. These plots support the steady-transient hybrid method because the were able to initialize relatively quickly using the steady solver, and then solve for the average values in the domain of a comparable transient case. As expected, there are not large oscillations in these plots because they are too coarse to detect these small differences in values. However, the solver is able to detect a slight periodic behavior, as is indicated by the very low amplitudes in the transient portion of the result that occur during each cycle. By taking the average value in the transient portion of the result, these plots are able to successfully calculate these flow parameters. In all of the results presented above, the development of the first shock cell can clearly be seen in the Mach contour plots, where the maximum mach number is between 3.5-4.3. The jet is under-expanded, as seen by the expansion of the jet in the mach contour just past the nozzle exit.

In all 3 cases the velocity contour plots show that a portion of the nozzle jet flow goes directly into the cavity, and the other portion bypasses the cavity. The amount of the flow that bypasses the cavity appears to be dependant on the opening diameter of the resonance cavity. In addition, the graphs of the velocity at each point and the average values listed in the tables, indicate that the velocity of the gas is sonic at the exit of the nozzle, and drops to close to zero in the cavity. This makes sense, as in the physical system as gas is flowing into the cavity from the nozzle, the gas inside of the cavity is flowing out. This means that the overall velocity magnitude of the gas should be near to zero as the flow of the gas in and out should be the same. The likely reason that the velocities are not exactly zero

inside of the cavity, is due to the shocks and turbulence causing the gas to swirl inside the cavity. The velocity at P1 is higher in all cases, which is likely due to the value being affected by the free jet in the gap region.

In these cases, the pressure in the nozzle inlet and exit regions are identical, as is to be expected, since they are all set to 19 bar inlet pressure. The plot of the pressure versus iteration curve for P1-4 show that in each case, the pressure becomes close to equal throughout the cavity, with the highest pressure at the opening of the cavity, P1, and then nearly the same pressures at P2, P3 and P4. This can be seen in both the pressure contour plots and the iterations plots, where the curves are extremely close together for each point. In Case 1, the average pressure in the cavity is around 3.54 bar, in Case 2 it is 3.86 bar, and in Case 3 it is 3.06 bar.

In the temperature contour plots, the temperature inside of the expansion region of the first shock cell is between 64-250K, because according to the ideal gas law, $PV = nRT$ as the pressure drops, ie expansion, the temperature must drop as well. The flat edge of this low temperature region, signifies the switch to the compression zone of the first shock cell, where the pressure and temperature increase. Inside of the cavity, the temperature contour plots and the temperature versus iteration plots show that the temperature increases rapidly with the highest temperature at the base, P4. This is the expected temperature gradient in a resonance cavity and looks very similar to the temperature contour by Narayanan [52]. As explained in chapter 3, this increase in temperature inside of the cavity is caused by the the gas dynamic phenomenon through shock wave irreversibilities and frictional losses. In addition, when comparing the 3 cases, it can be seen that as the temperature in the cavity increases, the pressure decreases. The average temperature and pressure values at P4 are, 3.54 bar and 593 K for Case 1, 3.86 bar and 468 K for Case 2, and 3.06 bar and 800 K for Case 3. This is due to conservation of energy and can be explained by the ideal gas law as well.

Now that the resulting plots and tables have been explained and agree with the expected behavior of a resonance heating cavity, the cases can be reviewed to determine which is able to meet the ethanol auto-ignition temperature. As stated, Cases 1-3 were conducted in order, with information from each case used to make changes in the design of the subsequent case. In *Case 1: Preliminary Design*, the final average temperature at the base of the cavity is less than 600K, which makes it insufficient to ignite this fuel. However this is still a substantial heating of the gas, meaning that the gas dynamic heating phenomenon is occurring successfully. This means that the preliminary design is promising, but some changes need to be made in order to increase the base temperature. In Marchan's paper, he stated that the optimal angle for a resonance heating device was $6°$ [48]. To test this assertion and see if the heating improved, in *Case 2: Large* α, the geometry of the device was adjusted such that the cavity conical angle was $6°$. As the cavity opening and base diameter remained unchanged, the increased angle resulted in a shorter cavity, where $L_{res} = 14.272$. After running this case it was found that the maximum temperature achieved at the cavity base was 468K. This is insufficient and lower in temperature than Case 1 by 130K. It is uncertain if this decrease in performance it attributed to the increased angle or decreased cavity length. However in the interest of time, it is suggested to investigate this further in future works. Based on the results of Cases 1 and 2, *Case 3: Large* D_{res} was designed. Since Case 1 performed better than Case 2, it was decided to maintain the $3°$ cavity conical angle. In the velocity contour plot from Case 1, Figure 12.7 it is evident that a portion of the exhaust jet never enters the cavity, and instead flows directly around the outside. It was then postulated that perhaps the base temperature could be increased by increasing the cavity opening diameter, such that more of the exhaust jet would flow into the cavity and participate in the gas dynamic heating process. Therefore in Case 3, the cavity opening diameter, D_{res} was increased from 4 to 6mm. The cavity angle of $3°$ and base diameter of 1mm were maintained, resulting in a cavity length of $L_{res} = 47.7mm$. The final average temperature at the cavity base in Case 3 was 800K. This is over 120K higher than the conservative minimum requirement of 680K. As Case 3 was successful in heating the gas at the cavity base to well above the ethanol auto-ignition temperature, it is chosen to be the system Detailed Design.

12.4. Cases 3.1, 3.2 and 3.3 Results

After Case 3 was chosen for the Detailed Design, it was decided to explore the effect that changes in the inlet gas pressure would have on the heating of the system. The main engine that this igniter was designed for, the Blizzard, uses a blow-down system, which means that the pressure in its tanks decreases over time. One option is to have the propellant for the ignition system be tapped off of these

main engine propellant lines, which would mean that the pressure of the igniter propellants would be tied to the value in the tank. The ignition lasts for only 1-2 seconds, meaning that the change in the tank pressure due to the blow-down effect, will not have a large impact on the supply pressure to the igniter. However, if the starting pressure in the main engine propellant tanks is increased or decreased, it will change the supply pressure to the igniter. As this engine is still under development, it is likely that this pressure will change, causing a change in igniter propellant supply pressure. In order to better understand how a change in the supply pressure to the ignition system changes the performance of the resonance heating device, 3 additional cases were run. These cases all use Case 3 Large D_{res}, but change the inlet pressure P_o. The cases used P_o = 10.25, 15, and 25 bar. Table 12.8-Table 12.10 list the values of pressure, temperature and velocity at P1-4 for each of these cases. Below the contour plots and parameter versus iteration plots are provided for each case. In the subsequent section these results are analysed.

12.4.1. Case 3.1, Po: 10.25 Bar Results

Table 12.8: Results Case 3.1: Large D_{res}, $P_o = 10.25$ bar, average values at P 1-4 in transient

Parameter	P1	P2	P3	P4
Pressure (Pa)	369255	344895	349388	356066
Temp (K)	294.12	457.3	492.2	692
Velocity (m/s)	161	18	30	1.3

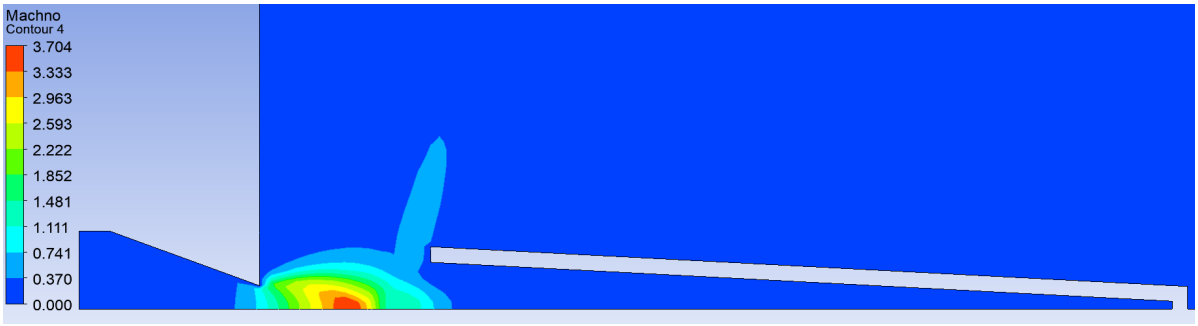

Figure 12.27: Case 3.1: Large D_{res}, $P_o = 10.25$ bar Mach Contour at End of Simulation

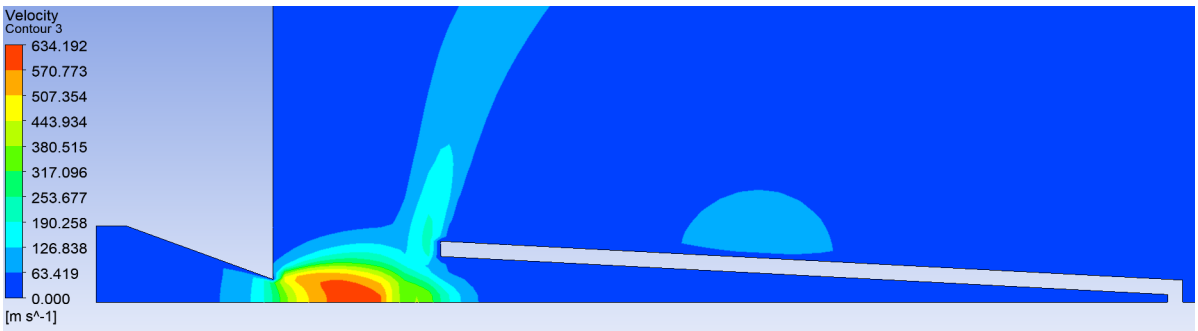

Figure 12.28: Case 3.1: Large D_{res}, $P_o = 10.25$ bar, Velocity Contour at End of Simulation

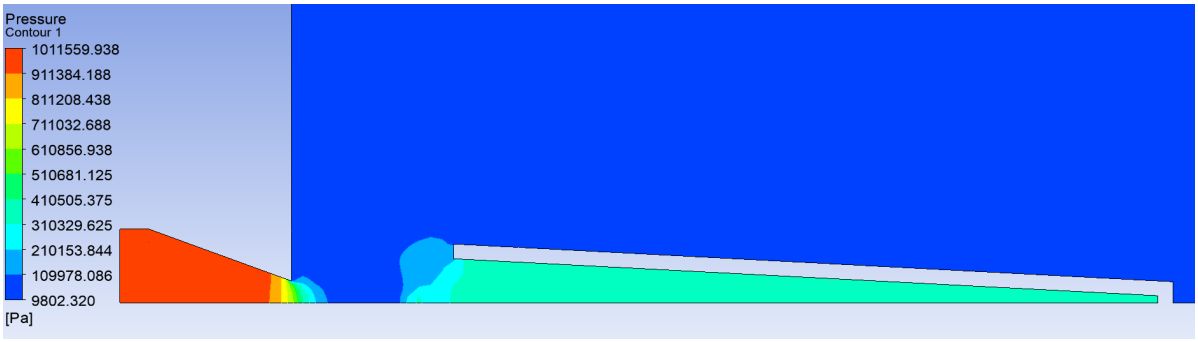

Figure 12.29: Case 3.1: Large D_{res}, P_o = 10.25 bar, Pressure Contour at End of Simulation

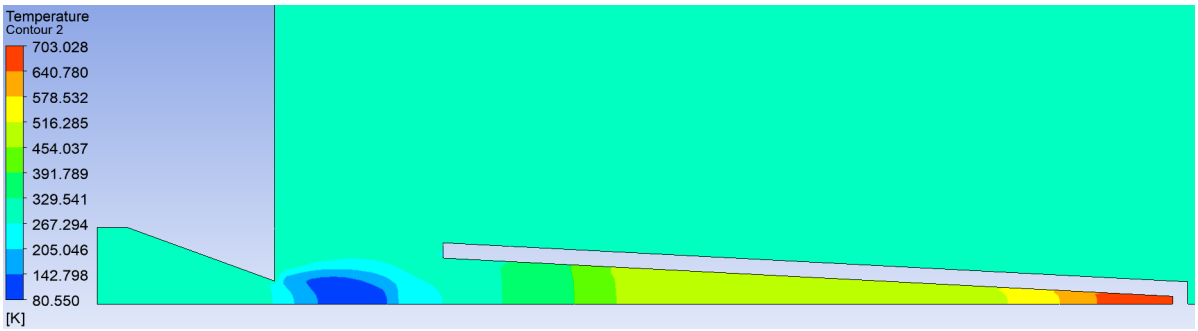

Figure 12.30: Case 3.1: Large D_{res}, P_o = 10.25 bar, Temperature Contour at End of Simulation

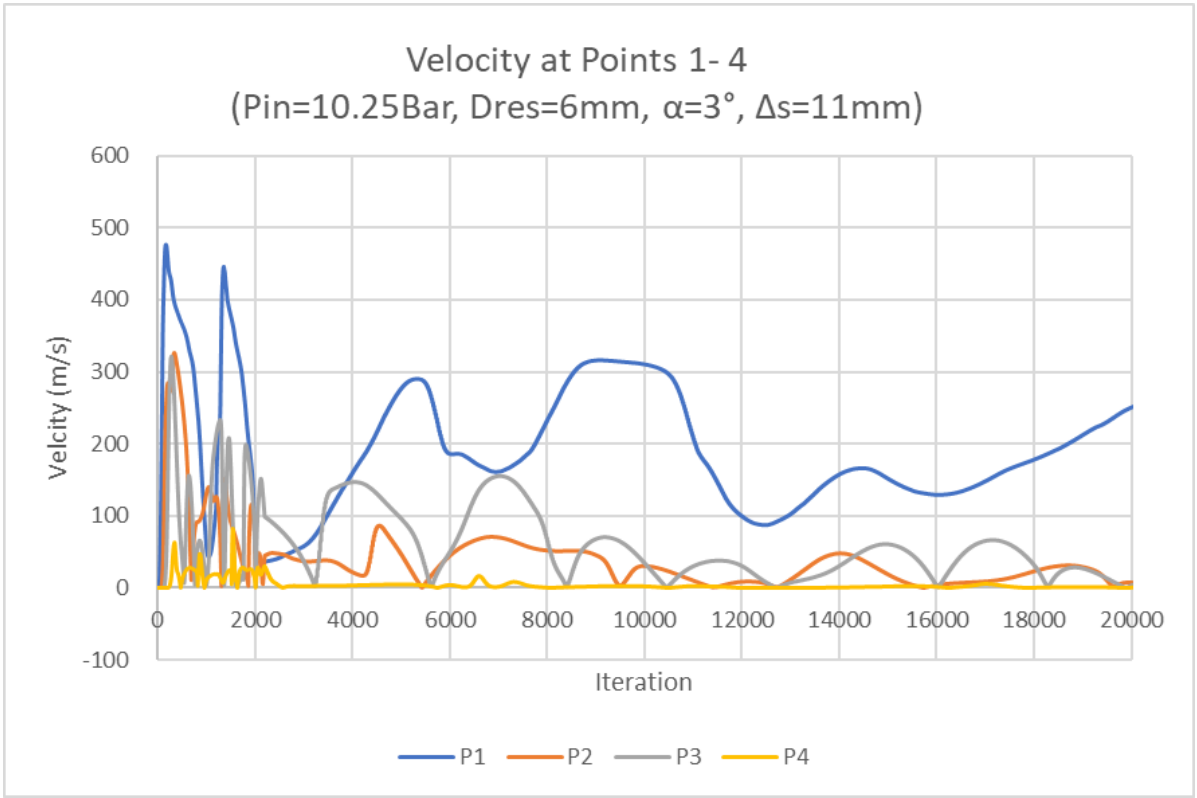

Figure 12.31: Case 3.1: Large D_{res}, P_o = 10.25 bar, Velocity Plot

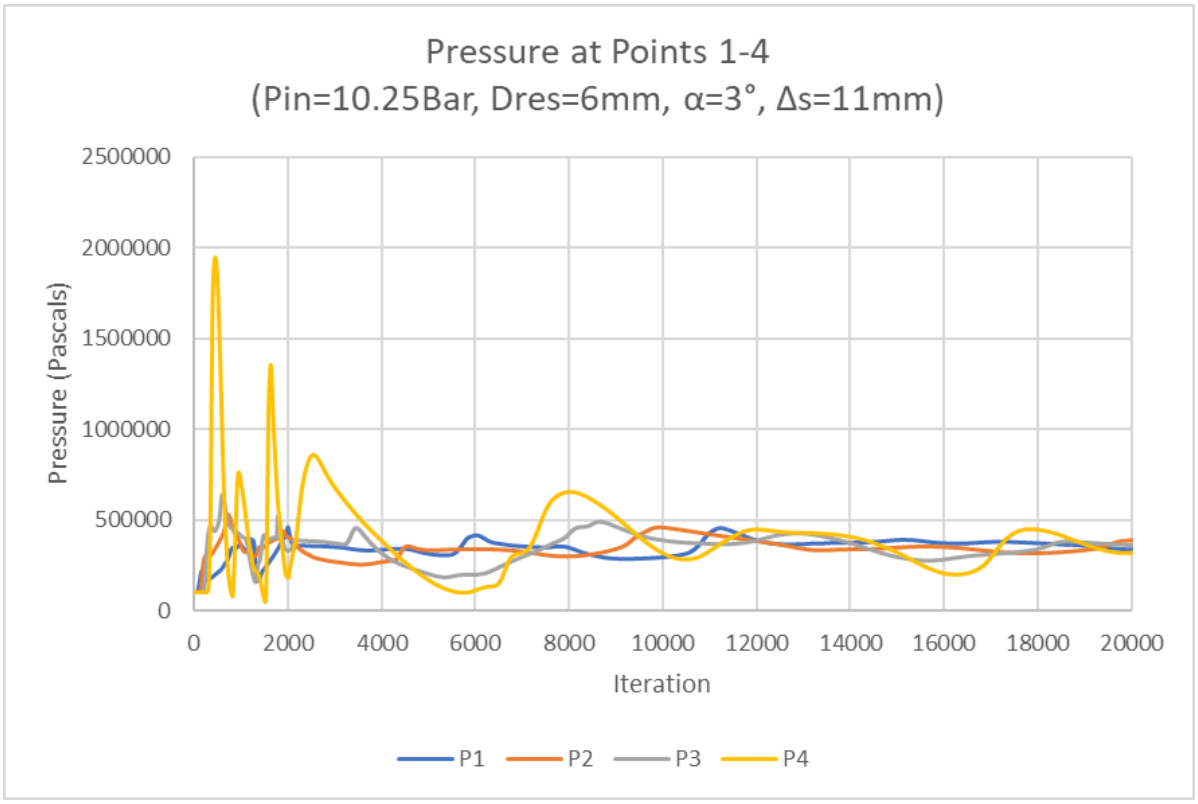

Figure 12.32: Case 3.1: Large D_{res}, $P_o = 10.25$ bar, Pressure Plot

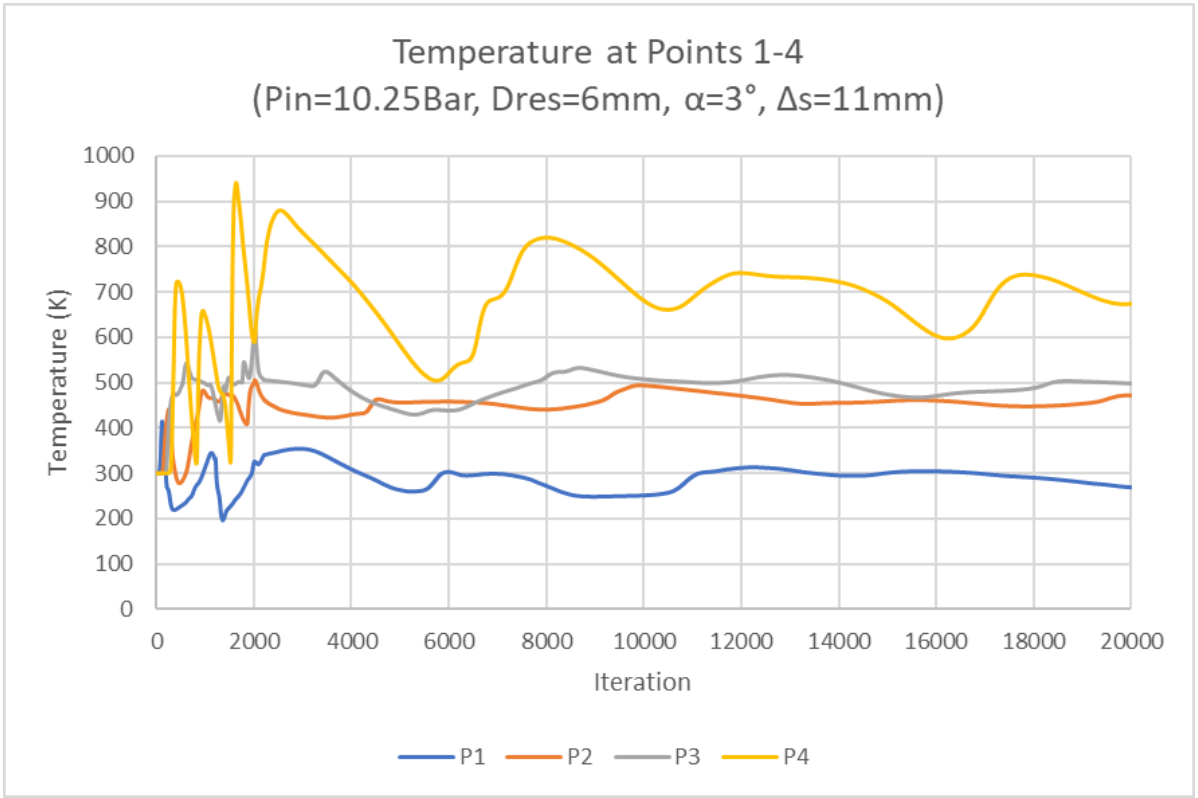

Figure 12.33: Case 3.1: Large D_{res}, $P_o = 10.25$ bar, Temperature Plot

12.4.2. Case 3.2, Po: 15 Bar Results

Table 12.9: Results Case 3.2: Large D_{res}, P_o = 15 bar, average values at P 1-4 in transient

Parameter	P1	P2	P3	P4
Pressure (Pa)	278771	302166	301208	301135
Temp (K)	315	401	465	744
Velocity (m/s)	38.65	9.42	8.25	0.38

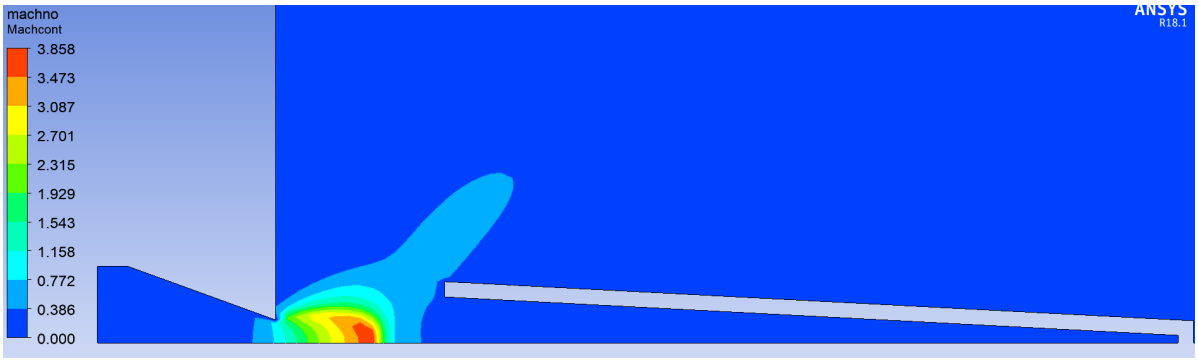

Figure 12.34: Case 3.2: Large D_{res}, P_o = 15 bar, Mach Contour at End of Simulation

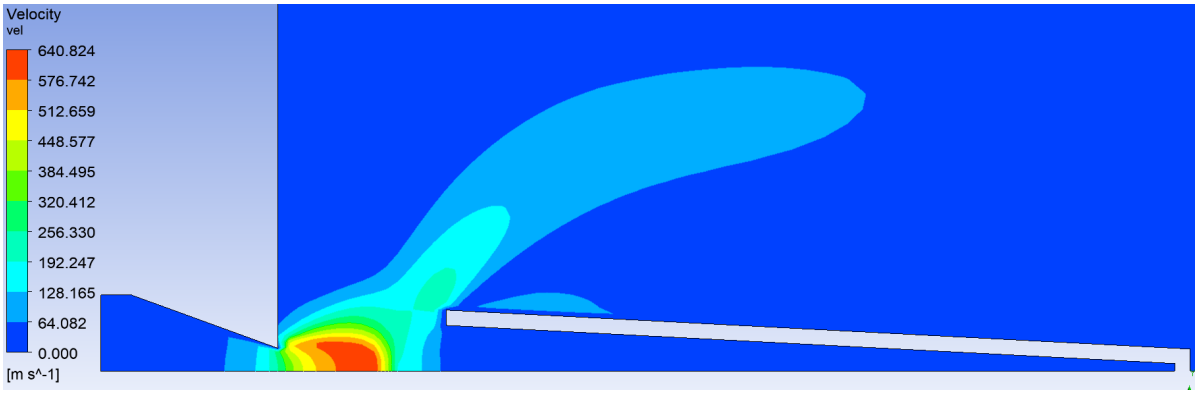

Figure 12.35: Case 3.2: Large D_{res}, P_o = 15 bar, Velocity Contour at End of Simulation

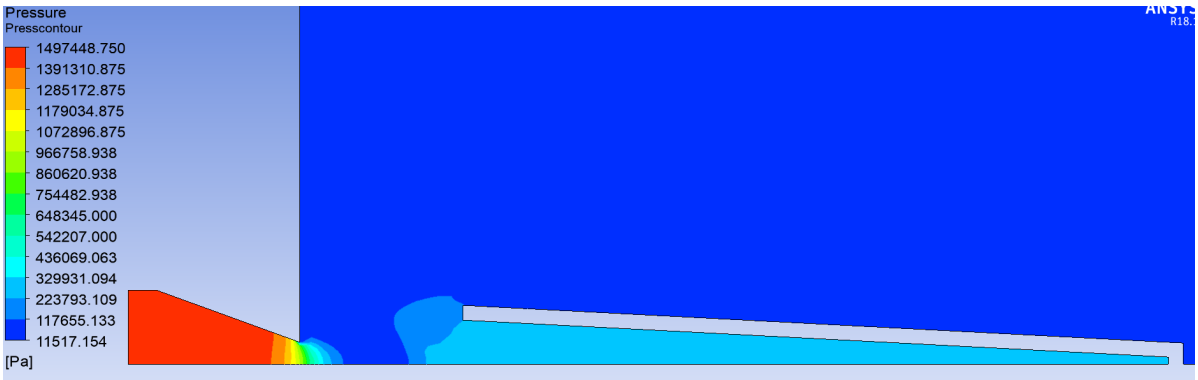

Figure 12.36: Case 3.2: Large D_{res}, P_o = 15 bar, Pressure Contour at End of Simulation

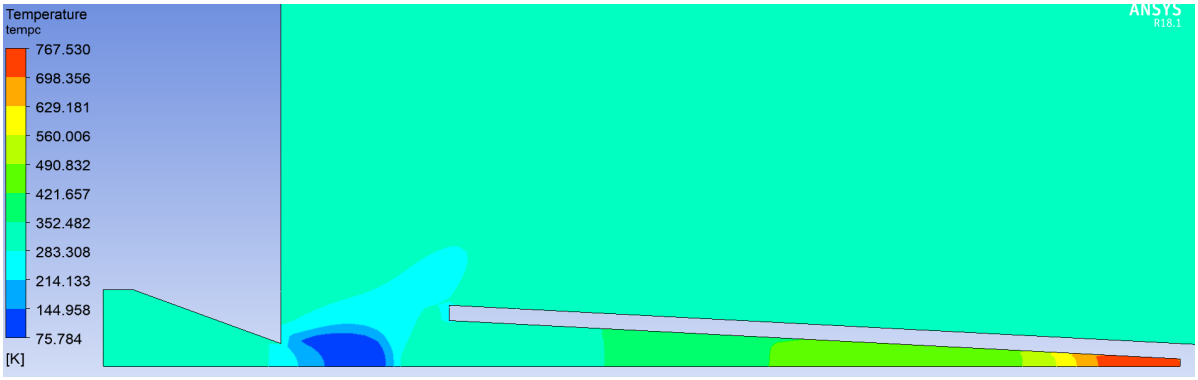

Figure 12.37: Case 3.2: Large D_{res}, P_o = 15 bar, Temperature Contour at End of Simulation

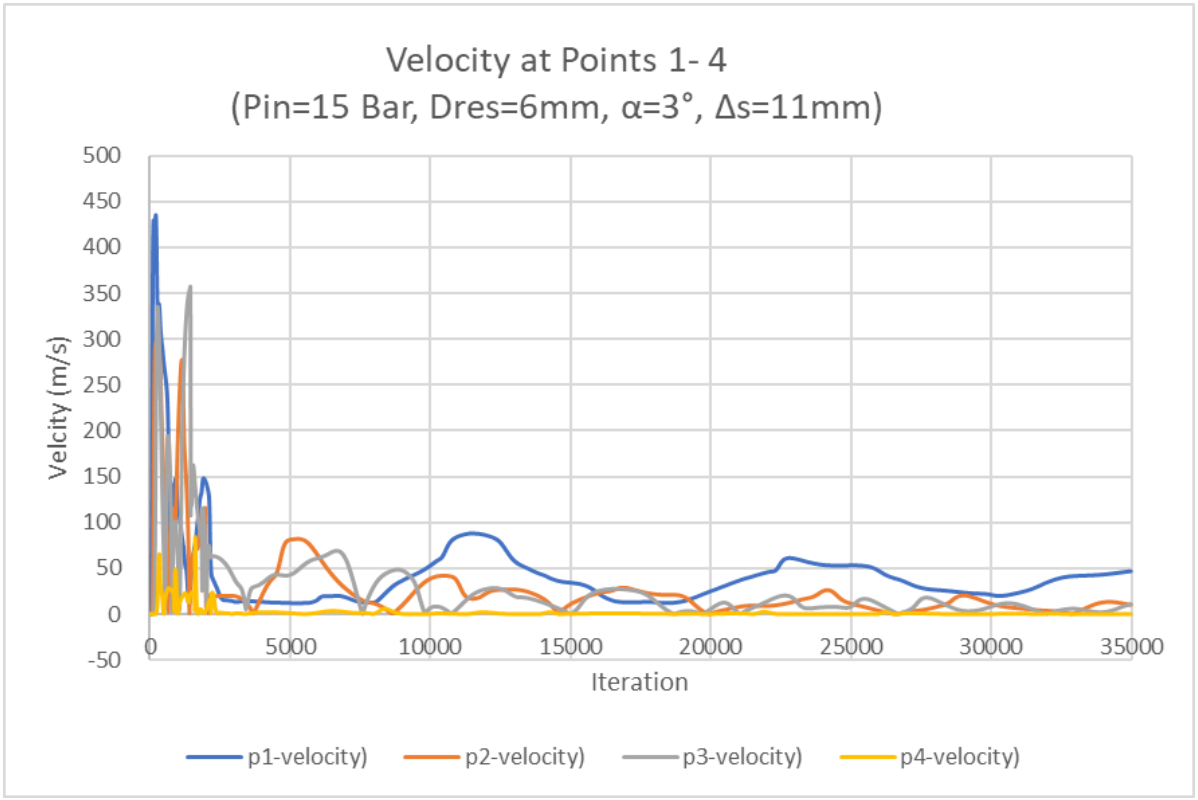

Figure 12.38: Case 3.2: Large D_{res}, P_o = 15 bar, Velocity Plot

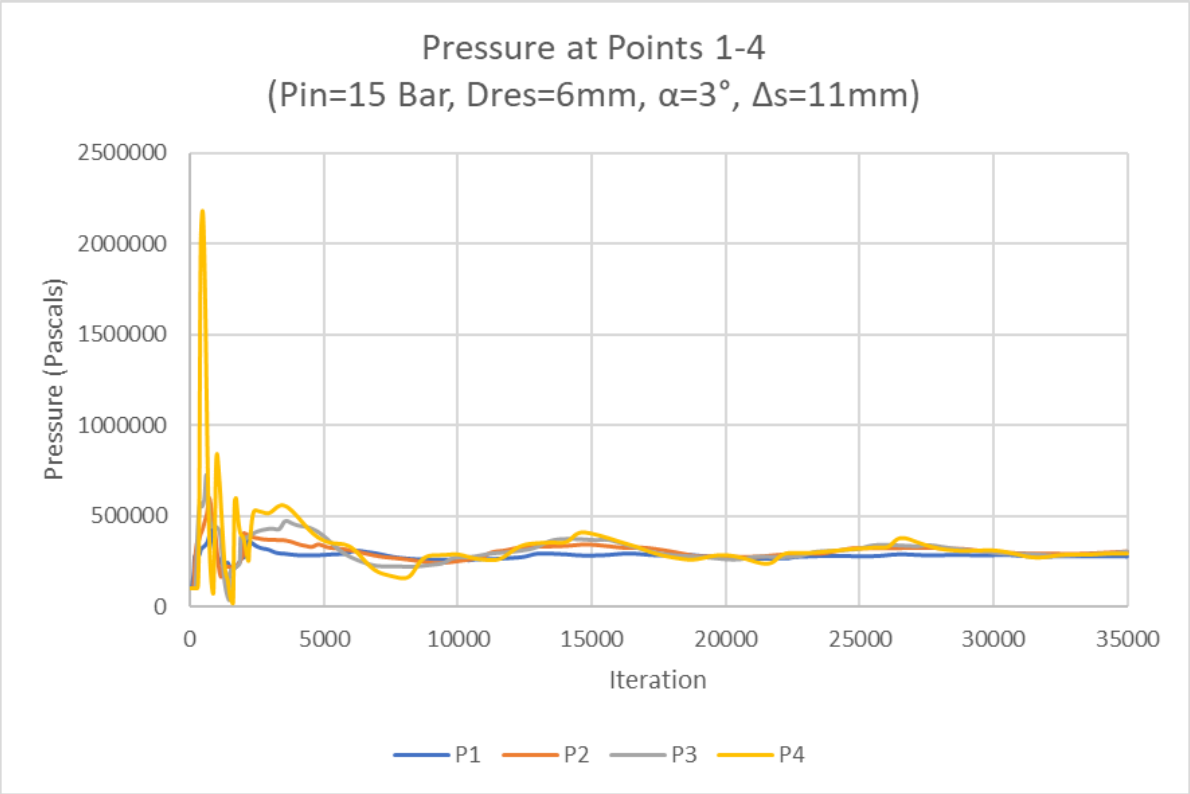

Figure 12.39: Case 3.2: Large D_{res}, P_o = 15 bar, Pressure Plot

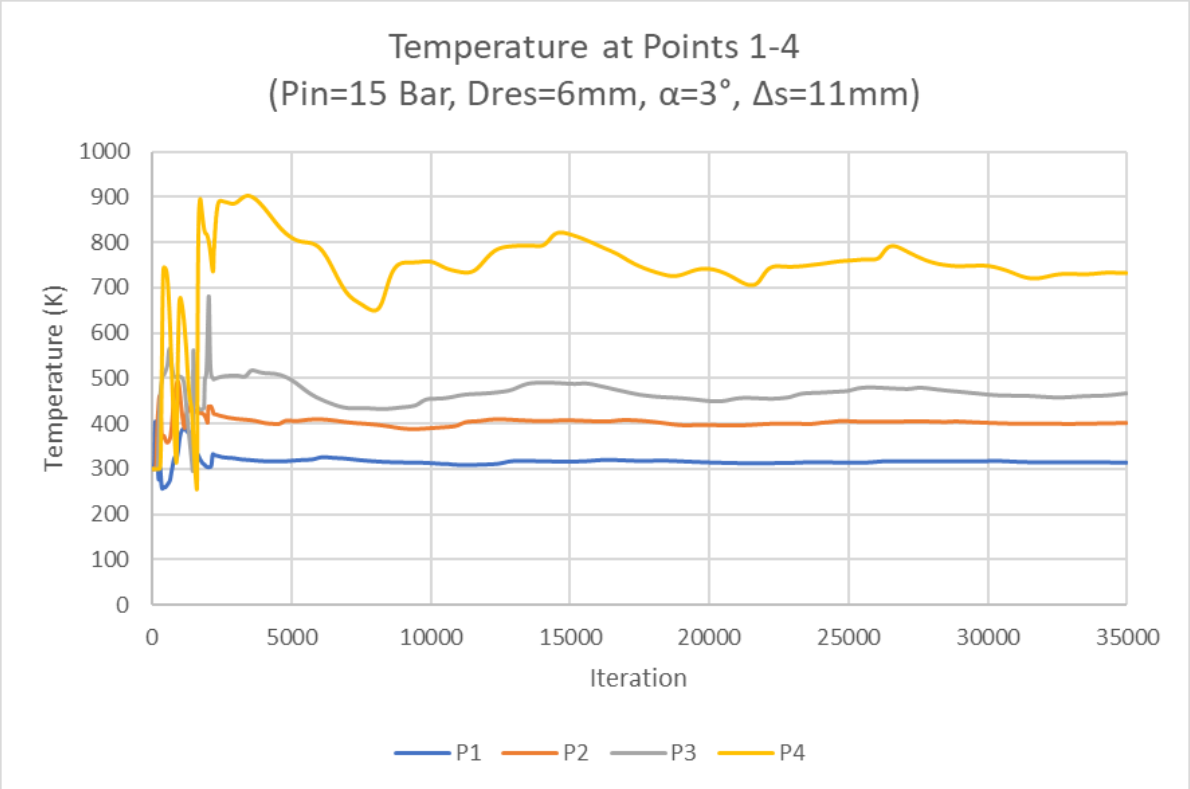

Figure 12.40: Case 3.2: Large D_{res}, P_o = 15 bar, Temperature Plot

12.4.3. Case 3.3, Po: 25 Bar Results

Table 12.10: Results Case 3.3: Large D_{res}, $P_o = 25$ bar, average values at P 1-4 in transient

Parameter	P1	P2	P3	P4
Pressure (Pa)	276941	306295	305450	305270
Temp (K)	316	450	676	800
Velocity (m/s)	22.13	4.65	4.16	0.13

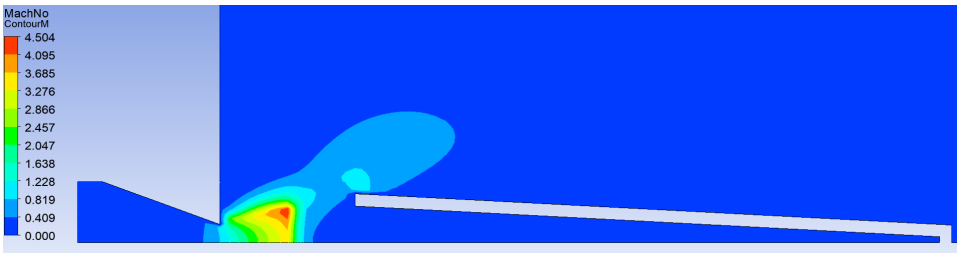

Figure 12.41: Case 3.3: Large D_{res}, $P_o = 25$ bar, Mach Contour at End of Simulation

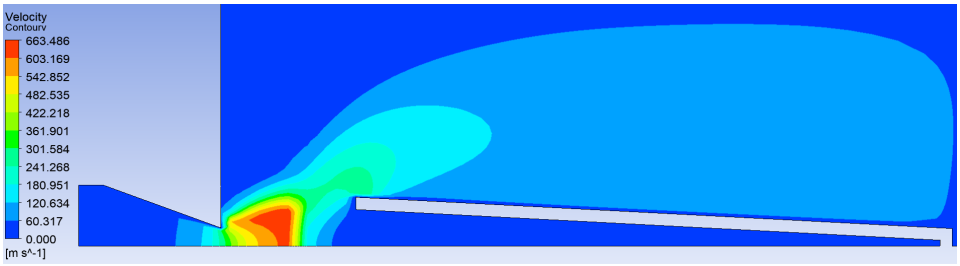

Figure 12.42: Case 3.3: Large D_{res}, $P_o = 25$ bar, Velocity Contour at End of Simulation

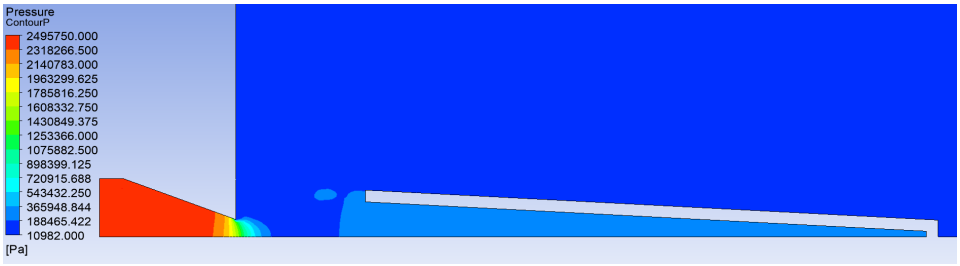

Figure 12.43: Case 3.3: Large D_{res}, $P_o = 25$ bar, Pressure Contour at End of Simulation

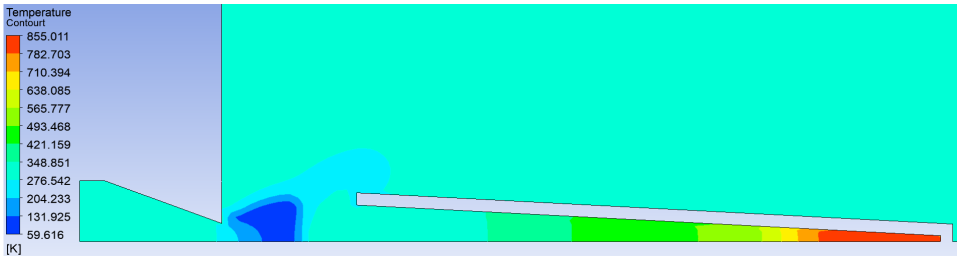

Figure 12.44: Case 3.3: Large D_{res}, $P_o = 25$ bar, Temperature Contour at End of Simulation

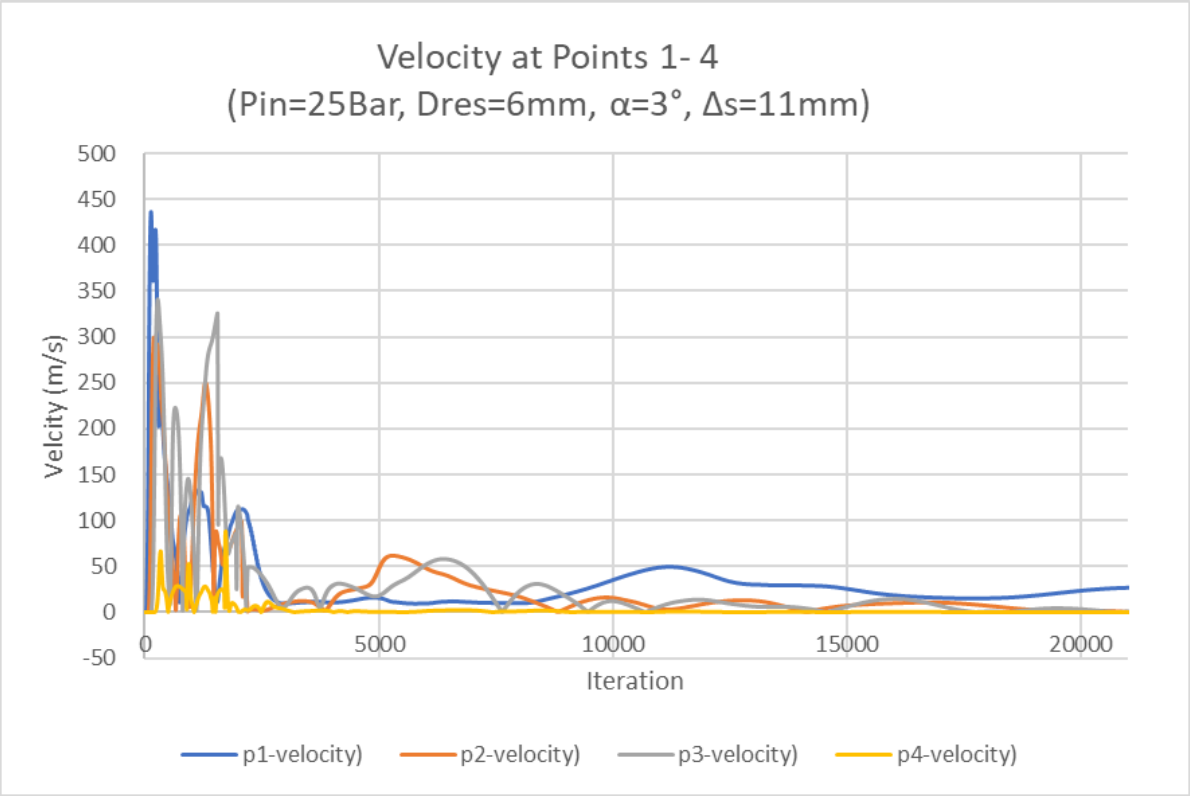

Figure 12.45: Case 3.3: Large D_{res}, P_o = 25 bar, Velocity Plot

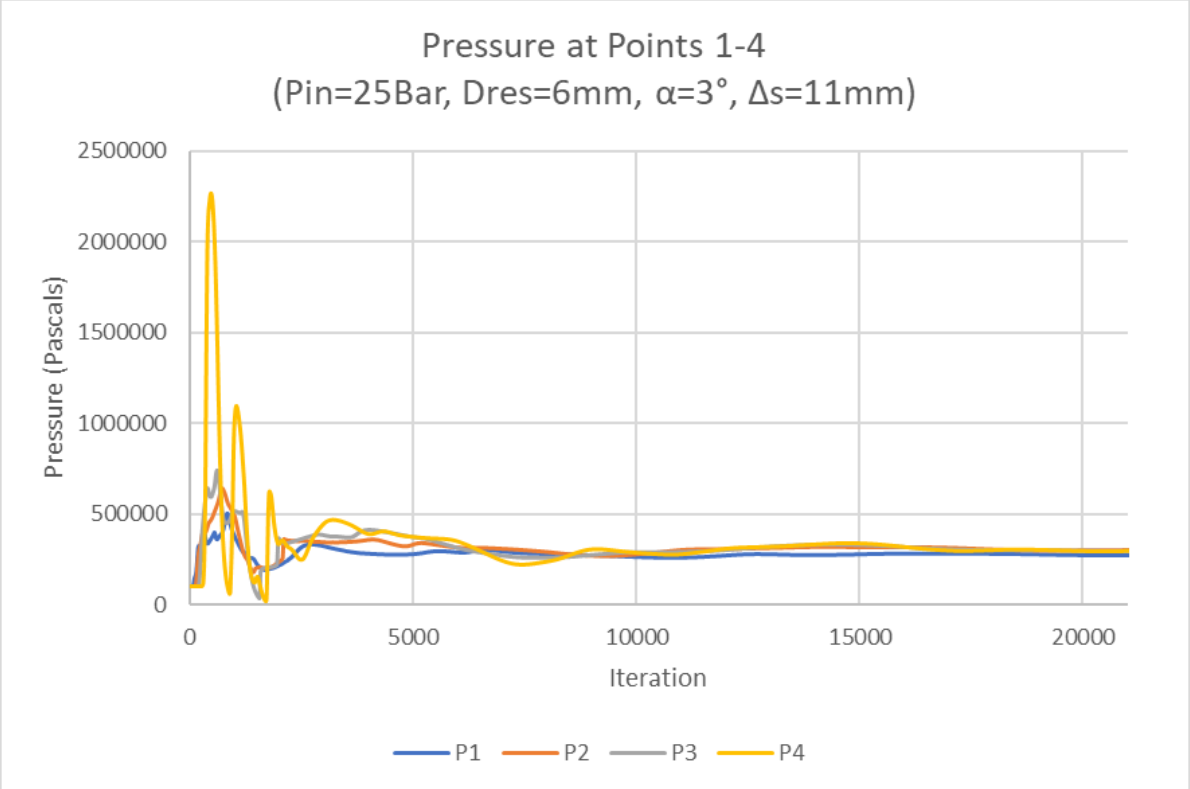

Figure 12.46: Case 3.3: Large D_{res}, P_o = 25 bar, Pressure Plot

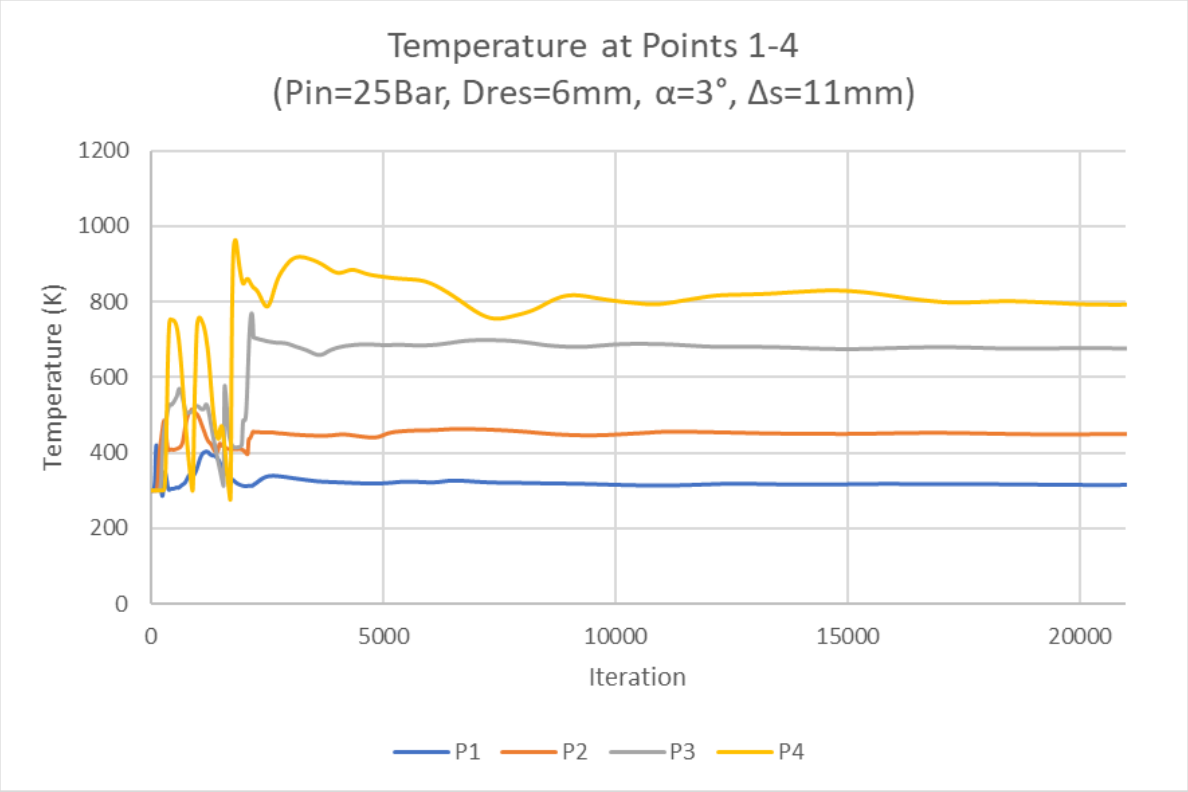

Figure 12.47: Case 3.3: Large D_{res}, $P_o = 25$ bar, Temperature Plot

12.5. Cases 3, 3.1, 3.2 and 3.3 Analysis

First, looking at the mach and velocity contours for each case, they show that the lower the inlet pressure, the smaller the physical expansion of the jet. This makes sense as a lower pressure inlet has less expanding to do, thus resulting in a smaller diameter jet. This can be seen clearly in the velocity contours, where the $P_o = 25$ bar contour has a much larger jet diameter than the $P_o = 10.25$ bar case, resulting in a larger portion of the jet bypassing the cavity.

Now the pressures and temperature contours, plots, and tables can be used to compare each case. In Table 12.11, the values at P4 are directly compared for all 4 cases, as well as the mass flow rate at the inlet. As the heating at the base, at P4, is the most important performance parameter of the device, P4 will be focused on in the analysis.

Table 12.11: Results Large D_{res} Comparisons of P_o, values are average in transient

Parameter	$P_o = 10.25$ **Bar**	$P_o = 15$ **Bar**	$P_o = 19$ **Bar**	$P_o = 25$ **Bar**
P4 Pressure (Pa)	356066	301135	306381	305270
P4 Temp (K)	692	744	800	800
Approx. Mass Flow Rate (kg/s)	17.6	26.3	32	33

The design case uses $P_o = 19$ bar, and the injection nozzle is sized such that the gas is choked when the pressure in 18 bar or higher. This means that if $P_o < 17$ bar, the gas will no longer be choked and therefore the mass flow rate will decrease proportional to the area, as is dictated by Equation 7.8. Once the nozzle is choked, when $P_o \geq 18$ bar, the mass flow rate will no longer change. This expectation is confirmed by the results in Table 12.11, in which the mass flow rate of the $P_o = 10.25$ bar and $P_o = 15$ bar cases was lower than the design case, because the flow is not choked. In the $P_o = 25$ bar case, the mass flow rate is nearly identical to that of the 19 bar design case, with the small error due

to estimations made in the solver. This is correct, because the nozzle is choked above $P_o = 18$ bar, so the mass flow rate should remain the same for all input pressures higher than 18 bar.

Comparing the pressures and temperatures of each case, when $P_o = 10.25$ bar, the resulting pressure at P4 is 0.5bar higher than that of the other 3 cases and the temperature is 50-100K lower. For $P_o = 15$, 19 and 25 bar, the pressure at P4 is very similar. The temperature at $P_o = 19$ and 25 bar, are the same at 800K, and the temperature at $P_o = 15$ bar, is 56K lower. This difference in temperate for the lower input pressure cases is due to the injection nozzle not being choked, resulting in a lower mass flow rate. This effects the shock formation in the cavity, leading to a lower final temperature. Once the nozzle is choked, $P_o \geq 18$ bar, the mass flow rate is constant, resulting in the same shock structure and the same temperature and pressure at the cavity base. The major insight from these results is that for a given design, if the user wants the resonance device to retain its performance, the supply pressure must be greater than or equal to the designed injection nozzle pressure for choked flow. It is important to also point out that the length of the first shock cell is dependant on the NPR, as seen in Equation 8.1. This equation states that if the ambient pressure is constant, than a larger P_o would result in a longer first shock cell. This means that the length of the expansion and compression zones in the first shock cell would increase and the transition location between zones would move further away from the nozzle exit. In the cases tested, a 6 bar increase in P_o above the designed pressure did not affect the performance. It should be cautioned, however, that drastically increasing the inlet pressure may lead to the cavity inlet being located in the expansion zone. Therefore, if the inlet pressure for the system is increased greatly above its design pressure, the user should calculate the expected location of these expansion and compression zones and adjust the cavity distance if necessary.

12.6. Conclusion and Detailed Design

In this chapter, 3 'Cavity' cases were tested in order to determine which case achieved sufficient heating in the base of the cavity to ensure auto-ignition of the fuel. This chapter described each of the cases and showed that the results met the convergence and validation criteria. After analyzing these results, it was seen that Case 3 was successful in heating the gas at the cavity base to far above the ethanol auto-ignition temperature. As Case 3 outperformed the adjusted preliminary design in Case 1, Case 3 was selected for the Detailed System Design. The full set of Detailed Design parameters for the resonance ignition device are listed in Table 12.12. With Case 3 chosen, a study on the effect of inlet pressure on resonance cavity performance was conducted, as this may change during igniter operation. Through this study, it was concluded that in order for the cavity to perform as designed, the inlet pressure should remain at or above the designed choked pressure of the injection nozzle. Overall this chapter was successful in generating a detailed design for the resonance ignition system and providing insights on its performance at different inlet pressures.

Table 12.12: Resonance Ignition Device Detailed Design Parameters

Parameter	Symbol	Value	Unit
Resonance Gas		Oxygen	
Fuel		Ethanol85	
Oxidizer Injection Temperature	$T_{0,ox}$	288.15	K
Fuel Injection Temperature	$T_{0,f}$	288.15	K
Minimum Required Ignition Power	P_{ign}	152.1	kW
Combustion Temperature	T_c	1960	K
Mixture Ratio	O/F	0.8	
Heating Value Exhaust	dH	2079469	J/kg
Materials			
Injection Nozzle Material	Material	SS304	
Resonance Tube Material	Material	PTFE/SS304	
Igniter Chamber Material	Material	SS304	
Mass Flow Rates			
Total Propellant Mass Flow Rate	m_o	70.12	g/s
Oxidizer Mass Flow Rate	m_o	31.165	g/s
Fuel Mass Flow Rate	m_f	38.956	g/s
GOX Sonic Injection Nozzle			
Injection Nozzle Exit Diameter	D_n	3	mm
Injection Nozzle Inlet Diameter	d_{in}	10	mm
Injection Nozzle Convergent Angle	β	20	Degree
NPR, Nozzle Pressure Ratio	P_o/P_{atm}	19	
Oxidizer Injection Pressure	P_o	19.0	Bar
Combustion Chamber Pressure	P_c	8.72	Bar
Area Ratio	ϵ	11.11	
Convergent Length	L_{conv}	9.616	mm
Nozzle radius	r_u	2.25	mm
Converging Radius	r_a	1.2	mm
Resonance Cavity			
Resonance Cavity Shape	Shape	Conical-Truncated	
Resonance Cavity Inlet diameter	d	6.0	mm
Resonance Cavity end diameter	d_e	1.0	mm
Resonance Cavity Angle	α	3	degrees
Resonance Cavity Length	L_{res}	47.7	mm
Resonance Tube wall thickness	t_w	1.0	mm
Gap Distance	ΔS	11	mm
Exhaust Orifice			
Exhaust Orifice Diameter	d_{exh}	12.0	mm
Exhaust Pressure Drop	ΔP_{exh}	1.74	Bar
Exhaust Velocity	v_{exh}	456	m/s
Fuel Injector			
Fuel Injection No. Holes		3	
Fuel Injection Hole Diameter	1.0	mm	
Fuel Injection Pressure Drop	ΔP_f	2.23	Bar
Fuel Injection Velocity	V_f	21	m/s
Fuel Exhaust Pressure Drop	ΔP_f	0.0009	Bar
Fuel Exhaust Velocity	V_f	0.32	m/s
Minimum Fuel Supply Pressure	$P_{f,min}$	26.3	Bar

13

Conclusion

13.1. Conclusions

The goal of this thesis was to design and test an innovative ignition system. To that end a custom python script was developed to generate a preliminary design of a resonance ignition system based on empirical equations and guidance from other researchers. In order to test the performance of this device a set of numerical simulations were conducted in ANSYS Fluent. First, the characteristics of the under-expanded flow from a converging nozzle were modelled in order to provide more detailed information, which was used to refine the placement and geometric design of the resonance cavity. Then a set of simulations were performed on the full geometry in order to determine the optimal resonance cavity design in order to achieve sufficient heating of the gas at the base of the nozzle. After much experimentation and research, a steady-transient hybrid method was developed which vastly decreased the computational time required for this model, without impacting the accuracy of the results. This model was validated against other experiments, and can be used in future works to model more more cases and further develop this technology. The results of the 'Nozzle-Steady' case characterized the geometry of the under-expanded exhaust jet from a converging nozzle. These results proved that the empirical equation used to calculate the length of the first shock cell was incorrect, and the gap distance was adjusted to match the simulation results. Therefore it is recommended that if the geometry or supply pressure of the nozzle changes markedly, this 'Nozzle-Steady' simulation be rerun in order to properly size the gap distance. The 'Cavity' cases were successful in finding a Detailed Design of the resonance ignition system that was capable of heating the resonant gas at the base of the cavity to more than 120K above the ethanol auto-ignition temperature. In addition to generating a detailed design, additional tests were conducted to characterize the relationship between the oxygen supply pressure and the heating at the base of the cavity. These tests found that the if the supply pressure was decreased such that the NPR was lower than the nozzle critical pressure ratio, the temperature at the base of the cavity decreased. However if the supply pressure was increased such that the NPR was above the nozzle critical pressure ratio, the temperature at the base of the cavity was unchanged because the nozzle was choked. This thesis was successful in developing and validating a functional Detailed Design of a resonance ignition system that was capable of heating gas up to 800K. This thesis adds valuable information to the current body of work on the innovative technology of resonance ignition systems.

13.2. Recommendations

In this thesis, a python script was developed to create the preliminary design, which was tested using ANSYS Fluent. Through these numerical simulations, 3 different designs were tested and a Detailed Design of the system was chosen. While this is a success, there are of course many recommendations that I, as a researcher, would make for future work. This steady-transient hybrid method was validated by inputting the Afzali fully transient case into this model and comparing the results. While they agreed quite well and the model was validated, in order to more robustly validate this model, one could run a validation case of a second and third study as well. In the interest of time this was not done in this thesis but is recommended. For further validation, one could run Case 3 in a fully transient solve with

a much more refined mesh, using the TU Delft cluster. By comparing the results of the fully transient case to the steady-transient hybrid case would provide very strong validation of this model.

In addition, it is foreseen that someone developing a resonance ignition system could input design parameters into the python script and directly generate a detailed system design, without the need to perform numerical simulations. This would greatly decrease the time between design iterations. To accomplish this, one could run more cases with ANSYS Fluent and characterize how changing specific parameters affected the performance of the system. If enough cases are run then one could reasonably predict the performance of a specific geometry and input pressure. This would take a great deal of simulation time, but would be extremely useful for design iterations.

Finally, it is recommended that the Detailed Design be manufactured and tested in a laboratory. The results of these physical experiments can be used to validate the numerical results. This resonance ignition system provides a low cost, low mass, and simple method for achieving ignition, making it an attractive option for small launch vehicles. Therefore it is hoped that students in the DARE rocket team at TU Delft , who are developing a small launch vehicle, will manufacture and test this design.

Bibliography

[1] Haynes 188 Alloy. Technical report, Haynes International Inc., .

[2] Manufacturing Planning Guide. Technical report, NASA Johnson Space Center, .

[3] INCOSE Systems Engineering Handbook, version 2.0 - AE4S12 Space Systems Engineering (2019/20 Q1), July 2000. URL https://brightspace.tudelft.nl/d2l/le/content/192153/viewContent/1355581/View.

[4] Liquid Oxygen Safetygram 6. Technical report, Air Products and Chemicals Inc., Allentown, PA, 2015.

[5] Thermal diffusivity, March 2020. URL https://en.wikipedia.org/w/index.php?title=Thermal_diffusivity&oldid=947686570. Page Version ID: 947686570.

[6] Babak Afzali and Hassan Karimi. Numerical investigation on thermo-acoustic effects and flow characteristics in semi-conical Hartmann–Sprenger resonance tube. *Proceedings of the Institution of Mechanical Engineers, Part G: Journal of Aerospace Engineering*, 231(14):2706–2722, December 2017. ISSN 0954-4100. doi: 10.1177/0954410016670419. URL https://doi.org/10.1177/0954410016670419. Publisher: IMECHE.

[7] Babak Afzali Khoshkbijari and Hassan Karimi. Effect of pipe geometry and material properties on flow characteristics and thermal performance of a conical Hartmann–Sprenger tube. *Journal of the Brazilian Society of Mechanical Sciences and Engineering*, 39(11):4489–4501, November 2017. ISSN 1678-5878, 1806-3691. doi: 10.1007/s40430-017-0843-4. URL http://link.springer.com/10.1007/s40430-017-0843-4.

[8] T Ahmad, S L Plee, and J P Myers. ANSYS_fluent_user's_guide_15.0. *ANSYS Inc.*, page 2692, November 2013.

[9] C Akkermans. *Ignition modeling in methane-oxygen rocket engines: Design and modeling of a methane-oxygen rocket engine igniter using reacting flows with computational fluid dynamics*. PhD thesis, Delft University of Technology, Delft, The Netherlands, August 2017.

[10] Christian Bauer, Martin Hauser, and Oskar J. Haidn. Investigation of Stabilization Effects in Hartmann-Sprenger Tubes. *TRANSACTIONS OF THE JAPAN SOCIETY FOR AERONAUTICAL AND SPACE SCIENCES, AEROSPACE TECHNOLOGY JAPAN*, 14(ists30):Pa_95–Pa_100, 2016. ISSN 1884-0485. doi: 10.2322/tastj.14.Pa_95. URL https://www.jstage.jst.go.jp/article/tastj/14/ists30/14_Pa_95/_article.

[11] Christian Bauer, Paul Lungu, and Oskar J Haidn. Numerical Investigation of a Resonance Ignition System. In *Technical University of Munich, Institute for Turbomachinery and Flight Propulsion*, Madrid, Spain, 2019. EUCASS.

[12] Tom Benson. Boyle's Law, 2014. URL https://www.grc.nasa.gov/WWW/BGH/boyle.html.

[13] E. Brocher and J. P. Ardissone. Heating characteristics of a new type of Hartmann-Sprenger tube. *International Journal of Heat and Fluid Flow*, 4(2):97–102, June 1983. ISSN 0142-727X. doi: 10.1016/0142-727X(83)90008-5. URL http://www.sciencedirect.com/science/article/pii/0142727X83900085.

[14] E. Brocher and M. Kawahashi. Wave and thermal phenomena in H.S.-tubes with an area constriction. pages 179–185, 1986. URL http://adsabs.harvard.edu/abs/1986swst.proc..179B. Conference Name: Shock Waves and Shock Tubes.

[15] E. BROCHER and C. MARESCA. *STUDY OF THERMAL PHENOMENA IN A HARTMANN-SPRENGER TUBE*. December 1974. URL http://archive.org/details/nasa_techdoc_19750005123.

[16] E. Brocher, C. Maresca, and M.-H. Bournay. Fluid dynamics of the resonance tube. *Journal of Fluid Mechanics*, 43(2):369–384, August 1970. ISSN 1469-7645, 0022-1120. doi: 10.1017/S0022112070002422. URL https://www.cambridge.org/core/journals/journal-of-fluid-mechanics/article/fluid-dynamics-of-the-resonance-tube/FBB3A269E54F5B91DABBB60F6B4E5A27.

[17] Eric Brocher. Heating Rate of the Driven Gas in a Hartmann-Sprenger Tube. *AIAA Journal*, 13 (10):1265–1266, 1975. ISSN 0001-1452. doi: 10.2514/3.60537. URL https://doi.org/10.2514/3.60537.

[18] S. M. Chang and S. Lee. ON THE JET REGURGITANT MODE OF A RESONANT TUBE. *Journal of Sound and Vibration*, 246(4):567–581, September 2001. ISSN 0022-460X. doi: 10.1006/jsvi.2000.3646. URL http://www.sciencedirect.com/science/article/pii/S0022460X00936460.

[19] M. W. Chase. NIST JANAF Themochemical Tables, Fourth Edition. pages 1–1951, 1998.

[20] E William Conrad, Albert J Pavli, and Bert R Phillips. Resonance Tube Igniter. *NASA Tech Brief Lewis Research Center*, (Brief 70-10618):2, November 1970.

[21] Christian J.R. Coronado, João A. Carvalho, José C. Andrade, Ely V. Cortez, Felipe S. Carvalho, José C. Santos, and Andrés Z. Mendiburu. Flammability limits: A review with emphasis on ethanol for aeronautical applications and description of the experimental procedure. *Journal of Hazardous Materials*, 241-242:32–54, November 2012. ISSN 03043894. doi: 10.1016/j.jhazmat.2012.09.035. URL https://linkinghub.elsevier.com/retrieve/pii/S0304389412009594.

[22] Hess Corporation and Hess Plaza. Kerosene Safety Data Sheet Hess. (0290):10.

[23] Krijn de Kievit, Eoghan Gilleran, and et al. Blizzard V1 System Review. Design Review Report-internal V2, Delft Aerospace Rocket Engineering Cryogenics Group, Delft, The Netherlands, April 2019.

[24] Zoe Dickert. Development of a Resonance Ignition System for Cryogenic LRE, Literature Study. Technical report, Delft University of Technology, Delft, The Netherlands, February 2020.

[25] Distill. Ethanol Material Safety Data Sheet - Europe, 2020. URL http://www.distill.com/materialsafety/msds-eu.html.

[26] Simone Elia. Design and development of a fluid system for a resonant igniter. page 121.

[27] Dr Ahmed Nagib Elmekawy. Introduction to ANSYS Meshing Module 01: Core Skills. page 82.

[28] Erwin Franquet, Vincent Perrier, Stéphane Gibout, and Pascal Bruel. Review on the under-expanded jets. 2015. doi: 10.13140/RG.2.1.2640.6883. URL http://rgdoi.net/10.13140/RG.2.1.2640.6883. Publisher: Unpublished.

[29] P.N. Fuller. Advanced Ignition Systems Final Report. R-8756, Rocketdyne North American Rockwell under contract NAS8-25126, Canoga Park, California, July 1971.

[30] Prof. Eberhard Gill. TU Delft AE4S12 Space Systems Engineering Lecture SLides, 2017.

[31] E.M. Greitzer, C.S. Tan, and M.B. Graf. *Internal Flow Concepts and Applications*. 2006.

[32] Zhang Guozhou, Song Yana, Yu Nanjia, Tong Xiaoyan, and Ma Bin. Coaxial Hydrogen/Oxygen Gas-Dynamic Resonance Ignition Technology for Rocket Repetitive Starting. In *AIAA SPACE 2007 Conference & Exposition*, Long Beach, California, September 2007. American Institute of Aeronautics and Astronautics. ISBN 978-1-62410-016-1. doi: 10.2514/6.2007-6157. URL http://arc.aiaa.org/doi/10.2514/6.2007-6157.

[33] Nancy Hall. Schlieren Flow Visualization NASA. URL https://www.grc.nasa.gov/www/k-12/airplane/tunvschlrn.html.

[34] Awatef Hamed, K Das, and D Basu. Numerical Simulation and Parametric Study of Hartmann-Sprenger Tube Based Powered Device. In *41st Aerospace Sciences Meeting and Exhibit*, Reno, Nevada, January 2003. American Institute of Aeronautics and Astronautics. ISBN 978-1-62410-099-4. doi: 10.2514/6.2003-550. URL http://arc.aiaa.org/doi/10.2514/6.2003-550.

[35] Jul Hartmann. Construction, performance and design of the acoustic air-jet generator. *Journal of Scientific Instruments*, 16(5):140–149, May 1939. ISSN 0950-7671. doi: 10.1088/0950-7671/16/5/302. URL http://stacks.iop.org/0950-7671/16/i=5/a=302?key=crossref.642c46c541eb38cfcda1cf33b0c53417.

[36] Stefan Hickel. 03_grid Generation, 2019.

[37] Stefan Hickel. 04_turbulence, 2019.

[38] Stefan Hickel. 05_rans.pdf, 2019.

[39] Dieter K Huzel. DESIGN OF LIQUID PROPELLANT ROCKET ENGINES. page 469, 1967.

[40] ANSYS Inc. ANSYS_fluent_12.0_theory_guide, January 2009. URL https://www.afs.enea.it/project/neptunius/docs/fluent/html/th/main_pre.htm.

[41] ANSYS Inc. ANSYS_fluent_12.0_tutorial_guide-Step_10:_saving_and_postprocessing_time-Dependent_data_sets, February 2009. URL https://www.afs.enea.it/project/neptunius/docs/fluent/html/tg/node71.htm.

[42] Babak Afzali Khoshkbijari and Hassan Karimi. Effect of pipe geometry and material properties on flow characteristics and thermal performance of a conical Hartmann–Sprenger tube. *Journal of the Brazilian Society of Mechanical Sciences and Engineering*, 39(11):4489–4501, November 2017. ISSN 1806-3691. doi: 10.1007/s40430-017-0843-4. URL https://link-springer-com.tudelft.idm.oclc.org/article/10.1007/s40430-017-0843-4. Company: Springer Distributor: Springer Institution: Springer Label: Springer Number: 11 Publisher: Springer Berlin Heidelberg.

[43] B. Lawver, D. Rousar, and W. Boyd. Ignition characterization of the GOX/ethanol propellant combination. In *20th Joint Propulsion Conference*, Cincinnati,OH,U.S.A., June 1984. American Institute of Aeronautics and Astronautics. doi: 10.2514/6.1984-1467. URL http://arc.aiaa.org/doi/10.2514/6.1984-1467.

[44] Paul Lungu, Christian Bauer, and Oskar J Haidn. Operational behaviour investigation of Hartmann-Sprenger Tube based resonance ignition systems for oxygen/methane in-orbit propulsion applications. Technical Report SP2018_00229, Technical University of Munich, Institute for Turbomachinery and Flight Propulsion, Garching, Germany, 2018.

[45] Paul Lungu, Christian Bauer, and Oskar J Haidn. Design aspects and characterisation of a resonance igniter for oxygen/methane in-orbit propulsion systems. In *Technical University of Munich, Institute for Turbomachinery and Flight Propulsion*, page 16, Madrid, Spain, 2019. EUCASS.

[46] Thuy Mai. Technology Readiness Level, May 2015. URL http://www.nasa.gov/directorates/heo/scan/engineering/technology/txt_accordion1.html.

[47] Mike Mannion and Barry Keepence. SMART requirements. *ACM SIGSOFT Software Engineering Notes*, 20(2):42–47, April 1995. ISSN 01635948. doi: 10.1145/224155.224157. URL http://portal.acm.org/citation.cfm?doid=224155.224157.

[48] Roman A. Marchan. Small-Scale Supersonic Combustion Chamber with a Gas-Dynamic Ignition System. *Combustion Science and Technology*, 183(11):1236–1265, November 2011. ISSN 0010-2202. doi: 10.1080/00102202.2011.589874. URL https://doi.org/10.1080/00102202.2011.589874. Publisher: Taylor & Francis _eprint: https://doi.org/10.1080/00102202.2011.589874.

[49] V. P. Rakowsky Marchese. A fluidic sounding rocket motor ignition system. New Orleans, LA, US, November 1972. URL https://ntrs.nasa.gov/search.jsp?R=19730028684.

[50] S. Murugappan and E. Gutmark. Parametric study of the Hartmann–Sprenger tube. *Experiments in Fluids*, 38(6):813–823, June 2005. ISSN 0723-4864, 1432-1114. doi: 10.1007/s00348-005-0977-5. URL http://link.springer.com/10.1007/s00348-005-0977-5.

[51] Ashish Narayan, Narayanan Subramanian, and Shallesh Kumar Jha. Numerical Simulation of Partially Covered Hartmann Whistle in a Sonic Underexpanded Jet. November 2018.

[52] S. Narayanan, Bholanath Behera, T. Sundararajan, and K. Srinivasan. Acoustic Heating Effects in Hartmann Whistle:. *International Journal of Aeroacoustics*, October 2013. ISSN 10.1260/1475-472X.12.5-6.557. URL https://journals-sagepub-com.tudelft.idm.oclc.org/doi/10.1260/1475-472X.12.5-6.557. Publisher: SAGE PublicationsSage UK: London, England.

[53] S. Narayanan, A. Samanta, Ashish Narayan, and Shailesh Kumar Jha. Computational Study of Partially Covered Hartmann Whistle in a Sonic-Underexpanded Jet. *Iranian Journal of Science and Technology, Transactions of Mechanical Engineering*, 43(4):639–661, December 2019. ISSN 2364-1835. doi: 10.1007/s40997-018-0232-3. URL https://doi.org/10.1007/s40997-018-0232-3.

[54] Mario Niwa, A. Santana, and Khoze Kessaev. Development of a Resonance Igniter for GO/Kerosene Ignition. *Journal of Propulsion and Power*, 17(5):995–997, 2001. doi: 10.2514/2.5860. URL https://doi.org/10.2514/2.5860.

[55] Dept. of Defencse Systems Management College. Systems Engineering Fundamentals - AE4S12 Space Systems Engineering (2019/20 Q1), January 2001. URL https://brightspace.tudelft.nl/d2l/le/content/192153/viewContent/1355580/View.

[56] B R Phillips and A J Pavli. Resonance tube ignition of hydrogen-oxygen mixtures. Technial Note E-6122, Lewis Research Center National Aeronautics and Space Administration, Cleveland, Ohio, May 1971.

[57] Bert R Phillips. RESONANCE TUBE HAZARDS IN OXYGEN SYSTEMS. page 25, Phoenix, Arizona, April 1982. National Aeronautics and Space Administation Lewis Research Center.

[58] George A. Repas. Hydrogen-Oxygen Torch Ignitor. Technical Report 106493, Lewis Research Center National Aeronautics and Space Administration, Cleveland, Ohio, March 1994.

[59] Paul D. Ronney. Laser versus conventional ignition of flames. Technical report, University of Southern California Department of Mechanical Engineering, Los Angeles, California, February 1994.

[60] Leon Stabinsky. Analytical and Experimental Study of Resonance Ignition Tubes. Final Report R-9403, Rocketdyne Division Rockwell International JPL Contract No. PO 953563, Canoga Park, California, December 1973.

[61] George Paul Sutton and Oscar Biblarz. *Rocket propulsion elements*. John Wiley & Sons, New Delhi, 2014. ISBN 978-81-265-2577-5. OCLC: 914504068.

[62] Charles K. Westbrook. Chemical kinetics of hydrocarbon ignition in practical combustion systems. *Proceedings of the Combustion Institute*, 28(2):1563–1577, January 2000. ISSN 15407489. doi: 10.1016/S0082-0784(00)80554-8. URL https://linkinghub.elsevier.com/retrieve/pii/S0082078400805548.

[63] Jeroen Wink, Rob Hermsen, Ralph Huijsman, Christ Akkermans, Luka Denies, Filipe Barreiro, Adriaan Schutte, Angelo Cervone, and Barry Zandbergen. Cryogenic Rocket Engine Development at Delft Aerospace Rocket Engineering. In *SP2016-3124644*, page 13, Rome, Italy, 2016. Space Propulsion Cinference.

[64] Desmond E. Winterbone and Ali Turan. *Advanced thermodynamics for engineers*. Elsevier, Amsterdam, 2nd ed edition, 2015. ISBN 978-0-444-63373-6. OCLC: 906700132.

[65] Rolf Wubben. Cryogenic Propulsion Team - Delft Aerospace Rocket Engineering. DARE internal report V1, Delft Aerospace Rocket Engineering Cryogenics Group, Delft, The Netherlands, September 2017.

[66] B T C Zandbergen. Thermal Rocket Propulsion (version 2.07). page 512, 2018.

[67] A.J. Zuckerwar. *Handbook of the Speed of Sound in Real Gases*. Academic Press, 2002. URL `https://pages.mtu.edu/~suits/SpeedofSoundOther.html`.

A

Appendix: Blizzard Lite

A.1. Overview of Main Engine

The main engine that this ignition system will be tested on is the Blizzard V1 Engine. Blizzard is a test bench version of a liquid bi-propellant engine. In October 2015 DARE established the Cryogenics project with the goal of research and development of a liquid bi-propellant engine using one or more cryogenic propellants [63, p.1]. The aim of the project is to develop an engine with a nominal thrust in the range of $10 - 15kN$. In order to achieve this, the team first aims to build and test a smaller version $2.6kN$ version whose most detailed designs can be found in the Blizzard v1 System Review V2. In the "Cryogenic Rocket Engine Development at Delft Aerospace Rocket Engineering" report, the team published their initial designs and plans for the cryogenic group [63]. As the design matured, changes were made and the most up to date document on the development of the engine is an internal DARE report, "Blizzard v1 System Review V2" [23]. This is an internal, unpublished report, and as such I have included relevant excerpts from this document in the appendix section of this document. The purpose of this thesis is to design an innovative ignition system that can be implemented on this engine. Therefore it is important to introduce the main parameters of the engine, its geometry and functionality. These will be necessary in order to develop a robust set of requirements for the ignition system and furthermore to create a design that takes into consideration the constraints presented by this engine.

A.1.1. Main Engine Parameters

The three main requirement of the Blizzard engine [23, p.2] are: the chamber pressure, $pc = 20$ bar, the fuel is 85% ethanol and 15% water, and the oxidizer is 100% LOX. The following engine parameters were found analytically using RPA and hand calculations. They should be seen as estimates.

Table A.1: Most Important Design Parameters of Blizzard V1

Parameter	Value	Unit
Engine Exit Velocity	2400.38	m/s
ISP	230.54	s
Total Mass Flow	1.1	kg/s
LOX Mass Flow	0.666	kg/s
Ethanol Mass Flow	0.477	kg/s
Thrust (Nozzle)	2.6	kN
OF	1.489	
Vandenkerchove Function	0.633	

A.1.2. Main Engine Components

When choosing an ignition system, the main physical components to consider on the engine are the combustion chamber, injector and manifold. The size of the combustion chamber dictates the space available for the ignition flame, as well as the orientation of the igniter to prevent eroding a hole in the side of the combustion chamber. The type of injector, its mass flow rate and its placement will dictate the size and location of the ignition flame as well as its power requirements. Finally the manifold, which sits at the top of the engine and houses the igniter, and injector will constrain the placement, orientation, and accessibility of the ignition system.

A.1.3. Combustion Chamber

Figure A.1 shows a cut-through image of the Blizzard V1 engine. In this figure you can identify the manifold on the right hand side of the image, and the steel tube, which acts as the combustion chamber for test, and the pressure ports along the top of the tube.

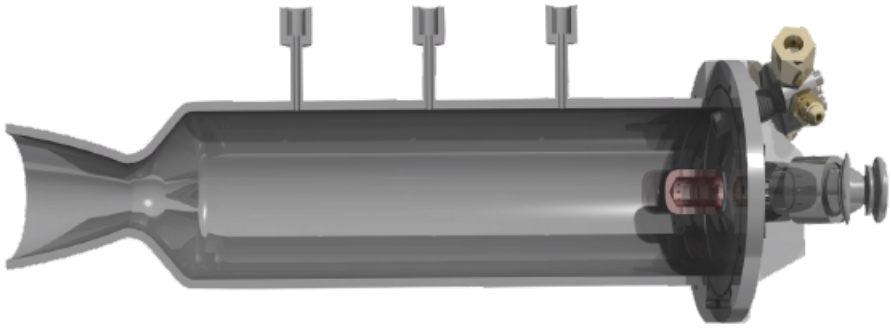

Figure A.1: Cryogenics Group Blizzard V1 Engine [23]

The engine parameters in Table A.1 were used to size the combustion chamber, the values of which are listed in Table A.2. The calculations for all of these values can be viewed in the appendix. The throat diameter was determined under the assumption of optimal expansion, $p_{exit} = p_{atm}$.

Table A.2: Combustion Chamber Sizing Blizzard V1

Parameter	Value	Unit
Throat Diameter	34.34	mm
Area Ratios	3.32	
Exit Diameter	61.75	mm
Chamber Diameter	90	mm
Chamber Length	220	mm

A.1.4. Injector Design and Placement and Manifold

This engine uses a pintle injector in order to inject the propellants from the feedsystem into the combustion chamber. The properties and mass flow rates of the propellants are in Table A.3. Figure A.2 provides a section view and mixing pattern of this injector, as well as highlights the 4 main parts of the injector, labeled a-d. These are the (a) fuel manifold, (b) pintle tip, (c) face plate, and (d) orifice plate. The oxidizer flows in through an adapter at the center of the manifold and is injected radially by the pintle tip. The fuel flows in through the adapter at a 45° angle in the manifold, pools up in the fuel manifold, and is spread out evenly by the orifice place before it is injected along the outside of the pintle time injector axially. When the fuel and oxidizer are both injected in this manner, perpendicularly

to one another, it results in the mixing pattern shown in Figure A.2, which helps increase atomization and encourages a more complete combustion [23].

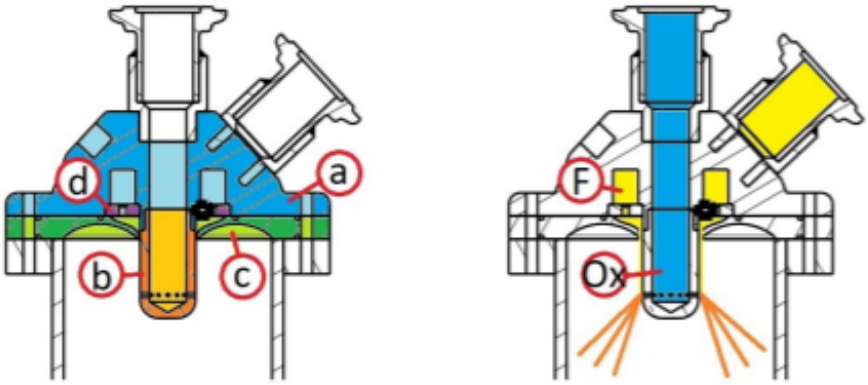

(a) Section view of the pintle injector manifold (b) Mixing pattern of a pintle injector

Figure A.2: Pintle Injector Blizzard V1 Engine [23]

In Figure A.1, one can see the location of the pintle injector and oxidizer line adapter in the manifold. The injector being located in the center of the manifold, and the subsequent placement of the oxidizer and fuel adapters, restrict the space available for the igniter. The space available on the manifold, location of the mixing propellants and flame size required will all need to be taken into consideration when designing the ignition system.

A.1.5. Main Engine Propellants

The purpose of the igniter is to initiate the combustion of the main engine propellants, 85% Ethanol and 100% LOX. Both of these propellants are stored in their liquid state in order to minimize the size of the storage tanks required. In order to achieve ignition, the igniter must be capable of providing enough power to vaporize and then ignite the propellants. The igniter power requirement is comprised of the amount of energy and the ignition time. In order to size the igniter properly, it is vital to calculate the power required to achieve a reliable ignition of the main engine propellants. To do so one must first determine the percentage of the main engine propellants that must be ignited in order to achieve a stable self-sustaining combustion. From this, the power required from the igniter can be calculated. To accomplish this, the physical parameters of the propellants, as well as all necessary equations and safety considerations and included below.

A.1.6. Propellant Physical Parameters

In order to minimize the volume and mass of the propellant storage tanks, the propellants are stored in their liquid state. As ethanol is liquid at STP (298K, 1 atm) [64], it is relatively simple to store in its liquid state, and only requires a tank kept at ambient temperature. Oxygen is a cryogenic liquid because it has a boiling point of $-183°C$ [4]. Therefore the liquid ethanol is stored at ambient temperature and the liquid oxygen is stored at cryogenic temperatures. The oxygen therefore has cryogenic storage requirements which include an insulated tank and feedsystem, cryogenic rated valves, and cryogenic o-rings, as well as specialized handling procedures to ensure the oxygen remains liquid in the feedsystem during injection. All relevant storage and mass flow information on the propellants is in Table A.3. Additional relevant information on the physical properties of these propellants are in Figure A.3 and Figure A.4.

It is necessary to mention that the testing procedures will influence the properties of the propellants. In order for the LOX to be in the liquid phase when it is injected into the combustion chamber, the LOX feedsystem, manifold and injector need to be pre-chilled. This is accomplished by flowing LOX through the system until it cools down the components enough to remain in the liquid phase during injection. While the ethanol is stored separately and has separate feed system lines, it will still flow through the same manifold and injector. This is very likely to lower the injection temperature of the ethanol. Therefore when determining the power requirements of the igniter, it is necessary to take into account that the ethanol will be at a temperature below ambient. CRYO has estimated this temperature to be

Table A.3: Main Engine Propellant Information [23]

Parameter	Ethanol 85%	LOX 100%
Stored State	Liquid	Liquid
Nominal Tank Operating Pressure	50 bar	55 bar
Temperature	298K	90 K
Injector Mass Flow Rate	0.478 kg/s	0.666 kg/s

Formula: CH_3CH_2OH / C_2H_6O
Molecular mass: 46.1
Boiling point: 78°C
Melting point: -114 °C
Relative density (water = 1): 0.79
Solubility in water: miscible
Vapour pressure, kPa at 20°C: 5.8
Relative vapour density (air = 1): 1.6
Relative density of the vapour/air-mixture at 20°C (air = 1): 1.03
Flash point: 12.0 °C c.c.
Auto-ignition temperature: 400°C
Explosive limits, vol% in air: 3.1-27.7
Octanol/water partition coefficient as log Pow: -0.32
Viscosity: 1.074 mPa*s at 20°C

Figure A.3: UN International Chemical Safety Card (ICSC) Ethanol/Ethyl Alcohol [25]

Table 1: Liquid Oxygen Physical and Chemical Properties

Molecular Formula	O_2
Molecular Weight	31.999
Boiling Point @ 1 atm	–297.4°F (–183.0°C)
Freezing Point @ 1 atm	–361.9°F (–218.8°C)
Critical Temperature	–181.8°F (–118.4°C)
Critical Pressure	729.1 psia (49.6 atm)
Density, Liquid @ BP, 1 atm	71.23 lb/scf (1141 kg/m³)
Density, Gas @ 68°F (20°C), 1 atm	0.0831 lb/scf (1.33 kg/m³)
Specific Gravity, Gas (air=1) @ 68°F (20°C), 1 atm	1.11
Specific Gravity, Liquid (water=1) @ 68°F (20°C), 1 atm	1.14
Specific Volume @ 68°F (20°C), 1 atm	12.08 scf/lb (0.754 m³/Kg)
Latent Heat of Vaporization at BP	91.7 Btu/lb (213 Kj/Kg)
Expansion Ratio, Liquid to Gas, BP to 68°F (20°C)	1 to 860
Solubility in Water @ 77°F (25°C), 1 atm	3.16% by volume

Figure A.4: Liquid Oxygen Safety Card Air Products [4]

a conservative value of 200K, and this value will be used for the rest of the report [23, p.9]. More information on the safety and handling of these propellants can be found here for ethanol [25] and here for liquid oxygen [4].

A.2. Main Engine Design Drawings

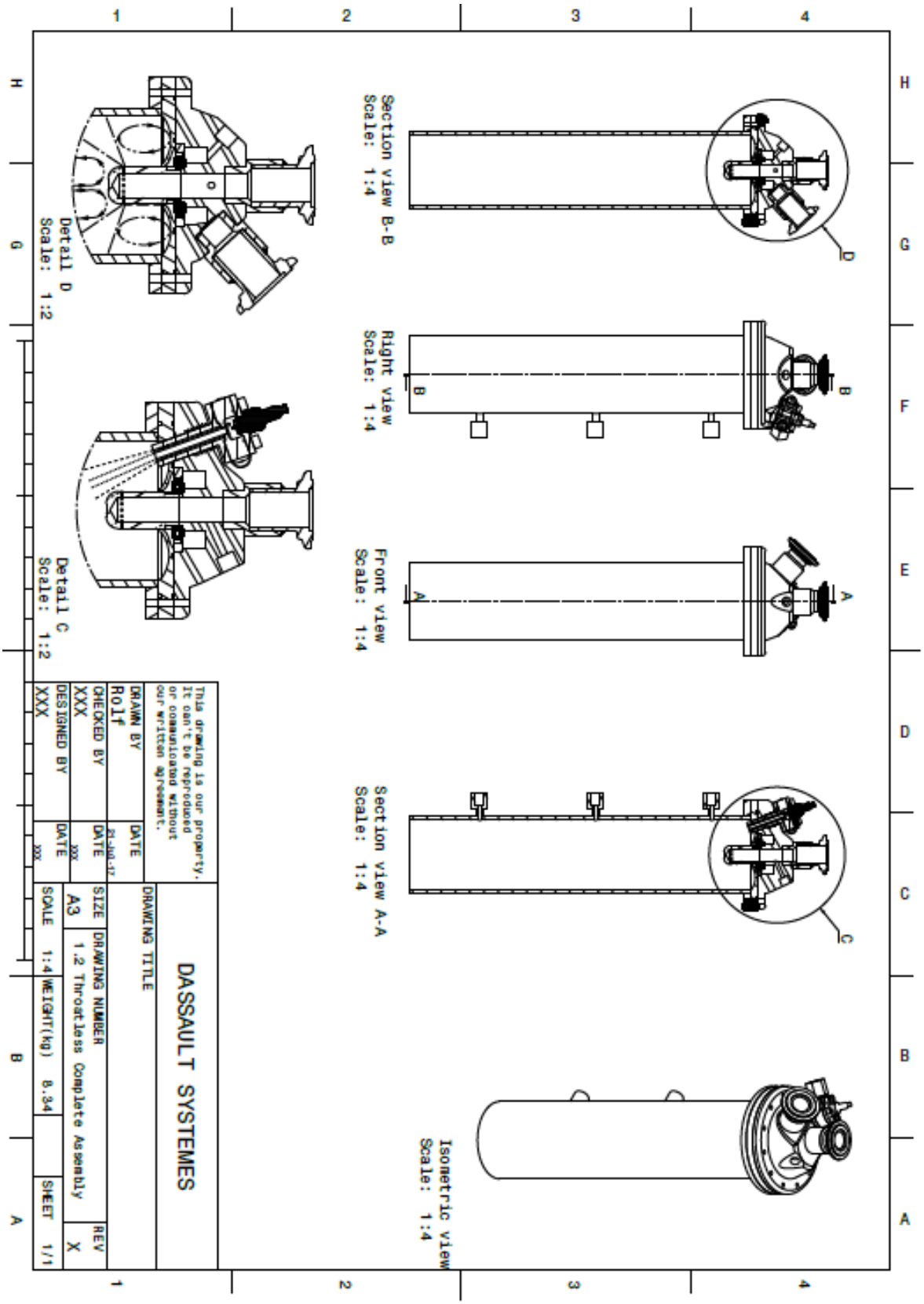
Section view B-B
Scale: 1:4
Right view
Scale: 1:4
Front view
Scale: 1:4
Section view A-A
Scale: 1:4
Isometric view
Scale: 1:4
Detail D
Scale: 1:2
Detail C
Scale: 1:2
This drawing is our property.
It can't be reproduced
or communicated without
our written agreement.
DRAWN BY
Rolf
DATE
CHECKED BY
XXX
DATE
DESIGNED BY
XXX
DATE
DASSAULT SYSTEMES
DRAWING TITLE
SIZE
A3
DRAWING NUMBER
1.2 Throatless Complete Assembly
REV
X
SCALE
1:4
WEIGHT(kg)
8.34
SHEET
1/1

Figure A.5: [23]

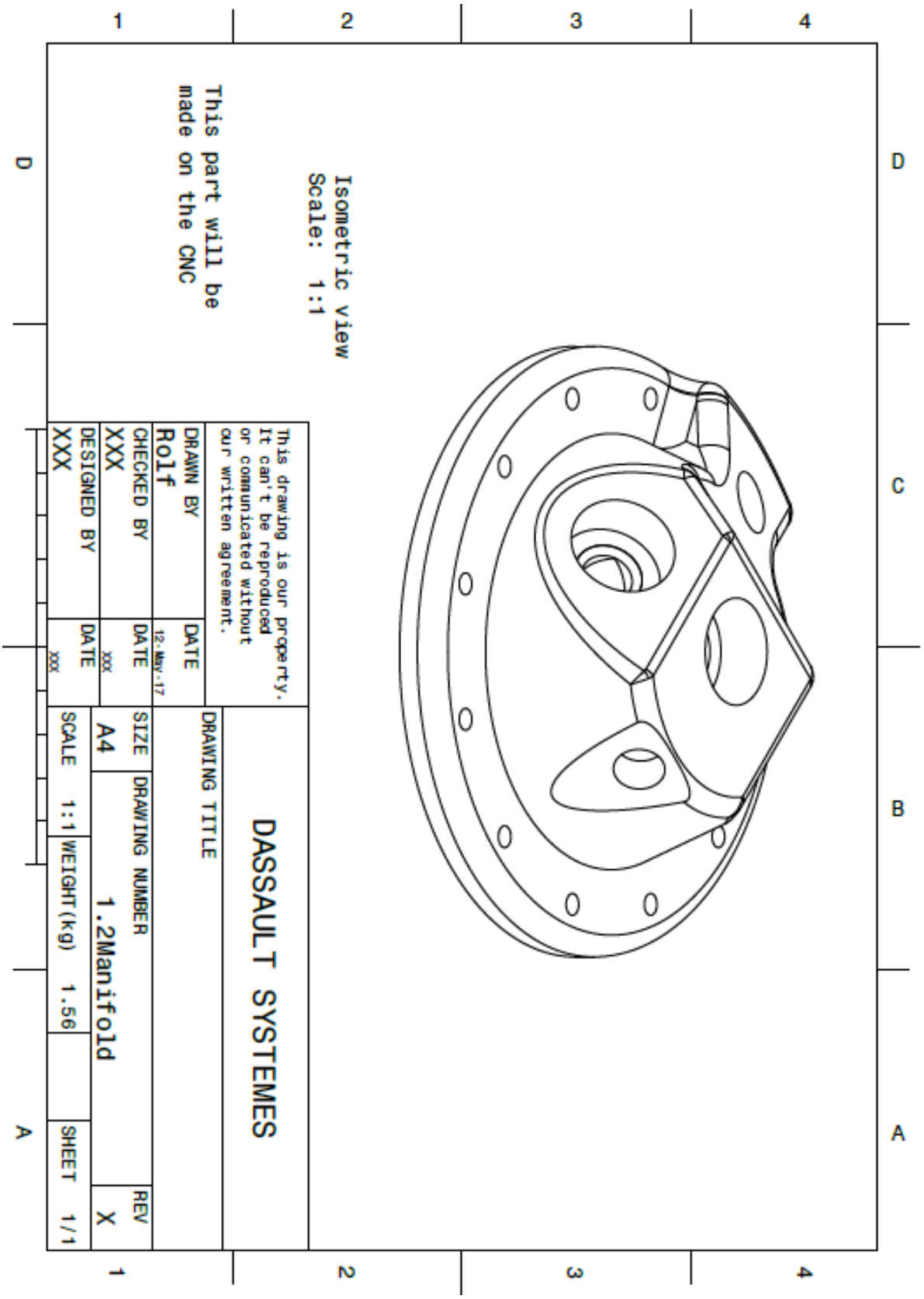
Isometric view
Scale: 1:1
This part will be made on the CNC
This drawing is our property. It can't be reproduced or communicated without our written agreement.
DRAWN BY
Rolf
DATE
12-May-17
CHECKED BY
XXX
DATE
XXX
DESIGNED BY
XXX
DATE
XXX
DRAWING TITLE
DASSAULT SYSTEMES
SIZE
A4
DRAWING NUMBER
1.2Manifold
REV
X
SCALE 1:1
WEIGHT(kg) 1.56
SHEET 1/1

Figure A.6: [23]

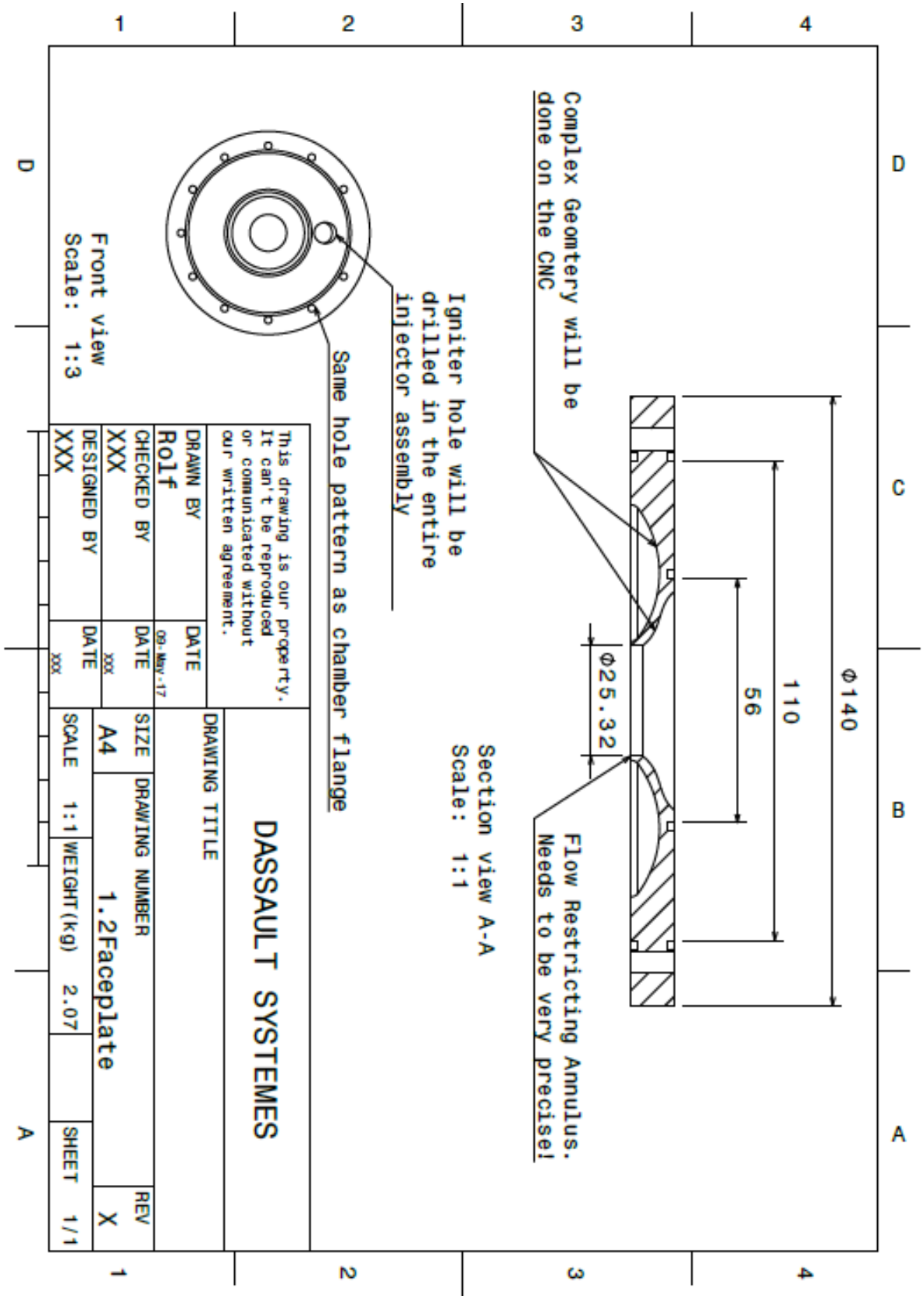
Complex Geomtery will be done on the CNC
Igniter hole will be drilled in the entire injector assembly
Same hole pattern as chamber flange
Flow Restricting Annulus. Needs to be very precise!
Section view A-A
Scale: 1:1
Front view
Scale: 1:3
Φ140
110
56
Φ25.32
This drawing is our property. It can't be reproduced or communicated without our written agreement.
DRAWN BY Rolf DATE 09-May-17
CHECKED BY XXX DATE XXX
DESIGNED BY XXX DATE XXX
DASSAULT SYSTEMES
DRAWING TITLE
SIZE A4
DRAWING NUMBER 1.2Faceplate
REV X
SCALE 1:1
WEIGHT(kg) 2.07
SHEET 1/1

Figure A.7: [23]

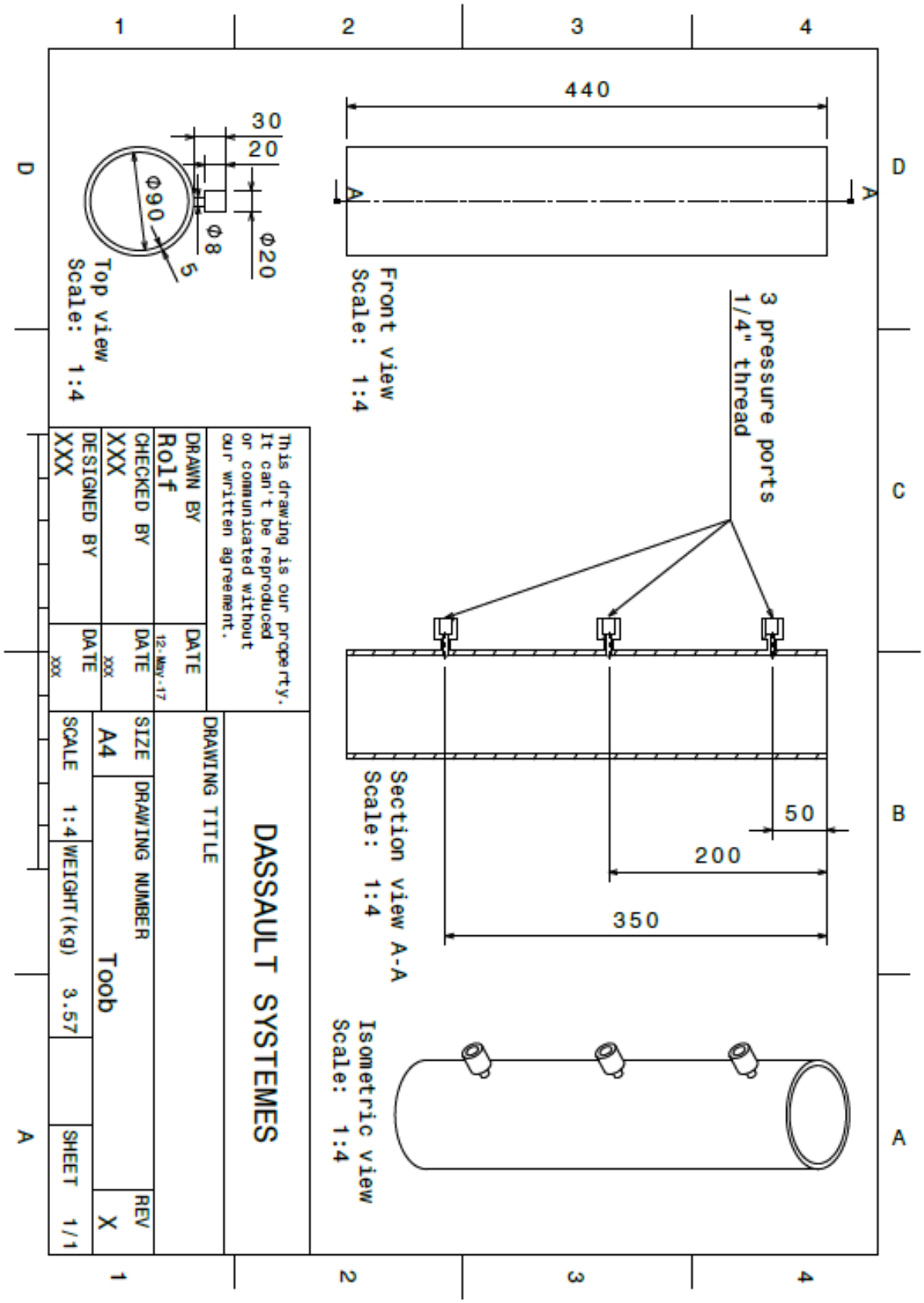
440
30
20
Φ90
Φ8
Φ20
5
Top view
Scale: 1:4
Front view
Scale: 1:4
3 pressure ports
1/4" thread
Section view A-A
Scale: 1:4
50
200
350
Isometric view
Scale: 1:4
This drawing is our property.
It can't be reproduced
or communicated without
our written agreement.
DRAWN BY
Rolf
DATE
12-May-17
CHECKED BY
XXX
DATE
XXX
DESIGNED BY
XXX
DATE
XXX
DASSAULT SYSTEMES
DRAWING TITLE
SIZE
A4
DRAWING NUMBER
Toob
REV
X
SCALE 1:4
WEIGHT(kg) 3.57
SHEET 1/1

Figure A.8: [23]

B

Python Code and Output

```
PYTHON OUTPUTS
Part 1: Import Main Engine Parameters
Blizzard Lite Parameters
Blizzard Lite
Isp = 227.738  ;  Thurst =  2600 N
mox =  0.696 kg/s  ;  mf =  0.468 kg/s  ;  mtot =  1.164 kg/s
-----                  ---------
Main Engine Parameters imported.
----------                                  -------------
Part 2: Main Engine Propellant Parameters
Stoichiometric Chem. Balance Eqn:
( 1.0 C2H5OH(l) +  0.4513 H2O(l)) +  3.0 O2(l) ->  2.0 CO2(g) +  3.4513 H2O(g)
Stoichiometric O/F ratio for 85% Ethanol-15% Water Fuel and 100% LOX:
1.7711454557294495
ER:  0.841 . It is  Fuel Rich .
----------                                  -------------
Part 3: Igniter OF vs. Tc
Take a look at the OF vs. T plot. Choose an OF that has a Tc < 2090K. (This is
about max reasonable operational temperature for SS304 for a combustion of <
3sec.) Choose a fuel rich combustion to prevent oxidation damage and corrosion.
OF of 0.8 gives Tc = 1960K
Choose an OF from the RPA vs OF Plot: >? 0.8
Which combustion temperature goes with that OF, in Kelvin: >? 1960
OF is type  <class 'float'>
Tc is type  <class 'float'>
For O/F =  0.8 . Combustion Temp =  1960.0 K
Chem. Balance Eqn:
3.2 ( 1.0 (C2H5OH(l)+ 0.4513 H2O(l))+ 3.0 O2(l)-> 2.0 CO2(g)+ 3.4513 H2O(g)+ 0.0
O2(l) + 2.2 ( 1.0 (C2H5OH(l)+ 0.4513 H2O(l))
----------                                  -------------
Part 4: Main Engine Minimum Ignition Energy Requirement
What percentage of main flow do we want to ignite? Write in decimal form. (ie.
10% -> 0.10) Recommended value: 0.05. >? 0.05
What safety factor on the ignition power? Recomended Value: 2. >? 2
To ignite  5.0 % of the main engine propellants requires 72.9 kW of power  ;
145.8 kW with SF of 2.0 .
----------                                  -------------
Part 5: Igniter Exhaust and power calculations
Dh CO2p IGN:  1649738.6627937732 . Dh O2p IGN:  1440106.246322037 . Dh_H2Op IGN:
 3207447.7343014404
Dh exhaust: 2079469.2717752566
gamma exhaust: 1.2176674017938485
R exhaust: 326.7996075485107
mm exhaust: 31.18275814658856
Total Mass Flow Rate =  70.12068806963524 g/sec
Fuel Mass Flow Rate =  38.95593781646402 g/sec
Oxidizer Mass Flow Rate =  31.16475025317122 g/sec
Part 6: Sonic injection nozzle
Critical Pressure ratio =  0.5282817877171742
Critical temperature ratio =  0.8333333333333334
R, oxygen =  259.82873929620604 J/kg*K
gamma, oxygen =  1.4
GOX diameters (mm): [1.5, 2, 2.5, 3, 3.5, 4, 4.5, 5, 5.5, 6, 6.5]
For the list of GOX nozzle exit diameters, these are the minimum allowable
```

values of Oxygen Total Supply Pressure required to maintain choked flow, as well as the maximum allowable combustion pressures that correspond to these supply pressures.
GOX P total supply (bar) : [71.908, 40.448, 25.887, 17.977, 13.208, 10.112, 7.99, 6.472, 5.349, 4.494, 3.829]
GOX P combustion (bar): [37.988, 21.368, 13.676, 9.497, 6.977, 5.342, 4.221, 3.419, 2.826, 2.374, 2.023]
Choose an exit diameter for the GOX nozzle, in mm: >? 3
Choose a supply pressure for the GOX nozzle, see list of GOX pressures to see minimum allowed P, in bar: >? 19
Choose an inlet diameter for the GOX nozzle, based on Goodridge flex hose sizes in mm: >? 10
Choose a converging angle for GOX nozzle, use range 20-60 degrees, in degrees : >? 20
Combustion Pressure, Pc: 8.72 Bar
GOX eta: 11.111
GOX Lcon: 9.616 mm
GOX NPR, during heating: 18.752
GOX ru: 2.25 mm
GOX ra: 1.2 mm
GOX Total Temperature at Inlet: 300 K
GOX Total Pressure at Inlet: 19.0 bar
GOX Velocity Inlet: 16.279033219884134 m/s
GOX Velocity throat: 301.563 m/s
GOX Static Temp. at Throat: 250.0 K
GOX Static Pressure at Throat: 1003735.397 Pascals
Part 7: Exhaust Orifice Sizing
Choose an exhaust orifice diameter, in mm: >? 12
Exhaust Orifice Diameter = 12.0 mm
Exhaust Orifice Area = 113.09733552923255 m2
Exhaust Density = 1.3608554138304894 kg/m3
Exhaust Orifice Pressure Drop = 1.7436551273572165 Bar
Exhaust Orifice Velocity = 455.59800132029545 m/s
Part 8: Resonance Cavity
How much larger is resonance cavity opening than GOX nozzle exit?>? 1.4
What is the end diameter at base of resonance cavity, in mm? >? 1
What is the angle of the resonance cavity, in degrees? >? 3
Resonance cavity is a truncated cone shape. optimal
Resonance Cavity Opening Diameter: 4.2 mm.
Resonance Cavity End Diameter: 1.0 mm.
Resonance Cavity Angle: 3.0 degrees.
Resonance Cavity Length: 30.529818700365137 mm.
Resonance Cavity Length Mach Disc: 8.441 mm.
Part 9: Ignter Fuel Injection
Fuel Injector No. Holes 3
Fuel Injector Hole Diameter 1.0 mm
Fuel Injector Pressure Drop 2.237 Bar
Fuel Injector Velocity 20.955 m/s
Fuel Injector Exhaust Pressure Drop 0.00093 Bar
Fuel Injector Exhaust Velocity 0.437 m/s
Fuel Injector Minimum Injection pressure 26.238 Bar

```
### Main.py ###

import matplotlib.pyplot as plt
from math import *
import numpy as np
import sympy
from sympy import S, symbols, printing
from scipy.optimize import fsolve
import ipdb

plotcp = 'No'                                          # Plot O2, H2O & CO2 Cp
figures? Yes or No
plotethcp = 'No'                                       # Plot Igniter Ethanol Cp
figures? Yes or No
plotRPA = 'Yes'                                         # Plot RPA OF vs. Tc Plot?
Yes or No
r_inlet = 0.005         # [m] diameter of sonic nozzle inlet from Goodridge hose
options D06 (9.53mm ID, figure can have a nozzzle with 8mm ID attached)

#~~~~~~~~~~~~~~~~~~~~~~~~~~~~~~~~~~~~~~~~~~~~~~~~~~~~~~~~~~~~~~~~~~~~~~~~~~~~#
print("Part 1: Import Main Engine Parameters")
print("Blizzard Lite Parameters")
from Blizzard_Lite import Blizzard_Lite
plt.interactive(False)
Bliz_Lite = Blizzard_Lite()
print("Blizzard Lite")
print("Isp =", round(Bliz_Lite.Isp,3), " ;  Thurst = ", Bliz_Lite.F, "N ")
print("mox = ", round(Bliz_Lite.MAIN_mox,3), "kg/s  ;  mf = ",
round(Bliz_Lite.MAIN_mf,3), "kg/s  ;  mtot = ", round(Bliz_Lite.MAIN_mtotal,3),
"kg/s")
print("-----                  ---------")

"""
print("Import Blizzard Heavy Parameters")
from Blizzard_Heavy import Blizzard_Heavy
plt.interactive(False)

Bliz_Heavy = Blizzard_Heavy()
print("Blizzard Heavy")
print("Isp =", round(Bliz_Heavy.Isp,3), " ;  Thurst = ", Bliz_Heavy.F, "N ")
print("mox = ", round(Bliz_Heavy.MAIN_mox,3), "kg/s  ;  mf = ",
round(Bliz_Heavy.MAIN_mf,3), "kg/s  ;  mtot = ",
round(Bliz_Heavy.MAIN_mtotal,3), "kg/s")
"""
Engine_1 = Blizzard_Lite()
"""
#All engine paramters are now imported.
#Import as Engine_1.Per_Eth, or Engine_1.gamma
"""
print("Main Engine Parameters imported. ")
print("----------                                      -------------")

#~~~~~~~~~~~~~~~~~~~~~~~~~~~~~~~~~~~~~~~~~~~~~~~~~~~~~~~~~~~~~~~~~~~~~~~~~~~~#~
```

```
print("Part 2: Main Engine Propellant Parameters")
"""
In this part we will calculate the stoichiometric O/F for the main engine and
ignition propellant mixture (since they are
the same propellants, Oxidizer: LOX, and Fuel: 85% Ethanol-15% Water.
We will also calculate the weighted molar mass of the fuel and the weighted
density of the fuel (since it is a mixture.)
Then we will calculate the equivalence ratio of the main engine propellants.
"""

from MolecularWeights import MolecularWeights
Mol_weights1 = MolecularWeights()
#ipdb.set_trace()
Stoich_OF, Wtmm_Fuel, Wtrho_Fuel = Mol_weights1.StoichMassFractions()
"""
The above is assuming M_C2H5OHr = 1gram.
Otherwise, if M_C2H5OHr = 2gram you would call:
    Mol_weights1 = MolecularWeights(2)
    Stoich_OF = Molecular_weights1.MassFractions()

Equivalence Ratio OF/OFstoich
    ER < 1: Fuel Rich, some fuel remains
    ER = 1: stoichiometric. all fuel and ox used
    ER > 1: Fuel Lean. some Oxidizer remains

"""
MAIN_ER = Engine_1.MAIN_OF / Stoich_OF

if MAIN_ER > 1:
    MEburn = 'Fuel Lean'
elif MAIN_ER < 1:
    MEburn = 'Fuel Rich'
else:
    MEburn = 'Stoichiometric'
print("Stoichiometric O/F ratio for 85% Ethanol-15% Water Fuel and 100% LOX: ",
Stoich_OF)
print("ER: ", round(MAIN_ER,3), ". It is ", MEburn, ".")

# ER = OF_IGN/1.8
print("----------                                    -------------")

#~~~~~~~~~~~~~~~~~~~~~~~~~~~~~~~~~~~~~~~~~~~~~~~~~~~~~~~~~~~~~~~~~~~~~~~~~~~~~~~~#

print("Part 3: Igniter OF vs. Tc")
"""
Call the RPA function to create the OF vs Tc plot at a range of igniter
combustion pressure, Pc_IGN.
Then choose a mixture ratio, OF, and the corresponding Combustion temperature,
Tc_IGN.
"""

from RPAFULL import RPAFULL_func
abc = RPAFULL_func(Stoich_OF)
```

```
print("Take a look at the OF vs. T plot. Choose an OF that has a Tc < 2090K. "
      "(This is about max reasonable operational temperature for SS304 for a
combustion of < 3sec.) "
      "Choose a fuel rich combustion to prevent oxidation damage and
corrosion.")

print("OF of 0.8 gives Tc = 1960K")
OF_IGN = float(input("Choose an OF from the RPA vs OF Plot: "))
Tc_IGN = float(input("Which combustion temperature goes with that OF, in Kelvin:
" ))

print("OF is type ", type(OF_IGN))
print("Tc is type ", type(Tc_IGN))

"""
Now call the next function to calc the chemical balance eqn for the igniter
combustion
given the chosen OF.

Chemical Balance Eqn Begin
    from ChemicalBalance import chembal_func
    A, B, C, D, E, F, burn = chembal_func(OFex, Tc, Stoich_OF, Wtmm_Fuel, mmO2,
As, ABs, Bs, Cs, Ds)
    get list of coefficients for the chemical balance equation

    A*(C2H5OH(l) + 0.45127*H2O(l)) + B*O2(l) -> C*CO2(g) + D*H2O(g) + E*O2(g) +
F*(C2H5OH(l) + 0.45127*H2O(l))

"""
A, B, C, D, E, F, burn = Mol_weights1.chembal_func(OF_IGN, Tc_IGN, Stoich_OF,
Wtmm_Fuel)

print("For O/F = ", OF_IGN, ". Combustion Temp = ", Tc_IGN, "K")
print("Chem. Balance Eqn:")
print("%.1f" % round(A, 1), "(", "%.1f" % round(Mol_weights1.As, 1),
"(C2H5OH(l)+", "%.4f" % round(Mol_weights1.ABs, 4), "H2O(l))+",
      "%.1f" % round(B, 1), "O2(l)->", "%.1f" % round(C, 1), "CO2(g)+", "%.4f" %
round(D, 4), "H2O(g)+",
      "%.1f" % round(E, 1), "O2(l) +", "%.1f" % round(F, 1), "(", "%.1f" %
round(Mol_weights1.As, 1), "(C2H5OH(l)+", "%.4f"
      % round(Mol_weights1.ABs, 4), "H2O(l))")

print("----------                                    -------------")

#~~~~~~~~~~~~~~~~~~~~~~~~~~~~~~~~~~~~~~~~~~~~~~~~~~~~~~~~~~~~~~~~~~~~~~~~~~~~~~~~#

print("Part 4: Main Engine Minimum Ignition Energy Requirement")
"""
To calculate the total power required to raise X% of the main engine propellants
to the ignition temp, you need to
calc how much power is required to raise the propellants from their injection
temp to the autoignition temp of ethanol
as well as the amount of power required to change the phase of the propellants
from liquid to vapor. Remember to
```

```
include the water in the ethanol, bc it does not contribute to the combustion,
but it requires a lot of power to heat
up to the combustion temp.

~~~~~~~~~~~~~~~~~ Main Engine H2O and O2 dH calcs  ~~~~~~~~~~~~~~~~~
"""
T_H2O = np.arange(Engine_1.T_ambient, Engine_1.T_EthAuto)
T_lox = np.arange(Engine_1.T_LoxStorage, Engine_1.T_EthAuto)

from CpO2CO2H2O import cp_func
cp_H2Or = cp_func('H2O', T_H2O)/(Mol_weights1.mmH2O/1000)
# [J/(kg*K)] Main Engine Reactant H2O cp
cp_O2r = cp_func('O2', T_lox)/(Mol_weights1.mmO2/1000)
# [J/(kg*K)] Main Engine Reactant O2 cp

if plotcp == 'Yes':
    plt.figure()
    plt.plot(T_lox, cp_O2r)
    plt.plot(T_H2O, cp_H2Or)
    plt.xlabel('Temperature [K]')
    plt.ylabel(r'$C_p$' + ' [J/kg/K]')
    plt.legend([r'$O_2$', r'$H_2O$'])
    plt.show()
else:
    pass

# Reactant enthalpies
Dh_watsumME = sum(cp_H2Or)                                          # [J/kg]
Main Engine Reactant Water enthalpy sum
Dh_oxsumME = sum(cp_O2r)                                            # [J/kg]
Main Engine Reactant Oxidizer enthalpy sum

"""
~~~~~~~~~~~~~~~~~ Main Engine Ethanol dH calcs  ~~~~~~~~~~~~~~~~~
Specific heat values for ethanol at the matching temperatures in List form.
Taken from NIST. See excel for 763K calc.
Calc the Cp values for ethanol over the temp values in the list below. Use exact
temp range, then just add margin for
final power to account for some heat losses due to the cooled manifold. Storage
temp of the fuel is 298.15K.
Auto-ignition temp is 763K.
"""
T_eth = [298.15, 300, 400, 500, 600, 700, 763]  # [K]
Cp_eth = [65.21, 65.49, 81.22, 95.78, 108.24, 118.83, 124.74]  # [J/mol*K]

Dh_eth = []
for i in range(len(T_eth) - 1):
    Dh_eth.append(((Cp_eth[i + 1] + Cp_eth[i]) / 2 * (T_eth[i + 1] - T_eth[i]))
* (1000 / Mol_weights1.mmC2H5OH))  # [J/kg]

Dh_ethsumME = sum(Dh_eth)                                           # [J/kg]
Main Engine Reactant Ethanol enthalpy sum

"""
```

```
~~~~~~~~~~~~~~~~~ Main Engine Power  ~~~~~~~~~~~~~~~~~

Here we calculate how much power is required to ignite a given percentage of the
main engine propellant flow
"""

PMF_ign = float(input("What percentage of main flow do we want to ignite? Write
in decimal form. (ie. 10% -> 0.10) "
                "Recommended value: 0.05. "))
SF_Power = float(input("What safety factor on the ignition power? Recomended
Value: 2. "))

from IgnitionPower import power_func
Q = power_func(PMF_ign, Engine_1.MAIN_mox, Engine_1.MAIN_mf, Engine_1.Per_Eth,
Engine_1.Per_Water, Dh_ethsumME,
                    Dh_watsumME,  Dh_oxsumME)
QSF = Q * SF_Power

print("To ignite ", PMF_ign*100, "% of the main engine propellants requires",
round(Q/1000,1), "kW of power  ; ", round(QSF/1000,1), "kW with SF of",
      SF_Power, ".")
"""
QFULL = power_func(1, Engine_1.MAIN_mox, Engine_1.MAIN_mf, Engine_1.Per_Eth,
Engine_1.Per_Water, Dh_ethsumME,
                    Dh_watsumME,  Dh_oxsumME)
print("To ignite ", 100, "% of the main engine propellants requires",
round(QFULL/1000,1), "kW of power.")
"""
print("----------                                    -------------")

#~~~~~~~~~~~~~~~~~~~~~~~~~~~~~~~~~~~~~~~~~~~~~~~~~~~~~~~~~~~~~~~~~~~~~~~~~~~~~~~~#

print("Part 5: Igniter Exhaust and power calculations")
"""

We are going to use a simple orifice for the igniter exhaust. This is easy to
replace during testing, as it will
likely melt multiple times, A nozzle is too complex and unnecessary. Therefore
it will be a simple orifice.
Begin by calculating the total change in enthalpy achieved by the given Tc
(which is a function of the selected OF).
Then we can calc the total mass flow rate of the igniter exhaust, given the
required power and the change in enthalpy.

~~~~~~~~~~~~~~~~~ Igniter Product Ethanol dH calcs ~~~~~~~~~~~~~~~~~
"""
Tethnp = np.arange(Engine_1.T_EthAuto, Tc_IGN)

from CpEthanol import  ethtest_func
cp_ethIGN = ethtest_func(Tethnp, plotethcp)                    # [J/(kg*K)]
Dh_EthpIGN = sum(cp_ethIGN)                                    # [J/kg] Igniter
Product in Exhaust Ethanol enthalpy sum

""" ~~~~~~~~~~~~~~~~~ Igniter Product CO2, H2O and CO2 dH calcs
```

```
~~~~~~~~~~~~~~~~~ """
Texhaust = np.arange(Engine_1.T_EthAuto, Tc_IGN)
cp_H2OpIGN = cp_func('H2O', Texhaust)/(Mol_weights1.mmH2O/1000)          #
[J/(kg*K)] Igniter Product H2O in Exhaust cp
cp_CO2pIGN = cp_func('CO2', Texhaust)/(Mol_weights1.mmCO2/1000)          #
[J/(kg*K)] Igniter Product CO2 in Exhaust cp
cp_O2pIGN = cp_func('O2', Texhaust)/(Mol_weights1.mmO2/1000)             #
[J/(kg*K)] Igniter Product O2 in Exhaust cp

if plotcp == 'Yes':
    plt.figure()
    plt.plot(Texhaust, cp_CO2pIGN, 'b')
    plt.plot(Texhaust, cp_O2pIGN, 'g')
    plt.plot(Texhaust, cp_H2OpIGN, 'r')
    plt.ylabel('Cp [J/(kg*K)]')
    plt.xlabel('Combustion Temperature [K]')
    plt.legend([r'CO2', r'O2', r'H2O'])
    plt.title('Cp v Temp, exhaust gases')
    plt.show()
else:
    pass

Dh_CO2pIGN = sum(cp_CO2pIGN)                                             # [J/kg]
Igniter Product in Exhaust CO2 Enthalpy Sum
Dh_O2pIGN = sum(cp_O2pIGN)                                               # [J/kg]
Igniter Product in Exhaust O2 Enthalpy Sum
Dh_H2OpIGN = sum(cp_H2OpIGN)                                             # [J/kg]
Igniter Product in Exhaust H2O Enthalpy Sum

print("Dh CO2p IGN: ", Dh_CO2pIGN, ". Dh O2p IGN: ", Dh_O2pIGN, ". Dh_H2Op IGN:
", Dh_H2OpIGN)

'''Weighted mass of the dH for the exhaust products. See the chemical balance
eqn above for the coefficients.
A*(C2H5OH(l) + 0.45127*H2O(l)) + B*O2(l) -> C*CO2(g) + D*H2O(g) + E*O2(g) +
F*(C2H5OH(l) + 0.45127*H2O(l)) '''

Dh_exhaustIGN = ((C*Dh_CO2pIGN) + (D*Dh_H2OpIGN) + (E*Dh_O2pIGN) +
                 (F*(Dh_EthpIGN +
(Mol_weights1.ABs*Dh_H2OpIGN))))/(C+D+E+F+(F*Mol_weights1.ABs))
print("Dh exhaust:", Dh_exhaustIGN)

## IGNITER Exhaust
RWT_Exhaust = ((C*Mol_weights1.R_CO2) + (D*Mol_weights1.R_H2O) +
(E*Mol_weights1.R_O2) + (F*(Mol_weights1.R_Eth +

(Mol_weights1.ABs*Mol_weights1.R_H2O))))/(C+D+E+F+(F*Mol_weights1.ABs))
        # [J/(kg*K)] Exhaust Gases Weighted Specific Gas Constant
mmWT_Exhaust = ((C*Mol_weights1.mmCO2) + (D*Mol_weights1.mmH2O) +
(E*Mol_weights1.mmO2) + (F*(Mol_weights1.mmC2H5OH +

(Mol_weights1.ABs*Mol_weights1.mmH2O))))/(C+D+E+F+(F*Mol_weights1.ABs))
    # [g/mol] Exhaust Gases Weighted Molar Mass
```

```
"""
specific heat ratio at combustion temp
https://www.grc.nasa.gov/www/k-12/airplane/specheat.html
cv = cp - R  ;  gamma = cp/cv  ;   calc cv at combustion temp, Tc
"""
cp_CO2plast = cp_CO2pIGN[-1]
cp_H2Oplast = cp_H2OpIGN[-1]
cp_O2plast = cp_O2pIGN[-1]
cp_Ethlast = cp_ethIGN[-1]

cpWT_exhaust = ((C*cp_CO2plast) + (D*cp_H2Oplast) + (E*cp_O2plast) +
(F*(cp_Ethlast +

(Mol_weights1.ABs*cp_H2Oplast))))/(C+D+E+F+(F*Mol_weights1.ABs))    # Exhaust
Gases Weighted Cp
cvWT_exhaust = cpWT_exhaust-RWT_Exhaust                             # Exhaust
Gases Weighted Cv
gammaWT_Exhaust = cpWT_exhaust/cvWT_exhaust                         # Exhaust
Gases Weighted gamma

print("gamma exhaust:", gammaWT_Exhaust)
print("R exhaust:", RWT_Exhaust)
print("mm exhaust:", mmWT_Exhaust)

""" Use the minimum ignition power and the change in enthalpy to calculate the
total igniter exhaust mass flow rate.
    then use the chosen OF and the calculated m_tot to calc the fuel and
oxidizer mass flow rates. """

m_tot = QSF / Dh_exhaustIGN                         # [kg/s] Igniter total mass
flow rate
m_f = m_tot / (1 + OF_IGN)                          # [kg/s] Igniter fuel mass
flow rate
m_ox = OF_IGN * m_f                                 # [kg/s] Igniter oxidizer
mass flow rate

print("Total Mass Flow Rate = ", m_tot*1000, "g/sec")
print("Fuel Mass Flow Rate = ", m_f*1000, "g/sec")
print("Oxidizer Mass Flow Rate = ", m_ox*1000, "g/sec")

#~~~~~~~~~~~~~~~~~~~~~~~~~~~~~~~~~~~~~~~~~~~~~~~~~~~~~~~~~~~~~~~~~~~~~~~~~~~~~~~~#

print("Part 6: Sonic injection nozzle")
"""
Now we will calculate the pressures and geometries required to achieve choked
flow in the GOX sonic injection nozzle
during the igniter heating and combustion phases of operation. The GOX sonic
nozzle must maintain choked flow during
this time, to prevent backflow of hot IGN combustion gases up the GOX line,
which could cause an explosion.

The corrected mass flow rate equation describes the relationship between mass
flow, supply temperature,
supply pressure and nozzle exit area. Pb/Pt < = P*/Pt.
```

```
See thesis report for more info on how this was done. Range of GOX nozzle areas
was chosen based on comparable systems.
"""

from GOXNozzle import GOXnozzle_func
GOXPressLists = GOXnozzle_func(Engine_1.To_supplyox, m_ox)

plt.figure()
plt.plot(GOXPressLists["Pc_plot"], GOXPressLists["de_plot"], 'g', label='IGN
Combustion Pressure, Pigncc')
plt.plot(GOXPressLists["Pt_plot"], GOXPressLists["de_plot"], 'b', label='IGN
Supply Total Pressure, Pt')
plt.xlabel('GOX Pressure (bar)')
plt.ylabel('Exit Diameter (mm)')
plt.legend(loc = 'upper right')
plt.title('GOX Nozzle Pressure vs. Exit Diameter, OF: 0.8')
plt.show()

print("GOX diameters (mm):", GOXPressLists["de_table"])
print("For the list of GOX nozzle exit diameters, these are the minimum
allowable values of Oxygen Total Supply "
      "Pressure required to maintain choked flow, as well as the maximum
allowable combustion pressures that correspond "
      "to these supply pressures.")
print("GOX P total supply (bar) :", GOXPressLists["Pt_table"])
print("GOX P combustion (bar):", GOXPressLists["Pc_table"])
GOX_de = float(input("Choose an exit diameter for the GOX nozzle, in mm: "))
GOX_Pt = float(input("Choose a supply pressure for the GOX nozzle, see list of
GOX pressures to see minimum allowed P, in bar: "))
GOX_din = float(input("Choose an inlet diameter for the GOX nozzle, "
                      "based on Goodridge flex hose sizes in mm: "))
GOX_Beta = float(input("Choose a converging angle for GOX nozzle, "
                       "use range 20-60 degrees, in degrees : "))

gamma = 1.4
CPR = (2 / (gamma + 1)) ** (gamma / (gamma - 1))
GOX_Pc = (GOX_Pt-(2.5))*CPR

from GOXNozzle import GOX_Geom
GOX_Geometries = GOX_Geom(Engine_1.To_supplyox, GOX_Pt, GOX_de, GOX_din,
GOX_Beta, m_ox)

print("Combustion Pressure, Pc: ", round(GOX_Pc,2), "Bar")
print("GOX eta: ", GOX_Geometries["GOX_eta"])
print("GOX Lcon: ", GOX_Geometries["GOX_Lcon"], " mm")
print("GOX NPR, during heating:", GOX_Geometries["GOX_NPR"])
print("GOX ru: ", GOX_Geometries["GOX_ru"], " mm")
print("GOX ra: ", GOX_Geometries["GOX_ra"], " mm")
print("GOX Total Temperature at Inlet: ", GOX_Geometries["GOX_Tin"], " K")
print("GOX Total Pressure at Inlet: ", GOX_Geometries["GOX_Pin"], " bar")
print("GOX Velocity Inlet: ", GOX_Geometries["GOX_vin"], " m/s")
print("GOX Velocity throat: ", GOX_Geometries["GOX_vt"], " m/s")
print("GOX Static Temp. at Throat: ", GOX_Geometries["GOX_Tts"], " K")
print("GOX Static Pressure at Throat: ", GOX_Geometries["GOX_Pts"], " Pascals")
```

```
#~~~~~~~~~~~~~~~~~~~~~~~~~~~~~~~~~~~~~~~~~~~~~~~~~~~~~~~~~~~~~~~~~~~~~~~~~~~~#

print("Part 7: Exhaust Orifice Sizing")

from IgniterExhaustOrifice import  EXHorifice_func
EXHOrifice = EXHorifice_func(m_tot, RWT_Exhaust, GOX_Pc, Tc_IGN)

plt.figure()
plt.plot(EXHOrifice["dexh"], EXHOrifice["DP"], 'g', label='Exhaust Orifice')
plt.xlabel('Orifice Diameter (mm)')
plt.ylabel('Pressure Drop (Bar)')
plt.legend(loc = 'upper right')
plt.title('Exhaust Orifice Diameter vs. Pressure Drop')
plt.show()

EXH_de = float(input("Choose an exhaust orifice diameter, in mm: "))

dexh_index = EXHOrifice["dexh"].index(EXH_de)
DP_orifice = EXHOrifice["DP"][dexh_index]       # [Pa] orifice DP
Vel_orifice = EXHOrifice["Vel"][dexh_index]       # [m/s] orifice velocity

EXH_area = (pi * (EXH_de ** 2) / 4)  # [m^2] x-sec area of all the orifice
print("Exhaust Orifice Diameter = ", EXH_de, " mm")
print("Exhaust Orifice Area = ", EXH_area, " m2")
print("Exhaust Density = ", EXHOrifice["density"], " kg/m3")
print("Exhaust Orifice Pressure Drop =", DP_orifice, " Bar")
print("Exhaust Orifice Velocity =", Vel_orifice, " m/s")

#~~~~~~~~~~~~~~~~~~~~~~~~~~~~~~~~~~~~~~~~~~~~~~~~~~~~~~~~~~~~~~~~~~~~~~~~~~~~#

print("Part 8: Resonance Cavity")
res_ratio = float(input("How much larger is resonance cavity opening than GOX
nozzle exit?"))
dres_end= float(input("What is the end diameter at base of resonance cavity, in
mm? "))
Angle_res= float(input("What is the angle of the resonance cavity, in degrees?
"))
Angle_resrad = Angle_res*(pi/180)
dres_in = round(GOX_de*res_ratio,3)
h = (dres_in-dres_end)/2
Lres =  h/tan(Angle_resrad)

Lmd = GOX_de * (0.645497*sqrt(GOX_Pt))

print("Resonance cavity is a truncated cone shape. optimal")
print("Resonance Cavity Opening Diameter: ", dres_in, " mm.")
print("Resonance Cavity End Diameter: ", dres_end, " mm.")
print("Resonance Cavity Angle: ", round(Angle_res,3), "degrees.")
print("Resonance Cavity Length: ", Lres, " mm.")
print("Resonance Cavity Length Mach Disc: ", round(Lmd,3), " mm.")

#~~~~~~~~~~~~~~~~~~~~~~~~~~~~~~~~~~~~~~~~~~~~~~~~~~~~~~~~~~~~~~~~~~~~~~~~~~~~#
```

```
print("Part 9: Ignter Fuel Injection")

Pcombme = Bliz_Lite.Pc*10**-5 # [bar] Main engine  combustion pressure
d_fuel = 0.001          # [m] diameter of fuel injection hole
num_f = 3               # number of fuel injection holes

from FuelInjector import FuelInj_func
FuelInj1 = FuelInj_func(m_f, d_fuel, num_f, Mol_weights1.rho_eth, EXH_de,
Pcombme)

print("Fuel Injector No. Holes", num_f)
print("Fuel Injector Hole Diameter", d_fuel*1000, " mm")
print("Fuel Injector Pressure Drop", round(FuelInj1["DPfuel"],3), " Bar")
print("Fuel Injector Velocity", round(FuelInj1["Vel_fuel"],3), " m/s")
print("Fuel Injector Exhaust Pressure Drop", round(FuelInj1["DPfuelexh"],5), "
Bar")
print("Fuel Injector Exhaust Velocity", round(FuelInj1["Vel_exhaustfuel"],3), "
m/s")
print("Fuel Injector Minimum Injection pressure", round(FuelInj1["Pfmin"],3), "
Bar")
```

```
### BLIZZARDLITE.PY ###
import math
class Blizzard_Lite:
### ~~~~~~~~~~~~~~~~~~~~~~~~~~ Main Engine ~~~~~~~~~~~~~~~~~~~~~~~~~~~~~~ ###
# Oxidizer: 100% LOX
# Fuel: 85% Ethanol + 15% Water
    def __init__(self):

        #ARE THESE PARAMETERS ALWAYS THE SAME OR DO THEY EVER CHANGE?
        self.T_LoxStorage = 90  # [K] Temperature of Stored Liquid Oxygen
        self.T_EthAuto = 673  # [K] Autoignition temperature of liquid ethanol
        self.To_supplyox = 300  # [K] Storage temperature of Gaseous Oxygen for
the igniter.
        self.T_ambient = 300  # [K]
        self.Per_Eth = 0.85  # Percentage of ethanol in fuel
        self.Per_Water = 0.15  # Percentage of ethanol in fuel
        self.F = 2600  # [N]  Design Ideal Thrust
        self.Pc = 20 * (10 ** 5)  # [Pa] Chamber Pressure
        self.Tc = 3167  # [K]  Chamber Temperature, from RPA
        self.Pe = 101325  # [Pa] Exit Pressure
        ## ** From RPA from 90% Ethanol, LOX mixture ** ##
        self.MM = 0.0233454  # [kgds1 = x1[-1]/mol] molar mass of the gas
        self.gamma = 1.1554  # of the gasses ** gamma varies,need to fix this
        self.MAIN_OF = 1.489  # O/F ratio
        self.mu = 1.81 * (10 ** -5)  # [Pa*s] viscosity
        self.eta_rxn = 0.9707  # Reaction Efficiency
        self.eta_nozzle = 0.9777  # Nozzle Efficiency
        self.eta_overall = 0.9490  # Overall Efficiency

        self.RA = 8.314  # [J/mol*K]
        self.go = 9.81  # [m/s^2] gravity
        self.R = self.RA / self.MM  # [J/kg*K] Gas Constant
        self.Vand = math.sqrt(self.gamma) * ((2 / (self.gamma + 1)) **
((self.gamma + 1) / (2 * (self.gamma - 1))))
        self.Vand = math.sqrt(self.gamma) * ((2 / (self.gamma + 1)) **
((self.gamma + 1) / (2 * (self.gamma - 1))))  # Vandenkerkhove
        self.rho_c = self.Pc / (self.R * self.Tc)  # density of gasses in
chamber, using ideal gas law

        ###~~~~~~ Ideal Rocket Theory Calculations ~~~~~~~~###
        # Exhaust Velocity, Isp & Mass Flow Rates
        self.Ve = math.sqrt(2 * (self.gamma / (self.gamma - 1)) * (self.RA /
self.MM) * self.Tc * (1 - ((self.Pe / self.Pc) ** ((self.gamma - 1) /
self.gamma))))  # [m/s]
        self.Isp = self.eta_overall * (self.Ve / self.go)  # [s]
        self.MAIN_mtotal = self.F / (self.eta_overall * self.Ve)  # [kg/s]
total mass flow rate
        self.MAIN_mox = self.MAIN_mtotal * (self.MAIN_OF / (1 + self.MAIN_OF))
# [kg/s]  oxidizer mass flow rate
        self.MAIN_mf = self.MAIN_mtotal * 1 / (1 + self.MAIN_OF)  # [kg/s]  fuel
mass flow rate
        # Nozzle is adapted so that Pexit = Patmosphere, therefore Ve = Veq
```

```
### MolecularWeights.py ###

import ipdb
class MolecularWeights():
    def __init__(self,grams_of_M_C2H5OHr = 1):

    #Add another entry to the class if the mass of M_C2H5OHr changes, I mean...
    #if you do Example_Molecular_Weight = MolecularWeights() it will assume the
mass of M_C2H5OHr is 1gram
    #if you do Example_Molecular_Weight = MolecularWeights(3) it will assume the
mass of M_C2H5OHr is 3 grams
        self.M_C2H5OHr=grams_of_M_C2H5OHr
    # Molecular Weights
        self.mmC = 12.011                                   # [g/mol]
        self.mmH = 1.008                                    # [g/mol]
        self.mmO = 15.999                                   # [g/mol]
        self.mmN = 14.007                                   # [g/mol]
        self.mmO2 = self.mmO * 2
        self.mmC2H5OH = (self.mmC * 2) + (self.mmH * 6) + self.mmO      #
[g/mol]
        self.mmCO2 = self.mmC + self.mmO2                           # [g/mol]
        self.mmH2O = (self.mmH * 2) + self.mmO                      # [g/mol]

        self.RA = 8.3145  # [(Pa*m^3)/(mol*K)]  Universal Gas Law Constant
        # Specific Gas Constants
https://www.engineeringtoolbox.com/individual-universal-gas-constant-d_588.html
        # R_WatVap = 461.52  # [J/(kg*K)] Specific Gas Constant Water Vapor
        # R_CDx = 188.92  # [J/(kg*K)] Specific Gas Constant Carbon Dioxide Gas
        self.R_Eth = (self.RA * 1000) / self.mmC2H5OH  # [J/(kg*K)] Specific Gas
Constant
        self.R_H2O = (self.RA * 1000) / self.mmH2O  # [J/(kg*K)] Specific Gas
Constant
        self.R_CO2 = (self.RA * 1000) / self.mmCO2  # [J/(kg*K)] Specific Gas
Constant
        self.R_O2 = (self.RA * 1000) / self.mmO2  # [J/(kg*K)] Specific Gas
Constant

        self.gammaO2 = 1.4      # specific heat ratio oxygen at STP
        ## densities at ambient temperature
        self.rho_eth = 789                                  # [kg/m3] ethanol
density at ambient temp.
        self.rho_H2O = 997                                  # [kg/m3] water density
at ambient temp.

        # Chemical Balance Eqn Stoichiometric
        # Given 100g Fuel == 85g Ethanol + 15g Water
        # A*C2H5OH(l) + AB*H2O(l) + B*O2(l) -> C*CO2(g) + D*H2O(g)
        self.MassEth = 85   # g
        self.MassWater = 15   # g
        self.unsimpA = self.MassEth/self.mmC2H5OH                  # mol
        self.unsimpAB = self.MassWater/self.mmH2O                   # mol
        self.unsimpC = self.unsimpA*2                           # mol
        self.unsimpD = ((self.unsimpA*6)+(self.unsimpAB*2))/2        # mol
        self.unsimpB = (((self.unsimpC*2) +
```

```
(self.unsimpD))-(self.unsimpA*1)-(self.unsimpAB*1))/2          # mol
        self.As = self.unsimpA/self.unsimpA                        # mol
        self.ABs = self.unsimpAB/self.unsimpA                        # mol
        self.Bs = self.unsimpB/self.unsimpA                        # mol
        self.Cs = self.unsimpC/self.unsimpA                        # mol
        self.Ds = self.unsimpD/self.unsimpA                        # mol

        self.Wtmm_Fuel =
((self.As*self.mmC2H5OH)+(self.ABs*self.mmH2O))/(self.As+self.ABs)

        print("Stoichiometric Chem. Balance Eqn:")
        print("(", "%.1f" % round(self.As, 1), "C2H5OH(l) + ", "%.4f" %
round(self.ABs, 4), "H2O(l)) + ",
          "%.1f" % round(self.Bs, 1), "O2(l) -> ", "%.1f" % round(self.Cs, 1),
"CO2(g) + ", "%.4f" % round(self.Ds, 4), "H2O(g)")
        # C2H5OH(l) + 0.45127*H2O(l) + 3*O2(l) -> 2*CO2(g) + 3.45127*H2O(g)
        # Calc Mass Fractions, given 1 gram C2H5OH

    def StoichMassFractions(self):
        FUNCTION_VARIALBE = self.M_C2H5OHr
        mol_C2H5OHr = FUNCTION_VARIALBE/self.mmC2H5OH         # [mol]
        M_H2Or = mol_C2H5OHr*self.ABs*self.mmH2O       # [g] per 1 gram C2H5OH
        M_O2r = mol_C2H5OHr*self.Bs*self.mmO2               # [g] per 1 gram
C2H5OH
        M_COp = mol_C2H5OHr*self.Cs*self.mmCO2              # [g] per 1 gram
C2H5OH
        M_H2Op = mol_C2H5OHr*self.Ds*self.mmH2O       # [g] per 1 gram C2H5OH

        Stoich_OF_var = M_O2r/(FUNCTION_VARIALBE+M_H2Or)
        Wtmm_Fuel = ((self.As * self.mmC2H5OH) + (self.ABs * self.mmH2O)) /
(self.As + self.ABs)        # [g] Weighted Fuel Molar Mass
        Wtrho_Fuel = ((self.As * self.rho_eth) + (self.ABs * self.rho_H2O)) /
(self.As + self.ABs)  # [kg/m3] fuel density at ambient temp.
        return Stoich_OF_var, Wtmm_Fuel, Wtrho_Fuel

        print("Stoichiometric O/F ratio for 85% Ethanol-15% Water Fuel and 100%
LOX: ", Stoich_OF_var)

    def chembal_func(self, OF, Tc, Stoich_OF, Wtmm_Fuel):
        # Determine Chemical Balance Eqn for given O/F
        # A*(C2H5OH(l) + 0.45127*H2O(l)) + B*O2(l) -> C*CO2(g) + D*H2O(g) +
E*O2(g) + F*(C2H5OH(l) + 0.45127*H2O(l))
        # Given O/F assume 1 mol of C2H5OH and 0.45127 mol of H2O reactants (bc
thats the fuel mass fraction)

        # Equivalence Ratio OF/OFstoich
        # ER < 1: Fuel Rich, some fuel remains
        # ER = 1: stoichiometric. all fuel and ox used
        # ER > 1: Fuel Lean. some Oxidizer remains
        ER = OF/Stoich_OF

        if  ER > 1:             # Fuel lean, excess oxidizer
            A = self.As                              # [mol]
            Mass_Fuel = A*Wtmm_Fuel             # [g]
```

```
            Mass_Ox = OF*Mass_Fuel            # [g]
            Mol_Ox = Mass_Ox/self.mmO2              # [mol]
            B = Mol_Ox                          # [mol]
            F = 0                               # [mol]
            C = self.Cs                             # [mol]
            D = self.Ds                             # [mol]
            E = B-self.Bs  # [mol]
            #print("ER = ", ER, "Combustion is Fuel Lean, excess Oxidizer")
            burn = 'Combustion is Fuel Lean, excess Oxidizer.'
        elif ER < 1:            # fuel rich, excess fuel
            B = self.Bs                             # [mol]
            Mass_Ox = B*self.mmO2                   # [g]
            Mass_Fuel = Mass_Ox/OF            # [g]
            Mol_Fuel = Mass_Fuel/Wtmm_Fuel      # [mol]
            A = Mol_Fuel                        # [mol]
            E = 0                               # [mol]
            F = A-self.As                           # [mol]
            C = self.Cs                             # [mol]
            D = self.Ds                             # [mol]
            #print("ER = ", ER, "Combustion is Fuel Rich, excess Fuel")
            burn = 'Combustion is Fuel Rich, excess Fuel.'
        else:                   # Stoichiometric
            A = self.As
            B = self.Bs
            C = self.Cs
            D = self.Ds
            E = 0
            F = 0
            #print("ER = ", ER, "Combustion is Stoichiometric, all components
used.")
            burn = 'Combustion is Stoichiometric, all components used.'
        return A, B, C, D, E, F, burn
```

```
###RPAFULL.py ###

import matplotlib.pyplot as plt
plt.style.use('classic')

from math import *
import numpy as np
import sympy
from sympy import S, symbols, printing

def RPAFULL_func(Stoich_OF):

    RPA_OF = [0.4, 0.45, 0.5, 0.55, 0.6, 0.65, 0.7, 0.75, 0.8, 0.84, 0.85, 0.9,
0.95, 1, 1.1, 1.2, 1.3, 1.4, 1.5, 1.6, 1.7, 1.8, 1.9, 2, 2.2,2.5, 2.7, 3, 3.3]

    # 5 bar
    Tc_5bar = [1004.1150, 1027.8626, 1064.0688, 1127.1262, 1270.5258,
1449.8212,1625.4904, 1794.7788, 1957.0609, 2081.3441, 2111.5747, 2257.1244,
2392.1168,2514.8096, 2717.4394, 2859.1916, 2947.3373, 2998.0227, 3025.6540,
         3039.3439, 3044.3142, 3043.5738, 3038.9244, 3031.4928,
3010.9829,2971.5724, 2941.7833, 2893.7107, 2842.7025]

    # 7 bar
    Tc_7bar = [1022.2167, 1047.6106, 1083.5719, 1141.8699, 1272.4342,
1449.9195,1625.5158, 1794.8593, 1957.3342,2081.9639,2112.3206, 2258.8223,
2395.4455,2520.5704, 2730.2789, 2880.3644, 2975.3755, 3030.3958,
3060.3961,3075.2459, 3080.6628, 3079.9376, 3075.0312, 3067.1637,
3045.4497,3003.7818, 2972.3297, 2921.6390, 2867.9370]

    # 9 bar
    Tc_9bar = [1036.1043, 1062.7967, 1098.6878, 1154.1363, 1274.7671,
1450.0484,1625.5380, 1794.9120, 1957.5110,2082.3660, 2112.8049, 2259.9330,
2397.6467,2524.4320, 2739.1638, 2895.4959, 2995.9162, 3054.4504,
3086.3894,3102.1909, 3107.9768, 3107.2702, 3102.1629, 3093.9511,
3071.2853,3027.8373, 2995.0781, 2942.3375, 2886.5378]

    # 11 bar
    Tc_11bar = [1047.4199, 1075.1944, 1111.0945, 1164.6321, 1277.4078,
1450.2080,1625.5598, 1794.9505, 1957.6375,2082.6540,2113.1521, 2260.7331,
2399.2441,2527.2616, 2745.8286, 2907.1329, 3012.0356, 3073.5542,
3107.1544,3123.7732, 3129.8775, 3129.1905, 3123.9168, 3115.4180,
3091.9581,3047.0280, 3013.1837, 2958.7473, 2901.2199]

    # 13 bar
    Tc_13bar = [1056.9936, 1085.7012, 1121.6512, 1173.8131, 1280.2558,
1450.3979,1625.5826, 1794.9806, 1957.7339,2082.8734,2113.4167, 2261.3451,
2400.4730, 2529.4545, 2751.0895, 2916.5063, 3025.2441, 3089.3724,
3124.4373,3141.7783, 3148.1649, 3147.4978, 3142.0815, 3133.3349,
3109.1897,3062.9833, 3028.2069, 2972.3180, 2913.3170]

    # 20 bar
    Tc_20bar = [1082.3253, 1113.5837, 1149.8333, 1199.2093, 1290.8751,
1451.2925,1625.6769, 1795.0536, 1957.9498,2083.3639,2114.0085, 2262.7209,
2403.2578,2534.4781, 2763.4802, 2939.3042, 3058.3146, 3129.7175,
```

```
3168.9320,3188.3274, 3195.5217, 3194.9221, 3189.1189, 3179.6946,
3153.6741,3103.9892, 3066.6850, 3006.8779, 2943.9304]

    # 35 bar
    Tc_35bar = [1118.0597, 1151.5207, 1188.5141, 1235.5768, 1312.4734,
1454.2768,1625.9785, 1795.1569, 1958.1752,2083.8666,2114.6149, 2264.1390,
2406.1615,2539.7998, 2777.1733, 2965.8387, 3098.8100, 3180.8709,
3226.3753,3248.9132, 3257.3525, 3256.8807, 3250.5293, 3240.1314,
3211.4210,3156.7885, 3115.9226, 3050.6518, 2982.2762]

    plt.plot(RPA_OF, Tc_5bar, 'r', label = '$P_{c}= 5 bar$')
    plt.plot(RPA_OF, Tc_7bar, 'b', label = '$P_{c}= 7 bar$')
    plt.plot(RPA_OF, Tc_9bar, 'g', label = '$P_{c}= 9 bar$')
    plt.plot(RPA_OF, Tc_11bar, 'c', label = '$P_{c}= 11 bar$' )
    plt.plot(RPA_OF, Tc_13bar, 'm', label = '$P_{c}= 13 bar$')
    plt.plot(RPA_OF, Tc_20bar, 'm', label='$P_{c}= 20 bar$')
    plt.plot(RPA_OF, Tc_35bar, 'm', label='$P_{c}= 35 bar$')
    #plt.axhline(y=763, color='red', linestyle='--')
    plt.axvline(Stoich_OF, 0, 3110, color='grey')
    # plt.axhline(y=750, color='grey', linestyle='--')
    # plt.axhline(y=1200, color='grey', linestyle='--')
    plt.xlabel('O/F')
    plt.ylabel('Combustion Temperature [K]')
    plt.legend(loc = 'lower right')
    plt.title('100% LOX, 85% Ethanol + 15% Water, Values from RPA')
    plt.show()

    # plt.figure()
    # plt.plot(RPA_OF, Tc_5bar, 'r', label='$P_{c}= 5 bar$')
    # plt.plot(RPA_OF, Tc_7bar, 'b', label='$P_{c}= 7 bar$')
    # plt.plot(RPA_OF, Tc_9bar, 'g', label='$P_{c}= 9 bar$')
    # plt.plot(RPA_OF, Tc_11bar, 'c', label='$P_{c}= 11 bar$')
    # plt.plot(RPA_OF, Tc_13bar, 'm', label='$P_{c}= 13 bar$')
    # # plt.axhline(y=763, color='red', linestyle='--')
    # plt.axvline(Stoich_OF, 0, 3110, color='grey')
    # # plt.axhline(y=750, color='grey', linestyle='--')
    # # plt.axhline(y=1200, color='grey', linestyle='--')
    # plt.xlabel('O/F')
    # plt.ylabel('Combustion Temperature [K]')
    # leg = plt.legend
    # plt.title('100% LOX, 85% Ethanol + 15% Water, Values from RPA')
    # plt.show()

    x = 1
    return x
```

```
### CpO2CO2H2O.PY ###
import numpy as np
import matplotlib.pyplot as plt

# element: which element are you choosing
# T: temperature range to calc cp


def cp_func(element,T):
    cp = []
    R = 8.314459
    T_mid = 1000.

    # Function constants
    # H2
    ah_H2 = [3.33727920E+00, -4.94024731E-05, 4.99456778E-07, -1.79566394E-10,
2.00255376E-14]
    al_H2 = [2.34433112E+00, 7.98052075E-03, -1.94781510E-05, 2.01572094E-08,
-7.37611761E-12]

    # O2
    ah_O2 = [3.28253784E+00, 1.48308754E-03, -7.57966669E-07, 2.09470555E-10,
-2.16717794E-14]
    al_O2 = [3.78245636E+00, -2.99673416E-03, 9.84730201E-06, -9.68129509E-09,
3.24372837E-12]

    # N2
    ah_N2 = [0.02926640E+02, 0.14879768E-02, -0.05684760E-05, 0.10097038E-09,
-0.06753351E-13]
    al_N2 = [0.03298677E+02, 0.14082404E-02, -0.03963222E-04, 0.05641515E-07,
-0.02444854E-10]

    # CH4
    ah_CH4 = [7.48514950E-02, 1.33909467E-02, -5.73285809E-06, 1.22292535E-09,
-1.01815230E-13]
    al_CH4 = [5.14987613E+00, -1.36709788E-02, 4.91800599E-05, -4.84743026E-08,
1.66693956E-11]

    # CO2
    ah_CO2 = [3.85746029E+00, 4.41437026E-03, -2.21481404E-06, 5.23490188E-10,
-4.72084164E-14]
    al_CO2 = [2.35677352E+00, 8.98459677E-03, -7.12356269E-06, 2.45919022E-09,
-1.43699548E-13]

    # H2O
    ah_H2O = [3.03399249E+00, 2.17691804E-03, -1.64072518E-07, -9.70419870E-11,
1.68200992E-14]
    al_H2O = [4.19864056E+00, -2.03643410E-03, 6.52040211E-06, -5.48797062E-09,
1.77197817E-12]

    if element == 'O2':
        al = al_O2
        ah = ah_O2
    elif element == 'CO2':
```

```
    al = al_CO2
    ah = ah_CO2
elif element == 'H2O':
    al = al_H2O
    ah = ah_H2O
elif element == 'N2':
    al = al_N2
    ah = ah_N2
elif element == 'CH4':
    al = al_CH4
    ah = ah_CH4
else:
    al = al_H2
    ah = ah_H2

for temp in T:
    if temp < T_mid:
        cpR = 0
        for i in range(len(al)):
            cpR = cpR + al[i]*temp**i
    else:
        cpR = 0
        for i in range(len(ah)):
            cpR = cpR + ah[i]*temp**i
    cp.append(cpR*R)
return np.array(cp)
```

```
### IgnitionPower.py ###

import matplotlib.pyplot as plt
from math import *
import numpy as np
import sympy
from sympy import S, symbols, printing
# Perc_mf:  percentage of the main engine propellant flow that must be ignited
[%]
# MAIN_Mox: main engine oxidizer mass flow rate [kg/s]
# MAIN_mf: main engine fuel mass flow rate [kg/s]
# Perc_eth: Percentage of the fuel mass flow rate that is ethanol [%]
# Perc_water: Percentage of the fuel mass flow rate that is water [%]
# Dh_ethsum: Sum of Ethnalpy of reactant ethanol [J/kg]
# Dh_watsum:Sum of Ethnalpy of reactant water [J/kg]
# Dh_oxsum: Sum of Ethnalpy of reactant oxidizer [J/kg]
# SF: safety factor of the power required

def power_func(Perc_mf, MAIN_mox, MAIN_mf, Perc_eth, Perc_water, Dh_ethsum,
Dh_watsum,  Dh_oxsum):
    PercMF_mox = (Perc_mf)*MAIN_mox                                          #
[kg/s] % of main engine mass flow rate Oxidizer
    PercMF_mf = (Perc_mf)*MAIN_mf                                            #
[kg/s] % of main engine mass flow rate Fuel
    Perc_meth = (Perc_eth)*PercMF_mf                                         #
[kg/s] Mass flow rate of the fuel that is ethanol
    Perc_mwater = (Perc_water)*PercMF_mf                                     #
[kg/s] Mass flow rate of the fuel that is water
    Lvap_ox = 214000                                                       # [J/kg]
 Latent heat of vaporization
    Lvap_eth = 854000                                                      # [J/kg]
 Latent heat of vaporization
    Lvap_wat = 2256000                                                     # [J/kg]
 Latent heat of vaporization
    # L, Latent heat of vaporization = amount of heat that must be added to
change the phase of the element
    # c, specific hea= amount of heat that must be added to change the
temperature of the element by 1C.
    # Q = m*c*deltaT :  Equation for change of temperature (where Q: power,
m:mass, c:specific heat, T: change of temp)
    # Q = m*L  : Eqn for change of phase. (where Q: power, m: mass, L: latent
heat of vaporization)
    # Begin with the Q = m*c*deltaT (c*deltaT == dH == change in enthalpy)
    # Power required to ignite a % of the main propellant flow
    # This is the amount og power the igniter must provide in order to achieve
ignition of the main engine prop flow
    # Power equation is from TRP p. 120
    Q = (Perc_meth * (Dh_ethsum + Lvap_eth)) + (Perc_mwater * (Dh_watsum +
Lvap_wat)) + (PercMF_mox * (Dh_oxsum + Lvap_ox))  # [J/s]
    #print("Power igniter must provide to ignite of 5% of the main engine prop
flow = ", Q, "J/s")
    return Q
```

```
### CpEthanol.py ###

import matplotlib.pyplot as plt
from math import *
import numpy as np
import sympy
from sympy import S, symbols, printing

# function to calc array for cp values of ethanol
def ethtest_func(T,plot):
    ## low Temp values
    T_ethLOWNIST = [298.15, 300, 400, 500, 600, 700, 763, 800, 900]  # [K]
    Cp_ethLOWNIST = [65.21, 65.49, 81.22, 95.78, 108.24, 118.83, 124.74, 127.92,
135.81]  # [J/mol*K]
    r = np.polyfit(T_ethLOWNIST, Cp_ethLOWNIST, 5)
    s = np.poly1d(r)
    # print(r)
    T_ethLOW = np.arange(290, 900)
    Cp_ethLOW = s(T_ethLOW)

    x = symbols("x")
    polyl = sum(S("{:6.2f}".format(v)) * x ** i for i, v in enumerate(r[::-1]))
    eq_latex1 = printing.latex(polyl)

    # High temp ethanol cp
    T_ethHIGHNIST = np.array([800, 900, 1000, 1200, 1300, 1400, 1500, 1750,
2000, 2250, 2500, 2750, 3000])  # [K]
    Cp_ethHIGHNIST = np.array(
        [127.92, 135.81, 142.68, 153.92, 158.49, 162.50, 166.01, 173, 178.20,
182, 184.9, 187, 189])  # [J/mol*K]
    p = np.polyfit(T_ethHIGHNIST, Cp_ethHIGHNIST, 4)
    f = np.poly1d(p)
    # print(p)
    T_ethHIGH = np.arange(900, 3500)
    Cp_ethHIGH = f(T_ethHIGH)

    x = symbols("x")
    poly = sum(S("{:6.2f}".format(v)) * x ** i for i, v in enumerate(p[::-1]))
    eq_latex = printing.latex(poly)
    # print(poly)

    if plot == 'Yes':
        plt.figure()
        plt.plot(T_ethLOW, Cp_ethLOW, label="${}$".format(eq_latex1))
        plt.plot(T_ethHIGH, Cp_ethHIGH, label="${}$".format(eq_latex))
        # plt.legend('Cp Low', 'Cp High')
        plt.xlabel('Combustion Temperature [K]')
        plt.ylabel('Cp, Specific Heat constant Pressure [J/mol*K]')
        plt.title('Ethanol High Temp Tc vs Cp')
        plt.show()
    else:
        pass

    rlist = r.tolist()
```

```
plist = p.tolist()

# now do the calcs
cp = []
Rpow = []
Ppow = []
Tmid = 800              #[K] when to switch high or low cp
for temp in T:
    i = 0
    if temp < Tmid:  #use low eqn
        cpeq = 0
        powr = len(r)-1
        for i in range(len(r)):
            cpeq = cpeq + r[i]*temp**powr
            powr = powr - 1
    else:
        cpeq = 0
        powp = len(p)-1
        for i in range(len(p)):
            cpeq = cpeq + p[i]*temp**powp
            powp = powp-1
    cp.append(cpeq)
return np.array(cp)
```

```
### GOXNozzle.py.py ###

import matplotlib.pyplot as plt
from math import *
import numpy as np
import sympy
from sympy import S, symbols, printing

## initial estimate of heat xfer in resonance cavity and ignition combustion
chamber
# First assume res. cavity is a right angle cylinder. Assume internal forced
convection.
# Material SS 316
###### Sonic Nozzle Stuff
## o : total values for pressure, temp and density, t : throat values, static
# Remember, Total Pressure/Temperature is ALWAYS Conserved!!! Total = dynamic +
static

def GOXnozzle_func(To, m):
    ### ~~~~~~~~~~~~~~ Constants ~~~~~~~~~~~~~~~~~~~ ###
    Runiv = 8.314                                           # [J/mol*K]
Universal Gas Constant
    go = 9.81                                               # [m/s^2] gravity
    mmO = 15.999/1000                                       # [kg/mol]
    mmO2 = mmO*2                                            # [kg/mol]
    RO2 = Runiv / mmO2                                      # [J/kg*K] Oxygen
Gas Gs Constant
    gamma = 1.4                                             # Ratio of specific
heat for Oxygen. Assume constant
    Patm = 101325                                           # [Pa] Atmospheric
Pressure at S.L.
    ### ~~~~~~~~~~~~~~ Calculations Throat Conditions ~~~~~~~~~~~~~~~~~~~ ###
    CTR = 2 / (gamma + 1)                                   # Critical
Temperature Ratio
    CPR = (2 / (gamma + 1)) ** (gamma / (gamma - 1))        # Critical Pressure
ratio
    print("Critical Pressure ratio = ", CPR)
    print("Critical temperature ratio = ", CTR)
    print("R, oxygen = ", RO2, "J/kg*K")
    print("gamma, oxygen = ", gamma)
    # for a set mass flow at Tt, and a given range of combustion pressures. calc
the total supply pressure values and
    # the corresponding exit area and then exit diameter values.
    pc_list = np.linspace(1,40,40)
    de_list = []
    pe_listpa = []
    pe_list = []

    # to keep choked conditions during entire operation. need PB/Pt <= P*/Pt,
where CPR = P*/Pt.
    # therefore Pt >= PB/CPR. where PB is the IGN combustion chamber pressure. I
will add a 2.5 bar margin to make sure
    # this requirement is met and choked flow remains during combustion.
    for i in pc_list:
```

```
        psupply = ((i*10**5)/CPR) + (2.5*10**5)          # add a 2.5 bar margin
to the supply pressure to ensure that you stay in the choked conditions.
        pe_listpa.append(psupply)
        exitArea =
((m*sqrt(To))/psupply)*sqrt(RO2/gamma)*(((gamma+1)/2)**((gamma+1)/(2*(gamma-1)))
)  # [m^2] exit area
        exitdiam = (2*sqrt(exitArea/pi))*1000              # [mm] throat
diameter
        de_list.append(exitdiam)

    for j in pe_listpa:
        pe = j*10**-5
        pe_list.append(pe)

    # make a list of the pressure values for specific diameters of 0.0 anf 0.5.
use the range we found in the plot.
    # this is a bit hardcoded so be aware.
    de_range = [1.5, 2, 2.5, 3, 3.5, 4, 4.5, 5, 5.5, 6, 6.5]  # [mm] nozzle exit
diameters
    pcomb_rangePA = []
    psupply_rangePA = []
    pcomb_range = []
    psupply_range = []

    for k in de_range:
        area = pi*(((k/1000)**2)/4)   # [m^2] nozzle exit area
        Ptot =
((m*sqrt(To))/area)*sqrt(RO2/gamma)*(((gamma+1)/2)**((gamma+1)/(2*(gamma-1))))
# [Pa] solve for total pressure for choked flow condition
        psupply_rangePA.append(Ptot)
        #pcc = (Ptot-(2.5*10**5))*CPR
        pcc = (Ptot) * CPR
        pcomb_rangePA.append(pcc)

    for l in pcomb_rangePA:
        pcign = round(l*10**-5,3)
        pcomb_range.append(pcign)

    for s in psupply_rangePA:
        ptign = round(s*10**-5,3)
        psupply_range.append(ptign)

    GOX_PressureLists = {"Pc_plot": pc_list, "Pt_plot": pe_list, "de_plot":
de_list,
                         "Pc_table": pcomb_range, "Pt_table": psupply_range,
"de_table": de_range}
    return GOX_PressureLists

def GOX_Geom(To, Po, d, din, beta, mox):
    ### ~~~~~~~~~~~~~~ Constants ~~~~~~~~~~~~~~~~~~~ ###
    Runiv = 8.314  # [J/mol*K] Universal Gas Constant
    go = 9.81  # [m/s^2] gravity
    mmO = 15.999 / 1000  # [kg/mol]
    mmO2 = mmO * 2  # [kg/mol]
```

```
    RO2 = Runiv / mmO2  # [J/kg*K] Oxygen Gas Gs Constant
    gamma = 1.4  # Ratio of specific heat for Oxygen. Assume constant
    Patm = 101325  # [Pa] Atmospheric Pressure at S.L.
    rho_o = (Po*(10**5))/(RO2*To)                  # [kg/m3] total density at
inlet
    CTR = 2 / (gamma + 1)  # Critical Temperature Ratio
    CPR = (2 / (gamma + 1)) ** (gamma / (gamma - 1))  # Critical Pressure ratio
    CDR = (2 / (gamma + 1)) ** (1 / (gamma - 1))           # Critical Density
ratio
    T_ts = round(To*CTR,3)                          # [K] Static temp at throat
    P_ts = round(Po*(10**5)*CPR,3)               # [Pa] Static pressure at
throat
    rho_ts = round(rho_o*CDR,3)                    # [kg/m3] static density at
throat
    A_throat = pi* (((d/1000)**2)/4)             # [m^2] Throat area
    M_t = 1                                  #  sonic nozzle, mach num at throat
    c_t = sqrt(gamma*RO2*T_ts)               # [m/s] speed of sound at throat
    v_t = round(c_t*M_t,3)                          # [m/s] velocity in throat

    ### ~~~~~~~~~~~~~~ Calculations Inlet Conditions ~~~~~~~~~~~~~~~~~~~ ###
    A_in = pi*(((din/1000)**2)/4)           # [m^2] Inlet area of nozzle
    NPR = round((Po*10**5)/Patm,3)                          # Nozzle Pressure
Ratio, see Lungu for definition
    r_u = round((d/2)*1.5, 3)                         # [mm] radius of exit
    r_a = round(d*.4,3)                             # [mm] radius at beginning
of convergent section
    Lcon = round((((din-d)/2)/tan(beta*(pi/180))),3) # [mm] length of converging
section of nozzle
    eta = round(A_in/A_throat,3)
    v_in = mox/(rho_o*A_in)                        # [m/s] velocity at nozzle
inlet

    # MESHING CALCS at throat conditions for GOX use this graph of Gaseous O2 as
a function of P and T to choose the dynamic viscosity
    #
https://www.engineeringtoolbox.com/oxygen-O2-dynamic-kinematic-viscosity-tempera
ture-pressure-d_2081.html?vA=-23&degree=C#
    mu = 18*10**-6          # [Pa*s] dynamic viscocity GOX at throat P and T
    Re_throat = (rho_ts*v_t*(d/1000))/mu            # Reynolds number at throat
    cf = 0.058/(Re_throat**0.2)
    tw = 0.5*cf*rho_ts*(v_t**2)
    ut = sqrt(tw/rho_ts)
    yplus = 1
    ycell1 = (yplus*mu)/(ut*rho_ts)                 # [m] height first cell
    GOX_Geom = {"GOX_eta": eta, "GOX_Lcon": Lcon, "GOX_NPR": NPR, "GOX_ru": r_u,
"GOX_ra": r_a, "GOX_vt": v_t, "GOX_vin": v_in,
                "GOX_Pin": Po, "GOX_Tin": To,"GOX_Tts": T_ts, "GOX_Pts": P_ts,
"GOX_rhots": rho_ts, "Re_throat": Re_throat, "yheight1": ycell1}
    return GOX_Geom
```

```
### IgniterExhaustOrifice.py ###

import matplotlib.pyplot as plt
from math import *
import numpy as np
import sympy
from sympy import S, symbols, printing


def EXHorifice_func(m_tot, R_Exh, Pc, To):
    """ first use the minimum ignition power and the change in enthalpy to
calculate the total igniter exhaust mass flow rate.
    then use the chosen OF and the calculated m_tot to calc the fuel and
oxidizer mass flow rates. """
    Cd = 0.9    # bc d>= 0.0015m

    rho_exho = (Pc*(10**5))/(R_Exh*To)                  # [kg/m3] total density
at inlet on orifice

    # make a list of the pressure values for specific diameters of 0.0 anf 0.5.
use the range we found in the plot.
    # this is a bit hardcoded so be aware.
    dexh_range = [10, 11, 12, 13, 14, 15, 16, 17, 18, 19, 20]  # [mm] exhaust
orifice diameters
    DPrange= []
    vel_range = []
    Arearange = []

    # A = (pi * (d ** 2) / 4)  # [m^2] x-sec area of all the orifice
    # DP = m_tot ** 2 / ((Cd ** 2) * (A ** 2) * 2 * rho_exho)  # [Pascals]
pressure drop across orifice
    # v = Cd * sqrt((2 * DP) / rho_exho)  # [m/s] velocity of exhaust gases
injected

    for i in dexh_range:
        area = (pi * ((i/1000) ** 2) / 4)  # [m^2] x-sec area of all the orifice
        DP = m_tot ** 2 / ((Cd ** 2) * (area ** 2) * 2 * rho_exho)  # [Pascals]
pressure drop across orifice
        v = Cd * sqrt((2 * DP) / rho_exho)  # [m/s] velocity of exhaust gases
injected
        DPbar = DP*10**-5
        DPrange.append(DPbar)
        vel_range.append(v)



    EXH_orifice  = {"dexh": dexh_range, "DP": DPrange, "Vel": vel_range,
"density": rho_exho}


    return EXH_orifice
```

```
### FuelInjector.py ###

import matplotlib.pyplot as plt
from math import *
import numpy as np
import sympy
from sympy import S, symbols, printing
from scipy.optimize import fsolve
import ipdb


# mf: fuel mass flow rate (kg/sec)
# d: inj. hole diameter (m)
# num: number of injector holes
# rhof: fuel density (kg/m^3)
# Cd: discharde coefficient


def FuelInj_func(mf,d,num,rhof, dexh, Pcombme):
    Cd = 0

    if d == .001:
        Cd = 0.88
    elif d >= 0.0015:
        Cd = 0.9
    else:
        print("you did not enter a proper value for d")
        return None

    A = num*(pi*(d**2)/4)                       # [m^2] x-sec area of all the
inj holes
    DP = (mf**2/((Cd**2)*(A**2)*2*rhof))          # [pascals] pressure drop
across fuel injector
    v = Cd*sqrt((2*DP)/rhof)                    # [m/s] velocity of fuel
injected
    DPbar = DP*(10**-5)

    dexhm = dexh/1000
    # calc pressure loss across exhaust orifice
    Aexh = (pi * (dexhm ** 2) / 4)  # [m^2] x-sec area of all the exhaust
orifice
    DPexh = (mf ** 2 / ((0.9 ** 2) * (Aexh ** 2) * 2 * rhof))  # [pascals]
pressure drop across exhasut orifice
    vexh = 0.9 * sqrt((2 * DPexh) / rhof)  # [m/s] velocity of fuel exhaust
    DPexhbar = DPexh*(10**-5)

    pdroptot = DPbar+ DPexhbar
    Pfmin = Pcombme+pdroptot+ 4
    FuelInj = {"DPfuel": DPbar, "Vel_fuel": v, "DPfuelexh": DPexhbar,
"Vel_exhaustfuel": vexh, "Pfmin": Pfmin}

    return FuelInj
```

C

RPA Fuel Input File Calculations

	Molar mass						
x*C2H5OH + y*H2O	**C**	12.011					
	H	1.008					
	O	15.999	31.998				
	C2H5OH	46.069					
	H2O	18.015					
					calc		
		0.4	**0.5**	**0.7**	**0.85**	**0.9**	**0.95**
RPA	**C**	0.4136	0.5622	0.9542		1.5575	1.7628
RPA	**H**	2.8272	3.1245	3.9085		5.1149	5.5255
RPA	**O**	1	1	1	1	1	1
Calc from RPA C, H, O Coef	**Mol WT.**	23.8166	25.9011	31.3997		39.8620	42.7417
RPA	**Mol. Wt RPA Given**	23.8164	25.9016	31.3998		39.8613	
BKWD CALC	**C**	0.3882	0.5622	0.9542	1.3769	1.5575	1.7628
BKWD CALC	**H**	2.7766	3.1246	3.9085	4.7538	5.1151	5.5256
BKWD CALC	**O**	1.0000	1.0000	1.0000	1.0000	1.0000	1.0000
BKWD CALC	**Mol WT.**	23.4607	25.9012	31.3999	37.3285	39.8625	42.7423
Calc from RPA C, H, O Coef	**x**	0.2068	0.2811	0.4771		0.7788	0.8814
Calc from RPA C, H, O Coef	**y**	0.7932	0.7190	0.5230		0.2212	0.1186
		23.8166	25.9019	31.4005		39.8612	42.7409
BKWD CALC	**x**	0.1941	0.2811	0.4771	0.6884	0.7788	0.8814
BKWD CALC	**y**	0.8060	0.7190	0.5229	0.3116	0.2212	0.1186

	perc.	0.4	0.5	0.7	0.85	0.9	0.95
Calc from RPA C, H, O Coef	**C2H5OH**	9.5271	12.9500	21.9795	0.0000	35.8762	40.6052
Calc from RPA C, H, O Coef	**H2O**	14.2895	12.9519	9.4209	0.0000	3.9849	2.1357
Calc from RPA C, H, O Coef	**Total Molar Mass**	23.8166	25.9019	31.4005	0.0000	39.8612	42.7409
PLOT Calcs	**Calc. C2H5OH**	8.9423	12.9501	21.9799	31.7158	35.8770	40.6061

PLOT Calcs	**Calc. H2O**	14.5197	12.9522	9.4207	5.6130	3.9855	2.1359
PLOT Calcs	Calc. Molar Mass	23.4620	25.9023	31.4006	37.3287	39.8625	42.7421

Given RPA	Heat of Formation (J/mol)	-284727.141	-283987.650	-282043.275		-279114.911	-278138.951
PLOT Calc	Heat of Formation (J/mol)	-284727.142	-283987.651	-282043.276	-279977.998	-279114.911	-278138.951

Check of my fuel input into RPA. If my value of Tc for 85% ethanol fits in the polynomial trendline, (R^2=1) then I know its right.

Pc = 9 bar, O/F = 2	**perc.**	0.4	0.5	0.7	0.85	0.9	0.95
RPA given	TC	2045.0546	2458.5451	2921.359	3090.9511	3135.5762	3171.1518

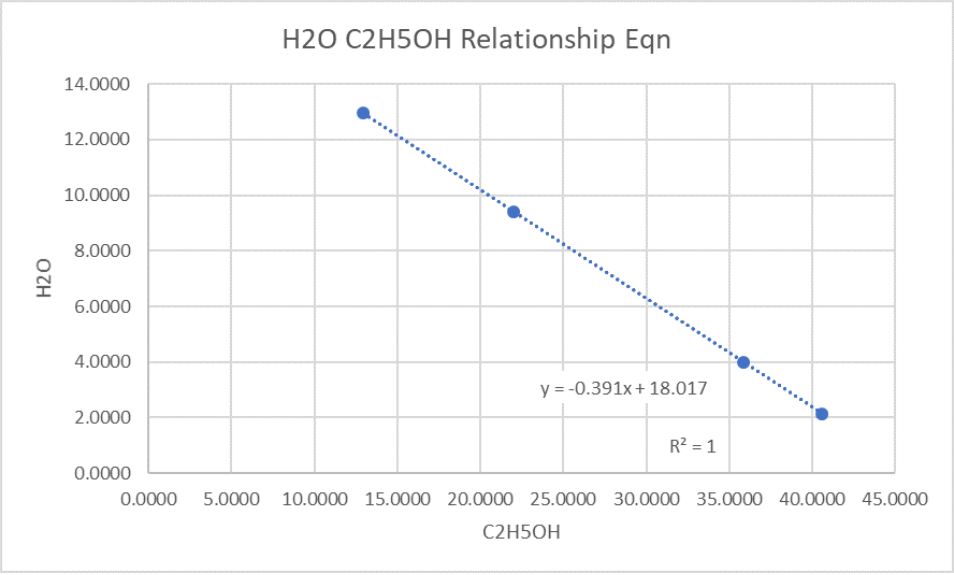

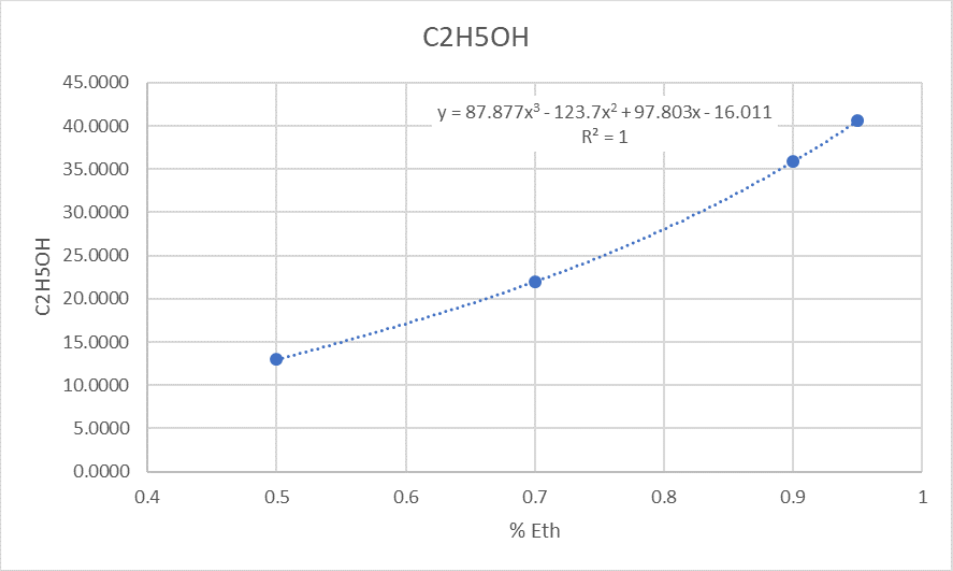
C2H5OH
y = 87.877x³ - 123.7x² + 97.803x - 16.011
R² = 1
C2H5OH
45.0000
40.0000
35.0000
30.0000
25.0000
20.0000
15.0000
10.0000
5.0000
0.0000
0.4
0.5
0.6
0.7
0.8
0.9
1
% Eth

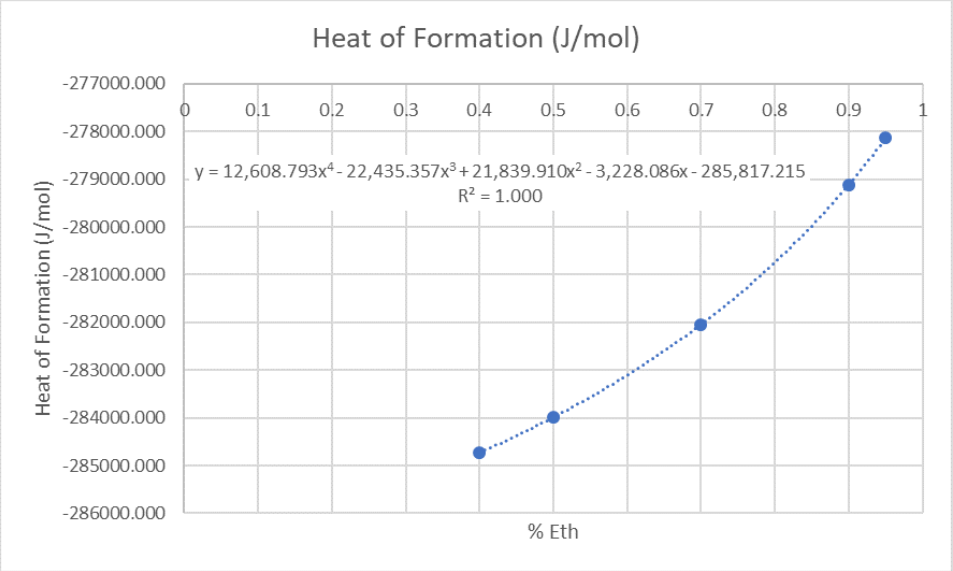
Heat of Formation (J/mol)
y = 12,608.793x⁴ - 22,435.357x³ + 21,839.910x² - 3,228.086x - 285,817.215
R² = 1.000
Heat of Formation (J/mol)
-277000.000
-278000.000
-279000.000
-280000.000
-281000.000
-282000.000
-283000.000
-284000.000
-285000.000
-286000.000
0
0.1
0.2
0.3
0.4
0.5
0.6
0.7
0.8
0.9
1
% Eth

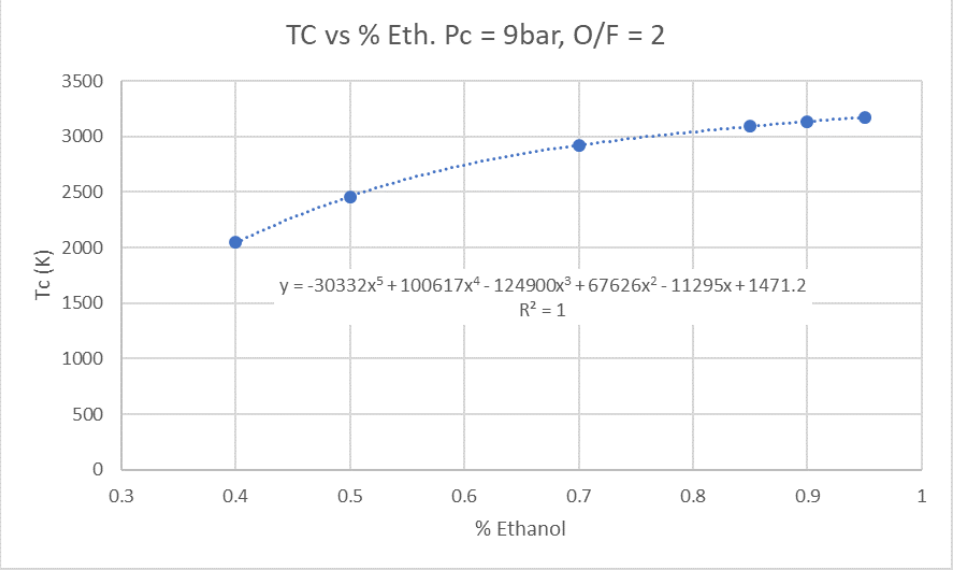
TC vs % Eth. Pc = 9bar, O/F = 2
y = -30332x⁵ + 100617x⁴ - 124900x³ + 67626x² - 11295x + 1471.2
R² = 1
Tc (K)
3500
3000
2500
2000
1500
1000
500
0
0.3
0.4
0.5
0.6
0.7
0.8
0.9
1
% Ethanol

D

ANSYS FLUENT: Mesh Refinement

This appendix includes the mesh details, mesh quality factors, residual plots and contour plots of the pressure, temperature mach and velocity for the LOW and HIGH Refinement cases. As the MEDIUM cases was the chosen level from this refinement study, the mesh information and results for that case are included in chapter 12 as 'Case 1: Preliminary Design.'

D.1. 1: HIGH Mesh

Details of "Mesh"	
Display	
Display Style	Body Color
Defaults	
Physics Preference	CFD
Solver Preference	Fluent
Relevance	0
Export Format	Standard
Element Order	Linear
Sizing	
Size Function	Proximity and Curvature
Relevance Center	Coarse
Span Angle Center	Fine
Curvature Normal ...	Default (18,0 °)
Num Cells Across ...	Default (3)
Proximity Size Functi...	Faces and Edges
Min Size	Default (3,4552e-002 mm)
Proximity Min Size	Default (3,4552e-002 mm)
Max Face Size	Default (3,45520 mm)
Growth Rate	Default (1,20)
Automatic Mesh Base...	On
Defeature Size	Default (1,7276e-002 mm)
Minimum Edge Length	0,50 mm
Quality	
Inflation	
Assembly Meshing	
Advanced	
Statistics	
Nodes	4792
Elements	4566

Figure D.1: Low Mesh Details

Table D.1: '1:HIGH' Mesh Quality Factors

Quality Factor	Value
Element Quality	
Average	0.77137
Stnd. Deviation	0.19172
Aspect Ratio	
Max	8.3976
Average	2.2477
Stnd. Deviation	1.2298
Orthogonal Quality	
Average	0.998
Stnd. Deviation	4.02e-03
Skewness	
Max	0.2222
Average	1.71e-02
Stnd. Deviation	2.32e-02

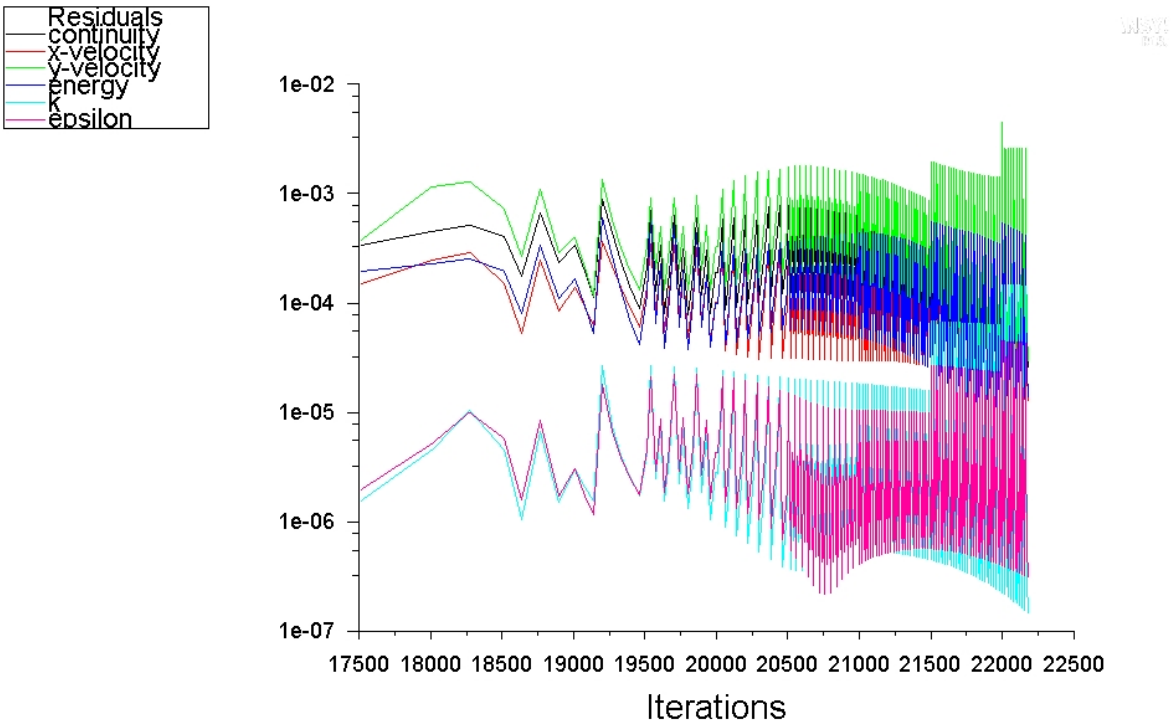

Figure D.2: 1: HIGH Mesh Residuals

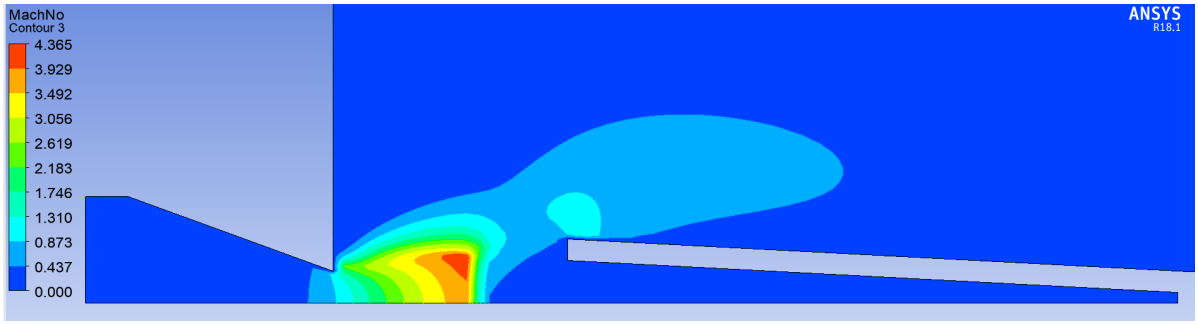

Figure D.3: 1: HIGH Mesh Mach Contour

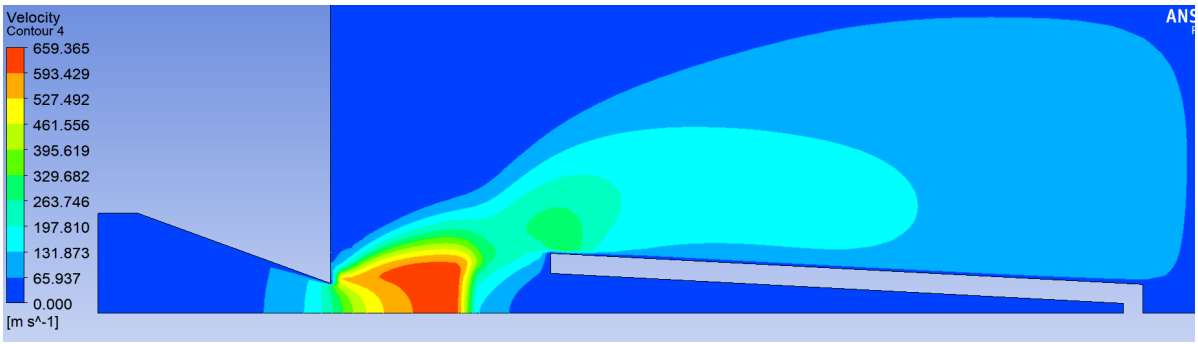

Figure D.4: 1: HIGH Mesh Velocity Contour

D.2. 3: LOW mesh

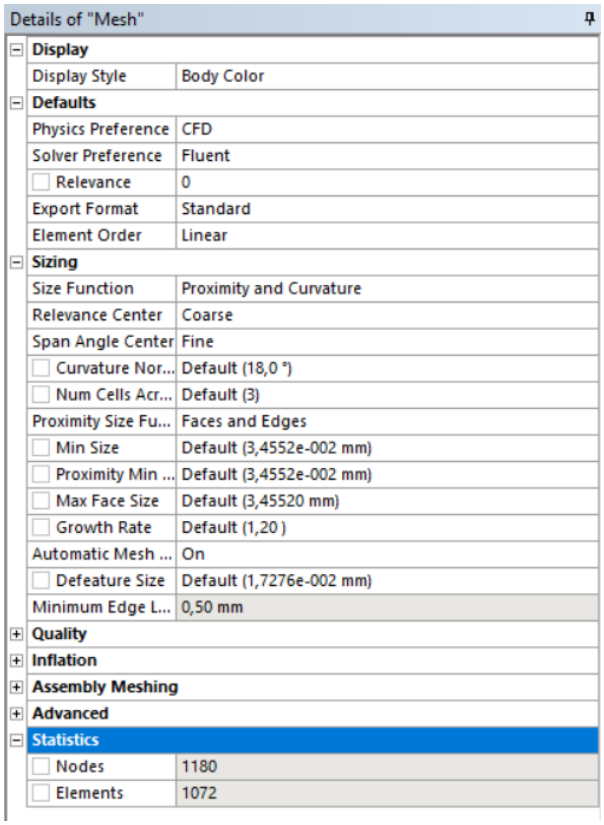

Figure D.5: Low Mesh Details

Table D.2: '3:Low' Mesh Quality Factors

Quality Factor	Value
Element Quality	
Average	0.751
Stnd. Deviation	0.205
Aspect Ratio	
Max	9.405
Average	2.38
Stnd. Deviation	1.43
Orthogonal Quality	
Average	0.998
Stnd. Deviation	4.6e-03
Skewness	
Max	0.2222
Average	2.05e-02
Stnd. Deviation	2.7e-02

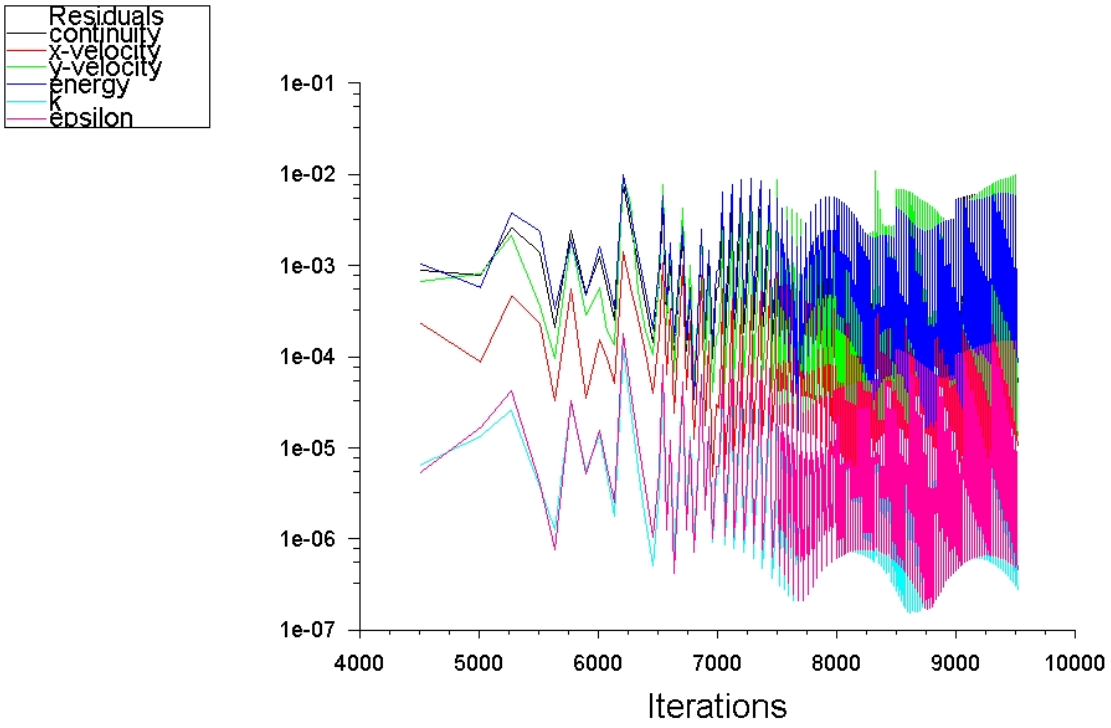

Figure D.6: 3: LOW Mesh Residuals

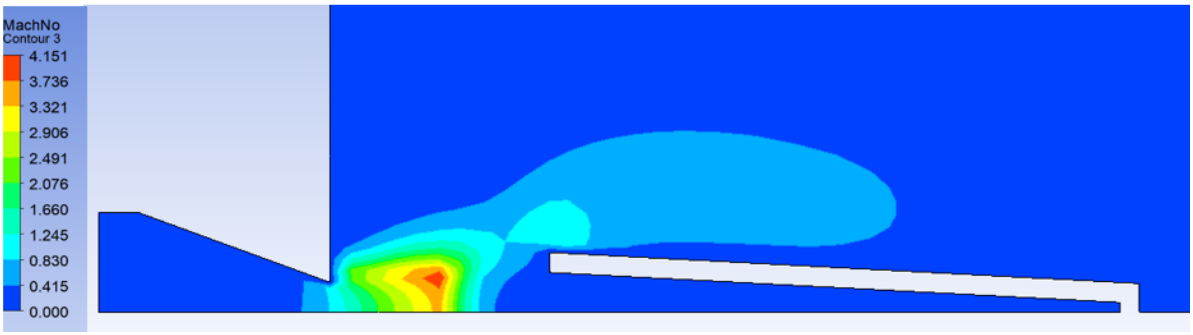

Figure D.7: 3: LOW Mesh Mach Contour

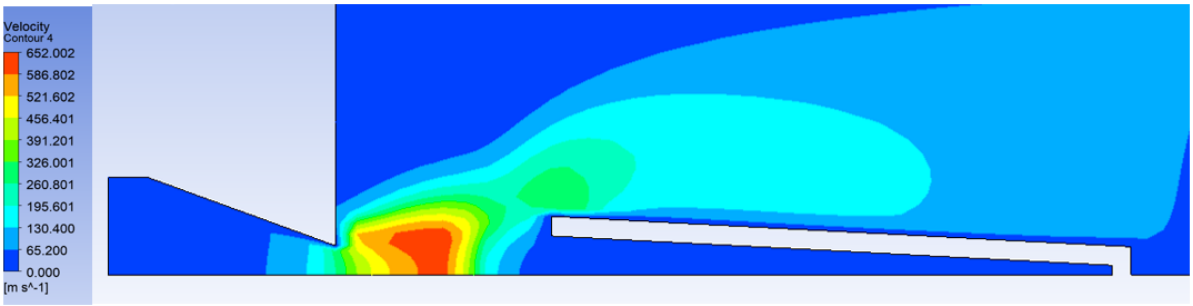

Figure D.8: 3: LOW Mesh Velocity Contour

E

ANSYS FLUENT: Mesh Validation

This appendix contains the ANSYS Fluent mesh, mesh quality factors and resulting residuals, contour plots, mass flow rates of inlet and outlet for the Afzali case mesh validation.

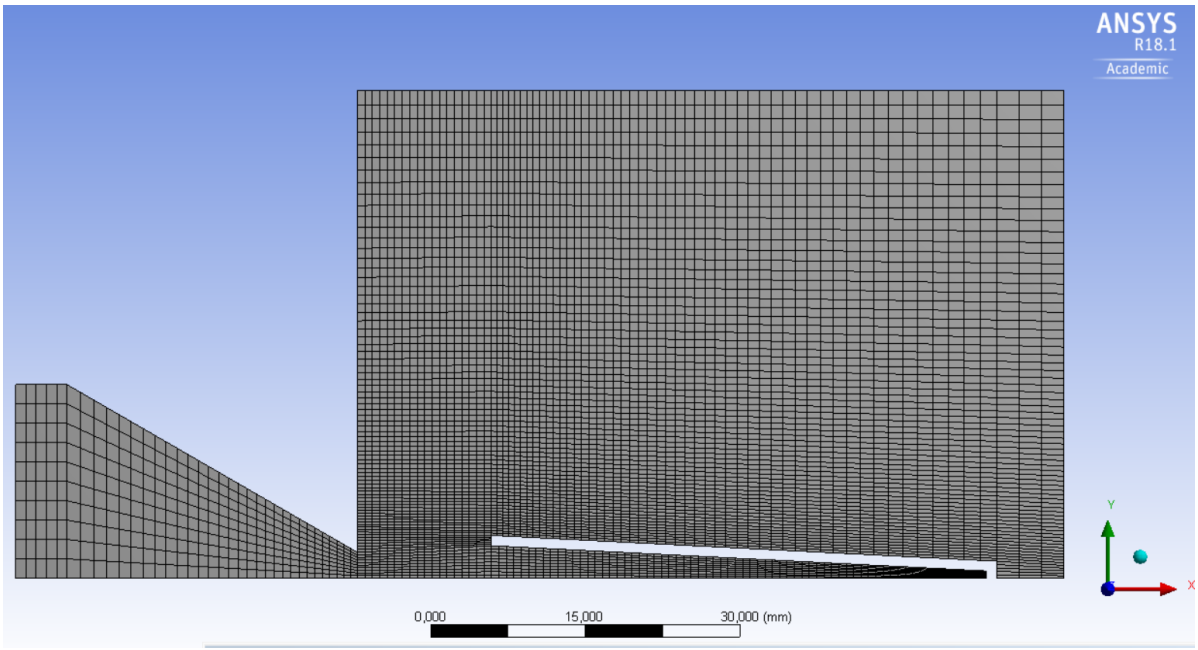

Figure E.1: Afzali Verification Mesh

Details of "Mesh"	
Display	
Display Style	Body Color
Defaults	
Physics Preference	CFD
Solver Preference	Fluent
Relevance	0
Export Format	Standard
Element Order	Linear
Sizing	
Size Function	Proximity and Curvature
Relevance Center	Coarse
Span Angle Center	Fine
Curvature Normal ...	Default (18,0 °)
Num Cells Across ...	Default (3)
Proximity Size Functi...	Faces and Edges
Min Size	Default (5,587e-002 mm)
Proximity Min Size	Default (5,587e-002 mm)
Max Face Size	Default (5,5870 mm)
Growth Rate	Default (1,20)
Automatic Mesh Base...	On
Defeature Size	Default (2,7935e-002 mm)
Minimum Edge Length	0,70 mm
Quality	
Inflation	
Assembly Meshing	
Advanced	
Statistics	
Nodes	6342
Elements	6080

Figure E.2: Afzali Verification Mesh Details

Table E.1: 'Afzali Verification' Mesh Quality Factors

Quality Factor	Value
Element Quality	
Average	0.76
Stnd. Deviation	0.20
Aspect Ratio	
Max	9.9975
Average	2.3292
Stnd. Deviation	1.4134
Orthogonal Quality	
Average	0.997
Stnd. Deviation	1.47e-02
Skewness	
Max	0.33333
Average	2.301e-02
Stnd. Deviation	4.5e-02

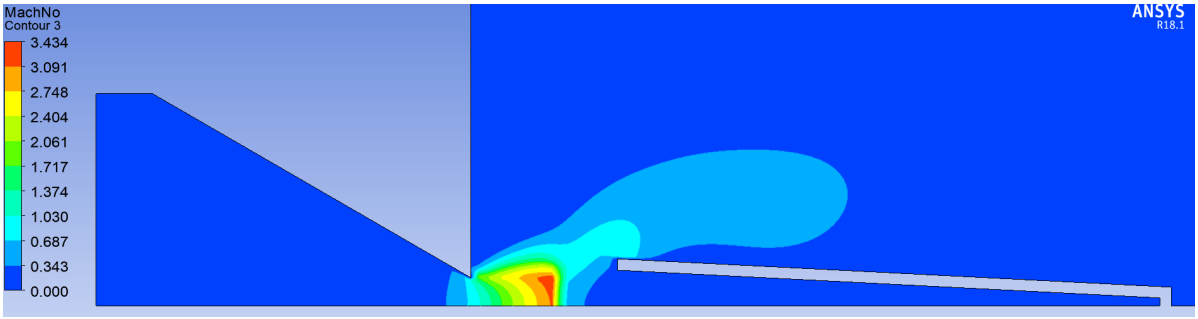

Figure E.3: Afzali Verification Mach Contour

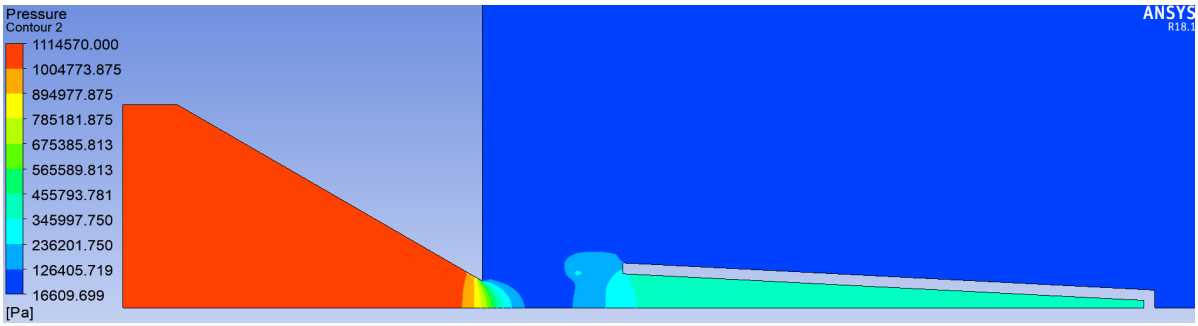

Figure E.4: Afzali Verification Pressure Contour

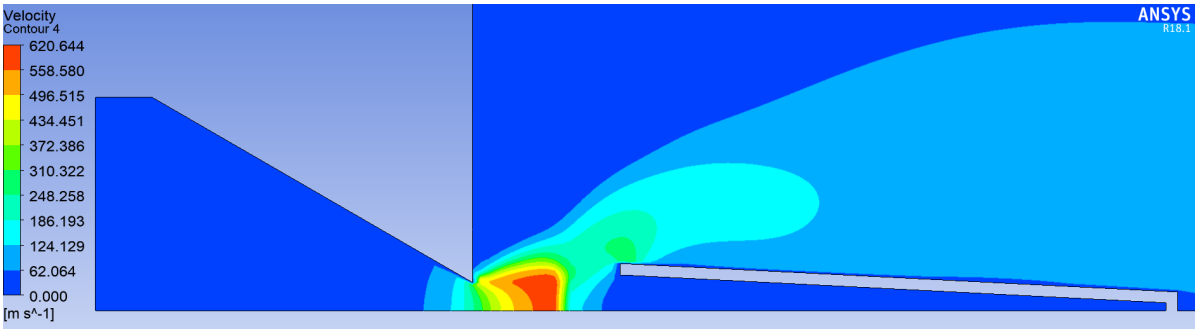

Figure E.5: Afzali Verification Velocity Contour

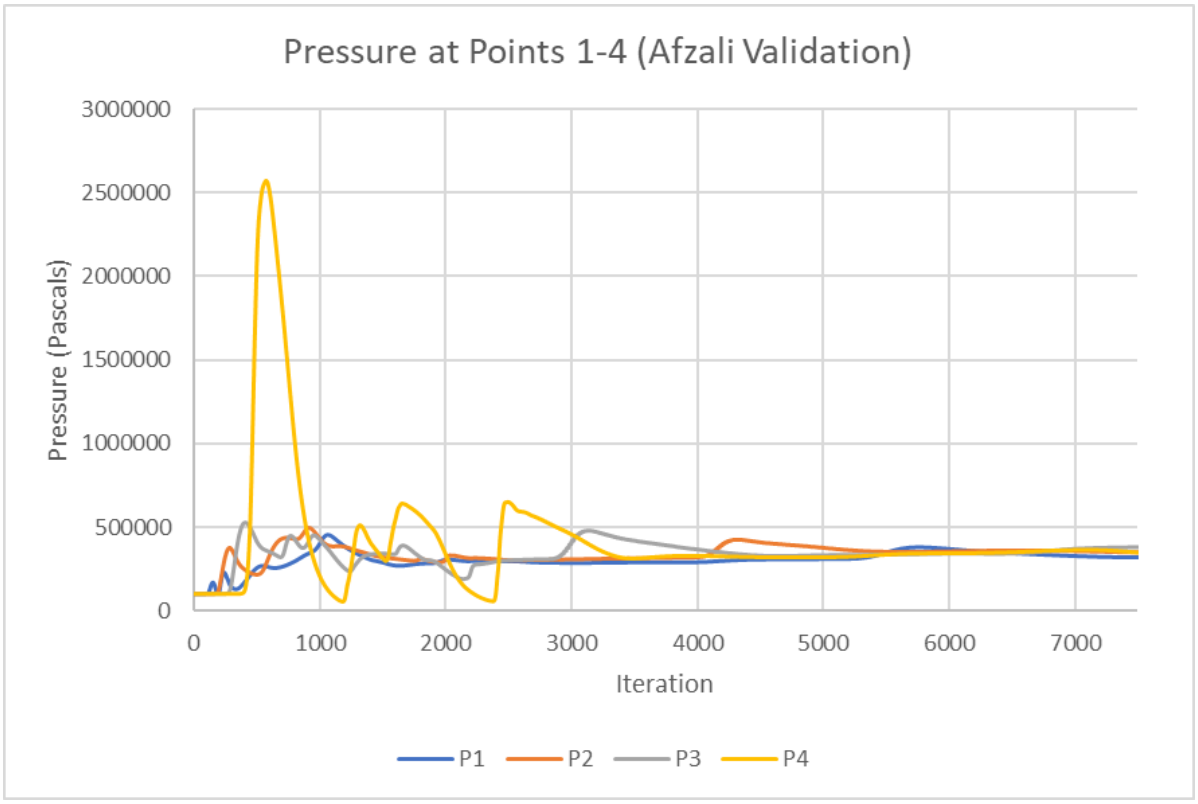

Figure E.6: Afzali Verification Pressure vs. Iteration plot

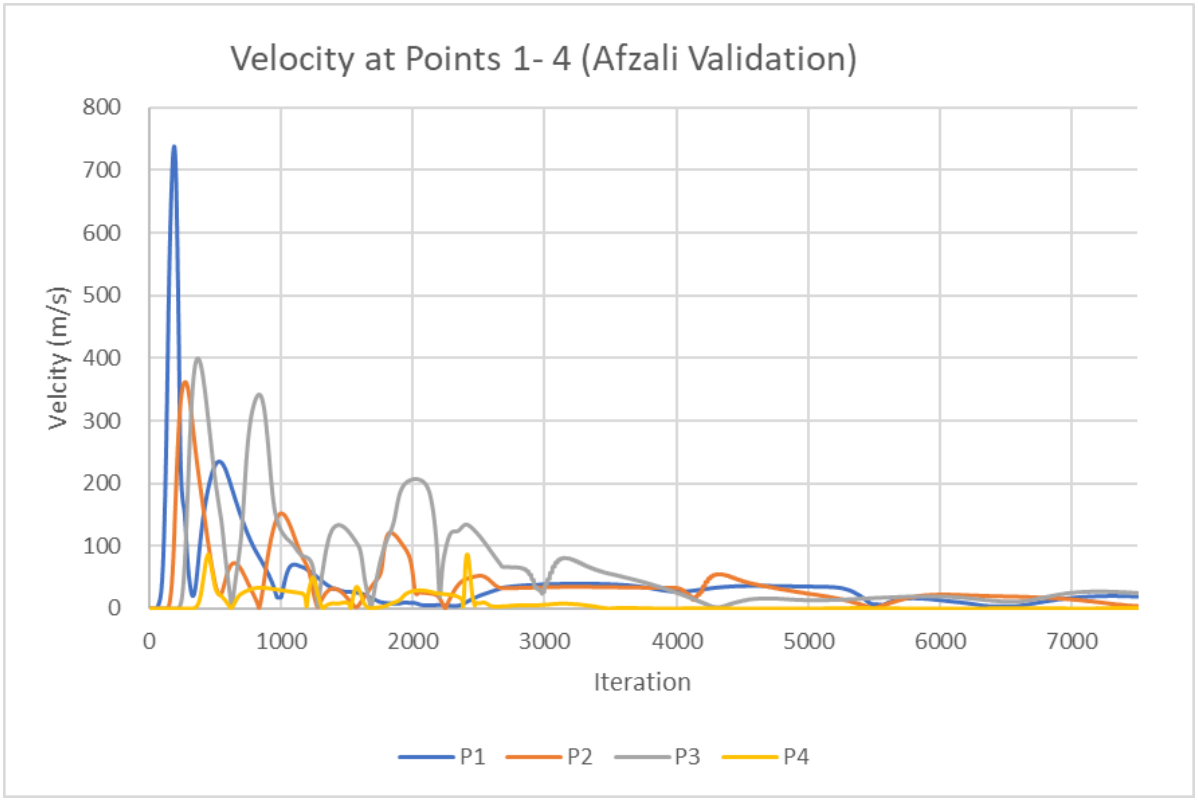

Figure E.7: Afzali Verification Velocity vs. Iteration plot

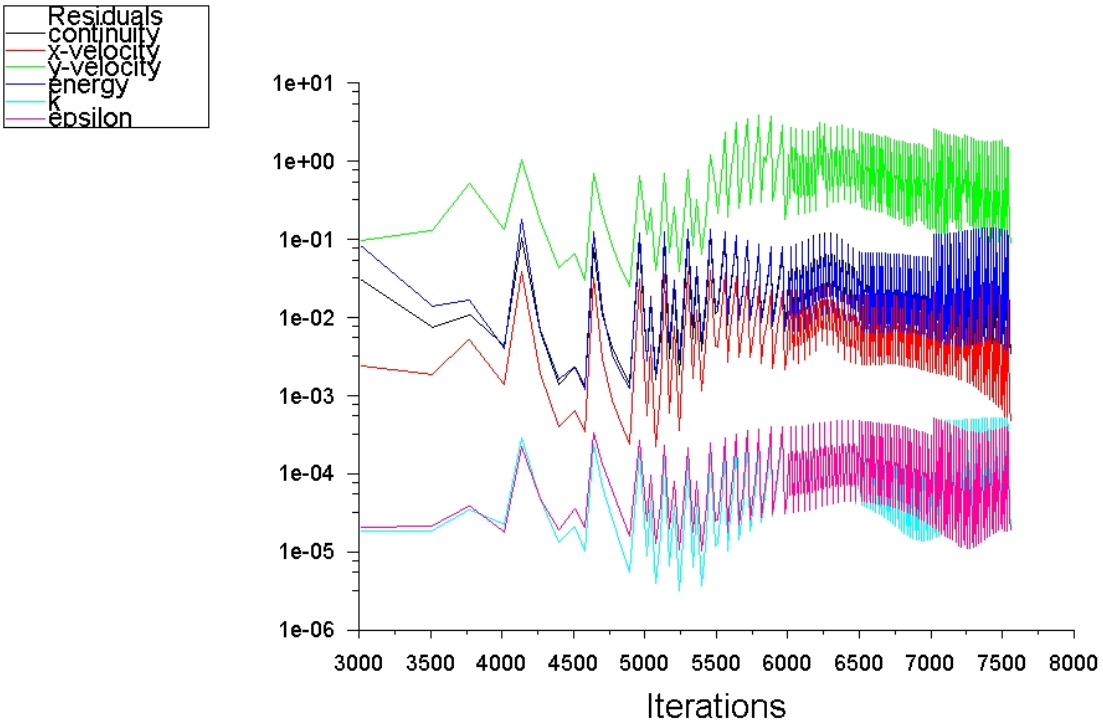

Figure E.8: Afzali Verification Residuals

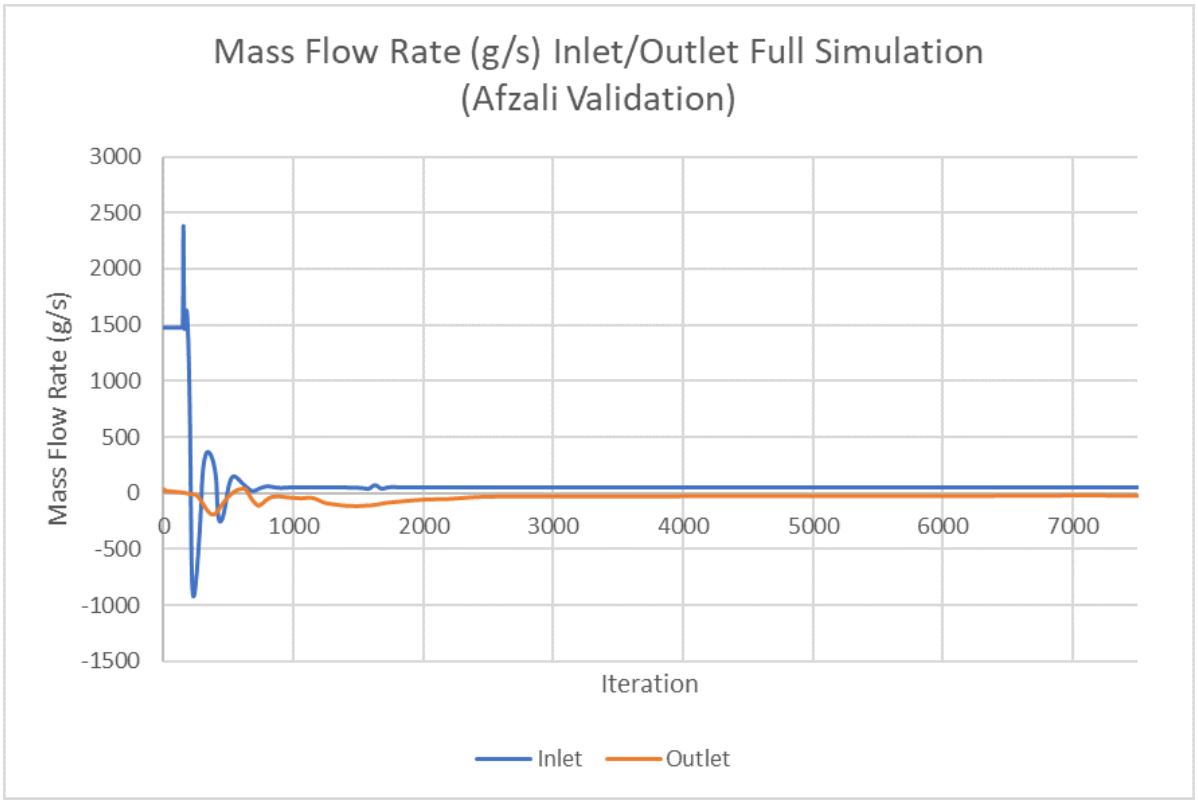

Figure E.9: Afzali Verification Mass Flow Rate vs. Iteration plot

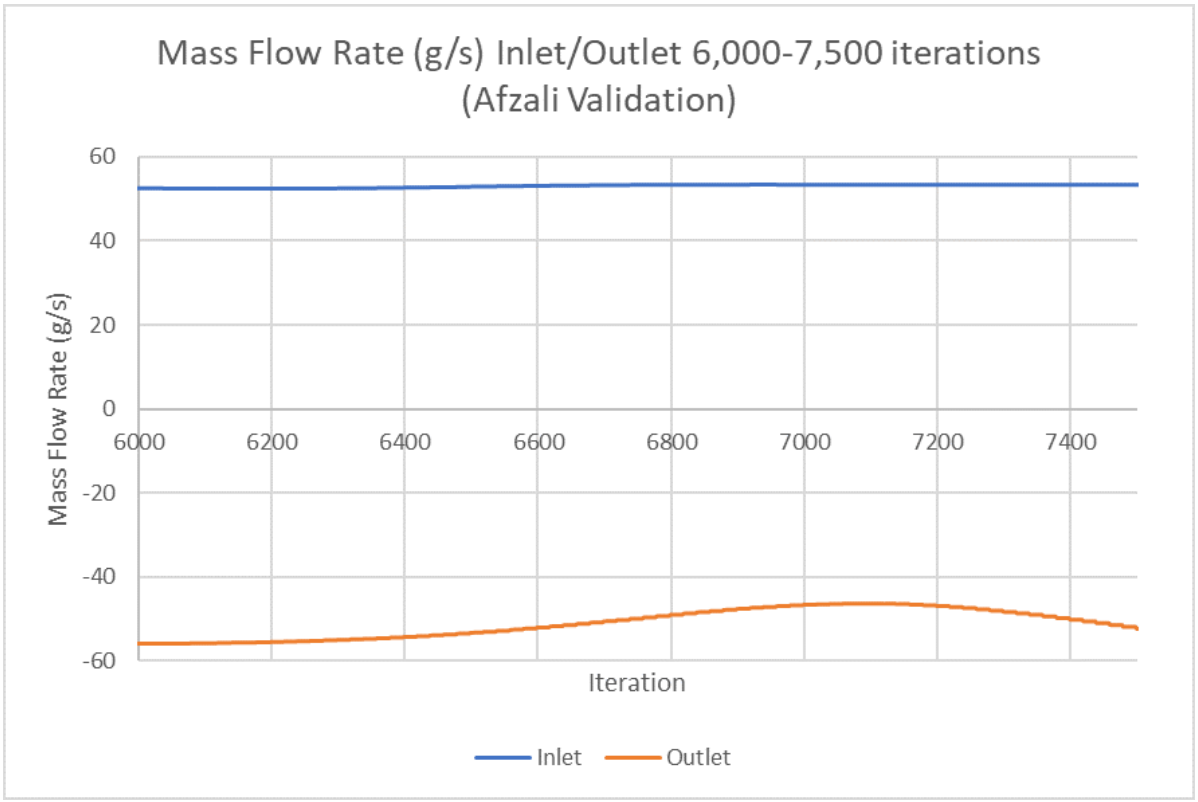

Figure E.10: Afzali Verification Mass Flow Rate vs. Iteration End plot

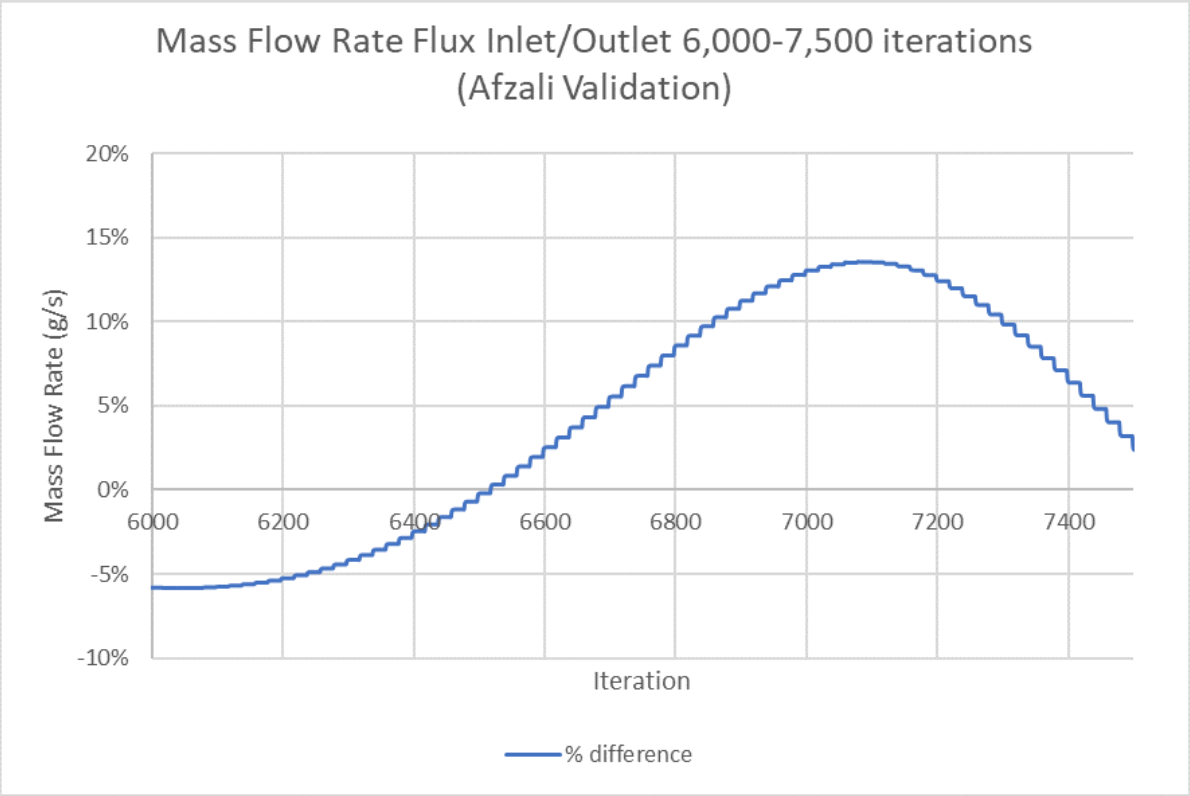

Figure E.11: Afzali Verification Mass Flow Rate FLUX vs. Iteration plot

F

ANSYS FLUENT: Nozzle-Steady

ANSYS Fluent mesh details and results of residuals, contour plots, mass flow rates of inlet and outlet. All plots are for the converging nozzle with the 3mm exit diameter and 19 bar inlet pressure gaseous oxygen.

Details of "Mesh"	
Display	
Display Style	Body Color
Defaults	
Physics Preference	CFD
Solver Preference	Fluent
Relevance	0
Export Format	Standard
Element Order	Linear
Sizing	
Size Function	Proximity and Curvature
Relevance Center	Coarse
Span Angle Center	Fine
Curvature Normal ...	Default (18,0 °)
Num Cells Across ...	Default (3)
Proximity Size Functi...	Faces and Edges
Min Size	Default (4,0887e-002 mm)
Proximity Min Size	Default (4,0887e-002 mm)
Max Face Size	Default (4,08870 mm)
Growth Rate	Default (1,20)
Automatic Mesh Base...	On
Defeature Size	Default (2,0443e-002 mm)
Minimum Edge Length	2,0 mm
Quality	
Inflation	
Assembly Meshing	
Advanced	
Statistics	
Nodes	63436
Elements	62850

Figure F.1: 'Nozzle-Steady' Mesh details

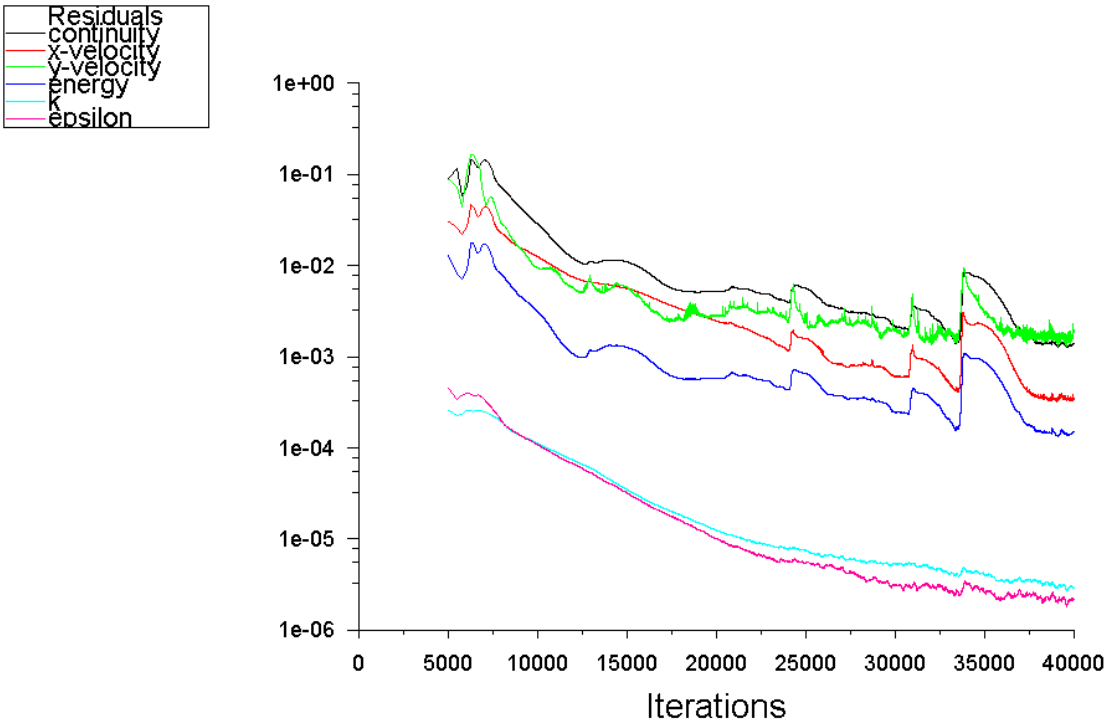

Figure F.2: Nozzle-Steady, Residuals

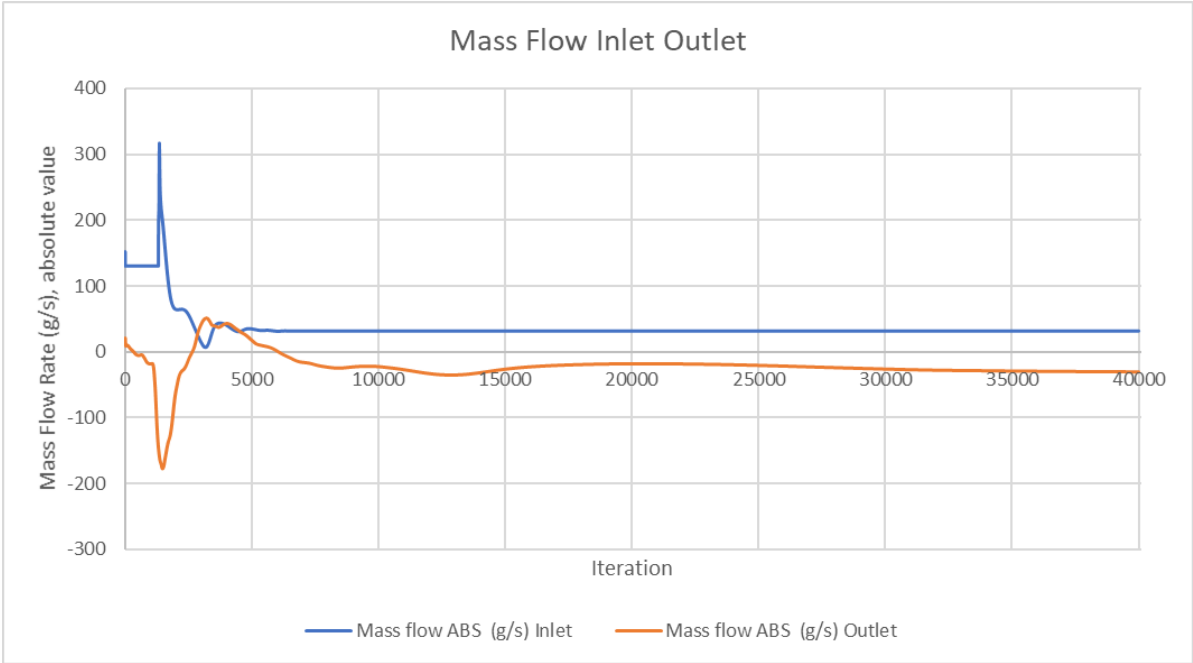

Figure F.3: Nozzle-Steady, Mass Flow Rates Inlet and Outlet, full simulation

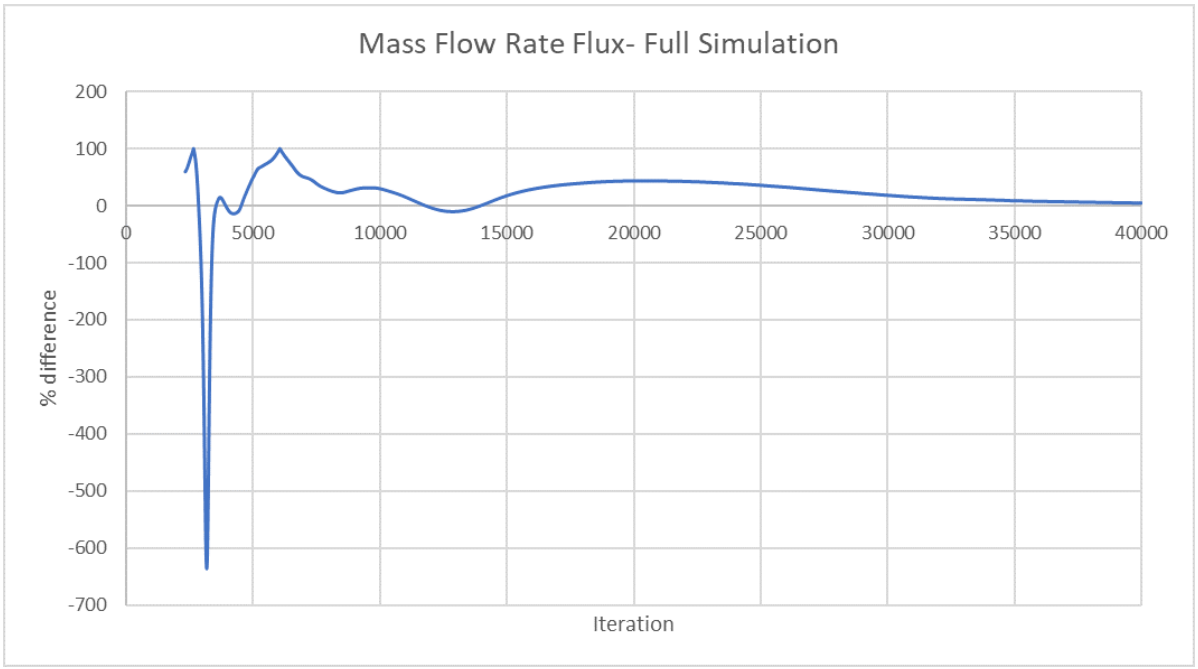

Figure F.4: Nozzle-Steady, Mass Flow Rate Flux, full simulation

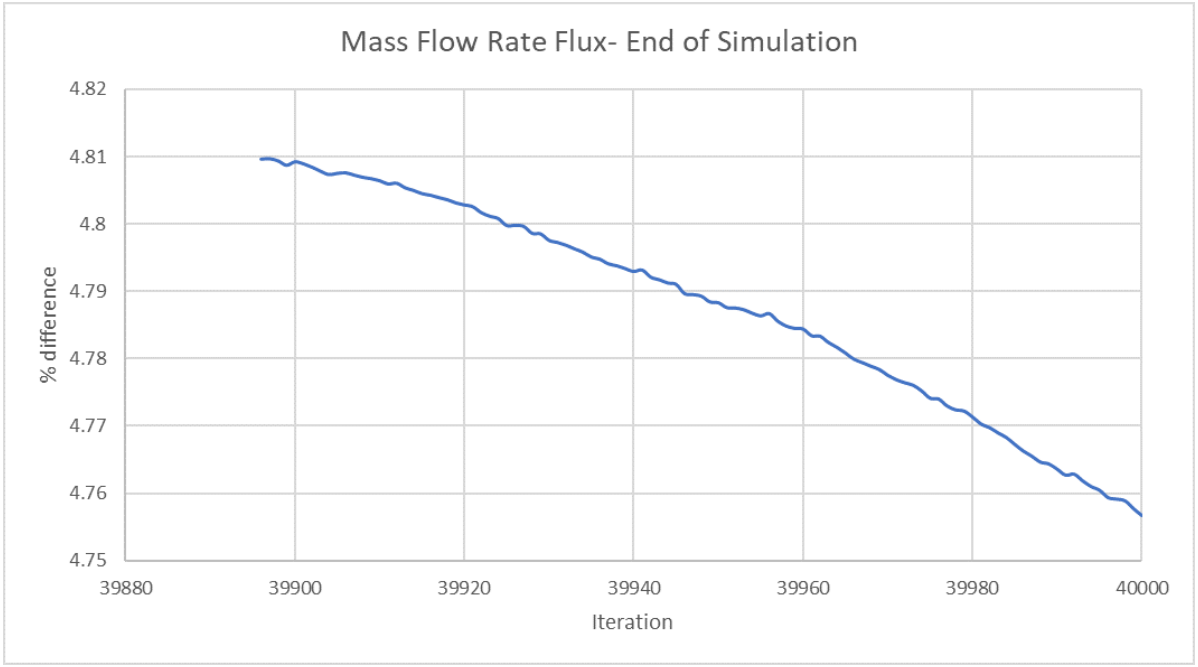

Figure F.5: Nozzle-Steady, Mass Flow Rate Flux, end of simulation

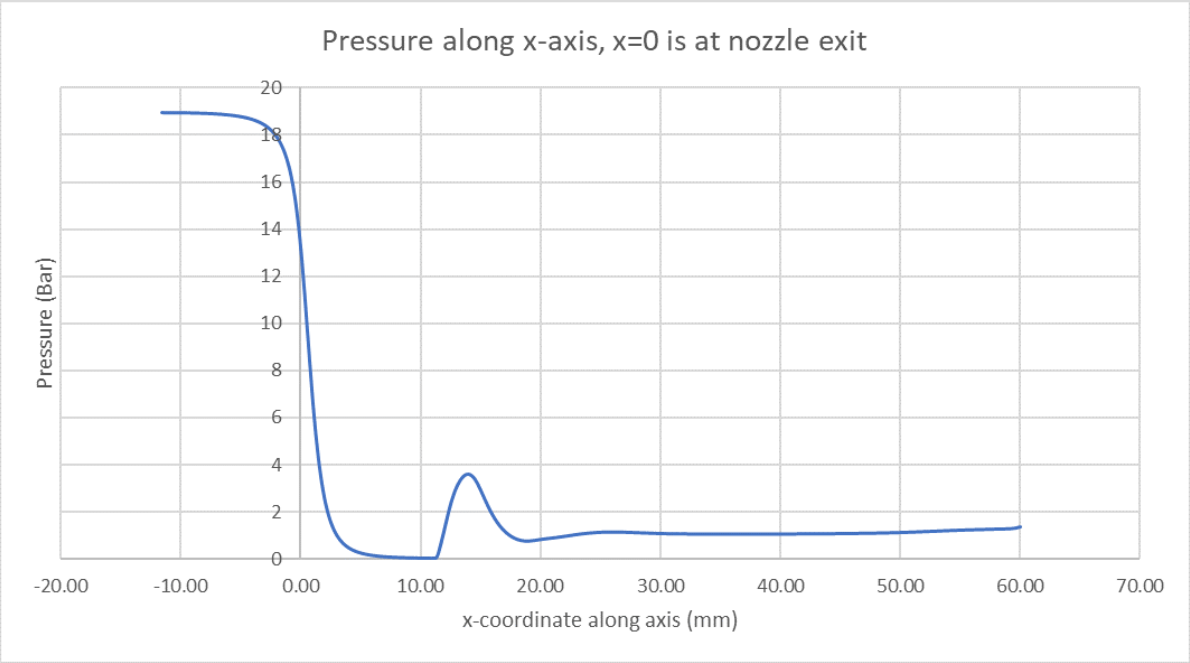

Figure F.6: Nozzle-Steady, Pressure along x-axis, x=0 is at nozzle exit

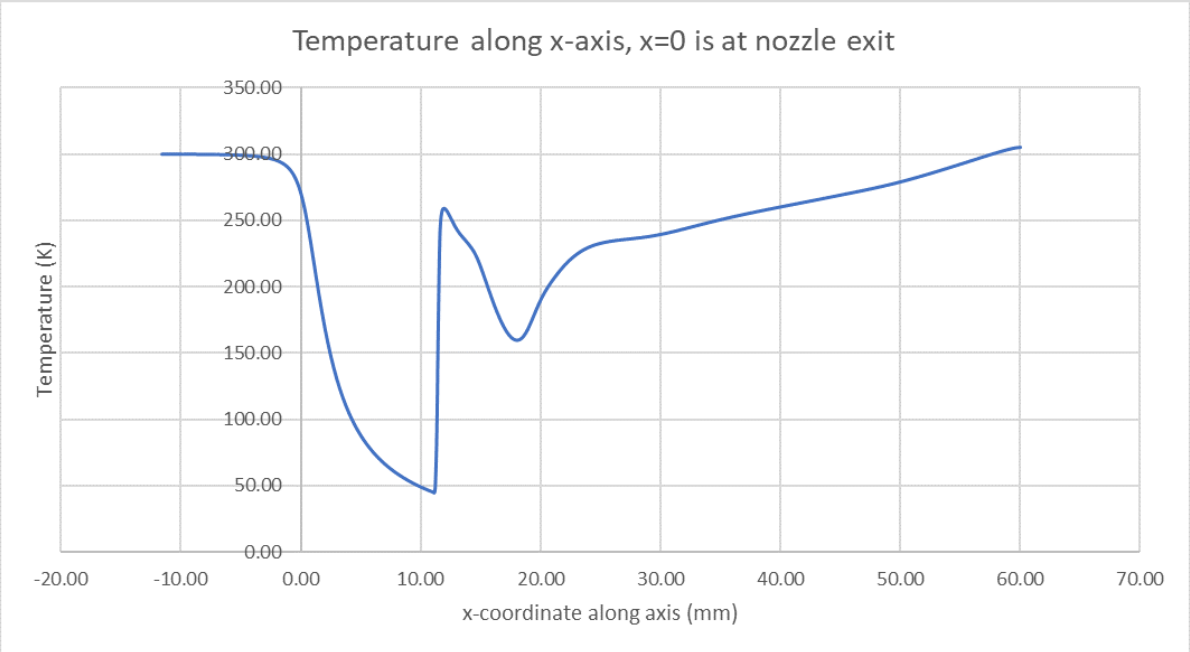

Figure F.7: Nozzle-Steady, Temperature along x-axis, x=0 is at nozzle exit

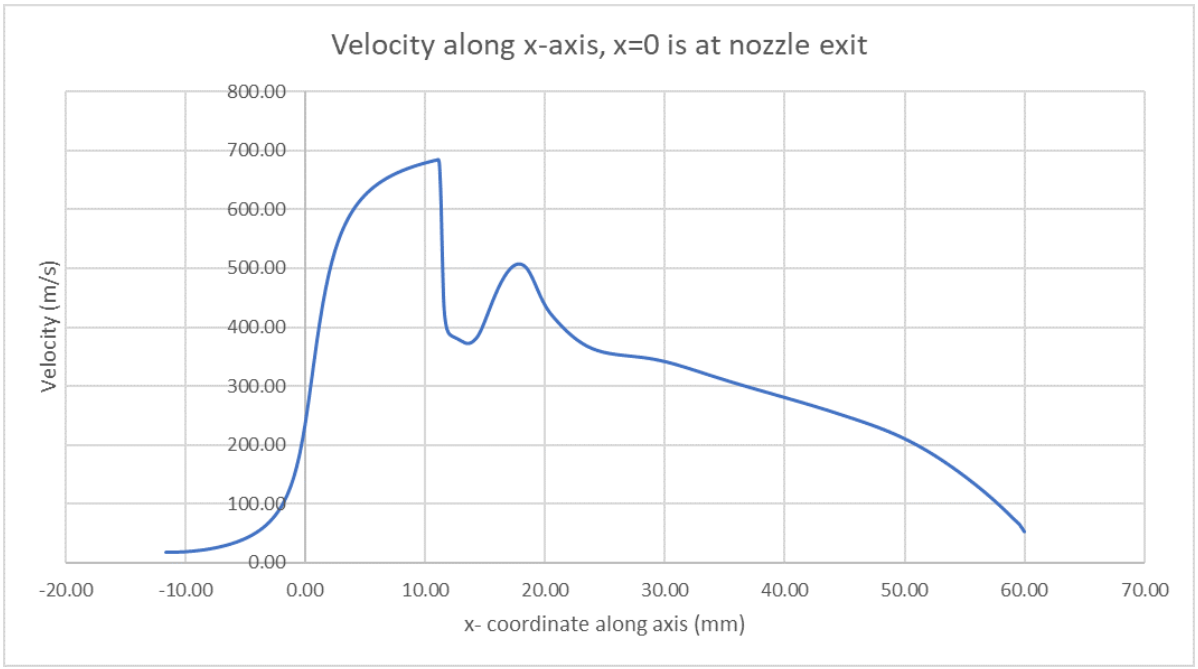

Figure F.8: Nozzle-Steady, Velocity along x-axis, x=0 is at nozzle exit

G

ANSYS FLUENT: Cavity

ANSYS Fluent residuals, mass flow rates of inlet and outlet, flux and contour plots for all of the cavity cases are given here. As Case 3 was used in the description of the solver convergence and validation in chapter 12, these plots are in that chapter and not included here. Additionally, in chapter 12, the explanation of the Case 3 convergence included a plot of the transient convergence, to validate the time-step size. That plot is not included for Cases 3.1-3.3 as they use the same mesh and time-step size.

G.1. Case 1: Preliminary Design Results

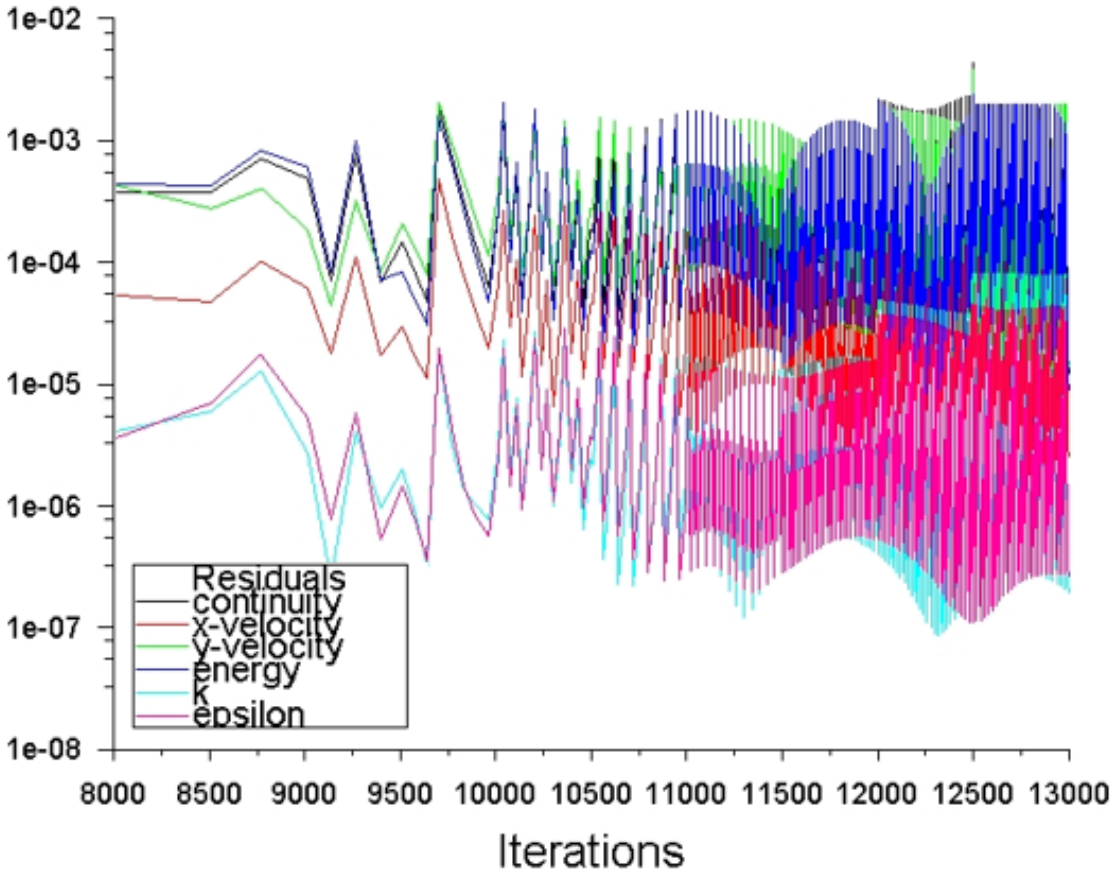

Figure G.1: Case 1: Preliminary Design, Residuals

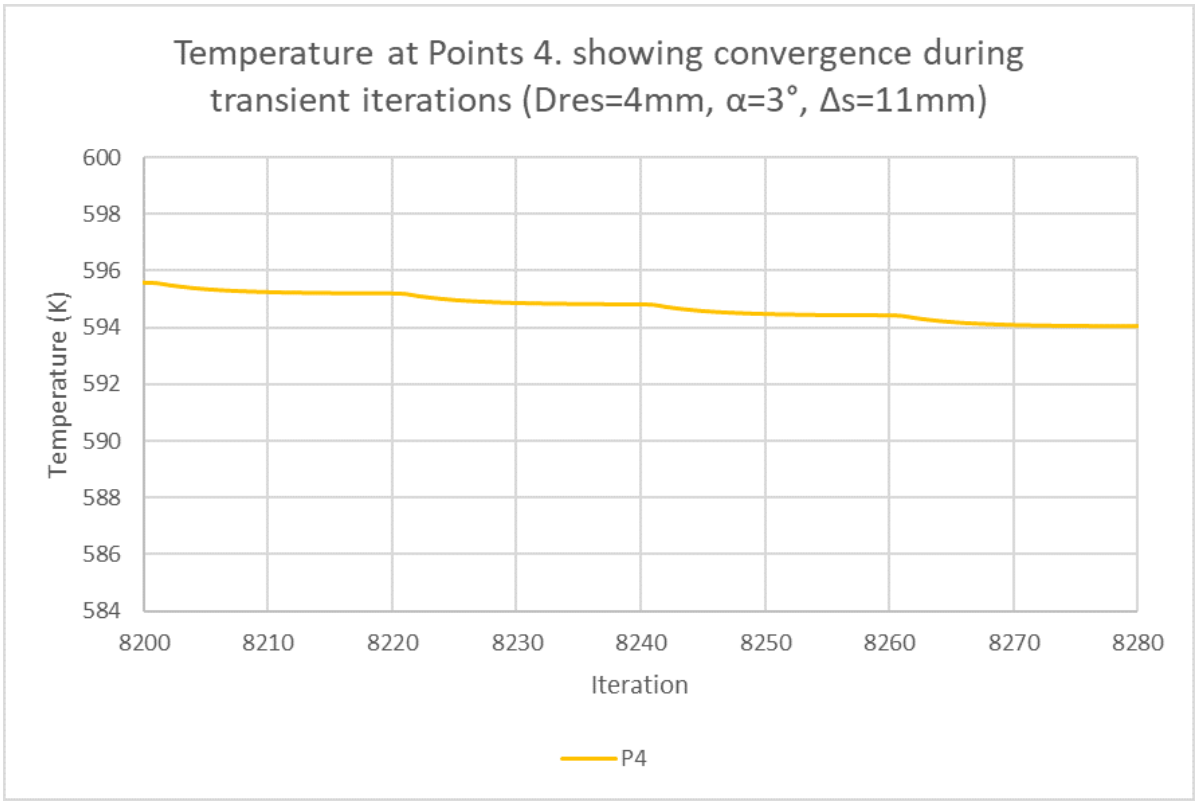

Figure G.2: Case 1: Preliminary Design, Transient Convergence

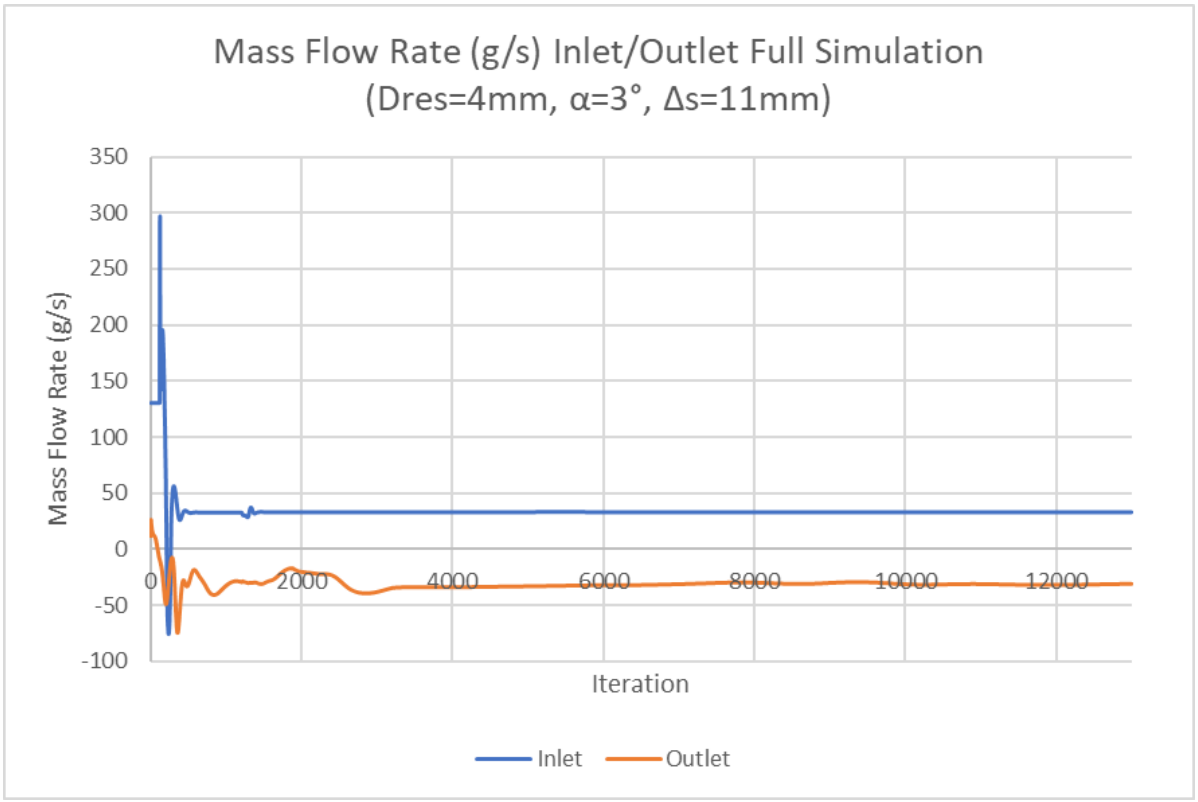

Figure G.3: Case 1: Preliminary Design, Mass Flow Rate Inlet/Outlet Full Simulation

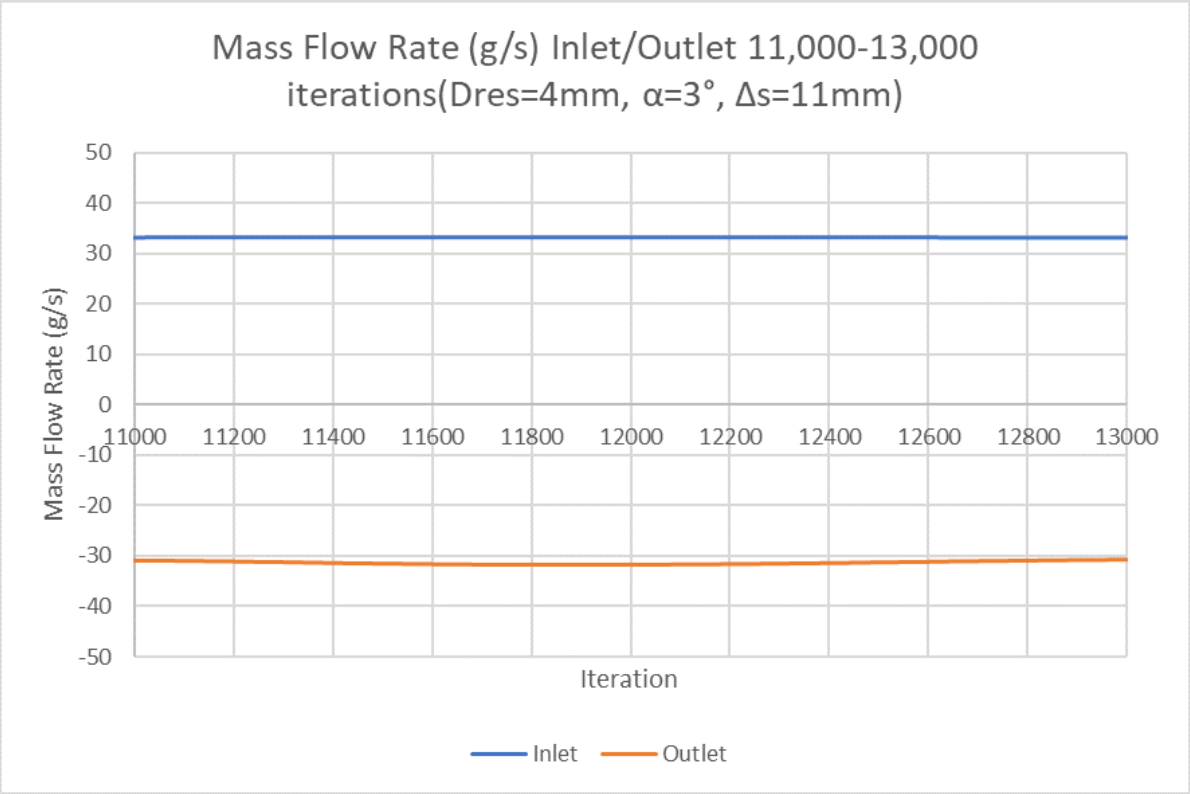

Figure G.4: Case 1: Preliminary Design, Mass Flow Rate Inlet/Outlet End of Simulation

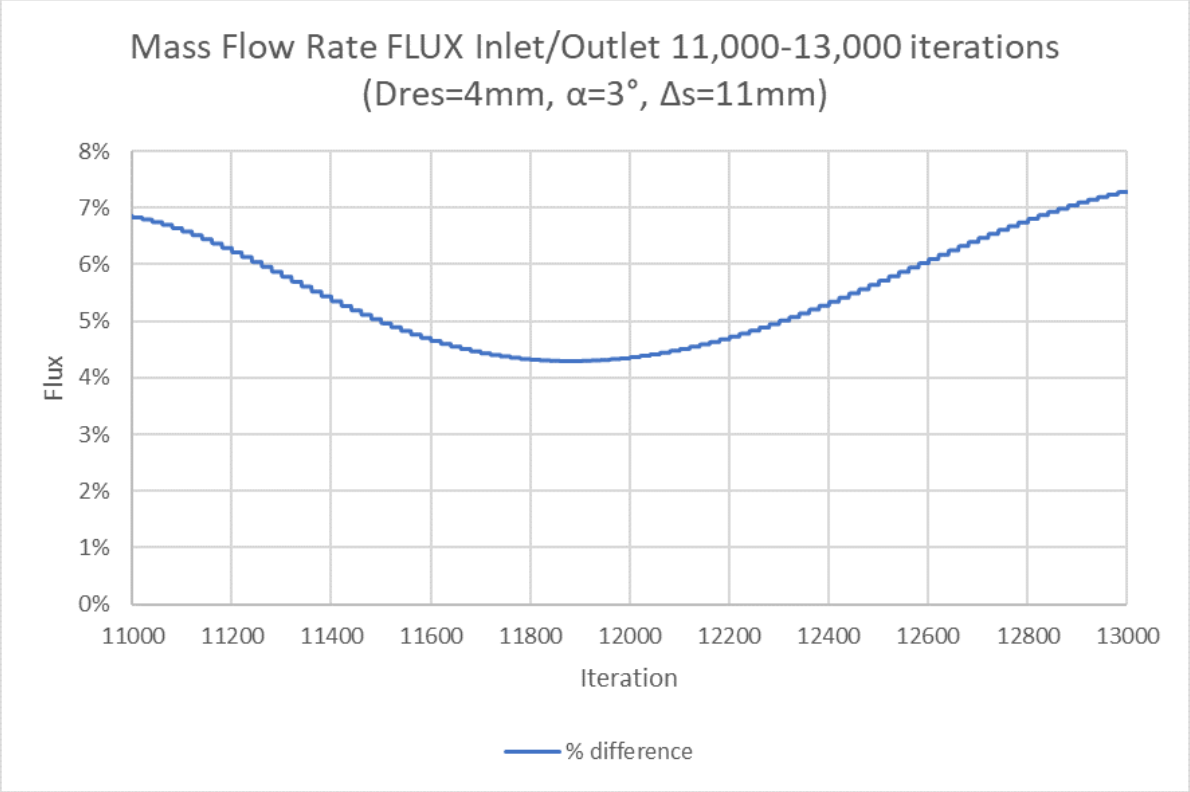

Figure G.5: Case 1: Preliminary Design, Mass Flow Rate Inlet/Outlet Flux, End of Simulation

G.2. Case 2: Large Alpha

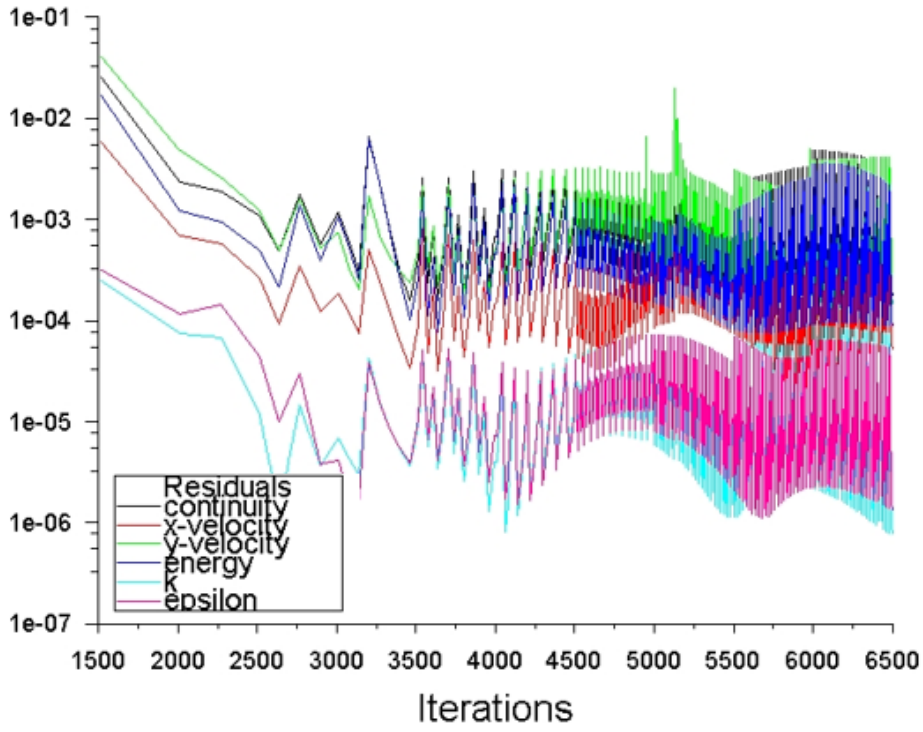

Figure G.6: Case 2: Large α , Residuals

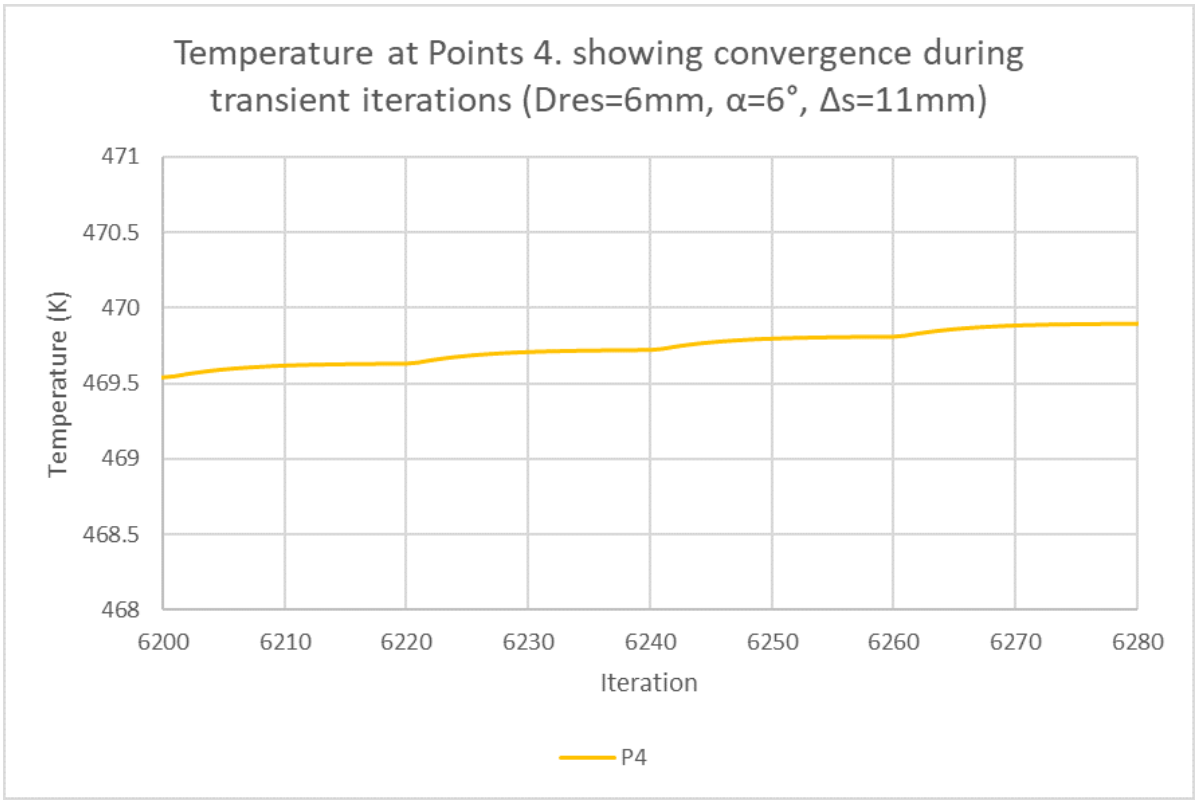

Figure G.7: Case 2: Large α, Transient Convergence

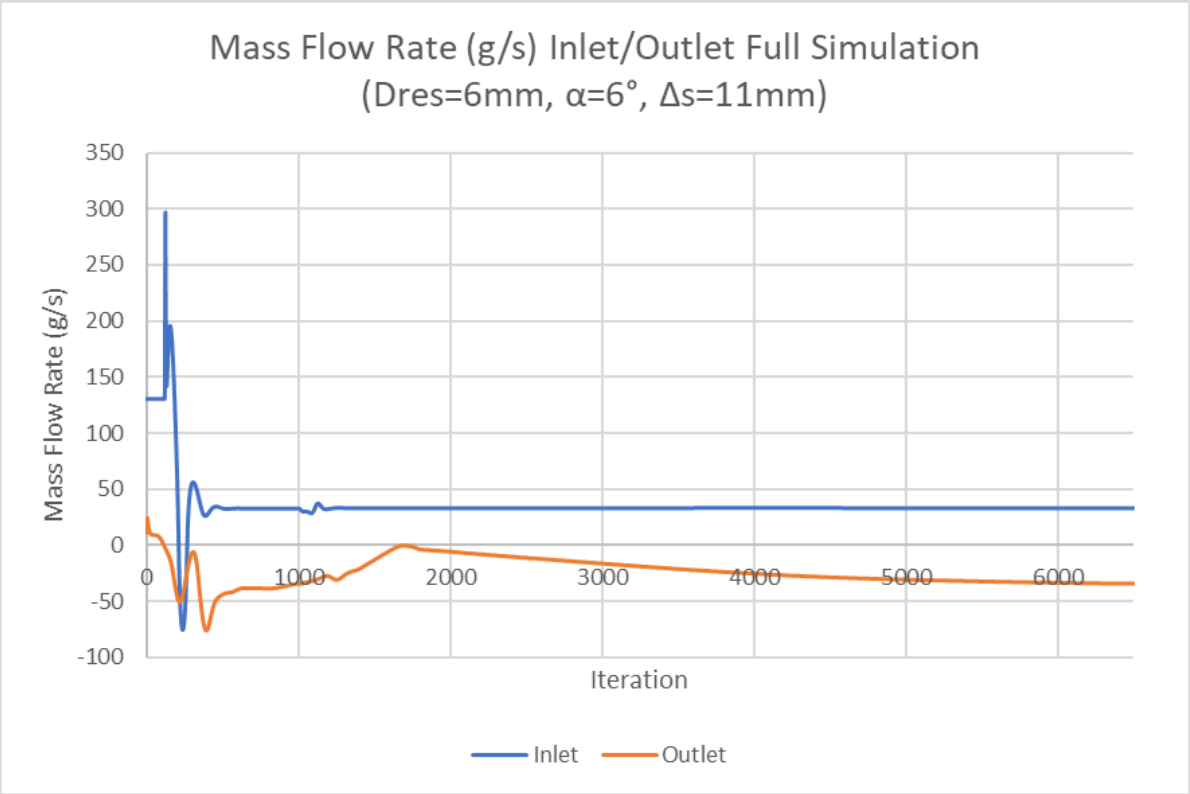

Figure G.8: Case 2: Large α, Mass Flow Rate Inlet/Outlet Full Simulation

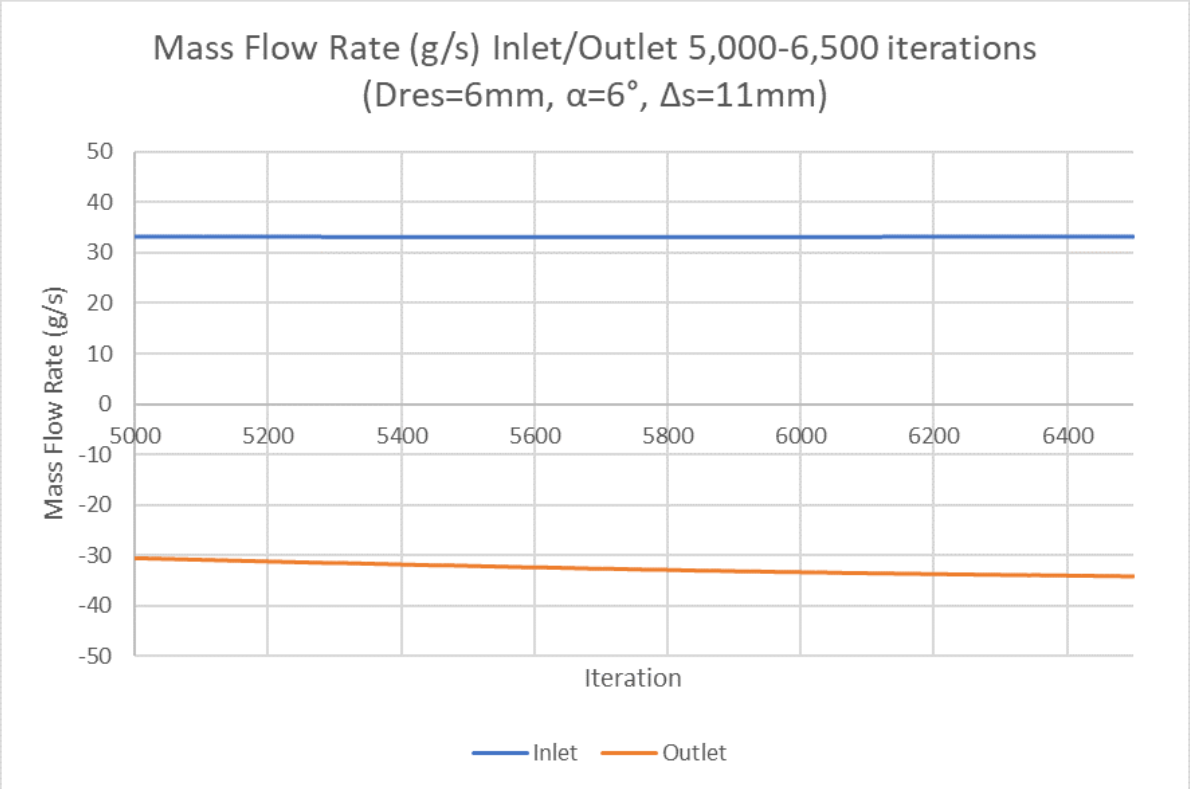

Figure G.9: Case 2: Large α, Mass Flow Rate Inlet/Outlet End of Simulation

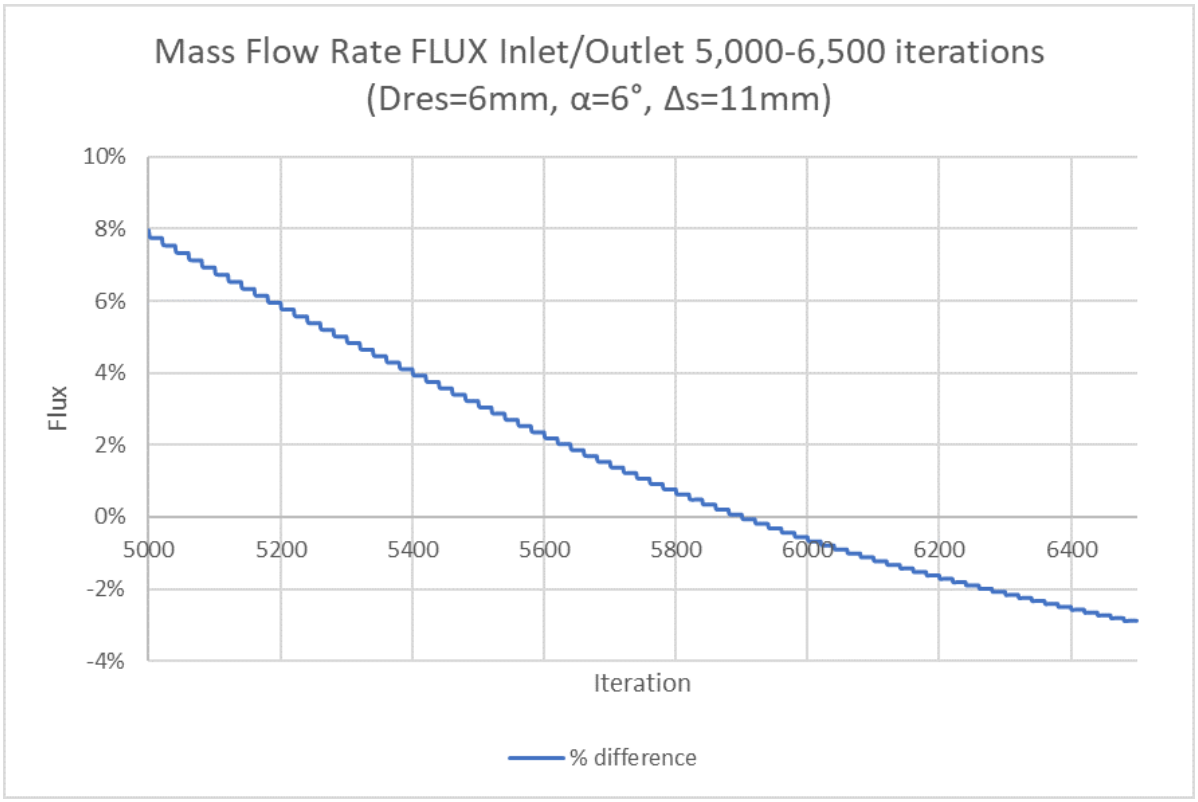

Figure G.10: Case 2: Large α, Mass Flow Rate Inlet/Outlet Flux, End of Simulation

G.3. Case 3.1: Large Dres Po: 10.25 bar

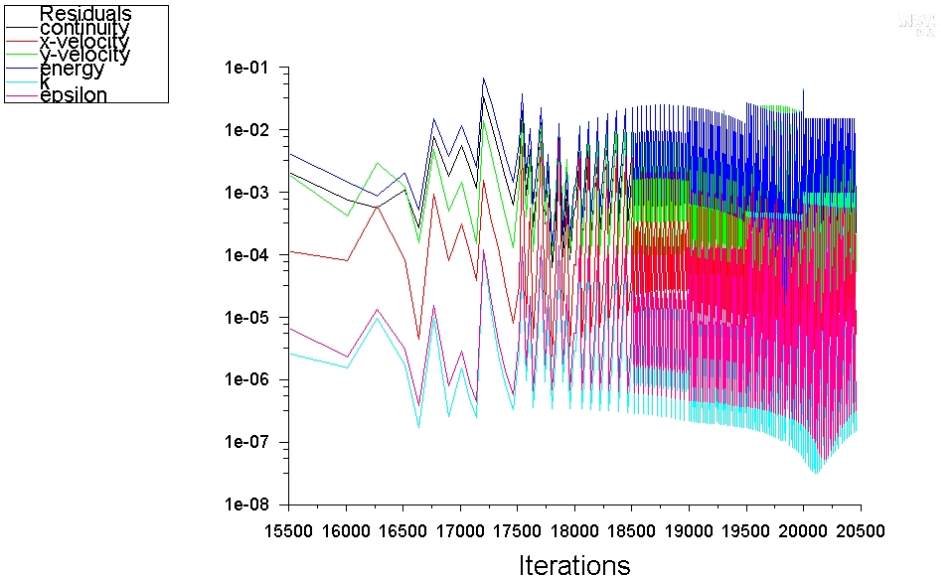

Figure G.11: Case 3.1: Large D_{res}, $P_o = 10.25$ bar, Residuals

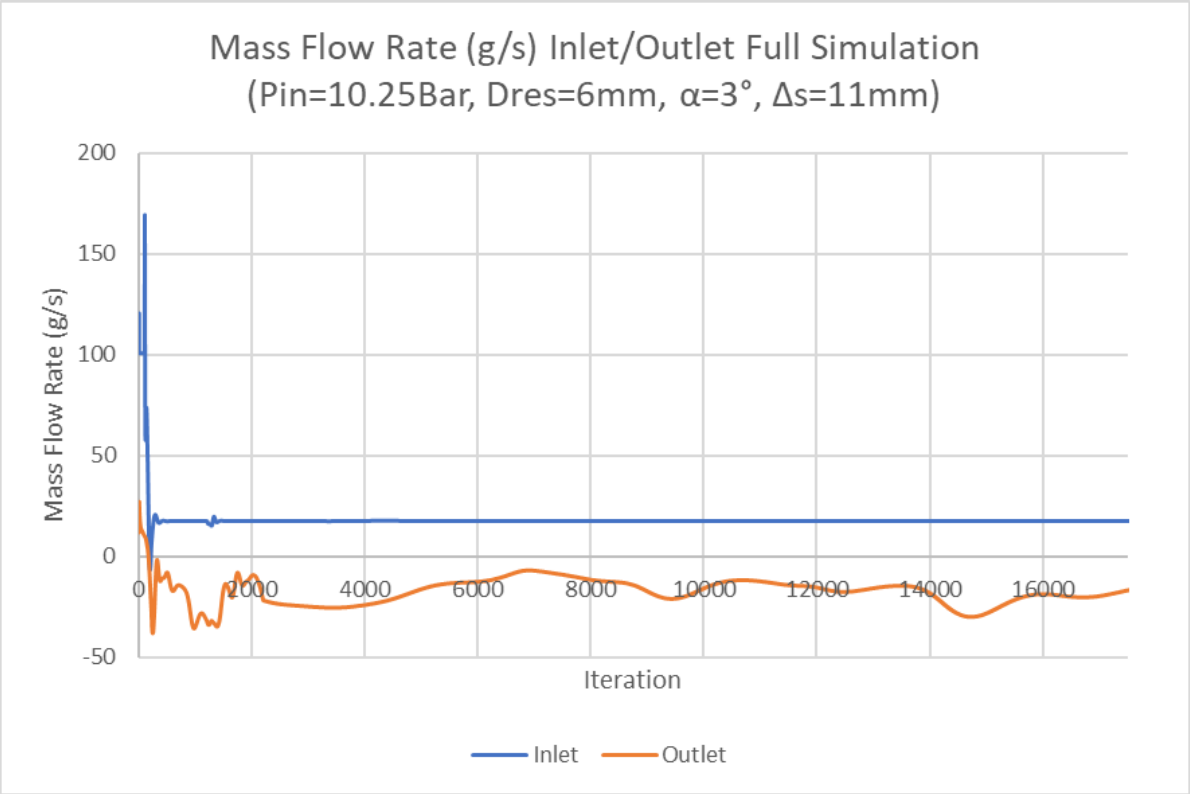

Figure G.12: Case 3.1: Large D_{res}, P_o = 10.25 bar, Mass Flow Rate Inlet/Outlet Full Simulation

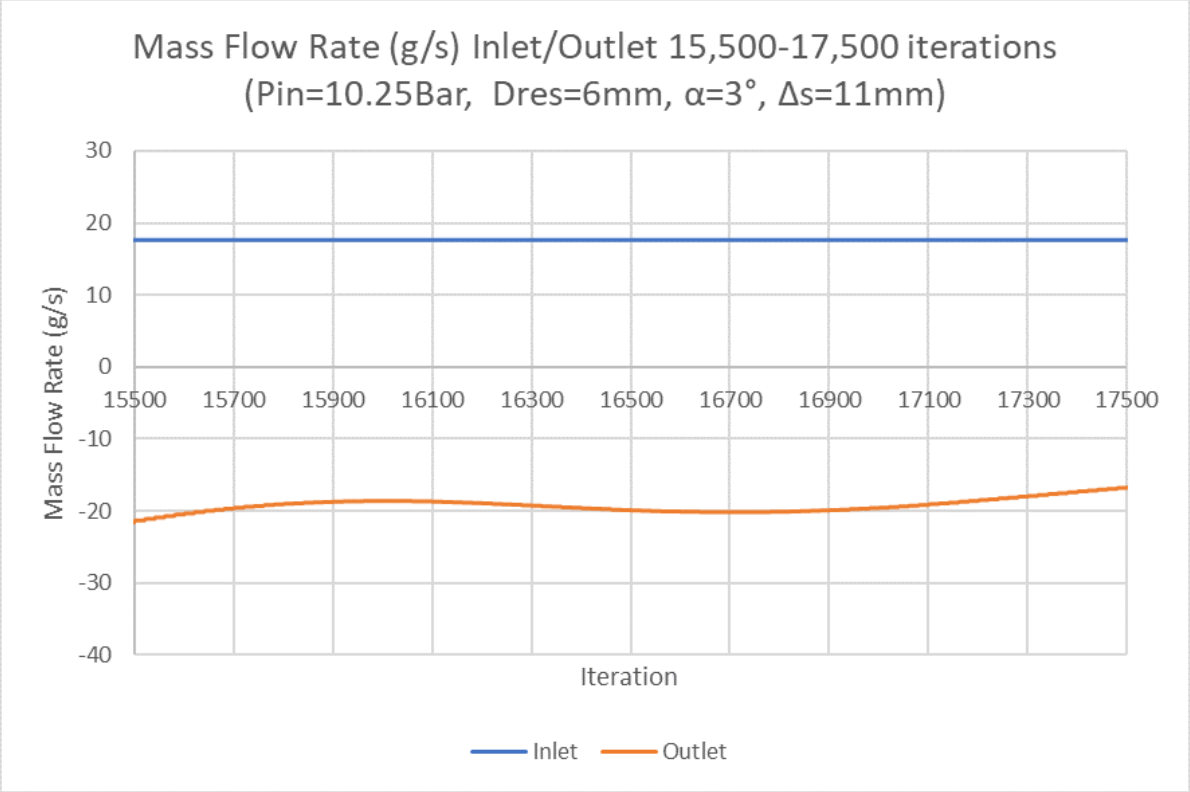

Figure G.13: Case 3.1: Large D_{res}, P_o = 10.25 bar, Mass Flow Rate Inlet/Outlet End of Simulation

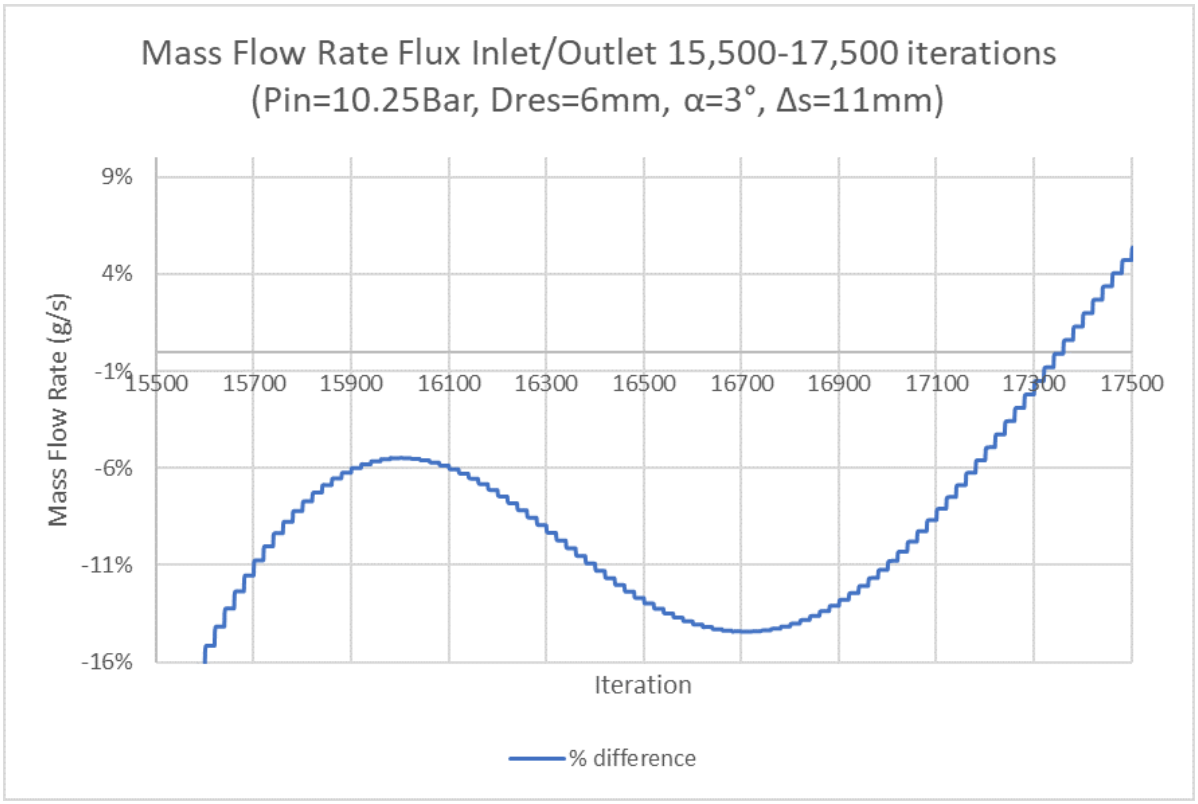

Figure G.14: Case 3.1: Large D_{res}, P_o = 10.25 bar, Mass Flow Rate Inlet/Outlet Flux, End of Simulation

G.4. Case 3.2: Large Dres Po: 15 bar

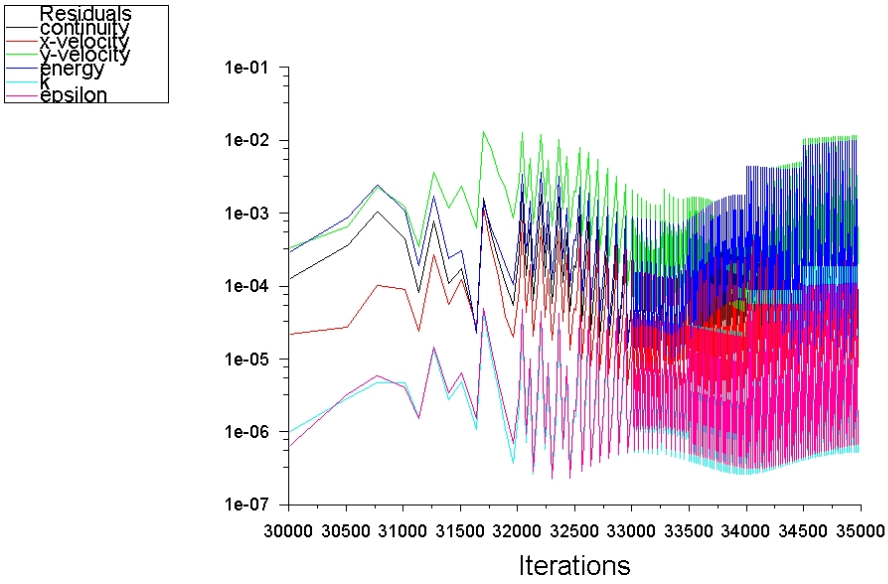

Figure G.15: Case 3.2: Large D_{res}, P_o = 15 bar, Residuals

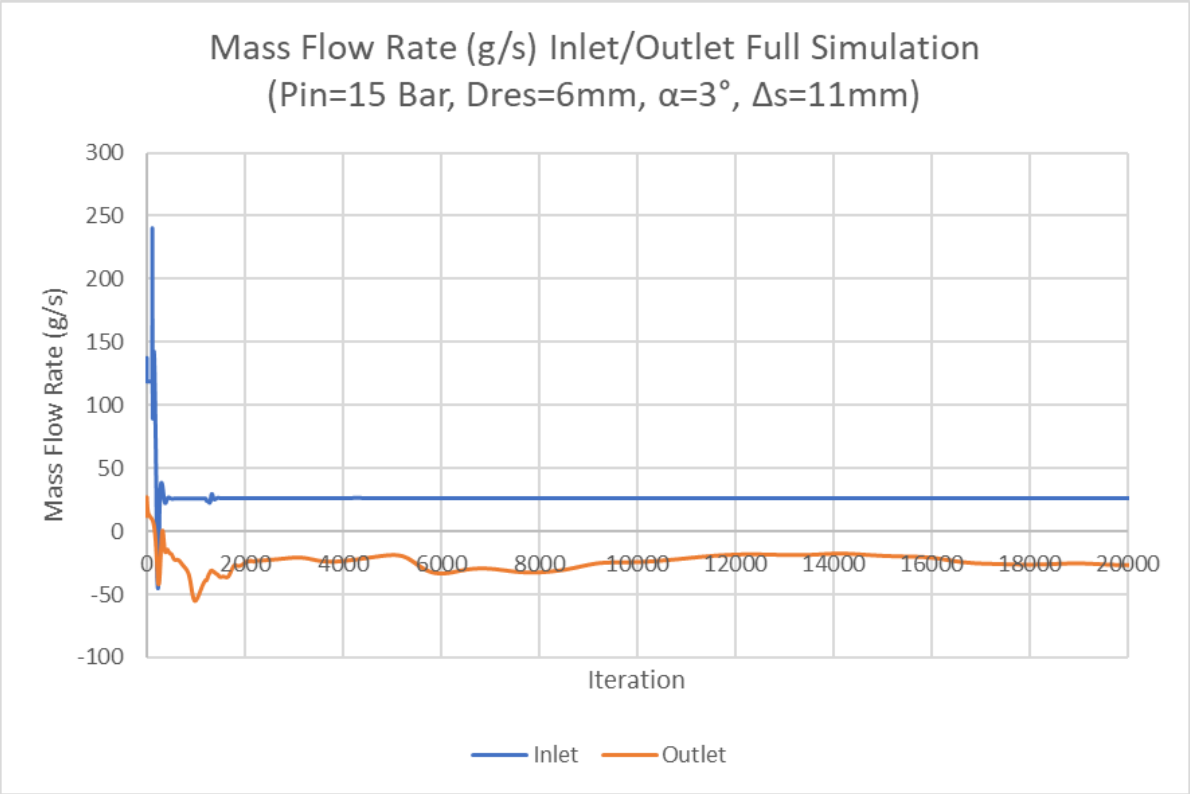

Figure G.16: Case 3.2: Large D_{res}, P_o = 15 bar, Mass Flow Rate Inlet/Outlet Full Simulation

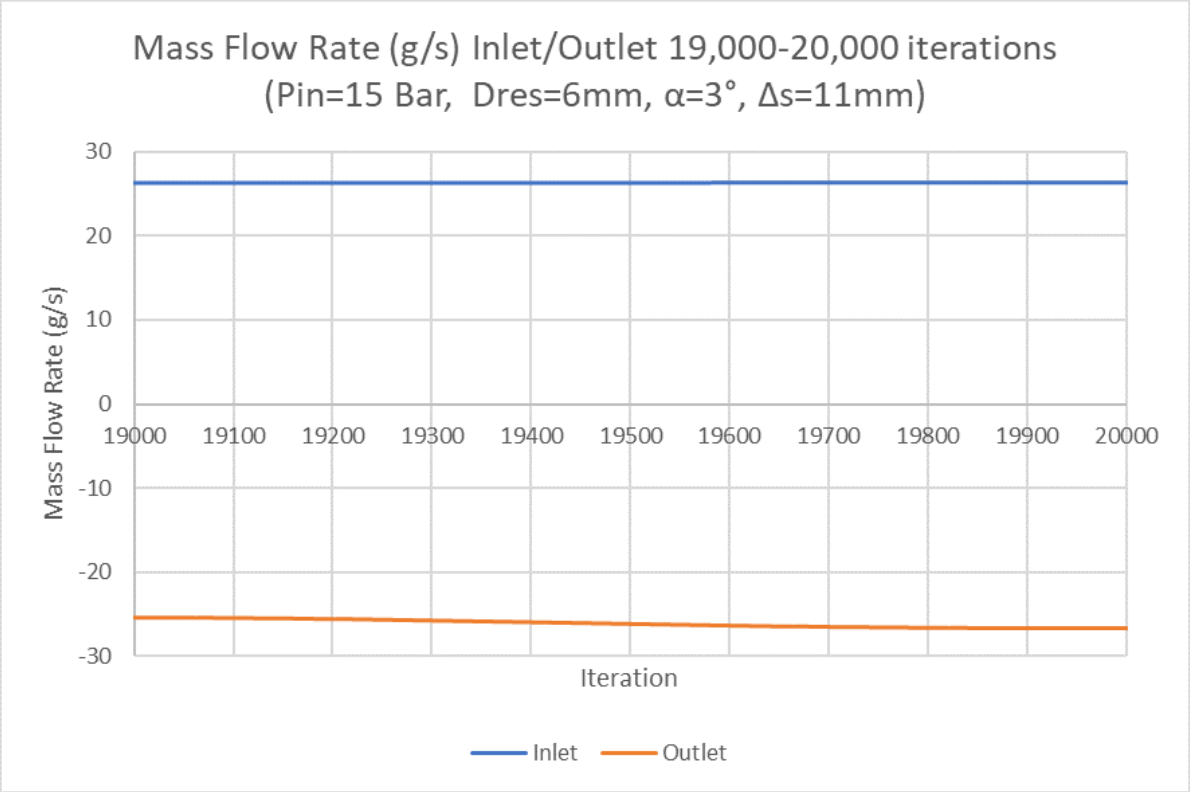

Figure G.17: Case 3.2: Large D_{res}, P_o = 15 bar, Mass Flow Rate Inlet/Outlet End of Simulation

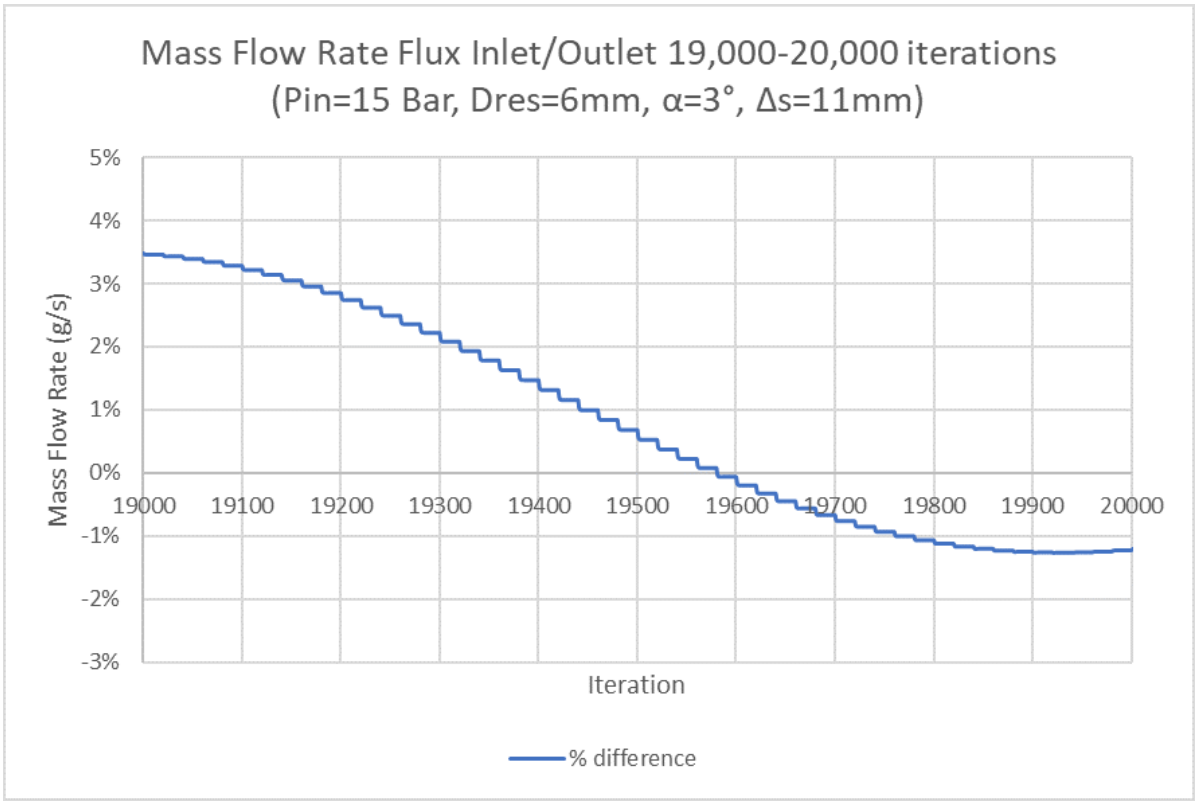

Figure G.18: Case 3.2: Large D_{res}, P_o = 15 bar, Mass Flow Rate Inlet/Outlet Flux, End of Simulation

G.5. Case 3.3: Large Dres Po: 25 bar

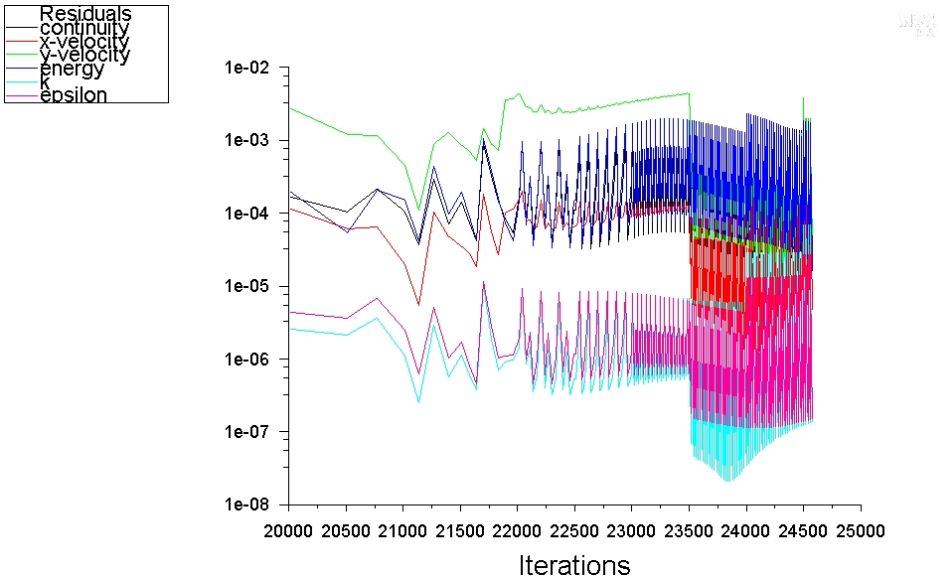

Figure G.19: Case 3.3: Large D_{res}, P_o = 25 bar, Residuals

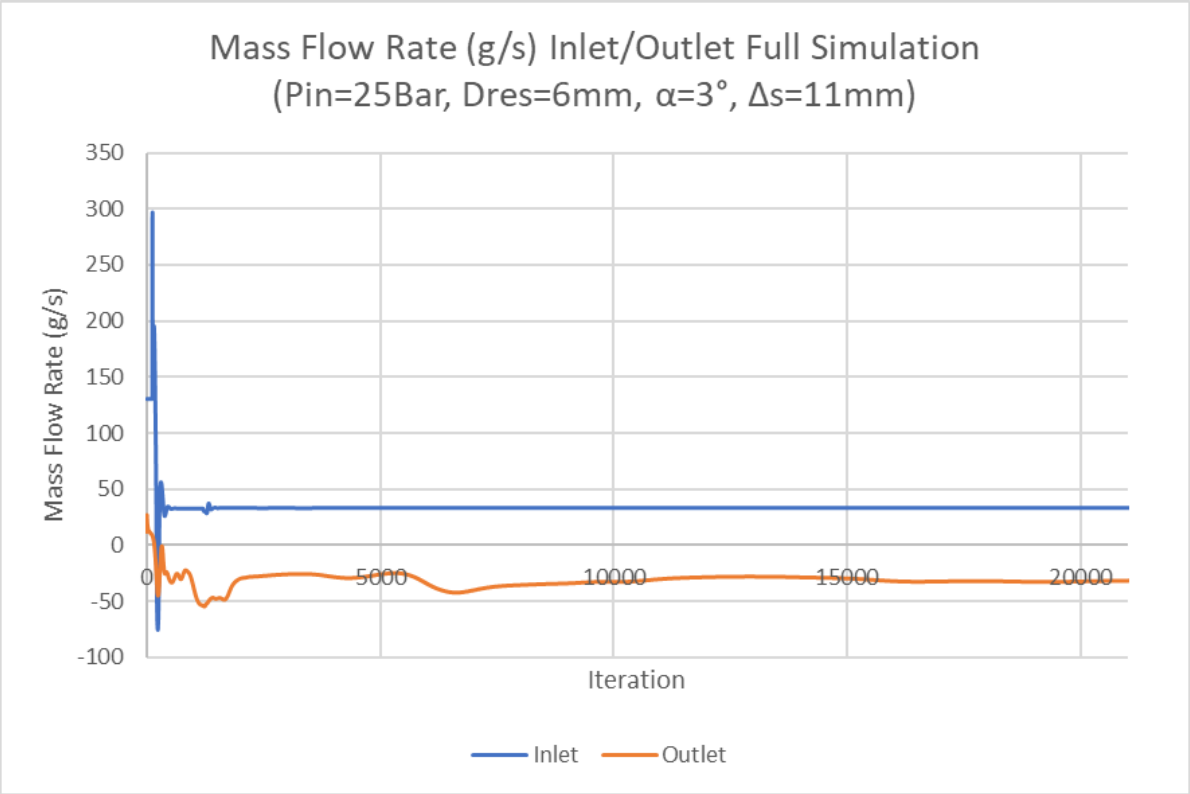

Figure G.20: Case 3.3: Large D_{res}, P_o = 25 bar, Mass Flow Rate Inlet/Outlet Full Simulation

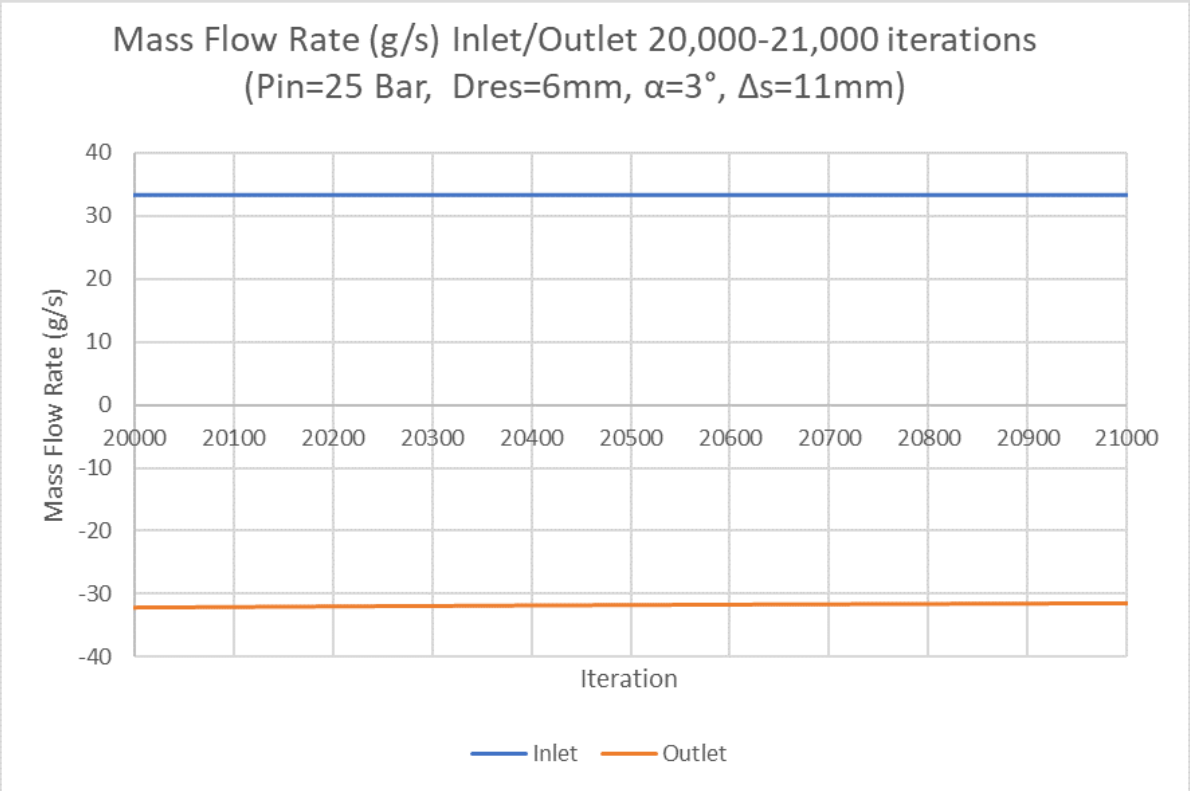

Figure G.21: Case 3.3: Large D_{res}, P_o = 25 bar, Mass Flow Rate Inlet/Outlet End of Simulation

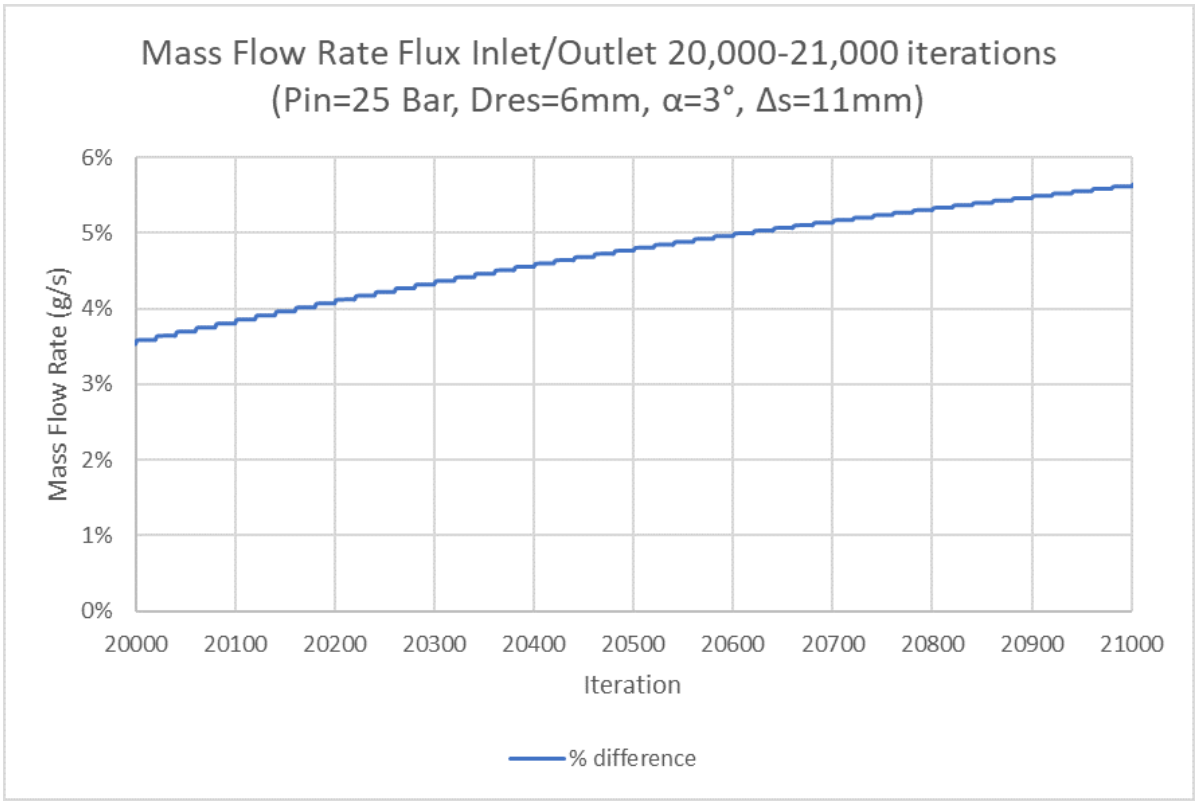

Figure G.22: Case 3.3: Large D_{res}, P_o = 25 bar, Mass Flow Rate Inlet/Outlet Flux, End of Simulation

H

Testing

H.1. Testing Purpose and Overview

Ignition systems are one of the most vital components of an engine. Failure of ignition systems can lead to delays in launches, explosive hard-starts, an even catastrophic engine failures. Therefore it is vital that an ignition system is properly tested prior to being integrated into a vehicle, in order to guarantee it's functionality and reliability. In addition to that verification testing, it is also critical to test an ignition system as an iterative part of the design and development process. Due to the nature of combustion, it is impossible to exactly predict how a system will function in reality. Therefore it is necessary to use estimations in the design, and then perform tests to adjust the design to fit the actual performance. In this project, ANSYS Fluent was used to test the design using numerical simulations. This has resulted in a verification of the preliminary and the generation of the detailed design. It is recommended that the next step in the development process it to perform physical experimentation of the system. This will demonstrate how well the physical system agrees with the theoretical one. This will be an iterative process between the design tools and the physical experiments. Results from the experimentation can be used to adjust the design tools such that they are more representative of reality. Then a more complete and reliable design can be developed using the design tools, changes can be made to the physical system and it can be retested. As it had been the original plan to perform such experiments, the literature study that accompanies this thesis provides detailed information on setting up the test campaign, and should be consulted for more information [24]. In this section, a summary of the test goals and phases are included as an addition to the work in the literature study.

H.2. Test Goals

Tests of the ignition system should be conducted in order to assess whether it meets the given requirements. Testing should be divided into test phases, determined by the stated testing sub-goals. The main goal of the test campaign is to build and demonstrate a working ignition system. This main goal cannot be achieved in one test and requires a number of smaller tests. The best way to conduct this test campaign, is to create a set of sub-goals from which a number of test phases can be developed. In these phases, each of the sub-goals will be achieved in the given order. This provides structure and pacing to the test campaign, but creating manageable goals and checkpoints. This main goal is refined below and broken down into smaller sub-goals, as follows. Following this, the test phases that developed to meet these sub-goals will be explained.

Main Goal: Demonstrate a GOX-Ethanol resonance ignition system that achieves ignition and meets the given system requirements.

Sub-Goals:

1. Determine relationship between GOX sonic nozzle inlet pressure, exit diameter and mass flow rate. Verify theoretical design.
2. Achieve heating of the resonance cavity using only a GOX nozzle and cavity. Determine best gap distance and cavity geometry combination, for heating.

3. Keeping geometry set, determine best material choice for maximum cavity heating.
4. Determine relationship between liquid ethanol injector hole size, inlet pressure, and mass flow rate. Verify theoretical design.
5. Achieve designed propellant mass flow rates in igniter.
6. Achieve ignition of GOX and Ethanol in the igniter combustion chamber.
7. Achieve ignition power and timing requirements.
8. Achieve ignition system reusability.

H.3. Test Phases

Testing will be conducted in phases, during each of which one or more of the given sub-goals will be met. These tests will be conducted using a test-bench version of the ignition system that has modular, adjustable components that can be changed to allow for adjustment during testing. The results of this testing will influence the final design of a flight version of the igniter. Once testing of the test-bench version of the igniter is completed, an optional fifth test phase will occur, during which a flight test version can be made and tested, prior to engine integration. Each of the phases described will be proceeded by a leak test with Nitrogen, to verify that the system is leak tight and ready for testing. Each of the phases is listed below with a short description. Expanded information on each phase is contained in the Literature Study.

Phase 1: Component Testing

Component testing will focus on two of the internal components–injection nozzle and gap distance. The injection nozzle will be tested first to see if it provides the calculated mass flow rate and pressure drop. This will be accomplished by flowing GOX through the injection nozzle into a cavity and measuring the pressures at the inlet and outlet of the nozzle to calculate the mass flow rate. Then a Schlieren imaging system will be used to see if the results of the Nozzle Exhaust Numerical simulation in Fluent provided an accurate depiction of the geometry of the injection nozzle exhaust plume. Schlieren imaging is a flow visualization tool that shows the flow away from an object's surface, in a manner than can be photographed [33]. The goal of this phase is to validate the detailed design choices on the relationship between the injection nozzle exit diameter and injection pressure, and the opening diameter of the resonance cavity and the gap distance.

Phase 2: Heating Test

In the heating test, gaseous oxygen will be injected through the nozzle into the resonance cavity. The temperature of the hot gasses at the bottom of the resonance cavity will be recorded using a thermocouple and a thermal camera. The testing will begin with an adjustable version that only contains the internal components–injection nozzle, resonance cavity and their gap distance. Once this version is tested, the complete version contained in a mixing chamber with an exit nozzle can be tested. The gap distance will be adjusted and resonance cavities of different materials and lengths will be tested, to assess the effect of these variables on heating. The goal of the heating test will be to determine the proper resonance cavity length, material and gap distance in order to reach the required temperature.

Phase 3: Cold Flow Testing

Cold flow tests will be used to evaluate the functionality and timing of the completed system. The complete prototype igniter, with the fuel injector, should be manufactured and tested. Cold flow means that no combustion will take place, as such no fuel will be used, so water will replace ethanol. The hot fire test procedures will be followed, but no flame will be produced. The goal of this testing phase is to work out any feedsystem, control system and/or procedural issues with the testing. Once completed the system will be ready for the hotfire.

Phase 4: Hot Fire Testing

Phase four is the hotfire testing. The feedsystem required is included in Appendix H. The procedures will be the same as for the cold flow, but now ethanol will be used instead of water. The goal of this phase is to learn the proper ignition timing, verify if the system meets all design parameters, and produces a flame. The system should be modular to allow replacement of components if they are thermally damaged. The test will be repeated a predetermined number of times to assess repeatability.

The plot below shows the ignition timing and relative igniter and main engine combustion pressures as a function of the timing of the ignition and main engine startup.

The combustion in the igniter will only last about 1-2 seconds from the moment the igniter fuel is injected until the point the GOX flow stops and the high pressure igniter fuel purge begins. The exact timing of the main engine achieving combustion and the igniter GOX stopping and fuel purge beginning is super dependant on many things. OF in reality (which is effected by many things, perhaps the injector is not impinging perfectly and the designed OF is not achieved), the size and length of the feedsystem lines can effect the achieved OF in reality. Therefore it is vital to note that much testing is required as systems in the real world do not behave as predicted and therefor there must be flexibility in the design to account for this and to allow for making adjustments during testing (like changing supply pressures, changing orifice sizes, etc) in order to set the actual optimal conditions for the physical engine in order to achieve the desired performance. Additionally, in order to ensure that a positive DP is maintained across the system, trial and error testing is necessary to determine the timing of ending the ignition combustion and beginning purging.

H.4. Safety Considerations

To ensure safety, these tests will be reviewed by the DARE Safety Board and consultation will be made with safety professionals at TU Delft Logistics and Management. In accordance with the TU Delft Dreamhall rules, no toxic materials will be used and proper personal protective equipment (PPE) will be work during all manufacturing and testing tasks. The level of PPE is dependant on the task, but in general includes safety googles, hearing protection, a lab coat, and steel-toed boots. All electronic equipment will be reviewed with a member of the DARE Electronics team for safety.

In accordance with the DARE Safety Board rules, any testing with pressures above 10 bar will require the presence of a safety officer. As this is not a very dangerous or large system, hot-fire testing will be done on the Fellowship Field on the TU Delft campus. CRYO team members will assist in the testing. The organization of the testing will be coordinated with the DARE Safety Board and the TU Delft Logistics and Management Department. These safety considerations will be expanded upon after meeting with the DARE safety personnel.

H.5. Conclusion

This section provides an overview of the experimental testing for the resonance ignition system. It provides an overview of the test goals and phases which can be used to set up a test campaign; in combination with the testing section of the literature study, and Appendix H which contains a feedsystem diagram and ignition timing chart.

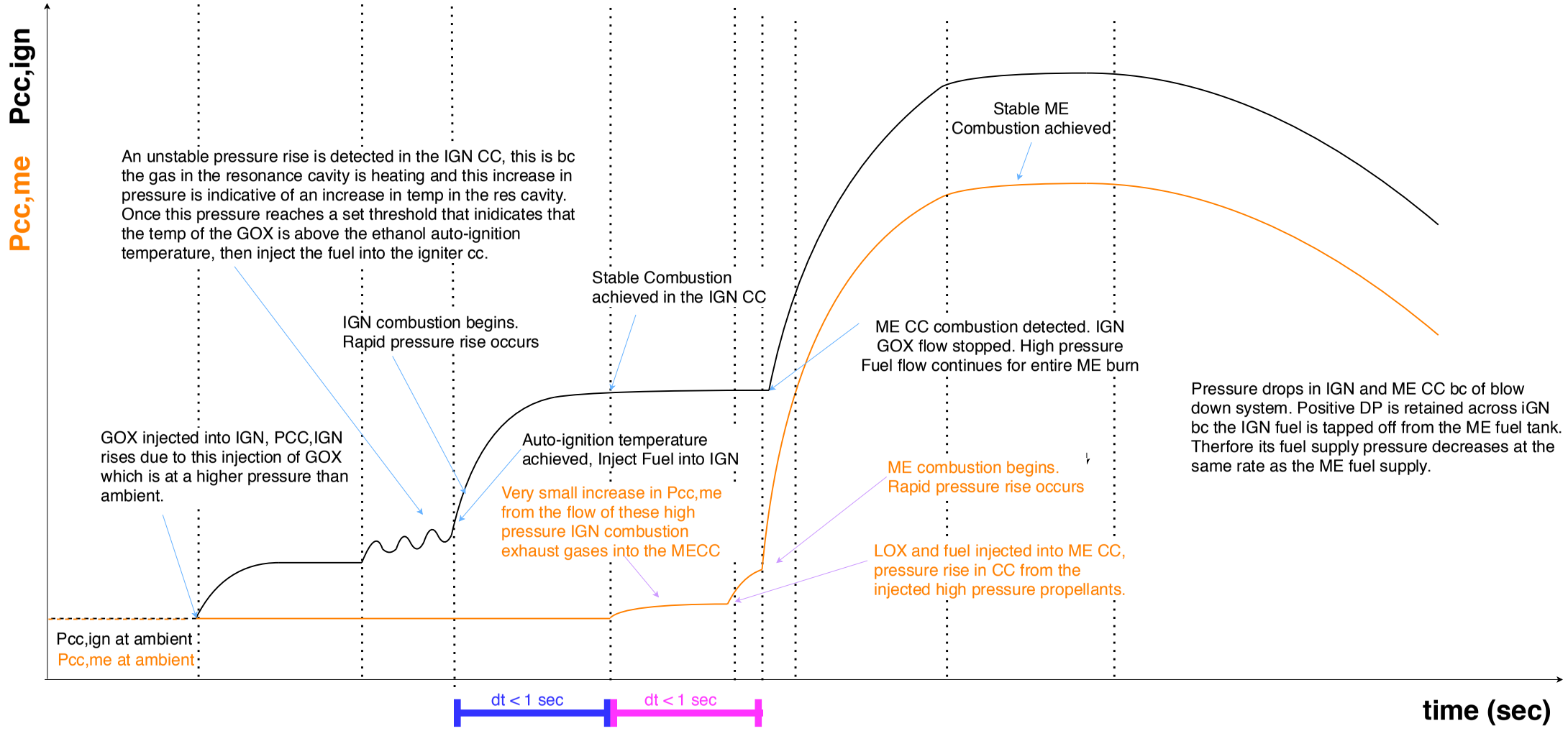
Pcc,ign
Pcc,me
An unstable pressure rise is detected in the IGN CC, this is bc the gas in the resonance cavity is heating and this increase in pressure is indicative of an increase in temp in the res cavity. Once this pressure reaches a set threshold that inidicates that the temp of the GOX is above the ethanol auto-ignition temperature, then inject the fuel into the igniter cc.
Stable ME Combustion achieved
Stable Combustion achieved in the IGN CC
IGN combustion begins. Rapid pressure rise occurs
ME CC combustion detected. IGN GOX flow stopped. High pressure Fuel flow continues for entire ME burn
Pressure drops in IGN and ME CC bc of blow down system. Positive DP is retained across iGN bc the IGN fuel is tapped off from the ME fuel tank. Therfore its fuel supply pressure decreases at the same rate as the ME fuel supply.
GOX injected into IGN, PCC,IGN rises due to this injection of GOX which is at a higher pressure than ambient.
Auto-ignition temperature achieved, Inject Fuel into IGN
Very small increase in Pcc,me from the flow of these high pressure IGN combustion exhaust gases into the MECC
ME combustion begins. Rapid pressure rise occurs
LOX and fuel injected into ME CC, pressure rise in CC from the injected high pressure propellants.
Pcc,ign at ambient
Pcc,me at ambient
dt < 1 sec
dt < 1 sec
time (sec)

DARE
Delft Aerospace Rocket Engineering

Title
GOX Heating Test Feed System

Project
ZED Thesis

Version	Date
2	2020/19/06

Author	Checked by
Zoe Dickert	KD

Symbol legend

- Crossing lines (not connected)
- Branch connection
- Check valve
- Hand-actuated valve
- Pneumatic-actuated ball-valve
- Compressed gas regulator
- Gas cylinder
- Resonance Tube
- Injection Nozzle
- Pressure gauge (analog)
- Temperature sensor (analog)
- Pressure sensor (electrical output)
- Temperature sensor (electrical output)
- Decibel sensor (electrical output)
- Oxygen (g) line
- Purge Nitrogen line
- Pressurizing Nitrogen line
- (NC) Normally Closed Valve
- (NO) Normally Open Valve

Glossary

TOD	Tank Opening Device
CGR	Compressed Gas Reg.
APG	Analog Pressure Gauge
DPS	Digital Pressure Sensor
DDS	Digital Decibel Sensor
DTS	Digital Temp. Sensor

V	Valve
VV	Vent Valve
DV	Dump Valve
SV	Service Valve
MV	Main Valve
XV	Extinguish Valve
XCV	Extin. Check Valve

Notes

Set Pressurizing N2 bottle to 8 bar.

Set O2(g) & N2(g) bottles to pressure specified in Test Plan.